I&EC research
Industrial & Engineering Chemistry Research

Article

pubs.acs.org/IECR

Highlighting Diffusional Coupling Effects in Ternary Liquid Extraction and Comparisons with Distillation

Rajamani Krishna*

Van 't Hoff Institute for Molecular Sciences, University of Amsterdam, Science Park 904, 1098 XH Amsterdam, The Netherlands

Supporting Information

ABSTRACT: Liquid extraction processes involve the separation of mixtures containing three or more species whose compositions are close to the binodal curve; this proximity causes the diffusion equilibration process to be strongly influenced by phase equilibrium thermodynamics. Due to thermodynamic factors, the interphase transfer flux of any component is influenced by the driving force of all the constituent species in the mixture, i.e. the diffusion process is strongly coupled. The transient diffusion equilibration process within spherical droplets dispersed within a continuous liquid phase is quantified by the classic Geddes model, used in combination with the Maxwell−Stefan diffusion formulation. For 13 different partially miscible ternary liquid mixtures, the equilibration trajectories in composition space are found to be curvilinear in shape. In all cases, the component Murphree efficiencies, E_i, are unequal to one another. The separations achieved are significantly different from those predicted by a simpler model that ignores coupling effects. In ternary distillation, the existence of azeotropes creates boundaries in composition space, whose crossings are disallowed in equilibrium-stage calculations. The application of the Geddes model for transient diffusion inside vapor bubbles yields curvilinear trajectories that demonstrate the possibility of boundary crossing; such crossings are in conformity with published experimental data.

1. INTRODUCTION

Liquid extraction, whose fundamental principles were elucidated in 1916 by W. K. Lewis,[1] is often used in the chemical and petroleum industries to separate mixtures that have boiling points close to one another, making distillation operations difficult and energy-intensive.[2−7] With the rapid development of a vast variety of ionic liquids[8,9] and eutectic[10] solvents, there is renewed interest in extractive separations for a variety of applications. To set the scene and define the objectives of this article, consider the separation a 25/75 heptane/toluene mixture, indicated by HT in Figure 1. Addition of the extraction agent, sulfolane (S), to HT results in a mixture of composition M that falls within the unstable region of the phase diagram. The mixture M will separate into two liquid phases that are in equilibrium with each other. In the extract phase E, the toluene/heptane ratio is 6.5, whereas this ratio is reduced to 2.4 in the raffinate phase R. Solvents such as sulfolane, NMP (*N*-methyl pyrrolidone), ionic liquids, and eutectics allow the reduction of aromatics of hydrocarbon mixtures for the purposes of improving the properties of kerosene, diesel, and lube-oils and manufacture of food-grade hexane.[2,9,11,12] The design and sizing of appropriate liquid−liquid contacting devices such as stirred vessels, sieve-tray columns, and rotating disc contactors (RDC) are crucially dependent on accurate estimation of the interphase transfer fluxes, and stage efficiencies, for achieving S-E, and HT-R equilibration.[2,5−7,13,14]

It is well established that the proper, and convenient, description of diffusion in ternary fluid mixtures is afforded by the Maxwell−Stefan (MS) diffusion formulation, that relates the diffusion fluxes to the chemical potential gradients[14−17]

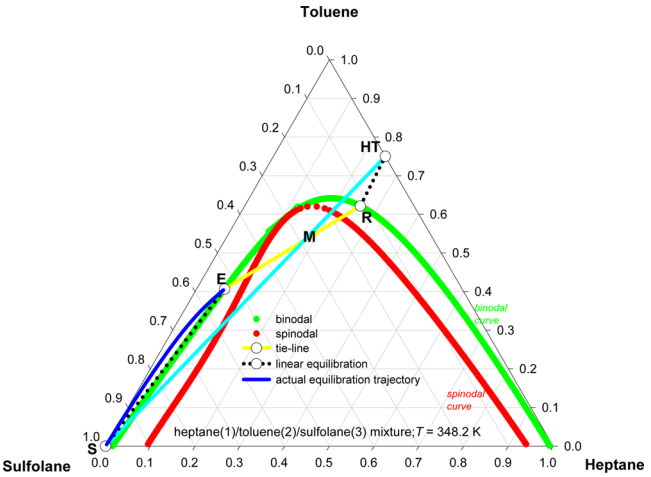

Figure 1. Phase equilibrium diagram for the system heptane(1)/toluene(2)/sulfolane(3) at 348.2 K. Pure sulfolane (S) is mixed with a 25/75 heptane/toluene mixture (HT) to yield mixture M. The mixture separates into two phases with compositions E and R at either ends of the tie-line shown. The blue colored lines show the actual composition trajectories for the S-E and HT-R equilibration.

$$-\frac{x_i}{RT}\frac{\mathrm{d}\mu_i}{\mathrm{d}z} = \sum_{\substack{j=1\\ j\neq i}}^{3}\frac{x_j J_i - x_i J_j}{c_t Đ_{ij}}; \qquad i = 1, 2, 3 \tag{1}$$

Received: November 17, 2015
Revised: January 1, 2016
Accepted: January 6, 2016
Published: January 6, 2016

DOI: 10.1021/acs.iecr.5b04236
Ind. Eng. Chem. Res. 2016, 55, 1053−1063

The diffusion fluxes in Equation 1 are defined with respect to the molar average reference velocity frame, $J_i \equiv c_i(u_i - u)$. At constant temperature, T, and pressure, p, only two of the three chemical potential gradients are independent because of the Gibbs–Duhem constraint $\sum_{i=1}^{3} x_i \frac{d\mu_i}{dz} = 0$. Also, the diffusion fluxes J_i sum to zero, $\sum_{i=1}^{3} J_i = 0$. The MS formulation is consistent with the theory of irreversible thermodynamics; the Onsager reciprocal relations demand that the MS pair diffusivities be symmetric $Đ_{ij} = Đ_{ji}$. For use in the design equations for separation devices, the chemical potential gradients are related to the mole fraction gradients by introducing a 2 × 2 matrix of thermodynamic factors $[\Gamma]$:

$$\frac{x_i}{RT}\frac{d\mu_i}{dz} = \sum_{j=1}^{2} \Gamma_{ij}\frac{dx_j}{dz}; \qquad \Gamma_{ij} = \delta_{ij} + x_i\frac{\partial \ln \gamma_i}{\partial x_j}; \qquad i, j = 1, 2 \tag{2}$$

The Γ_{ij} can be calculated from models describing phase equilibrium thermodynamics such as UNIQUAC or NRTL;[16,18] explicit analytic formulas for the calculation of the derivatives are provided in Appendix D of the work of Taylor and Krishna.[16] In the special case of thermodynamically ideal fluid mixtures, $[\Gamma]$ degenerates to the identity matrix

$$\Gamma_{ij} = \delta_{ij}; \qquad \text{(thermodynamically ideal fluid mixtures)} \tag{3}$$

For a ternary mixture, Equation 1 may be recast into the Fickian form

$$(J) = -c_t[D]\frac{d(x)}{dz} \tag{4}$$

in which the two-dimensional matrix of Fick diffusivities $[D]$ is a product of two matrices

$$[D] = [\Lambda][\Gamma] \tag{5}$$

Equation 1 allows the matrix $[\Lambda]$ to be expressed explicitly in terms of the MS diffusivities of the constituent binary pairs in the ternary mixture[17]

$$\begin{bmatrix} \Lambda_{11} & \Lambda_{12} \\ \Lambda_{21} & \Lambda_{22} \end{bmatrix} = \frac{\begin{bmatrix} Đ_{13}(x_1Đ_{23} + (1 - x_1)Đ_{12}) & x_1Đ_{23}(Đ_{13} - Đ_{12}) \\ x_2Đ_{13}(Đ_{23} - Đ_{12}) & Đ_{23}(x_2Đ_{13} + (1 - x_2)Đ_{12}) \end{bmatrix}}{x_1Đ_{23} + x_2Đ_{13} + x_3Đ_{12}} \tag{6}$$

Experimental data for a wide variety of ternary liquid mixtures[19−27] confirm that the off-diagonal elements of the Fick matrix $[D]$ are generally nonzero; this causes the diffusion flux of a given species to be engendered by the driving force of its partner species in the mixture; i.e., the ternary diffusion process is coupled. The work of Korchinsky et al.,[28] for example, underscores the importance of coupling effects for diffusion of acetone/methanol/benzene mixtures within films and inside drops. If the diffusion coupling effects are completely ignored, and the simplest Fickian relation

$$J_i = -c_t D\frac{dx_i}{dz}; \qquad i = 1, 2, 3 \tag{7}$$

is employed, the equilibration trajectories S-E and HT-R will be linear, as indicated by the dotted lines in Figure 1. The primary objective of this article is to demonstrate that the actual diffusion equilibration trajectories must be expected to be strongly curvilinear in composition space. To verify that the conclusions drawn for the system heptane/toluene/sulfolane have a generic character, we investigated diffusion equilibration trajectories in 13 partially miscible ternary liquid mixtures of relevance in different separation applications. The secondary objective is to compare the diffusional coupling effects in extraction with those for ternary azeotropic distillation; in the latter case, curvilinear diffusion equilibration trajectories may follow paths that are distinctly different from those predicted by Equation 7, resulting in crossing of boundaries that are forbidden by equilibrium stage calculations.

All calculations of diffusion trajectories, mass transfer coefficients, and efficiencies that are reported in this article involve explicit analytic formulas that were implemented in MathCad 15.[29] The Supporting Information accompanying this publication provides additional modeling details, input data on diffusivities, tabulated data on the NRTL and UNIQUAC parameters required for the determination of phase equilibrium thermodynamics, along with detailed calculations for all systems investigated.

2. EQUILIBRATION TRAJECTORIES AND MURPHREE EFFICIENCIES

The combination of eqs 5 and 6 shows that two kinds of "coupling" may contribute to off-diagonal contributions of the Fickian matrix $[D]$: (a) differences in the MS diffusivities of the binary pairs, $Đ_{ij}$, and (b) thermodynamic coupling, quantified by the off-diagonal elements of $[\Gamma]$. The first task is to estimate the MS diffusivities of the three binary pairs $Đ_{12}$, $Đ_{13}$, and $Đ_{23}$ in the extract phase. The MS binary pair diffusivities are composition dependent.[16,17,30] The Vignes interpolation formula for binary liquid mixtures[30,31] can be extended to ternary mixtures as follows[30]

$$Đ_{ij} = (Đ_{ij}^{x_i \to 1})^{x_i}(Đ_{ij}^{x_j \to 1})^{x_j}(Đ_{ij}^{x_k \to 1})^{x_k} \tag{8}$$

The six infinite dilution values of the pair diffusivities $Đ_{ij}^{x_j \to 1}$ can be estimated using say the Wilke–Chang correlation.[32] For estimation of $Đ_{ij}^{x_k \to 1}$, the i–j pair diffusivity when both i and j are present in infinitely dilute concentrations, the following formula has been suggested[30]

$$Đ_{ij}^{x_k \to 1} = (Đ_{ik}^{x_k \to 1})^{x_i/(x_i + x_j)}(Đ_{jk}^{x_k \to 1})^{x_j/(x_i + x_j)} \tag{9}$$

For the extract phase at the average composition between S and E, the estimated MS diffusivity values are $Đ_{12} = 0.94$; $Đ_{13} = 0.82$; $Đ_{23} = 0.96 \times 10^{-9}$ m^2 s^{-1}. The values of the pair diffusivities are close to one another primarily because of the closeness of the molar masses of heptane, toluene, and sulfolane: 0.1, 0.092, and 0.12 kg mol^{-1}, respectively. Consequently, the off-diagonal elements of $[\Lambda]$ are practically zero and any diffusional coupling effects must arise from the thermodynamic nonidealities, quantified by $[\Gamma]$. A pragmatic approach is to take $[\Lambda]$ to be a scalar diffusivity times the identity matrix, $[I]$, where the value of the scalar diffusivity is the square-root of the determinant of $[\Lambda]$,[17] that can be determined from eq 6

DOI: 10.1021/acs.iecr.5b04236
Ind. Eng. Chem. Res. 2016, 55, 1053−1063

$$|\Lambda|^{1/2} = \sqrt{\frac{Đ_{12}Đ_{13}Đ_{23}}{x_1Đ_{23} + x_2Đ_{13} + x_3Đ_{12}}} \quad (10)$$

Equation 10 yields $|\Lambda|^{1/2} = 0.9 \times 10^{-9}$ m^2 s^{-1}.

Turning to the thermodynamic influences on the Fick diffusivities, we note that at the three vertices of the composition space in Figure 1, $[\Gamma]$ reduces to the identity matrix $[I]$. As the compositions approach the binodal curve, the magnitude of the off-diagonal elements progressively increase. As illustration, Figure 2a presents the values of the elements of

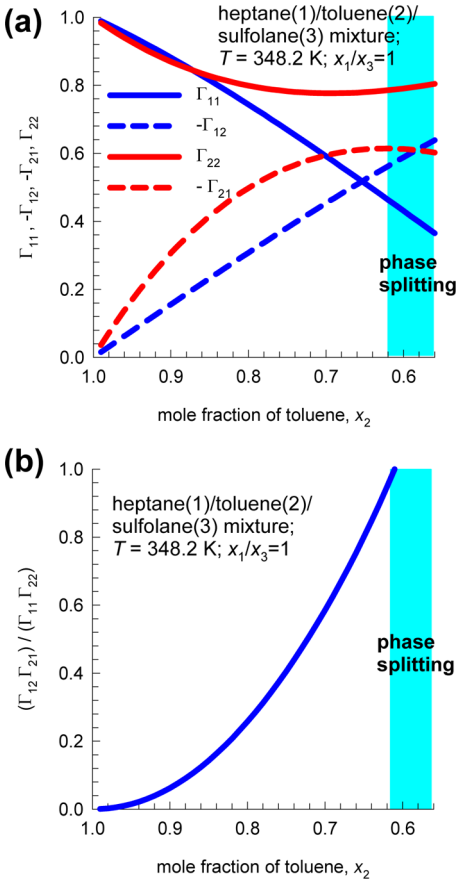

Figure 2. (a) Four elements of the matrix of thermodynamic factors, Γ_{11}, $-\Gamma_{12}$, $-\Gamma_{21}$, and Γ_{22} plotted as a function of the mole fraction of toluene, x_2 in the heptane(1)/toluene(2)/sulfolane(3) mixture at 348.2 K (b) Plot of the ratio $(\Gamma_{12}\Gamma_{21})/(\Gamma_{11}\Gamma_{22})$ as a function of the mole fraction of toluene, x_2. In these calculations, the ratio x_1/x_3 equals unity. The shaded region indicates phase splitting.

$[\Gamma]$ as a function of the mole fraction of toluene, x_2, starting at the toluene vertex of the composition triangle, maintaining $x_1/x_3 = 1$. Since both off-diagonal elements are negative, the data are plotted are for Γ_{11}, $-\Gamma_{12}$, $-\Gamma_{21}$, and Γ_{22}. The magnitudes of both off-diagonal elements are seen to increase as x_2 approaches 0.62, at which phase splitting occurs. In industrial practice, sulfolane is used along with 3 wt % water; the presence of water will serve to enhance the phase splitting tendencies and thermodynamic coupling.

An alternative method of highlighting the thermodynamic coupling effects is to plot the ratio $(\Gamma_{12}\Gamma_{21})/(\Gamma_{11}\Gamma_{22})$ as a function of x_2 (cf. Figure 2b); this ratio reaches an asymptotic value of unity along the spinodal curve, that defines the limit of phase stability[17]

$$(\Gamma_{12}\Gamma_{21})/(\Gamma_{11}\Gamma_{22}) = 1; \qquad \text{spinodal curve} \quad (11)$$

Equation 11 implies that for any partially miscible ternary mixture, thermodynamic coupling effects become of paramount importance in the regions close to phase splitting. On careful examination of available experimental data on Fick matrix $[D]$ for ternary liquid mixtures,[17] it has been established that coupling effects in the Fick matrix emanate predominantly from $[\Gamma]$. This leads to the conclusion that coupled diffusion should be expected to be the norm, rather than the exception, in liquid−liquid extraction processes.

A simple procedure for the estimation of the matrix of Fick diffusivities for partially miscible liquid mixtures is

$$[D] = |\Lambda|^{1/2}[\Gamma] \quad (12)$$

with the scalar diffusivity $|\Lambda|^{1/2}$ calculated from Equation 10; the accuracy of this estimation procedure has been established in earlier work on examination of published experimental data on Fick diffusivities.[17] At a composition that is the average of those at S (= (x_0)) and E (= (x_{eq})), the Fick matrix is estimated as $[D] = \begin{bmatrix} 0.643 & -0.148 \\ -0.769 & 0.733 \end{bmatrix} \times 10^{-9}$ m^2 s^{-1}. The off-diagonal contributions are non-negligible in magnitude. Particularly noteworthy is the large negative value of the D_{21} with respect to D_{22}. At the start of the equilibration process, the driving forces of heptane and toluene are $\Delta x_1 = x_{10} - x_{1eq} = 0.0 - 0.0627 = -0.0627$, and $\Delta x_2 = x_{20} - x_{2eq} = 0.0 - 0.4064 = -0.4064$. The magnitude of the coupling contributions to fluxes are indicated by ratios $\frac{D_{12}\Delta x_2}{D_{11}\Delta x_1} = -1.49$ and $\frac{D_{21}\Delta x_1}{D_{22}\Delta x_2} = -0.1616$. We conclude that the heptane flux, J_1, will be strongly influenced, in a negative sense, by the contribution of $D_{12}\Delta x_2$.

If sulfolane is dispersed as rigid spherical droplets of diameter, d_{drop}, within a continuous phase consisting of the hydrocarbon phase, the transient equilibration process inside a droplet is described by Geddes model,[33] that was originally developed for describing binary diffusion inside vapor bubbles on distillation trays. For ternary mixtures, the Geddes model can be written in two-dimensional matrix differential equation[16,34]

$$(x - x_{eq}) = [Q](x_0 - x_{eq});$$
$$[Q] \equiv \frac{6}{\pi^2}\sum_{m=1}^{\infty}\frac{1}{m^2}\exp\left[-m^2\pi^2\frac{4[D]t}{d_{drop}^2}\right] \quad (13)$$

The matrix $[Q]$ quantifies the departure from equilibrium. The Sylvester theorem, detailed in Appendix A of the work of Taylor and Krishna,[16] is required for explicit calculation of the composition trajectories described by eq 13. The fractional approaches to equilibrium, also termed as the Murphree efficiencies,[2−4,35,36] are calculated from

$$E_1 = \frac{x_{10} - x_1}{x_{10} - x_{1eq}} = 1 - Q_{11} - Q_{12}\frac{\Delta x_2}{\Delta x_1}$$
$$E_2 = \frac{x_{20} - x_2}{x_{20} - x_{2eq}} = 1 - Q_{22} - Q_{21}\frac{\Delta x_1}{\Delta x_2}$$
$$E_3 = \frac{x_{30} - x_3}{x_{30} - x_{3eq}} = \frac{\frac{\Delta x_1}{\Delta x_2}E_1 + E_2}{\frac{\Delta x_1}{\Delta x_2} + 1} \quad (14)$$

DOI: 10.1021/acs.iecr.5b04236
Ind. Eng. Chem. Res. 2016, 55, 1053−1063

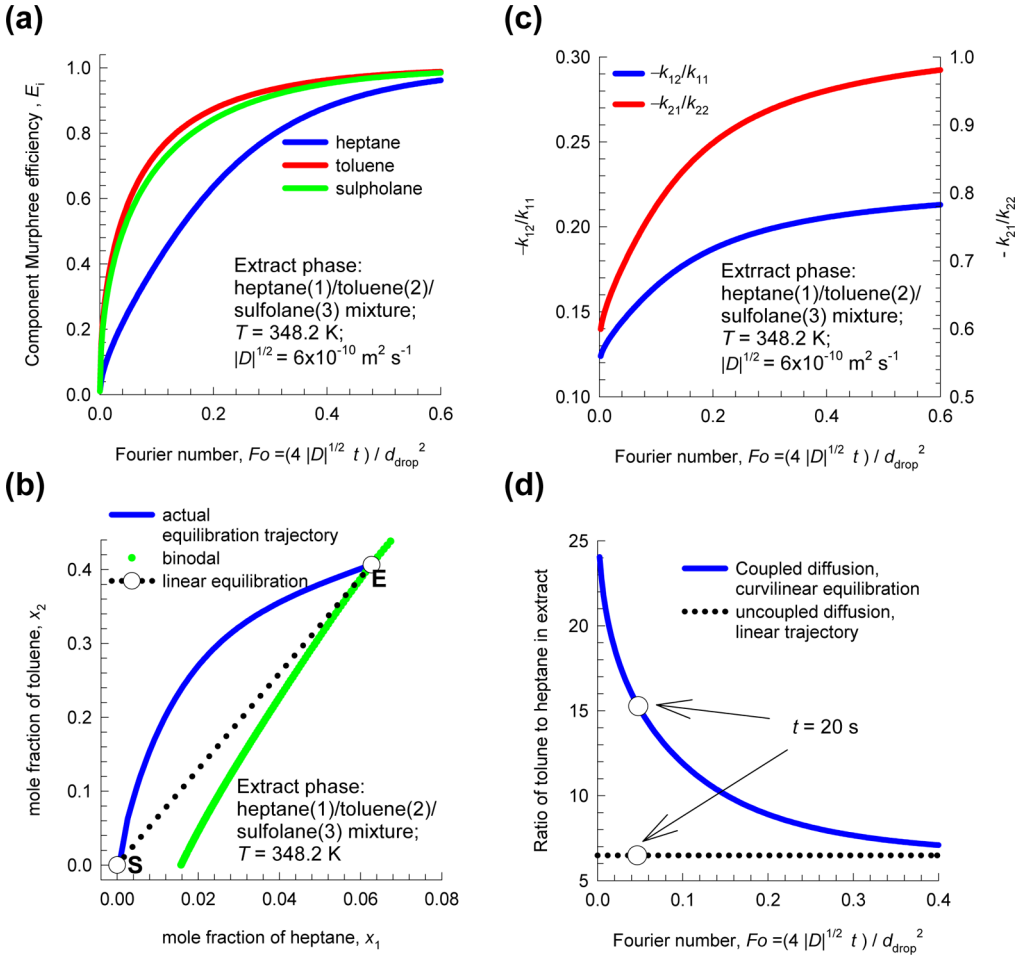

Figure 3. (a) Plot of the component Murphree efficiencies in the extract phase of heptane(1)/toluene(2)/sulfolane(3) mixture, E_i, as a function of the Fourier number. (b) Composition trajectory followed during S−E equilibration. (c) Calculations of the ratios $-k_{12}/k_{11}$ and $-k_{21}/k_{22}$ as a function of the Fourier number. (d) Plot of the toluene/heptane ratio in the extract phase as a function of the Fourier number.

The remark made by E. V. Murphree[35,36] in 1925 "The concept of the theoretical plate does not offer a satisfactory basis for calculation of rectifying columns when the mixture... contains more than two components" holds also for extractive separations, as we shall demonstrate below. Figure 3a present a plot of the component Murphree efficiencies in the extract phase as a function of the Fourier number, $\frac{4|D|^{1/2}t}{d_{drop}^2}$, wherein the value of the diffusivity is chosen as the square root of the determinant of the Fick matrix, $|D|^{1/2} = 0.6 \times 10^{-9}$. The quantity $|D|^{1/2}$ serves as a representative diffusivity value in order to express the obtained results in dimensionless time coordinates. For long contact times, each of the three efficiencies approaches unity. In practice, the contact time will be limited, and for $Fo < 0.4$, the component efficiencies are unequal to one another. The Murphree efficiency of heptane, E_1, is significantly lower than that of partner species; the reason for this can be traced to the large negative contribution of $D_{12}\Delta x_2$ to the heptane flux, J_1. This negative contribution of $D_{12}\Delta x_2$ also causes the equilibration trajectory to veer away from the heptane vertex in composition space, resulting in the curvilinear path; see Figure 1 and 3b.

The use of nonequilibrium stagewise simulation programs[13,14] require input data on the mass transfer coefficient to calculate separation performance. The two-dimensional matrix of mass transfer coefficients, $[k]$, defined by

$$(J) = c_t[k](x - x_{eq}) \tag{15}$$

and time-averaged for the interval $0-t$ can be calculated using the following expression[16]

$$[k_d] = -\ln[Q]\frac{d_{drop}}{6t}; \qquad [Q] = \exp\left[-[k_d]\frac{6}{d_{drop}}t\right] \tag{16}$$

Figure 3c presents calculations of the ratios $-k_{12}/k_{11}$ and $-k_{21}/k_{22}$ as a function of the Fourier number. The first thing to note is that the magnitude of the ratio $-k_{21}/k_{22}$ is significantly higher than that of $-k_{12}/k_{11}$; this is a reflection of the corresponding values of ratios $-D_{21}/D_{22}$ and $-D_{12}/D_{11}$. Second, both the ratios $-k_{12}/k_{11}$ and $-k_{21}/k_{22}$ increase with contact time, signifying that diffusional coupling effects increase with time. In the limit $t \to \infty$, an asymptotic value is reached

$$[k] = \frac{2\pi^2}{3}\frac{[D]}{d_{drop}} \tag{17}$$

In this asymptotic limit, the coupling effects of $[k]$ are directly proportional to those of the corresponding Fick matrix $[D]$.

Since the objective of the sulfolane extraction process is to reduce the aromatics contact in the feed mixture, the influence of coupling effects are best quantified by plotting the ratio of toluene to heptane in the extract phase as a function of the

DOI: 10.1021/acs.iecr.5b04236
Ind. Eng. Chem. Res. 2016, 55, 1053−1063

Fourier number; see Figure 3d. Taking coupling effects into account leads to a significantly higher toluene/heptane ratio in the extract than for the scenario in which coupling effects are ignored. In an actual liquid−liquid contactor, the contact time between the dispersed phase droplets with the surrounding continuous phase will be limited and the final equilibrium composition will not be reached. As illustration, let us assume that the droplet of 1 mm diameter rises at a velocity of 20 mm s^{-1} on a sieve tray with a dispersion height of 400 mm. The contact time, t = 20 s, and the Fourier number $Fo = \frac{4|D|^{1/2}t}{d_{drop}^{2}} = 0.048$. For this contact time, E_1 = 0.245; E_2 = 0.577; E_3 = 0.532, and the toluene/heptane ratio in the extract phase is 15.3. If coupling effects are ignored, the use of eq 7 predicts a linear equilibration trajectory with the toluene/heptane ratio = 6.5, a significantly lower value. For the chosen set of conditions, coupled diffusion effects enhances the uptake of aromatics in the extract phase, improving separation performance to a significant extent.

We now investigate the influence of the resistance to interphase mass transfer offered by the continuous (raffinate) phase; see the schematic in Figure 4. The mass transfer

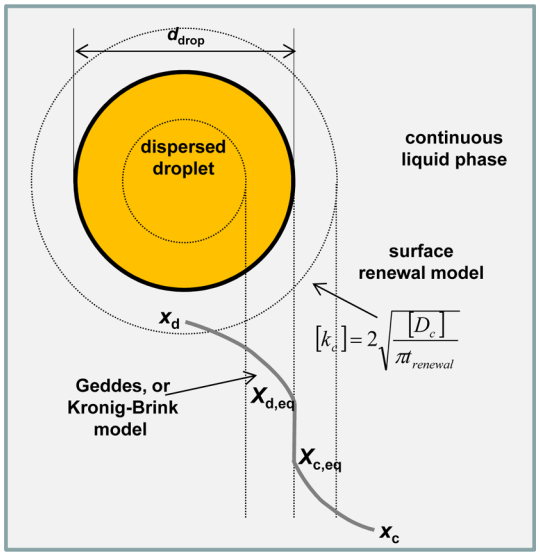

Figure 4. Interphase mass transfer resistances in liquid−liquid extraction.

coefficient external to the droplet can be estimated from the surface renewal theory[6,37]

$$[k_c] = 2\sqrt{\frac{[D_c]}{\pi t_{renewal}}} \tag{18}$$

The Fick matrix $[D_c]$ is evaluated using eq 12 at the average between the compositions of HT and R. The characteristic time for surface renewal can be estimated is $t_{renewal} = d_{drop}/V_{drop}$ = 0.05 s; this value is significantly lower than the time the droplet takes to rise through the dispersion, i.e. 20 s. The overall mass transfer coefficient is obtainable from the addition of resistances formula

$$[K_{Od}]^{-1} = [k_d]^{-1} + \frac{c_{tL,d}}{c_{tL,c}}\begin{bmatrix} \frac{x_{1d,eq}}{x_{1c,eq}} & 0 \\ 0 & \frac{x_{2d,eq}}{x_{2c,eq}} \end{bmatrix}[k_c]^{-1} \tag{19}$$

in which the distribution ratios are determined from those at the ends of the tie-line, E, and R; details of all calculations are provided in the Supporting Information. For a surface renewal time of 0.05 s, the estimated value of $[K_{Od}]$, used in combination with eqs 14 and 16, results in component efficiency values E_1 = 0.238; E_2 = 0.57; E_3 = 0.526; these values are only very slightly smaller than the those determined by ignoring the resistance of the continuous phase. In this case, the mass transfer resistance resides predominantly within the dispersed phase; this is a common occurrence.[38]

The Kronig−Brink[39] model that takes account of circulation within the droplet, leads to the following expression for the departure from equilibrium

$$(x - x_{eq}) = [Q](x_0 - x_{eq});$$
$$[Q] \equiv \frac{3}{8}\sum_{m=1}^{\infty} A_m^{\,2}\exp\left[-16\lambda_m\frac{4[D]t}{d_{drop}^{\,2}}\right] \tag{20}$$

The values of A_m and λ_m are tabulated by Sideman and Shabtai.[40] Equation 20 predicts a more rapid equilibration than the rigid sphere model eq 13. In composition space, the diffusion equilibration trajectory calculated using eq 20 follows a curvilinear path that is practically indistinguishable from that presented in Figure 3b. In other words, curvilinear diffusion trajectories are not the exclusive province of the Geddes eq 13.

The extraction of propylbenzene from mixtures with tetradecane with NMP solvent displays analogous characteristics; see Figure 5. Diffusion is strongly coupled due to the significant off-diagonal contributions of the elements of $[\Gamma]$, whose values at the average composition in the extract phase are $[\Gamma] = \begin{bmatrix} 0.0514 & -0.911 \\ 0.452 & 1.69 \end{bmatrix}$. The component efficiency of

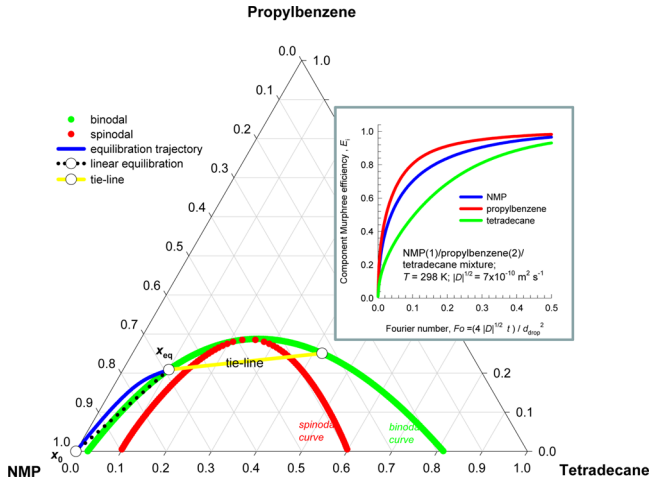

Figure 5. Transient equilibration trajectories for the system NMP(1)/propylbenzene(2)/tetradecane(3) at 298 K. The initial mole fractions in the drop are x_{10} = 1.0, x_{20} = 0.0, and x_{30} = 0.0. The final equilibrium composition is $x_{1,eq}$ = 0.6895, $x_{2,eq}$ = 0.2089, and $x_{3,eq}$ = 0.1016. The inset is a plot of the component Murphree efficiencies in the extract phase, E_i, as a function of the Fourier number.

DOI: 10.1021/acs.iecr.5b04236
Ind. Eng. Chem. Res. 2016, 55, 1053−1063

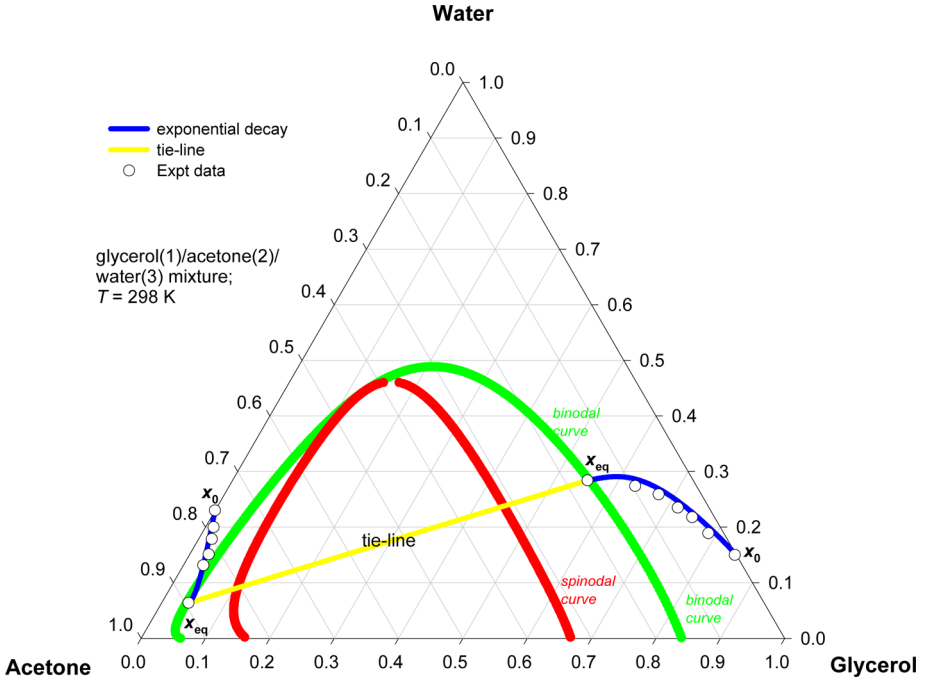

Figure 6. Transient equilibration trajectories for the system glycerol(1)/acetone(2)/water(3) mixtures at 298 K. The experimental data for the equilibration paths for glycerol(1)/acetone(2)/water(3) mixture measured in a stirred Lewis cell by Krishna et al.[41] are indicated by the symbols. The trajectories calculated using eq 21 are indicated by the continuous blue lines.

tetradecane is significantly lower than that of partner species (see inset to Figure 5); consequently, the equilibration trajectory tends to veer away from the tetradecane vertex. Diffusional coupling effects cause the extract phase to be significantly richer in aromatics than predicted by the linear equilibration process implicit in the assumption of the uncoupled flux relation 7.

The experimental data on transient equilibration of glycerol-rich and acetone-rich phases of the glycerol/acetone/water mixture measured in a stirred Lewis cell[41] confirm that the diffusion equilibration process follows curvilinear trajectories; see Figure 6. In a Lewis cell, the interface between the two liquid phases is flat; the appropriate expression for the departure from equilibrium in either the glycerol-rich or the acetone-rich phase is exponential decay model[41]

$$(x - x_{eq}) = [Q](x_0 - x_{eq}); \qquad [Q] \equiv \exp[-\beta[D]t] \tag{21}$$

where β is the Lewis cell constant. The Fick diffusivity in either phase can be estimated from eq 12, wherein the thermodynamic factors are calculated using the NRTL parameters reported in the literature.[42] The equilibration trajectories determined using eq 21 are shown by the continuous solid lines in Figure 6. It is remarkable to note that the experimentally determined *diffusion* trajectories can be reproduced, nearly quantitatively, using essentially input data on phase equilibrium *thermodynamics*.

The diffusion equilibration trajectories in ten other partially miscible systems encountered in a variety of separation technologies, water/acetone/phenol, water/acetone/ethyl-acetate, water/caprolactam/toluene, water/acetic-acid/isophorone, water/acetic-acid/MTBE, [omim][Cl]/ethanol/TAEE, [bmim][TfO]/ethanol/TAEE, water/ethanol/cyclohexane, toluene/ethanol/water, and water/acetone/toluene were also investigated; see Figures S8−S26 of the Supporting Information. For each of these mixtures we find (a) component Murphree efficiencies are different for one another and (b) the diffusion equilibration trajectories are curvilinear. As a small sample of the obtained results, Figures 7 and 8 show the

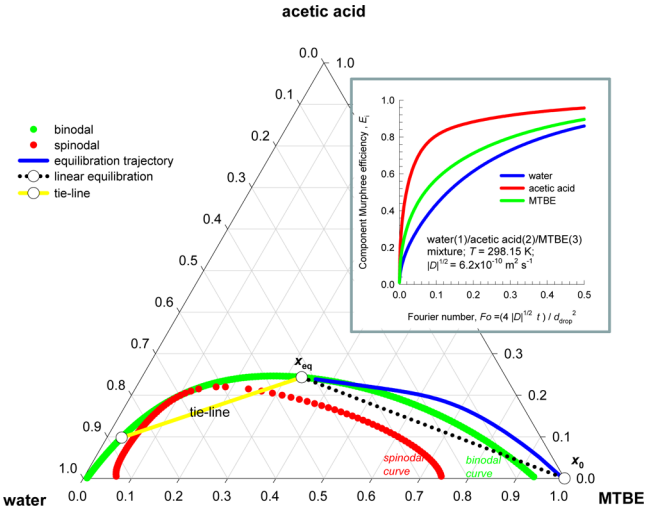

Figure 7. Transient equilibration trajectories for the system water(1)/acetic acid(2)/MTBE(3) at 298.15 K. The initial mole fractions in the drop are x_{10} = 0.0, x_{20} = 0.0, and x_{30} = 1. The final equilibrium composition is $x_{1,eq}$ = 0.4244, $x_{2,eq}$ = 0.2432, and $x_{3,eq}$ = 0.3324.

transient diffusion equilibration trajectories for the systems water/acetic acid/MTBE and [omim][Cl]/ethanol/TAEE mixtures. The use of the Geddes model (eq 13) predicts a circuitous path to equilibrium, proceeding almost parallel to the binodal curve. For both these mixtures, the path followed is concave in relation to the composition vertex of the component that has the lowest component Murphree efficiency: water in Figure 7 and TAEE in Figure 8. In sharp contrast, the linear

DOI: 10.1021/acs.iecr.5b04236
Ind. Eng. Chem. Res. 2016, 55, 1053−1063

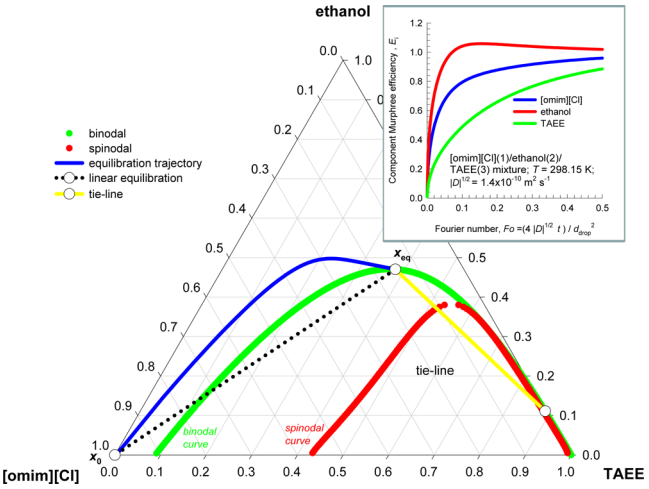

Figure 8. Transient equilibration trajectories for the system [omim]-[Cl](1)/ethanol(2)/TAEE(3) at 298.15. Here we denote the ionic liquid 1-octyl-3-methylimidazolium chloride in the abbreviated form [omim][Cl]. TAEE is the abbreviated name for tert-amyl ethyl ether. The initial mole fractions in the drop are x_{10} = 1.0, x_{20} = 0.0, and x_{30} = 0.0. The final equilibrium composition is $x_{1,eq}$ = 0.1501, $x_{2,eq}$ = 0.4703, and $x_{3,eq}$ = 0.3797.

equilibration trajectory predicted by eq 7 crosses the binodal curve while approaching equilibrium, implying the possibility of emulsification.[17]

3. DIFFUSIONAL COUPLING EFFECTS IN TERNARY DISTILLATION

We now draw comparisons between the diffusional coupling effects in ternary liquid extraction with corresponding effects in distillation; this exercise helps provide a broader perspective of diffusional coupling effects in separations technologies. In distillation, residue curve maps (RCM) are widely used for examining feasible separation schemes for ternary mixtures that form homogeneous or heterogeneous azeotropes;[43,44] RCMs describe the change of the composition of the liquid phase during continuous evaporation under conditions in which vapor−liquid equilibrium is maintained and serve as "tramlines" for column composition trajectories in a distillation tower. As illustration, consider the ternary mixture water/ethanol/acetone; the pure component boiling points are water = 373.2 K; ethanol = 351.6 K; acetone = 329.7 K. The water/ethanol azeotrope (12% water, 88% ethanol) has a boiling point of 351.4 K. The RCM for this mixture are also shown in Figure 9a. The solid black line joining the acetone vertex with the ethanol/water azeotrope is the distillation boundary that divides the ternary composition space into two distinct regions. The distillation boundary can be compared to the binodal curve for liquid extraction; they divide the ternary composition space into subregions and influence the equilibration paths. For an equilibrium (EQ) stage column, any feed mixture with composition in the left-triangular region will yield an acetone-rich distillate and ethanol-rich bottoms product. Any feed mixture with composition in the right-triangular region will yield an acetone-rich distillate and a water-rich bottoms product. As argued by Levy et al.,[45] the column composition trajectories calculated by an EQ stage model cannot cross the straight-line boundary in Figure 9a.

The blue circles in Figure 9b represent the experimental data of Springer et al.[46−49] for compositions measured in a bubble-cap tray column operating at total reflux, that implies $x_i = y_i$. The condenser composition is left of the distillation boundary. Therefore, the RCM dictates that the reboiler composition should be in the top left corner, richer in ethanol. The measurement data show that the reboiler composition is toward the right of the distillation boundary, and is richer in water. The experimentally determined Murphree point efficiencies are plotted in Figure 9c; on stage 2 just below the total condenser

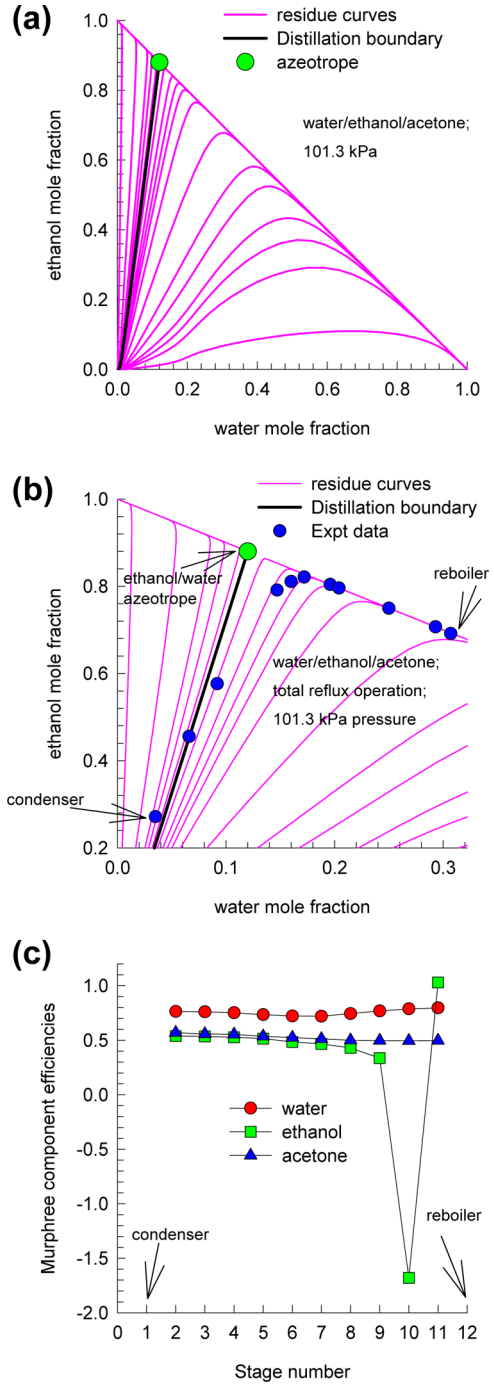

Figure 9. (a) Residue curve maps for distillation of water(1)/ethanol(2)/acetone(3) mixtures. (b) Blue circles represent the experimental data for T2−26 of Springer et al.[46−49] for composition trajectories in a bubble-cap tray column operating at total reflux implying $x_i = y_i$. (c) Experimentally determined Murphree component efficiencies in the 12-stage bubble cap column: stage 1 = total condenser; stage 12 = partial reboiler.

DOI: 10.1021/acs.iecr.5b04236
Ind. Eng. Chem. Res. 2016, 55, 1053−1063

where boundary crossing is experienced, we note the hierarchy of point efficiencies is $E_1 > E_2 \approx E_3$.

We aim to demonstrate that the phenomena of boundary crossing can be rationalized using the same set of equations that describe the equilibration trajectories for liquid extraction; the interphase mass transfer between rising vapor bubbles and the liquid phase on a tray is analogous to that sketched in Figure 4. For the vapor phase in distillation, the matrix of thermodynamic factor $[\Gamma]$ degenerates to the identity matrix, i.e. $\Gamma_{ij} = \delta_{ij}$; any diffusional coupling effects must therefore originate from differences in the MS diffusivities of the three binary pairs $Đ_{12}$, $Đ_{13}$, and $Đ_{23}$ in the vapor phase.

Consider a tray in the column for which the entering vapor composition is $y_{10} = 0.067$, $y_{20} = 0.44$, and $y_{30} = 0.493$ (cf. Figure 10a). This composition corresponds to that of stage 2 that experiences boundary crossing in the Springer experiments. For total reflux operations, the compositions of the liquid leaving that stage will be equal to that of the vapor entering the stage, i.e. $x_1 = 0.067$, $x_2 = 0.44$, and $x_3 = 0.493$. The composition of vapor in equilibrium with the liquid leaving the tray can be determined: $y_{1,eq} = 0.04335$, $y_{2,eq} = 0.25907$, and $y_{3,eq} = 0.69758$. The equilibrated vapor composition is also right of the distillation boundary. Use of the uncoupled flux eqs 7 will result in a linear equilibration trajectory that is parallel to the distillation boundary, remaining within the right-triangular region.

The values of the vapor phase MS diffusivities of the three binary pairs, calculated using the Fuller–Schettler–Giddings[50] method, are $Đ_{12} = 1.97$; $Đ_{13} = 1.71$; $Đ_{23} = 0.851 \times 10^{-5}$ m^2 s^{-1}; these diffusivities are independent of composition. At the average composition between the entering vapor compositions and the equilibrated compositions, use of eqs 5 and 6 yields $[D] = \begin{bmatrix} 1.79675 & -0.0067 \\ -0.36845 & 0.87989 \end{bmatrix} \times 10^{-5}$ m^2 s^{-1} in which D_{21} is seen to non-negligible in comparison with D_{22}. The driving forces are $\Delta y_1 = y_{10} - y_{1,eq} = 0.02365$, and $\Delta y_2 = y_{1o} - y_{2,eq} = 0.18093$. Both driving forces are positive, i.e. directed from vapor to the liquid phase.

Assuming that the vapor phase is dispersed in the form of spherical rigid bubbles (of diameter d_{bubble}) the diffusion equilibration trajectory, calculated using the Geddes equation, eq 13, is shown in Figure 10a. The curvilinear equilibration trajectory crosses the distillation boundary during a portion of its trajectory. The contact time of the vapor bubble with the liquid phase is finite. For a 4.5 mm bubble, with a rise velocity of 0.2 m s^{-1} in a froth dispersion of height 9.2 mm, the contact time $t = 0.046$ s; these input parameters are those reported by Springer et al.[47] and are representative values for their experiments. For a contact time $t = 0.046$ s, the composition of the vapor bubble leaving the tray is $y_1 = 0.0465$, $y_2 = 0.3118$, and $y_3 = 0.64175$; this vapor composition is on the left side of the distillation boundary. The hierarchy of the calculated point efficiencies $E_1 > E_2 \approx E_3$ (cf. Figure 10b) is in agreement with the experimentally determined values for stage 2 (cf. Figure 9c). The Murphree point efficiency of ethanol is the lower than that of water largely because of the negative contribution of the term $D_{21}\Delta y_1$. Consequently, a larger amount of water is transferred to the liquid phase than predicted by the uncoupled eq 7; i.e. the vapor phase is poorer in water, i.e. to the left of the distillation boundary. Put another way, the differences in the component efficiencies cause boundary crossing.

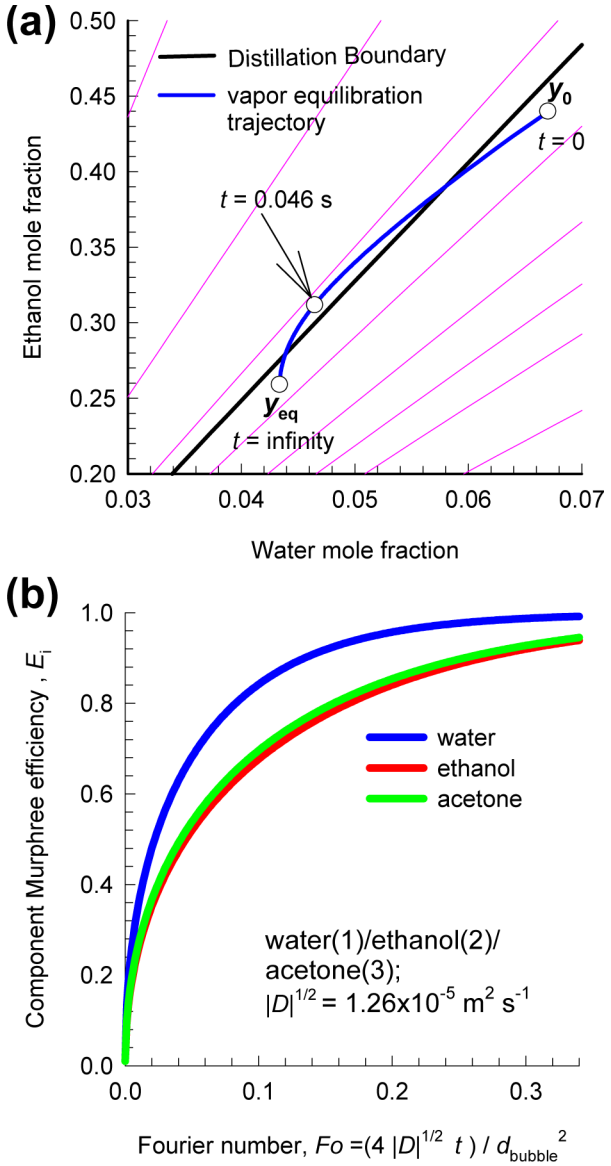

Figure 10. (a) Transient vapor equilibration trajectory obtained for initial mole fractions in the rigid spherical vapor bubble $y_{10} = 0.067$, $y_{20} = 0.44$, and $y_{30} = 0.493$. The final equilibrium compositions are $y_{1,eq} = 0.04335$, $y_{2,eq} = 0.25907$, and $y_{3,eq} = 0.69758$. (b) Plot of the component Murphree efficiencies, E_i, as a function of the Fourier number. All simulation details are provided in the Supporting Information.

The inclusion of the liquid phase resistance using the surface renewal model (cf. Figure 4) has a negligible influence on the equilibration trajectory, and boundary crossing is maintained; the detailed calculations verifying this conclusion are provided in the Supporting Information.

Analogous boundary crossing phenomena have been reported by Springer et al.[46−49] for water/ethanol/methanol and water/ethanol/methyl-acetate mixtures; see Figure 11a, and b. For each of these mixtures, we simulated the vapor equilibration trajectory for one tray that is close to the distillation boundary, lying on the right-hand side; the simulated results are shown Figure 11c, and d. For both systems, the vapor composition leaving the tray crosses the boundary and at the contact time $t = 0.046$ s, lies on the left-hand side of the boundary.

DOI: 10.1021/acs.iecr.5b04236
Ind. Eng. Chem. Res. 2016, 55, 1053−1063

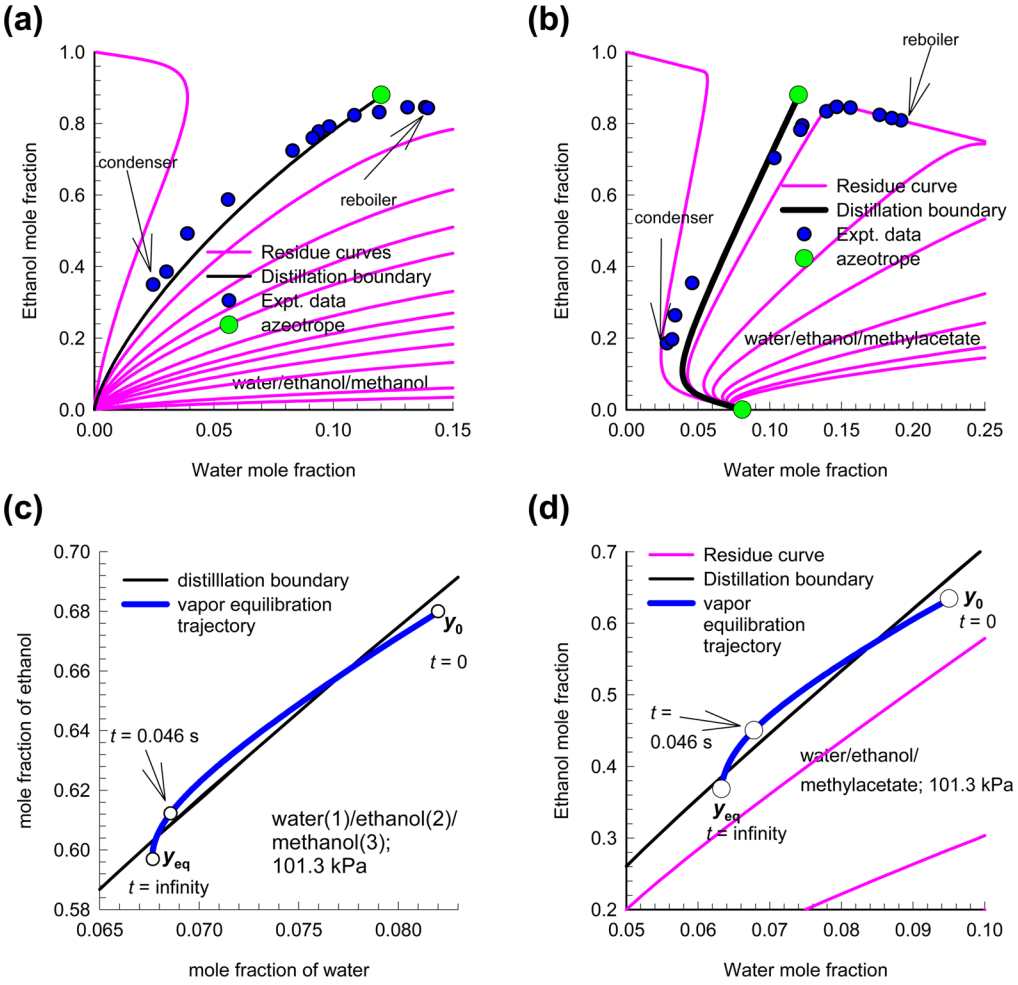

Figure 11. (a) Experimental data (run T4−13) on composition trajectories for water/ethanol/methanol.[46−49] (b) Experimental data (run T3−23) on composition trajectories for water/ethanol/methyl-acetate.[46−49] (c) Transient vapor equilibration trajectory for the system water/ethanol/methanol obtained for initial mole fractions in the rigid spherical vapor bubble y_{10} = 0.082, y_{20} = 0.68, and y_{30} = 0.238. The final equilibrium compositions are $y_{1,eq}$ = 0.06767, $y_{2,eq}$ = 0.59691, and $y_{3,eq}$ = 0.33542. (d) Transient vapor equilibration trajectory obtained for the system water/ethanol/methyl-acetate for initial mole fractions in the rigid spherical vapor bubble: y_{10} = 0.095, y_{20} = 0.6345, and y_{30} = 0.2705. The final equilibrium compositions are $y_{1,eq}$ = 0.06324, $y_{2,eq}$ = 0.36863, and $y_{3,eq}$ = 0.56813. All simulation details are provided in the Supporting Information.

For heterogeneous azeotropic distillation, experimental data on column composition trajectories for water/acetone/toluene (see TOC graphic), and water/ethanol/cyclohexane show boundary crossing characteristics that are also attributable to diffusional coupling effects;[51] see Figures S40−S42.

In a complementary analysis, Taylor et al.[52] have analyzed the mass transfer effects in ternary distillation to define the "non-equilibrium distillation boundaries" that cannot be crossed in actual column operation.

Diffusional coupling effects can be exploited to separate 2-propanol/water, ethanol/water, and acetone/methanol mixtures of azeotropic composition by distillation in the presence of an inert gas such as nitrogen, argon, or helium.[53,54] The Geddes model can be used to demonstrate the separation principle of diffusional distillation; see Figures S45−S48.

4. CONCLUSIONS

The following major conclusions can be drawn from the investigations reported in this work.

(1) In partially miscible liquid mixtures, diffusional coupling effects become increasingly significant as the compositions approach regions in which phase splitting occurs. The coupling effects originate predominantly from the matrix of thermodynamic factors, [Γ]. Strongly coupled diffusion is the norm, rather than the exception, in liquid extraction. The Fick diffusivity matrix can be estimated by multiplying [Γ] with a scalar diffusivity $|\Lambda|^{1/2}$.

(2) For all the 13 ternary partially miscible liquid mixtures that were investigated, the transient equilibration process follows curvilinear trajectories. In all cases, the Murphree component efficiencies are significantly different from one another. In ternary composition space, the curvature of the trajectory has a concave shape in relation to the vertex of the component with the lowest efficiency. Differences in Murphree component leave strong imprints on the separation performance.

(3) The experimentally observed curvilinear diffusion equilibration trajectories for glycerol/acetone/water mixtures can be reproduced accurately using estimates of the Fick diffusivity matrix in both glycerol-rich and acetone-rich phases by combining eq 12 with eq 21.

(4) The model used to calculate the transient equilibration trajectory for liquid extraction applies equally well to ternary azeotropic distillation. Diffusional coupling

DOI: 10.1021/acs.iecr.5b04236
Ind. Eng. Chem. Res. 2016, 55, 1053−1063

effects cause the crossing of distillation boundaries; such boundary crossings are not realized by the use of the uncoupled flux eqs 7.

The focus in this article has been on equilibration on a single stage in extraction and distillation columns. A few studies have demonstrated that the inclusion of diffusional coupling effects has a significant influence on the number of stages required to reach the desired level of purity in distillation columns (see Figures S36–S37);[55,56] similar studies are warranted for extraction column design. A further point to note is that axial mixing effects need to be additionally accounted for in models for RDC and packed extraction columns.

■ ASSOCIATED CONTENT

Supporting Information

The Supporting Information is available free of charge on the ACS Publications website at DOI: 10.1021/acs.iecr.5b04236.

Background information on liquid extraction and distillation processes, additional modeling details, input data on diffusivities, and tabulated data on the NRTL and UNIQUAC parameters required for the determination of phase equilibrium thermodynamics, along with detailed calculation results for all systems investigated (PDF)

■ AUTHOR INFORMATION

Corresponding Author

*E-mail: r.krishna@contact.uva.nl.

Notes

The authors declare no competing financial interest.

■ ACKNOWLEDGMENTS

Dr. J. M. van Baten is gratefully acknowledged for providing the code for calculation of the binodal curve.

■ NOTATION

A_m = constant in Kronig–Brink model, dimensionless
c_t = total molar concentration of mixture, mol m^{-3}
d_{bubble} = bubble diameter, m
d_{drop} = droplet diameter, m
$Đ_{ij}$ = MS binary pair diffusivity, m^2 s^{-1}
$[D]$ = Fick diffusivity matrix, m^2 s^{-1}
$|D|$ = determinant of the Fick diffusivity matrix, m^4 s^{-2}
$|D|^{1/2}$ = square-root of determinant of $[D]$, m^2 s^{-1}
E_i = component Murphree efficiency, dimensionless
Fo = Fourier number, dimensionless
$[I]$ = identity matrix, dimensionless
J_i = molar diffusion flux of species i with respect to u, mol m^{-2} s^{-1}
$[k]$ = matrix of mass transfer coefficients, m s^{-1}
$[K]$ = matrix of overall mass transfer coefficients, m s^{-1}
p = system pressure, Pa
$[Q]$ = matrix quantifying fractional departure from equilibrium, dimensionless
R = gas constant, 8.314 J mol^{-1} K^{-1}
t = time, s
T = absolute temperature, K
x_i = mole fraction of component i in liquid phase, dimensionless
y_i = mole fraction of component i in vapor phase, dimensionless
u = molar average mixture velocity, m s^{-1}
V_{drop} = droplet rise velocity, m s^{-1}
z = direction coordinate, m

Greek Letters

β = constant used for equilibration in Lewis stirred cell, m^{-2}
δ_{ij} = Kronecker delta, dimensionless
γ_i = activity coefficient of component i, dimensionless
$[\Gamma]$ = matrix of thermodynamic factors, dimensionless
$|\Gamma|^{1/2}$ = square-root of determinant of $[\Gamma]$, dimensionless
λ_m = constant in Kronig–Brink model, dimensionless
$[\Lambda]$ = matrix defined by eq 6, m^2 s^{-1}
$|\Lambda|^{1/2}$ = square-root of determinant of $[\Lambda]$, m^2 s^{-1}
μ_i = molar chemical potential, J mol^{-1}

Subscript

0 = referring to starting compositions, $t = 0$
bubble = referring to bubble
c = referring to continuous phase
d = referring to dispersed phase
drop = referring to droplet
eq = referring to final equilibrated compositions, $t \to \infty$
i = component number
j = component number
O = referring to overall parameter
renewal = referring to surface renewal

■ REFERENCES

(1) Lewis, W. K. The principles of countercurrent extraction. *J. Ind. Eng. Chem.* **1916**, *8*, 825–833.
(2) Seader, J. D.; Henley, E. J.; Roper, D. K. *Separation Process Principles*, 3rd ed.; John Wiley: New York, 2011.
(3) Treybal, R. E. *Mass-Transfer Operations*, 3rd ed.; McGraw-Hill: New York, 1980.
(4) Robbins, L. A.; Cusack, R. W. Chaper 15, Liquid-Liquid Extraction Operations and Equipment. *Perry's Chemical Engineers' Handbook*, 7th ed.; Perry, R. H., Green, D.W., Eds.; McGraw-Hill: New York, 1999.
(5) Wankat, P. C. *Separation Process Engineering*, 3rd ed.; Prentice-Hall: Upper Saddle River, NJ, 2012.
(6) Sherwood, T. K.; Pigford, R. L.; Wilke, C. R. *Mass Transfer*; McGraw Hill: New York, USA, 1975.
(7) Bart, H.-J. *Reactive Extraction*; Springer-Verlag: Berlin, 2001.
(8) Meindersma, G. W.; de Haan, A. Conceptual process design for aromatic/aliphatic separation with ionic liquids. *Chem. Eng. Res. Des.* **2008**, *86*, 745–752.
(9) Meindersma, G. W. Extraction of Aromatics from Naphtha with Ionic Liquids. Ph.D. Dissertation, University of Twente, The Nethelands, Enschede, 2005.
(10) Rodriguez, N. R.; Requejo, P. F.; Kroon, M. C. Aliphatic-aromatic separation using deep eutectic solvents as extracting agents. *Ind. Eng. Chem. Res.* **2015**, *54*, 11404–11412.
(11) Krishna, R.; Goswami, A. N.; Nanoti, S. M.; Rawat, B. S.; Khanna, M. K.; Dobhal, J. Extraction of aromatics from 63–69 °C Naphtha fraction for food grade hexane production using sulpholane and NMP as solvents. *Ind. J. Technol.* **1987**, *25*, 602–606.
(12) Al-Jimaz, A. S.; Fandary, M. S.; Al-Kandary, J. A.; Fahim, M. A. Liquid–liquid equilibria for n-alkanes (C12, C14,C17) + propylbenzene + NMP mixtures at temperatures between 298 and 328K. *Fluid Phase Equilib.* **2005**, *231*, 163–170.
(13) Kooijman, H. A.; Taylor, R. *The ChemSep Book*, 2nd ed.; ChemSep, 2006; www.chemsep.com.
(14) Lao, M. Z.; Kingsley, J. P.; Krishnamurthy, R.; Taylor, R. A Nonequilibrium Stage Model of Multicomponent Separation Processes 0.6. Simulation of Liquid Liquid Extraction. *Chem. Eng. Commun.* **1989**, *86*, 73–89.
(15) Krishna, R. Uphill Diffusion in Multicomponent Mixtures. *Chem. Soc. Rev.* **2015**, *44*, 2812–2836.

DOI: 10.1021/acs.iecr.5b04236
Ind. Eng. Chem. Res. 2016, 55, 1053–1063

(16) Taylor, R.; Krishna, R. *Multicomponent mass transfer*; John Wiley: New York, 1993.
(17) Krishna, R. Serpentine Diffusion Trajectories and the Ouzo Effect in Partially Miscible Ternary Liquid Mixtures. *Phys. Chem. Chem. Phys.* **2015**, *17*, 27428−27436.
(18) Sandler, S. I. *Chemical, Biochemical, and Engineering Thermodynamics*, 3rd ed.; John Wiley: New York, 1999.
(19) Grossmann, T.; Winkelmann, J. Ternary Diffusion Coefficients of Glycerol + Acetone + Water by Taylor Dispersion Measurements at 298.15 K. *J. Chem. Eng. Data* **2005**, *50*, 1396−1403.
(20) Grossmann, T.; Winkelmann, J. Ternary Diffusion Coefficients of Glycerol + Acetone + Water by Taylor Dispersion Measurements at 298.15 K. 2. Acetone-Rich Region. *J. Chem. Eng. Data* **2007**, *52*, 336−340.
(21) Grossmann, T.; Winkelmann, J. Ternary Diffusion Coefficients of Glycerol + Acetone + Water by Taylor Dispersion Measurements at 298.15 K. 3. Water-Rich Region. *J. Chem. Eng. Data* **2007**, *52*, 341−344.
(22) Vitagliano, V.; Sartorio, R.; Scala, S.; Spaduzzi, D. Diffusion in a Ternary System and the Critical Mixing Point. *J. Solution Chem.* **1978**, *7*, 605−621.
(23) Buzatu, D.; Buzatu, F. D.; Paduano, L.; Sartorio, R. Diffusion Coefficients for the Ternary System Water + Chloroform + Acetic Acid at 25 °C. *J. Solution Chem.* **2007**, *36*, 1373−1384.
(24) Alimadadian, A.; Colver, C. P. A New Technique for the Measurement of Ternary Diffusion Coefficients in Liquid Systems. *Can. J. Chem. Eng.* **1976**, *54*, 208−213.
(25) Cullinan, H. T.; Toor, H. L. Diffusion in the Three-Component Liquid System: Acetone-Benzene Carbon Tetrachloride. *J. Phys. Chem.* **1965**, *69*, 3941−3949.
(26) Shuck, F. O.; Toor, H. L. Diffusion in the Three Component Liquid System Methyl Alcohol - n-Propyl Alchohol - Isobutyl alcohol. *J. Phys. Chem.* **1963**, *67*, 540−545.
(27) Rehfeldt, S.; Stichlmair, J. Measurement and prediction of multicomponent diffusion coefficients in four ternary liquid systems. *Fluid Phase Equilib.* **2010**, *290*, 1−14.
(28) Korchinsky, W. J.; Grassia, P.; Harrison, C. H. Multicomponent mass transfer in films and rigid drops: The influence of concentration-variable diffusivity. *Chem. Eng. Sci.* **2009**, *64*, 433−442.
(29) PTC MathCad 15.0. http://www.ptc.com/, Needham, November 2015.
(30) Krishna, R.; van Baten, J. M. The Darken relation for multicomponent diffusion in liquid mixtures of linear alkanes. An investigation using Molecular Dynamics (MD) simulations. *Ind. Eng. Chem. Res.* **2005**, *44*, 6939−6947.
(31) Krishna, R.; van Baten, J. M. Unified Maxwell-Stefan description of binary mixture diffusion in micro- and meso- porous materials. *Chem. Eng. Sci.* **2009**, *64*, 3159−3178.
(32) Reid, R. C.; Prausnitz, J. M.; Poling, B. E. *The Properties of Gases and Liquids*, 4th ed.; McGraw-Hill: New York, 1986.
(33) Geddes, R. L. Local efficiencies of bubble-plate fractionators. *Trans. Am. Inst. Chem. Engrs.* **1946**, *42*, 79−105.
(34) Krishna, R. Model for prediction of point efficiencies for multicomponent distillation. *Chem. Eng. Res. Des. Trans. I. Chem. E* **1985**, *63*, 312−322.
(35) Murphree, E. V. Graphical rectifying column calculations. *Ind. Eng. Chem.* **1925**, *17*, 960−964.
(36) Murphree, E. V. Rectifying column calculations with particular reference to n-component mixtures. *Ind. Eng. Chem.* **1925**, *17*, 747−750.
(37) Cussler, E. L. *Diffusion: Mass Transfer in Fluid Systems*, 3rd ed.; Cambridge University Press: Cambridge, 2007.
(38) Sun, Y.; Zhao, Q.; Zhang, L.; Jiang, B. Measurement and Correlation of the Mass-Transfer Coefficient for the Methyl Isobutyl Ketone−Water−Phenol System. *Ind. Eng. Chem. Res.* **2014**, *53*, 3654−3661.
(39) Kronig, R.; Brink, J. C. On the Theory of Extraction from Falling Droplets. *Appl. Sci. Res.* **1951**, *2*, 142−154.
(40) Sideman, S.; Shabtai, H. Direct-Contact Heat Transfer Between a Single Drop and an Immiscible Liquid Medium. *Can. J. Chem. Eng.* **1964**, *42*, 107−116.
(41) Krishna, R.; Low, C. Y.; Newsham, D. M. T.; Olivera-Fuentes, C. G.; Standart, G. L. Ternary mass transfer in liquid-liquid extraction. *Chem. Eng. Sci.* **1985**, *40*, 893−903.
(42) Krishna, R.; Low, C. Y.; Newsham, D. M. T.; Olivera Fuentes, C. G.; Paybarah, A. Liquid Liquid Equilibrium in the System Glycerol Water Acetone at 25 °C. *Fluid Phase Equilib.* **1989**, *45*, 115−120.
(43) De Villiers, W. E.; French, R. N.; Koplos, G. J. Navigate Phase Equilibria via Residue Curve Maps. *Chem. Eng. Prog.* **2002**, *98* (11), 66−71.
(44) Doherty, M. F.; Malone, M. F. *Conceptual Design of Distillation Systems*; McGraw-Hill: New York, 2001.
(45) Levy, S. G.; Van Dongen, D. B.; Doherty, M. F. Design and synthesis of homogeneous azeotropic distillation. 2. Minimum reflux calculations for nonideal and azeotropic columns. *Ind. Eng. Chem. Fundam.* **1985**, *24*, 463−474.
(46) Springer, P. A. M.; Baur, R.; Krishna, R. Influence of interphase mass transfer on the composition trajectories and crossing of boundaries in ternary azeotropic distillation. *Sep. Purif. Technol.* **2002**, *29*, 1−13.
(47) Springer, P. A. M.; Buttinger, B.; Baur, R.; Krishna, R. Crossing of the distillation boundary in homogeneous azeotropic distillation: Influence of interphase mass transfer. *Ind. Eng. Chem. Res.* **2002**, *41*, 1621−1631.
(48) Springer, P. A. M.; van der Molen, S.; Baur, R.; Krishna, R. Experimental verification of the necessity to use the Maxwell-Stefan formulation in describing trajectories during azeotropic distillation. *Chem. Eng. Res. Des.* **2002**, *80*, 654−666.
(49) Springer, P. A. M.; van der Molen, S.; Krishna, R. The need for using rigorous rate-based models for simulations of ternary azeotropic distillation. *Comput. Chem. Eng.* **2002**, *26*, 1265−1279.
(50) Fuller, E. N.; Schettler, P. D.; Giddings, J. C. A new method for prediction of binary gas-phase diffusion coefficients. *Ind. Eng. Chem.* **1966**, *58*, 18−27.
(51) Springer, P. A. M.; Baur, R.; Krishna, R. Composition trajectories for heterogeneous azeotropic distillation in a bubble-cap tray column: Influence of mass transfer. *Chem. Eng. Res. Des.* **2003**, *81*, 413−426.
(52) Baur, R.; Krishna, R.; Taylor, R. Influence of Mass Transfer in Distillation: Feasibility and Design. *AIChE J.* **2005**, *51*, 854−866.
(53) Fullarton, D.; Schlünder, E. U. Diffusion Distillation - A New Separation.Process for Azeotropic Mixtures - Part I: Selectivity and Transfer Efficiency. *Chem. Eng. Process.* **1986**, *20*, 255−263.
(54) Singh, N.; Prasad, R. Experimental studies on the effect of inert gases on diffusion distillation of ethanol−water mixtures. *J. Chem. Technol. Biotechnol.* **2011**, *86*, 1495−1500.
(55) Taylor, R.; Krishna, R.; Kooijman, H. Real-World Modeling of Distillation. *Chem. Eng. Prog.* **2003**, *99* (7), 28−39.
(56) Krishnamurthy, R.; Taylor, R. A nonequilibrium stage model of multicomponent separation processes. Part III: the influence of unequal component efficiencies in process design problems. *AIChE J.* **1985**, *31*, 1973−1985.

DOI: 10.1021/acs.iecr.5b04236
Ind. Eng. Chem. Res. 2016, 55, 1053−1063

Supplementary Information (SI) to accompany:

Highlighting Diffusional Coupling Effects in Ternary Liquid Extraction and Comparisons with Distillation

Rajamani Krishna

Van 't Hoff Institute for Molecular Sciences, University of Amsterdam, Science Park 904,

1098 XH Amsterdam, The Netherlands

email: r.krishna@contact.uva.nl

Table of Contents

1. Preamble 3
2. Transient equilibration in heptane(1)/toluene(2)/sulpholane(3) mixtures 3
3. Transient equilibration in NMP(1)/propylbenzene(2)/tetradecane(3) 12
4. Transient equilibration in glycerol(1)/acetone(2)/water(3) 12
5. Transient equilibration in water(1)/acetone(1)/ethyl-acetate(3) 13
6. Transient equilibration in water(1)/caprolactam(2)/toluene(3) 14
7. Transient equilibration in water(1)/acetic acid(2)/isophorone(3) 14
8. Transient equilibration in water(1)/acetic acid(2)/MTBE(3) 15
9. Transient equilibration in [omim][Cl](1)/ethanol(2)/TAEE(3) 15
10. Transient equilibration in [bmim][TfO](1)/ethanol(2)/TAEE(3) 16
11. Transient equilibration in water(1)/ethanol(2)/cyclohexane(3) 17
12. Transient equilibration in toluene(1)/ethanol(2)/water(3) 17
13. Transient equilibration in water(1)/acetone(2)/toluene(3) 18
14. Springer experiments for boundary crossing in homogeneous azeotropic distillation 18
15. Transient equilibration inside vapor bubble rising through a liquid on a distillation tray 22
16. Boundary crossing in water/ethanol/acetone mixture 25
17. NEQ vs EQ models for design of column to separate water/ethanol/acetone mixtures 31
18. Boundary crossing in water/ethanol/methanol mixture 33
19. Boundary crossing in water/ethanol/methylacetate mixture 38
20. Boundary crossing in heterogeneous azeotropic distillation 43
21. Separating azeotropic alcohol/water mixture by diffusional distillation 44
22. Notation 51
23. References 65
24. Caption for Figures 68

1. Preamble

This Supporting Information (SI) accompanying the manuscript *Highlighting Diffusional Coupling Effects in Ternary Liquid Extraction and Comparisons with Distillation* provides background information on liquid extraction and distillation processes, additional modelling details, input data on diffusivities, tabulated data on the NRTL and UNIQUAC parameters required for the determination of phase equilibrium thermodynamics, along with detailed simulation results (in graphical form) for all systems investigated.

All calculations of Geddes diffusion trajectories, mass transfer coefficients, and efficiencies that are reported in this article involve explicit analytic formulae that were implemented in MathCad 15.[1] The calculation details are provided herein, in the event the interested reader would like to reproduce our calculations. For ease of reading, this SI is written with some overlap of material with the main manuscript.

2. Transient equilibration in heptane(1)/toluene(2)/sulpholane(3) mixtures

Figure 1 is a schematic showing a variety of applications of liquid extraction processes in petroleum refining. Most of these applications involve the separation of aromatics from hydrocarbon mixtures, for example for production of food grade hexane,[2] improving the smoke point of kerosene, and flow properties of lube oils. There are also other applications in the petrochemical industries.[3]

The contactors used in industry are either agitated, or un-agitated columns; see Figure 2.

Figure 3 is a schematic of single-stage contacting in sieve-tray column. This principle also applies to other stage-wise operations. On a given stage, the continuous liquid phase can be considered to be well-mixed; this is a reasonably good approximation.

For a ternary mixture, the diffusion in either continuous or dispersed phase is described by the generalized Fick's law

$$(J) = -c_t [D] \frac{d(x)}{dz} \tag{1}$$

in which the two-dimensional matrix of Fick diffusivities [D] is a product of two matrices

$$[D] = [\Lambda][\Gamma] \tag{2}$$

The 2 × 2 matrix of thermodynamic factors $[\Gamma]$

$$\frac{x_i}{RT}\frac{d\mu_i}{dz} = \sum_{j=1}^{2}\Gamma_{ij}\frac{dx_j}{dz}; \quad \Gamma_{ij} = \delta_{ij} + x_i\frac{\partial \ln \gamma_i}{\partial x_j}; \quad i,j = 1,2 \tag{3}$$

can be calculated from UNIQUAC or NRTL models describing phase equilibrium thermodynamics.[4, 5]

The matrix $[\Lambda]$ to be expressed explicitly in terms of the M-S diffusivities of the constituent binary pairs in the ternary mixture:

$$\begin{bmatrix} \Lambda_{11} & \Lambda_{12} \\ \Lambda_{21} & \Lambda_{22} \end{bmatrix} = \frac{\begin{bmatrix} Đ_{13}\left(x_1 Đ_{23} + (1-x_1)Đ_{12}\right) & x_1 Đ_{23}\left(Đ_{13} - Đ_{12}\right) \\ x_2 Đ_{13}\left(Đ_{23} - Đ_{12}\right) & Đ_{23}\left(x_2 Đ_{13} + (1-x_2)Đ_{12}\right) \end{bmatrix}}{x_1 Đ_{23} + x_2 Đ_{13} + x_3 Đ_{12}} \tag{4}$$

For partially miscible ternary mixtures, the coupling effects in the Fick matrix are primarily due to the thermodynamic factors; this has been demonstrated in earlier work.[6] For all the simulations presented in this article, we use the following, simplified expression for the calculation of the Fick matrix

$$[D] = |\Lambda|^{1/2}[\Gamma]$$

with the scalar diffusivity $|\Lambda|^{1/2}$ calculated from

$$|\Lambda|^{1/2} = \sqrt{\frac{Đ_{12}Đ_{13}Đ_{23}}{x_1 Đ_{23} + x_2 Đ_{13} + x_3 Đ_{12}}}$$

Let us consider the dispersion to consist of uniform and rigid droplets of diameter, d_{drop}. The transient equilibration process within a rigid spherical droplet is described by Geddes model that was originally developed for describing binary diffusion inside vapor bubbles on distillation trays.[7] For ternary mixtures, the Geddes model can be written in two-dimensional matrix differential equation[4]

$$\left(x - x_{eq}\right) = [Q]\left(x_0 - x_{eq}\right); \quad [Q] \equiv \frac{6}{\pi^2}\sum_{m=1}^{\infty}\frac{1}{m^2}\exp\left[-m^2\pi^2\frac{4[D]t}{d_{drop}^2}\right] \tag{5}$$

The Sylvester theorem, detailed in Appendix A of Taylor and Krishna,[4] is required for explicit calculation of the composition trajectories described by Equation (5). For extraction equipment such as a sieve tray or rotating disc contactors, the effective contact time of the dispersed phase droplets with the surrounding continuous phase is $t = h_f / V_{drop}$, where h_f is the liquid/liquid dispersion height, and V_{drop} is the droplet rise velocity.[8]

The fractional approaches to equilibrium for contact time *t*, also termed as the Murphree efficiencies,[3, 9, 10] are calculated from

$$\begin{aligned} E_1 &= \frac{x_{10} - x_1}{x_{10} - x_{1eq}} = 1 - Q_{11} - Q_{12}\frac{\Delta x_2}{\Delta x_1}; \\ E_2 &= \frac{x_{20} - x_2}{x_{20} - x_{2eq}} = 1 - Q_{22} - Q_{21}\frac{\Delta x_1}{\Delta x_2}; \\ E_3 &= \frac{x_{30} - x_3}{x_{30} - x_{3eq}} = \frac{\frac{\Delta x_1}{\Delta x_2}E_1 + E_2}{\frac{\Delta x_1}{\Delta x_2} + 1} \end{aligned} \tag{6}$$

Let us define a two-dimensional matrix of mass transfer coefficients, $[k]$, defined by

$$(J) = c_t[k]\left(x - x_{eq}\right) \tag{7}$$

The matrix of Sherwood numbers $[Sh]$

$$[Sh_t] = [k]d_{drop}[D]^{-1} \tag{8}$$

can be calculated as a function of the contact time using the following expression[4]

$$[Sh_t] = \frac{2}{3}\pi^2\left[\sum_{m=1}^{\infty}\exp\left[-m^2\pi^2\frac{4[D]t}{d_{drop}^2}\right]\right]\left[\frac{6}{\pi^2}\sum_{m=1}^{\infty}\frac{1}{m^2}\exp\left[-m^2\pi^2\frac{4[D]t}{d_{drop}^2}\right]\right]^{-1} \tag{9}$$

In the limit $t \to \infty$, an asymptotic value is reached

$$[Sh_t] = \frac{2\pi^2}{3} = 6.58 \tag{10}$$

It must be emphasized that Equation (9), is the value of the matrix at any time *t*, and not the time-averaged value. The time-averaged Sherwood number, $[Sh]$, for the interval 0 – *t*, is given by the expression

$$[Sh] = -\frac{2}{3}\ln[[Q]][D]^{-1}\frac{d_{drop}^2}{4t} \tag{11}$$

In the limit $t \to \infty$, an asymptotic value is also reached for the time-averaged Sherwood number

$$[Sh] = \frac{2\pi^2}{3} = 6.58 \tag{12}$$

The corresponding time-averaged matrix of mass transfer coefficients in the dispersed phase is

$$[k_d] = \frac{[Sh][D]}{d_{drop}} = -\frac{2}{3}\ln[[Q]][D]^{-1}\frac{d_{drop}^2}{4t}\frac{[D]}{d_{drop}} = -\ln[[Q]]\frac{d_{drop}}{6t} \tag{13}$$

In this asymptotic limit $t \to \infty$, the coupling effects of $[k]$ are directly proportional to those of the Fick matrix $[D]$.

Let us denote the interfacial area per unit volume of drop as

$$a = \frac{6}{d_{drop}} \tag{14}$$

With this definition, the time-averaged matrix of mass transfer coefficients is

$$[k_d] = -\ln[[Q]]\frac{1}{at} \tag{15}$$

In chemical engineering practice, it is conventional to define the number of transfer units for the dispersed phase as

$$[NTU_d] = [k_d]at = -\ln[[Q]] \tag{16}$$

Therefore an alternative expression for the fractional departure from equilibrium is

$$[Q] = \exp[-NTU_d] = \exp[-[k_d]at] \tag{17}$$

Let us examine the diffusion equilibration trajectories for heptane(1)/toluene(2)/sulpholane(3) mixtures at 348.2 K. Please note that in the SI we use the English spelling of sulpholane. The US spelling is sulfolane, as used in the main manuscript. In particular, we examine the trajectory followed as droplets containing pure sulpholane (composition: x_{10} = 0.0, x_{20} = 0.0, and x_{30} = 1.0) equilibrates to the equilibrium composition E, at the tie-line indicated in Figure 4: $x_{1,eq}$ = 0.062684992, $x_{2,eq}$ = 0.406432625, and $x_{3,eq}$ = 0.53088.

The first task is to estimate the M-S diffusivities if the three binary pairs $Đ_{12}$, $Đ_{13}$, and $Đ_{23}$ using the following interpolation formulation[11]

$$Đ_{ij} = \left(Đ_{ij}^{x_i \to 1}\right)^{x_i} \left(Đ_{ij}^{x_j \to 1}\right)^{x_j} \left(Đ_{ij}^{x_k \to 1}\right)^{x_k} \tag{18}$$

The six infinite dilution values of the pair diffusivities $Đ_{ij}^{x_j \to 1}$ are estimated the Wilke-Chang correlation.[12] For estimation of $Đ_{ij}^{x_k \to 1}$, the *i* - *j* pair diffusivity when both *i* and *j* are present in infinitely dilute concentrations, the following formula has been suggested[11]

$$Đ_{ij}^{x_k \to 1} = \left(Đ_{ik}^{x_k \to 1}\right)^{x_i/(x_i+x_j)} \left(Đ_{jk}^{x_k \to 1}\right)^{x_j/(x_i+x_j)} \tag{19}$$

At the arithmetic average composition between S and E, we calculate the following values of the M-S diffusivities of the binary pairs

$$Đ_{12} = 0.94; \quad Đ_{13} = 0.82; \quad Đ_{23} = 0.96 \times 10^{-9} \text{ m}^2\text{s}^{-1}$$

The value of the scalar diffusivity is

$$|\Lambda|^{1/2} = \sqrt{\frac{Đ_{12}Đ_{13}Đ_{23}}{x_1Đ_{23} + x_2Đ_{13} + x_3Đ_{12}}} = 0.9 \times 10^{-9} \text{ m}^2\text{s}^{-1}$$

The matrix of thermodynamic factors is determined from the NRTL parameters provided in Table 1.

$$[\Gamma] = \begin{bmatrix} 0.71695 & -0.16465 \\ -0.85701 & 0.81773 \end{bmatrix}$$

The Fick matrix is calculated as

$$[D] = |\Lambda|^{1/2}[\Gamma] = \begin{bmatrix} 0.643 & -0.148 \\ -0.769 & 0.733 \end{bmatrix} \times 10^{-9}$$

We can also determine a "magnitude" of the Fick diffusivity for use in the calculation of the Fourier number

$$|D|^{1/2} = 0.6 \times 10^{-9}$$

Let us assume that the droplet of 1 mm diameter rises at a velocity of 20 mm s^{-1} on a sieve tray with a dispersion height of 400 mm. The contact time, t = 20 s. For this set of input values, we calculate the following set of parameters:

Interfacial area per unit volume of droplet

$$a = \frac{6}{d_{drop}} = 6 \times 10^{3}$$

The matrix describing the departure from equilibrium is

$$[Q] = \begin{bmatrix} 0.4133 & 0.0527 \\ 0.2743 & 0.38105 \end{bmatrix}$$

The matrix for the number of transfer units for the dispersed phase

$$[NTU_d] = \begin{bmatrix} 0.93041 & -0.13707 \\ -0.713443 & 1.01431 \end{bmatrix}$$

The time-average matrix of mass transfer coefficients is

$$[k_d] = \begin{bmatrix} 7.75341 & -1.1422 \\ -5.94533 & 8.45255 \end{bmatrix} \times 10^{-6}$$

The component Murphree efficiencies are

$$E_1 = \frac{x_{10} - x_1}{x_{10} - x_{1eq}} = 1 - Q_{11} - Q_{12}\frac{\Delta x_2}{\Delta x_1} = 0.245$$

$$E_2 = \frac{x_{20} - x_2}{x_{20} - x_{2eq}} = 1 - Q_{22} - Q_{21}\frac{\Delta x_1}{\Delta x_2} = 0.577$$

$$E_3 = \frac{x_{30} - x_3}{x_{30} - x_{3eq}} = \frac{\frac{\Delta x_1}{\Delta x_2}E_1 + E_2}{\frac{\Delta x_1}{\Delta x_2} + 1} = 0.532$$

The toluene/heptane ratio in dispersed phase leaving the stage at contact time of 20 s can be calculated from

$$\left(x - x_{eq}\right) = [Q]\left(x_0 - x_{eq}\right); \quad [Q] = \exp[-[K_{od}]at]$$

The value is calculated as $\frac{0.23437}{0.01536} = 15.26$.

The Kronig-Brink[13] model that takes account of circulation within the droplet, leads to the following expression for the departure from equilibrium

$$\left(x - x_{eq}\right) = [Q]\left(x_0 - x_{eq}\right); \quad [Q] \equiv \frac{3}{8}\sum_{m=1}^{\infty} A_m^2 \exp\left[-16\lambda_m \frac{4[D]t}{d_{drop}^2}\right] \tag{20}$$

The values of A_m and λ_m are tabulated by Sideman and Shabtai;[14] see Table 2. Equation (20) predicts a more rapid equilibration than the rigid sphere model (5). In composition space, the diffusion equilibration trajectory calculated using equation (20) follows a curvilinear path that is practically indistinguishable from that predicted by the Geddes model for equilibration.

We now examine the influence of the resistance to interphase mass transfer offered by the continuous phase, i.e. the raffinate. Figure 27 presents a schematic of mass transfer resistances in liquid-liquid extraction.

All the calculations of the parameters for the raffinate phase are an average between the compositions HT (x_{10} = 0.25, x_{20} = 0.75, and x_{30} = 0.0) and the final equilibrium compositions of R ($x_{1,eq}$ = 0.258578176, $x_{2,eq}$ = 0.621464559, and $x_{3,eq}$ = 0.11996), as indicated in Figure 4.

At the arithmetic average composition between S and E, we calculate the M-S diffusivities of the binary pairs

$$Đ_{12} = 2.8; \quad Đ_{13} = 2.55; \quad Đ_{23} = 2.95\times10^{-9}\ \mathrm{m^2 s^{-1}}$$

The scalar diffusivity value is

$$|\Lambda|^{1/2} = \sqrt{\frac{Đ_{12}Đ_{13}Đ_{23}}{x_1Đ_{23} + x_2Đ_{13} + x_3Đ_{12}}} = 2.58\times10^{-9}\ \mathrm{m^2 s^{-1}}$$

The matrix of thermodynamic factors is calculated from the NRTL parameters

$$[\Gamma] = \begin{bmatrix} 0.46322 & -0.646785 \\ -0.017851 & 1.243143 \end{bmatrix}$$

The Fick matrix for the continuous (raffinate) phase is

$$[D] = |\Lambda|^{1/2}[\Gamma] = \begin{bmatrix} 1.19536 & -1.669058 \\ -0.04607 & 3.20799 \end{bmatrix} \times 10^{-9}$$

The magnitude of the Fick matrix is

$$|D|^{1/2} = 1.94 \times 10^{-9}$$

It is noticeable that all diffusivity values for the raffinate phase are higher than the corresponding ones for the extract phase; the primary reason is the lower concentration of sulpholane in the raffinate phase.

The mass transfer coefficient external to the droplet can be estimated from the surface renewal theory[15, 16]

$$[k_c] = 2\sqrt{\frac{[D_c]}{\pi t_{renewal}}} \tag{21}$$

The Fick matrix $[D_c]$ is evaluated using $[D_c] = |\Lambda_c|^{1/2}[\Gamma_c]$ at the average between the compositions of HT and R. The characteristic time for surface renewal can be estimated is $t_{renewal} = d_{drop}/V_{drop}$ = 0.05 s; this value is significantly lower than the time the droplet takes to rise through the dispersion, 20 s.

For a surface renewal time of 0.05 s, the mass transfer in the continuous phase can be estimated from the surface renewal theory

$$[k_c] = 2\sqrt{\frac{[D]}{\pi t_{renewal}}} = \begin{bmatrix} 173.79033 & -92.55819 \\ -2.55464 & 285.40194 \end{bmatrix} \times 10^{-6}$$

The overall mass transfer coefficient can be calculated

$$[K_{Od}]^{-1} = [k_d]^{-1} + \frac{c_{tL,d}}{c_{tL,c}} \begin{bmatrix} \frac{x_{1d,eq}}{x_{1c,eq}} & 0 \\ 0 & \frac{x_{2d,eq}}{x_{2c,eq}} \end{bmatrix} [k_c]^{-1}$$

Inserting the values of the partial mass transfer coefficients, we have for the overall mass transfer coefficients

$$[K_{Od}]^{-1} = \begin{bmatrix} 7.75341 & -1.1422 \\ -5.945333 & 8.45255 \end{bmatrix}^{-1} \times 10^6 + \frac{10132}{8981} \begin{bmatrix} \frac{0.062684992}{0.258578176} & 0 \\ 0 & \frac{0.406432625}{0.621464559} \end{bmatrix} \begin{bmatrix} 173.79033 & -92.55819 \\ -2.55464 & 285.40194 \end{bmatrix}^{-1} \times 10^6$$

$$[K_{Od}] = \begin{bmatrix} 7.66559 & -1.13673 \\ -5.76671 & 8.28557 \end{bmatrix} \times 10^{-6}$$

The matrix for the overall number of transfer units

$$[NTUO_d] = \begin{bmatrix} 0.91987 & -0.13641 \\ -0.69201 & 0.99427 \end{bmatrix}$$

The Murphree component efficiencies are

$$E_1 = \frac{x_{10} - x_1}{x_{10} - x_{1eq}} = 1 - Q_{11} - Q_{12} \frac{\Delta x_2}{\Delta x_1} = 0.23785$$

$$E_2 = \frac{x_{20} - x_2}{x_{20} - x_{2eq}} = 1 - Q_{22} - Q_{21} \frac{\Delta x_1}{\Delta x_2} = 0.57032$$

$$E_3 = \frac{x_{30} - x_3}{x_{30} - x_{3eq}} = \frac{\frac{\Delta x_1}{\Delta x_2} E_1 + E_2}{\frac{\Delta x_1}{\Delta x_2} + 1} = 0.52589$$

The toluene/heptane ratio in dispersed phase leaving the stage at contact of 0.05 s can be calculated from

$$(x - x_{eq}) = [Q](x_0 - x_{eq}); \quad [Q] = \exp[-[K_{od}]at]$$

The value is calculated as $\frac{0.2318}{0.01491} = 15.54$. The toluene/heptane ratio is very slightly higher than the corresponding value obtained by ignoring the continuous phase mass transfer resistances.

3. Transient equilibration in NMP(1)/propylbenzene(2)/tetradecane(3)

The solvent NMP (=N-methyl-2-pyrrolidone) is dispersed as droplets in the hydrocarbon phase. Figure 6 shows the equilibration trajectory. The trajectory calculations are obtained from the following input data (see also legend to Figure 6).

$$\left|\Lambda\right|^{1/2} = 1\times10^{-9}\ \mathrm{m^2 s^{-1}}$$

$$[\Gamma] = \begin{bmatrix} 0.05136 & -0.91061 \\ 0.45016 & 1.68594 \end{bmatrix}$$

$$[D] = \left|\Lambda\right|^{1/2}[\Gamma] = \begin{bmatrix} 0.05136 & -0.91061 \\ 0.45016 & 1.68594 \end{bmatrix}\times10^{-9}$$

$$\left|D\right|^{1/2} = 7\times10^{-10}$$

4. Transient equilibration in glycerol(1)/acetone(2)/water(3)

The experimental data on transient equilibration of glycerol-rich and acetone-rich phases of the glycerol/acetone/water mixture were measured in a stirred Lewis cell by Krishna et al.;[17] see Figure 7. In this case, the interface between the two liquid phases is flat; the appropriate expression for the departure from equilibrium in either the glycerol-rich or the acetone-rich phase is[17]

$$\left(x - x_{eq}\right) = [Q]\left(x_0 - x_{eq}\right); \quad [Q] \equiv \exp[-\beta[D]t] \tag{22}$$

where β is the Lewis cell constant. The value of the constant used in our calculations is $\beta = 10^7$. The precise choice of the value of this constant has no influence on the trajectories in composition space.

The start and end compositions in the glycerol-rich and acetone-rich phase are those in the experiments of Krishna et al.;[17] see legend to Figure 7. The two trajectories are calculated using $[D] = \left|\Lambda\right|^{1/2}[\Gamma]$ with $\left|\Lambda\right|^{1/2} = \left(D_{1,self}\right)^{x_1}\left(D_{2,self}\right)^{x_2}\left(D_{3,self}\right)^{x_3}$, taking $D_{1,\mathrm{self}}$= 0.01, $D_{2,\mathrm{self}}$= 3.2, $D_{3,\mathrm{self}}$= 0.5 with units 10^{-9} m^2 s^{-1}; this diffusivity information has been derived from our earlier work.[6]

For the glycerol-rich phase the following input data are calculated:

$$\left|\Lambda\right|^{1/2} = 3.75\times10^{-11}\ \mathrm{m^2 s^{-1}}$$

$$[\Gamma]=\begin{bmatrix}2.151617 & 1.171495\\ 0.019193 & 0.687462\end{bmatrix}$$

$$[D]=|\Lambda|^{1/2}[\Gamma]=\begin{bmatrix}8.069819 & 4.39379\\ 0.071986 & 2.578383\end{bmatrix}\times 10^{-11}$$

$$|D|^{1/2}=4.53\times 10^{-11}$$

For the acetone-rich phase the following input data are calculated:

$$|\Lambda|^{1/2}=2.23\times 10^{-9}\ \mathrm{m^2 s^{-1}}$$

$$[\Gamma]=\begin{bmatrix}1.064438 & 0.177947\\ 0.9564073 & 0.766246\end{bmatrix}$$

$$[D]=|\Lambda|^{1/2}[\Gamma]=\begin{bmatrix}2.296962 & 0.383994\\ 2.06384 & 1.653491\end{bmatrix}\times 10^{-9}$$

$$|D|^{1/2}=1.73\times 10^{-9}$$

5. Transient equilibration in water(1)/acetone(1)/ethyl-acetate(3)

Figure 8 and Figure 9 show the transient equilibration trajectories for the system water(1)/acetone(2)/ethylacetate(3) at 293 K.

The trajectory calculations in Figure 8 are obtained from the following input data (see also legend to Figure 8).

$$|\Lambda|^{1/2}=2.14\times 10^{-9}\ \mathrm{m^2 s^{-1}}$$

$$[\Gamma]=\begin{bmatrix}0.335504 & -0.287411\\ -5.6\times 10^{-3} & 1.233074\end{bmatrix}$$

$$[D]=|\Lambda|^{1/2}[\Gamma]=\begin{bmatrix}0.717637 & -0.614767\\ -0.012094 & 2.637524\end{bmatrix}\times 10^{-9}$$

$$|D|^{1/2}=1.37\times 10^{-9}$$

6. Transient equilibration in water(1)/caprolactam(2)/toluene(3)

Figure 10 and Figure 11 show the transient equilibration trajectories for the system water(1)/caprolactam(2)/toluene(3) at 298 K.

The trajectory calculations in Figure 10 are obtained from the following input data (see also legend to Figure 10).

$$|\Lambda|^{1/2} = 1\times10^{-9}\ \mathrm{m^2 s^{-1}}$$

$$[\Gamma] = \begin{bmatrix} 0.9312464 & -0.1564682 \\ -0.9630304 & 0.6333638 \end{bmatrix}$$

$$[D] = |\Lambda|^{1/2}[\Gamma] = \begin{bmatrix} 0.9312464 & -0.1564682 \\ -0.9630304 & 0.6333638 \end{bmatrix}\times10^{-9}$$

$$|D|^{1/2} = 6.63\times10^{-10}$$

7. Transient equilibration in water(1)/acetic acid(2)/isophorone(3)

Figure 12 and Figure 13 show the transient equilibration trajectories for the system water(1)/acetic acid(2)/isophorone(3) at 298 K.

The trajectory calculations in Figure 12 are obtained from the following input data (see also legend to Figure 12).

$$|\Lambda|^{1/2} = 1\times10^{-9}\ \mathrm{m^2 s^{-1}}$$

$$[\Gamma] = \begin{bmatrix} 0.7352077 & -0.47604686 \\ -0.13916565 & 1.38146886 \end{bmatrix}$$

$$[D] = |\Lambda|^{1/2}[\Gamma] = \begin{bmatrix} 0.7352077 & -0.47604686 \\ -0.13916565 & 1.38146886 \end{bmatrix}\times10^{-9}$$

$$|D|^{1/2} = 9.74\times10^{-10}$$

8. Transient equilibration in water(1)/acetic acid(2)/MTBE(3)

Figure 14 and Figure 15 show the transient equilibration trajectories for the system water(1)/acetic acid(2)/MTBE(3) at 298.15 K.

The trajectory calculations in Figure 14 are obtained from the following input data (see also legend to Figure 14).

$$|\Lambda|^{1/2} = 1\times10^{-10}\ \mathrm{m^2 s^{-1}}$$

$$[\Gamma] = \begin{bmatrix} 0.33765906 & -0.75846144 \\ -0.26661839 & 1.75009021 \end{bmatrix}$$

$$[D] = |\Lambda|^{1/2}[\Gamma] = \begin{bmatrix} 0.33765906 & -0.75846144 \\ -0.26661839 & 1.75009021 \end{bmatrix}\times10^{-9}$$

$$|D|^{1/2} = 6.2\times10^{-10}$$

9. Transient equilibration in [omim][Cl](1)/ethanol(2)/TAEE(3)

There is increasing amount of fundamental and technological interest in the use of ionic liquids in separations in liquid-liquid extraction. We shall examine the diffusion trajectories in ternary mixtures of [omim][Cl](1)/ethanol(2)/TAEE(3). Here we denote the ionic liquid 1-octyl-3-methylimidazolium chloride in the abbreviated form [omim][Cl]. TAEE is the abbreviated name for tert-amyl ethyl ether.

Figure 16, Figure 17, and Figure 18 show the transient equilibration trajectory for the system [omim][Cl](1)/ethanol(2)/TAEE(3) at 298.15 K.

The trajectory calculations in Figure 16 are obtained from the following input data (see also legend to Figure 16). The final equilibrium composition is $x_{1,eq}$ = 0.150072736, $x_{2,eq}$ = 0.47026855, and $x_{3,eq}$ = 0.379658714.

$$|\Lambda|^{1/2} = 1\times10^{-10}\ \mathrm{m^2 s^{-1}}$$

$$[\Gamma] = \begin{bmatrix} 1.155617836 & -2.5088582 \\ -0.71005985 & 3.20938546 \end{bmatrix}$$

$$[D] = |\Lambda|^{1/2}[\Gamma] = \begin{bmatrix} 1.155617836 & -2.5088582 \\ -0.71005985 & 3.20938546 \end{bmatrix} \times 10^{-10}$$

$$|D|^{1/2} = 1.4 \times 10^{-10}$$

The trajectory calculations in Figure 17 are obtained from the following input data (see also legend to Figure 17). The final equilibrium composition is $x_{1,eq}$ = 0.397919131, $x_{2,eq}$ = 0.381690314, and $x_{3,eq}$ = 0.22039056.

$$|\Lambda|^{1/2} = 1 \times 10^{-10}\ \mathrm{m^2 s^{-1}}$$

$$[\Gamma] = \begin{bmatrix} 1.04814698 & -2.42905971 \\ -0.40060012 & 3.22825358 \end{bmatrix}$$

$$[D] = |\Lambda|^{1/2}[\Gamma] = \begin{bmatrix} 1.04814698 & -2.42905971 \\ -0.40060012 & 3.22825358 \end{bmatrix} \times 10^{-10}$$

$$|D|^{1/2} = 1.55 \times 10^{-10}$$

10. Transient equilibration in [bmim][TfO](1)/ethanol(2)/TAEE(3)

We also investigation the diffusion trajectories using a different ionic liquid [bmim][TfO] = 1-butyl-3-methylimidazolium trifluoromethanesulfonate.

Figure 19 and Figure 20 the transient equilibration trajectories for the system [bmim][TfO](1)/ethanol(2)/TAEE(3) at 298.15 K.

The trajectory calculations in Figure 19 are obtained from the following input data (see also legend to Figure 19).

$$|\Lambda|^{1/2} = 1 \times 10^{-10}\ \mathrm{m^2 s^{-1}}$$

$$[\Gamma] = \begin{bmatrix} 0.6048285 & -1.8612996 \\ 0.0978455 & 3.1563742 \end{bmatrix}$$

$$[D] = |\Lambda|^{1/2}[\Gamma] = \begin{bmatrix} 0.6048285 & -1.8612996 \\ 0.0978455 & 3.1563742 \end{bmatrix} \times 10^{-10}$$

$$|D|^{1/2} = 1.44 \times 10^{-10}$$

11. Transient equilibration in water(1)/ethanol(2)/cyclohexane(3)

Figure 21 and Figure 22 show the transient equilibration trajectory for the system water(1)/ethanol(2)/cyclohexane(3) at 298 K.

The trajectory calculations in Figure 21 are obtained from the following input data (see also legend to Figure 21).

$$|\Lambda|^{1/2} = 3.13\times10^{-9}\ \mathrm{m^2 s^{-1}}$$

$$[\Gamma] = \begin{bmatrix} 0.08686 & -0.49724 \\ 0.33949 & 1.04153 \end{bmatrix}$$

$$[D] = |\Lambda|^{1/2}[\Gamma] = \begin{bmatrix} 0.27222 & -1.5584 \\ 1.06401 & 3.42367 \end{bmatrix}\times10^{-9}$$

$$|D|^{1/2} = 1.6\times10^{-9}$$

12. Transient equilibration in toluene(1)/ethanol(2)/water(3)

Figure 23 and Figure 24 show the transient equilibration trajectory for the system toluene(1)/ethanol(2)/water(3) at 298 K.

The trajectory calculations in Figure 23 are obtained from the following input data (see also legend to Figure 23).

$$|\Lambda|^{1/2} = 1\times10^{-9}\ \mathrm{m^2 s^{-1}}$$

$$[\Gamma] = \begin{bmatrix} 0.17105226 & -0.32119791 \\ 0.41999696 & 1.14665716 \end{bmatrix}$$

$$[D] = |\Lambda|^{1/2}[\Gamma] = \begin{bmatrix} 0.17105226 & -0.32119791 \\ 0.41999696 & 1.14665716 \end{bmatrix}\times10^{-9}$$

$$|D|^{1/2} = 5.75\times10^{-10}$$

13. Transient equilibration in water(1)/acetone(2)/toluene(3)

Figure 25 and Figure 26 show the transient equilibration trajectory for the system water(1)/acetone(2)/toluene(3) at 298 K.

The trajectory calculations in Figure 25 are obtained from the following input data (see also legend to Figure 25).

$$\left|\Lambda\right|^{1/2} = 1\times10^{-9}\ \mathrm{m^2 s^{-1}}$$

$$[\Gamma] = \begin{bmatrix} -0.303576 & -0.636406 \\ 1.12334 & 1.593812 \end{bmatrix}$$

$$[D] = \left|\Lambda\right|^{1/2}[\Gamma] = \begin{bmatrix} -0.303576 & -0.636406 \\ 1.12334 & 1.593812 \end{bmatrix}\times10^{-9}$$

$$\left|D\right|^{1/2} = 4.8\times10^{-10}$$

14. Springer experiments for boundary crossing in homogeneous azeotropic distillation

Design and simulation procedures for distillation are commonly based on the equilibrium stage model, developed by Sorel more than a hundred years ago.[18] Departures from thermodynamic equilibrium between the vapor and liquid phases on a distillation tray are commonly accounted for by introducing the component Murphree point efficiencies

$$E_i = \frac{y_{iE} - y_{iL}}{y_{iE} - y_{i,eq}} = 1 - \frac{y_{iL} - y_{i,eq}}{y_{iE} - y_{i,eq}} = 1 - \frac{\Delta y_{iL}}{\Delta y_{iE}};\quad i = 1,2,...n \tag{23}$$

where y_{iE}, and y_{iL} are, respectively, the vapor phase mole fractions, entering and leaving a tray, and $y_{i,eq}$ is the vapor composition in thermodynamic equilibrium with the liquid leaving the tray. See schematic in Figure 27. For a tray in thermodynamic equilibrium, the component efficiencies are 100% for each component. Mass transfer resistances on either side of the vapor/liquid interface reduce the component efficiencies to values below 100%. For binary distillation, the Murphree component efficiencies are bounded, i.e. $0 \le E_{1,} = E_2 \le 1$. For multicomponent distillation, with the number of

species $n \geq 3$, coupled diffusion effects in either vapor or liquid phases cause the component efficiencies to be distinctly different from one another, $E_1 \neq E_2 \neq E_3$. Phenomena such as osmotic diffusion, diffusion barrier, and uphill diffusion lead to component efficiencies that are unbounded ($E_i \to \pm\infty$), zero ($E_i = 0$), or negative ($E_i < 0$); this has been demonstrated in several experimental studies.[19-27]

The values of the component Murphree efficiencies influence the composition profiles along the height of distillation columns.

Levy et al.[28] have put forward the following two "rules" regarding that are applicable to continuous azeotropic distillation columns operating with each stage in thermodynamic equilibrium:

- If the simple distillation boundary is perfectly linear, then the steady-state composition profile in a continuous distillation column cannot cross the boundary from either side.
- If the simple distillation boundary is curved, then the steady-state composition profile in a continuous distillation column cannot cross the boundary from the concave side but may cross the boundary from the convex side when moving from the product compositions inward.

Consider, for example, the system methanol – isopropanol – water; the residue curve maps for this system are shown in Figure 28a. A straight-line distillation boundary connects the binary isopropanol-water azeotrope with pure methanol and divides the composition space into two regions. According to Rule 1, the column composition trajectories cannot cross this straight line distillation boundary, whichever side the feed is located. For either of the two feed locations, F1 and F2 in Figure 28a boundary crossing is forbidden.

For the system acetone - chloroform – methanol we have three binary and one ternary azeotrope dividing the composition space into four regions by means of four distillation boundaries, that are all curved; see the residue curve map shown in Figure 28b. According to Rule 2, the column trajectory obtained for operation with the feed located on the concave side of a boundary, with say composition indicated by F1 is able to cross that boundary. This has been demonstrated experimentally by Li et al.[29]

Conversely, if the feed is located on the convex side, with say composition indicated by F2 the boundary cannot be crossed.[28]

In a series of papers, Springer et al. [21, 23, 25, 26] have reported a set of experiments in a bubble-cap tray column operating at total reflux for homogeneous azeotropic distillation using mixtures: water/ethanol/methanol, water/ethanol/acetone, water/ethanol/methylacetate, water/ethanol/methanol/acetone to demonstrate that the Levy rules are violated. The experimental set-up used by Springer can be viewed at: http://krishna.amsterchem.com/distillation/. A schematic of the experimental set-up is shown in Figure 29. The set-up consists of a 12-stage distillation column wherein all the experiments were conducted under total-reflux conditions at 101.3 kPa. The condenser is a total condenser, and is considered to be stage 1. The numbering of the stages is downwards, and the Stage 12 is the partial reboiler. Stages 2, to 11 are bubble-cap trays.

As an example of boundary crossing in homogeneous azeotropic distillation, we present the experimental results for Run T2-26 for water(1)/ethanol(2)/acetone(3) mixture in Figure **30**, In Run T2-26, the condenser composition is left of the distillation boundary. Therefore, the residue curves dictate that the reboiler composition should be in the top left corner, rich in ethanol. The measured compositions along the column operating at total reflux shows that the reboiler composition is towards the right of the distillation boundary, and is rich in water. Boundary crossing occurs at stage 2, just below the total condenser.

For Run T2-26, the values of $\Delta y_{2E} = \left(y_{2E} - y_{2,eq}\right)$ are plotted in Figure 31a. We note that the ethanol driving force $\Delta y_{2E} = \left(y_{2E} - y_{2,eq}\right) > 0$ for Stages 2 – 9, $\Delta y_{2E} = \left(y_{2E} - y_{2,eq}\right) \approx 0$ for Stage 10, and $\Delta y_{2E} = \left(y_{2E} - y_{2,eq}\right) < 0$ for Stage 11. The values of the E_2 for ethanol is negative on Stage 10; on Stage 11, $E_i > 1$; see Figure 31b. This implies reverse or uphill diffusion on stages 10 and 11; the transfer of ethanol is dictated by the driving forces of the other two components $\Delta y_{1E} = \left(y_{1E} - y_{1,eq}\right)$, and $\Delta y_{3E} = \left(y_{3E} - y_{3,eq}\right)$, that are both finite.[21]

We shall demonstrate later that the boundary crossing is primarily due to the factor that the Murphree efficiency of water is higher than that of ethanol, i.e. $E_1 > E_2$.

The experimental data for Run T4-13 with water(1)/ethanol(2)/methanol(3) mixture are shown in Figure 32, In Run T4-13, the condenser composition is left of the distillation boundary. Therefore, the residue curves dictate that the reboiler composition should be in the top left corner, rich in ethanol. The measured compositions along the column operating at total reflux shows that the reboiler composition is towards the right of the distillation boundary, and is rich in water. Also shown in Figure 32 are the Murphree component efficiencies along the column for Run T4-13. We shall demonstrate later that the boundary crossing is primarily due to the factor that the Murphree efficiency of water is higher than that of ethanol, i.e. $E_1 > E_2$.

The experimental data for Run T3-23 with water(1)/ethanol(2)/methylacetate(3) mixture are shown in Figure 33. In Run T3-23, the condenser composition is left of the distillation boundary. Therefore, the residue curves dictate that the reboiler composition should be in the top left corner, rich in ethanol. The measured compositions along the column operating at total reflux shows that the reboiler composition is towards the right of the distillation boundary, and is rich in water. Also shown in Figure 33 are the Murphree component efficiencies along the column for Run T4-13. We shall demonstrate later that the boundary crossing is primarily due to the factor that the Murphree efficiency of water is higher than that of ethanol, i.e. $E_1 > E_2$.

Experimental data (blue circles) of Springer et al.[25] for Run Q6 with quaternary water(1)/ethanol(2)/methanol(3)/acetone(4) mixtures are indicated by the blue circles in Figure 34; the data are plotted in ternary composition space by combining the mole fractions of methanol and acetone in the left bottom vertex. Two distillation boundaries are shown: the “acetone” boundary is the same as for the water/ethanol/acetone mixture; the “methanol” boundary is the same as for the water/ethanol/methanol mixture. The experimental data shows that both the “acetone” and “methanol” boundaries are crossed in Run Q6. Also shown as insets are the Murphree component efficiencies and component driving forces. The component Murphree efficiency of methanol is negative on stage 3, and

slightly exceeds unity on stage 4. This implies that uphill diffusion of methanol manifests on stages 3 and 4. The reason is to found in the fact that the driving force of methanol is practically zero on these two stages; the direction of transport of methanol is dictated by the transfer of the three partner species in the mixture: water, ethanol, and acetone. The boundary crossing is primarily due to the factor that the Murphree efficiency of water is higher than that of ethanol, i.e. $E_1 > E_2$.

For rationalization and quantitative description of the observed experimental boundary crossing phenomena, Springer et al. Springer et al.[21, 23, 25, 26] used rigorous non-equilibrium (NEQ) stage-wise contacting model, as implemented in ChemSep.[18, 30] The NEQ model uses the Maxwell-Stefan formulation for diffusion in the vapor and the two liquid phases. The important conclusion reached in their work is that boundary crossing effects are primarily attributable to diffusional coupling effects, that cause the component Murphree efficiencies to be unequal to one another. Unequal component efficiencies cause column composition trajectories to deviate from those of the residue curve maps. Put another way, the NEQ model does not follow the tramline guides of the RCM.

Our aim below is to show that the boundary crossing phenomena can be explained on the basis of the Geddes model for transient equilibration of vapor bubbles rising through the liquid on a tray.

15. Transient equilibration inside vapor bubble rising through a liquid on a distillation tray

For a ternary mixture, the diffusion, in either the dispersed vapor bubbles or in the continuous liquid phase surrounding the bubbles, is described by the generalized Fick's law

$$(J) = -c_t [D] \frac{d(x)}{dz}$$

in which the two-dimensional matrix of Fick diffusivities [D] is a product of two matrices

$$[D] = [\Lambda][\Gamma]$$

The vapor phase can often be considered to thermodynamically ideal; in this event, the matrix of thermodynamic factor degenerates to the identity matrix

$$\Gamma_{ij} = \delta_{ij}; \quad i, j = 1,2$$

The matrix $[\Lambda]$ to be expressed explicitly in terms of the M-S diffusivities of the constituent binary pairs in the ternary mixture:

$$\begin{bmatrix} \Lambda_{11} & \Lambda_{12} \\ \Lambda_{21} & \Lambda_{22} \end{bmatrix} = \frac{\begin{bmatrix} Đ_{13}\left(x_1 Đ_{23} + (1-x_1) Đ_{12}\right) & x_1 Đ_{23}\left(Đ_{13} - Đ_{12}\right) \\ x_2 Đ_{13}\left(Đ_{23} - Đ_{12}\right) & Đ_{23}\left(x_2 Đ_{13} + (1-x_2) Đ_{12}\right) \end{bmatrix}}{x_1 Đ_{23} + x_2 Đ_{13} + x_3 Đ_{12}}$$

Let us consider the dispersion to consist of uniform and rigid vapor bubbles of diameter, d_{bubble}. The transient equilibration process within a rigid spherical bubble is described by Geddes model that was originally developed for describing binary diffusion inside vapor bubbles on distillation trays.[7] For ternary mixtures, the Geddes model can be written in two-dimensional matrix differential equation[4, 31]

$$\left(y - x_{eq}\right) = [Q]\left(y_0 - x_{eq}\right); \quad [Q] \equiv \frac{6}{\pi^2} \sum_{m=1}^{\infty} \frac{1}{m^2} \exp\left[-m^2 \pi^2 \frac{4[D]t}{d_{bubble}^2}\right]$$

In the above equation, (y_0) denotes the vapor composition entering the tray. The Sylvester theorem, detailed in Appendix A of Taylor and Krishna,[4] is required for explicit calculation of the composition trajectories described by the Geddes model. For vapor bubbles rising on a sieve or bubble-cap tray, the effective contact time of the dispersed phase bubbles with the surrounding continuous phase is $t = h_f / V_{bubble}$, where h_f is the froth dispersion height, and V_{bubble} is the bubble rise velocity.

The fractional approaches to equilibrium for contact time *t*, also termed as the Murphree efficiencies,[3, 9, 10] are calculated from

$$E_1 = \frac{y_{10} - y_1}{y_{10} - y_{1eq}} = 1 - Q_{11} - Q_{12} \frac{\Delta y_2}{\Delta y_1};$$

$$E_2 = \frac{y_{20} - y_2}{y_{20} - y_{2eq}} = 1 - Q_{22} - Q_{21} \frac{\Delta y_1}{\Delta y_2};$$

$$E_3 = \frac{y_{30} - y_3}{y_{30} - y_{3eq}} = \frac{\frac{\Delta y_1}{\Delta y_2} E_1 + E_2}{\frac{\Delta y_1}{\Delta y_2} + 1}$$

Let us define a two-dimensional matrix of mass transfer coefficients, $[k]$, defined by

$$(J) = c_t [k](y - y_{eq})$$

The matrix of Sherwood numbers $[Sh]$

$$[Sh_t] = [k] d_{bubble} [D]^{-1}$$

can be calculated as a function of the contact time using the following expression[4]

$$[Sh_t] = \frac{2}{3}\pi^2 \left[\sum_{m=1}^{\infty} \exp\left[-m^2\pi^2 \frac{4[D]t}{d_{bubble}^2}\right]\right]\left[\frac{6}{\pi^2}\sum_{m=1}^{\infty}\frac{1}{m^2}\exp\left[-m^2\pi^2\frac{4[D]t}{d_{bubble}^2}\right]\right]^{-1}$$

In the limit $t \to \infty$, an asymptotic value is reached

$$[Sh_t] = \frac{2\pi^2}{3} = 6.58$$

It must be emphasized that $[Sh_t]$ is the value of the matrix at any time *t*, and not the time-averaged value. The time-averaged Sherwood number, $[Sh]$, for the interval 0 – *t*, is given by the expression

$$[Sh] = -\frac{2}{3}\ln[[Q]][D]^{-1}\frac{d_{bubble}^2}{4t}$$

In the limit $t \to \infty$, an asymptotic value is also reached for the time-averaged Sherwood number

$$[Sh] = \frac{2\pi^2}{3} = 6.58$$

The corresponding time-averaged matrix of mass transfer coefficients in the dispersed vapor phase is

$$[k_d] = \frac{[Sh][D]}{d_{bubble}} = -\frac{2}{3}\ln[[Q]][D]^{-1}\frac{d_{bubble}^2}{4t}\frac{[D]}{d_b} = -\ln[[Q]]\frac{d_{bubble}}{6t}$$

In this asymptotic limit $t \to \infty$, the coupling effects of $[k]$ are directly proportional to those of the Fick matrix $[D]$.

Let us denote the interfacial area per unit volume of bubble as

$$a = \frac{6}{d_{bubble}}$$

With this definition, the time-averaged matrix of mass transfer coefficients is

$$[k_d] = -\ln[[Q]]\frac{1}{at}$$

In chemical engineering practice, it is conventional to define the number of transfer units for the dispersed phase as

$$[NTU_d] = [k_d]at = -\ln[[Q]]$$

Therefore an alternative expression for the fractional departure from equilibrium is

$$[Q] = \exp[-NTU_d] = \exp[-[k_d]at]$$

We now apply the Geddes model to rationalize the boundary effects for for water(1)/ethanol(2)/acetone(3), water(1)/ethanol(2)/methanol(3), and water(1)/ethanol(2)/methylacetate(3) mixtures.

16. Boundary crossing in water/ethanol/acetone mixture

Consider distillation of water(1)/ethanol(2)/acetone(3) mixture in a tray column operating at total reflux at a total pressure of 101.3 kPa. For a specified tray, the composition of the vapor entering the tray is y_{10} = 0.067, y_{20} = 0.44, and y_{30} = 0.493. This composition is right of the distillation boundary. For total reflux operations, the compositions of the liquid leaving that stage will be equal to that of the vapor entering the stage, i.e. x_1 = 0.067, x_2 = 0.44, and x_3 = 0.493. The composition of vapor in equilibrium with the liquid leaving the tray can be determined using the NRTL parameters provided in Table **15**. The bubble point temperature is 335.5 K and the equilibrium composition is $y_{1,eq}$ = 0.04335, $y_{2,eq}$ = 0.25907, and $y_{3,eq}$ = 0.69758. The equilibrium composition is also right of the distillation boundary, as is to be expected.

The driving forces are $\Delta y_1 = y_{10} - y_{1,eq} = 0.02365$, and $\Delta y_2 = y_{20} - y_{2,eq} = 0.18093$. Both driving forces are positive, i.e. directed from vapor to the liquid phase.

The values of the vapor phase M-S diffusivities of the binary pairs, calculated using the Fuller-Schettler-Giddings (FSG)[32] method, are $Đ_{12} = 1.97$; $Đ_{13} = 1.71$; $Đ_{23} = 0.851 \times 10^{-5}$ m^{2}s^{-1}. These diffusivities are independent of composition. The differences in the binary pair diffusivities cannot be ignored, as we demonstrate below. At the average composition between the entering compositions and the equilibrated compositions, use of

$$[D] = \begin{bmatrix} \Lambda_{11} & \Lambda_{12} \\ \Lambda_{21} & \Lambda_{22} \end{bmatrix} = \frac{\begin{bmatrix} Đ_{13}\left(x_1 Đ_{23} + (1-x_1)Đ_{12}\right) & x_1 Đ_{23}\left(Đ_{13} - Đ_{12}\right) \\ x_2 Đ_{13}\left(Đ_{23} - Đ_{12}\right) & Đ_{23}\left(x_2 Đ_{13} + (1-x_2)Đ_{12}\right) \end{bmatrix}}{x_1 Đ_{23} + x_2 Đ_{13} + x_3 Đ_{12}}$$

results in

$$[D] = \begin{bmatrix} 1.79675 & -0.0067 \\ -0.36845 & 0.87989 \end{bmatrix} \times 10^{-5} \text{ m}^2 \text{ s}^{-1}$$ in which the D_{21} is seen to non-negligible in comparison with D_{22}.

We can also determine a "magnitude" of the Fick diffusivity for use in the calculation of the Fourier number: $|D|^{1/2} = 1.26 \times 10^{-5}$ in order to plot the results in terms of dimensionless times.

The diffusion equilibration trajectory, calculated using the Geddes model is shown in Figure 35a. The curvilinear equilibration trajectory crosses the distillation boundary during a portion of this traject. Figure 35b presents a plot of the component Murphree efficiencies, E_i, as function of the Fourier number. The Murphree point efficiency of ethanol, E_2, is the lowest; this is because of the negative contribution of $D_{21}\Delta y_1$; the Murphree point efficiency of water, E_1, is higher than that of ethanol: $E_1 > E_2$. Due to $E_1 > E_2$, a higher proportion of water is transferred to the liquid phase as compared to ethanol; this implies that the vapor phase is poorer in water than predicted by calculations based on equal component efficiencies. The hierarchy of point efficiencies $E_1 > E_2 \approx E_3$ is in agreement with the experimentally determined values for Stage 2; see Figure 31b.

The contact time of the bubble with the liquid phase is finite. For a 4.5 mm bubble, with a rise velocity of 0.2 m s^{-1} in a dispersion of height 9.2 mm, the contact time t = 0.046 s; these are the input parameters used by Springer et al. in the NEQ model implementation.[23]

For this contact time, the composition of the vapor bubble leaving the tray is

y_1 =0.0465, y_2 = 0.3118, and y_3 = 0.64175.

This vapor composition is on the other side of the distillation boundary. Such boundary crossing is observed in Run T2-26 of the experiments of Springer et al.[21, 23, 25, 26] (cf. Figure **30**).

The time-averaged mass transfer coefficient for the dispersed bubbles, for contact time t = 0.046 s is

$$[k_d] = -\ln[Q]\frac{d_{bubble}}{6t}$$

For t = 0.046 s, we have the matrix describing the departure from equilibrium is

$$[Q] = \begin{bmatrix} 0.12178 & 1.17915\times10^{-3} \\ 0.06477 & 0.38105 \end{bmatrix}$$

and

$$[k_d] = \begin{bmatrix} 343.52901 & -1.00639 \\ -55.27758 & 205.97396 \end{bmatrix}\times10^{-4}$$

If the diffusion coupling effects are completely ignored, and the simplest Fickian relation

$$J_i = -c_t D\frac{dx_i}{dz};\quad i = 1,2,3 \tag{24}$$

is employed, the equilibration trajectory will be linear, running parallel to the residue curves (pink lines) in Figure 35a.

Let us examine what influence inclusion of liquid phase mass transfer resistance has on the composition trajectories.

The first task is to estimate the M-S diffusivities if the three binary pairs $Đ_{12}$, $Đ_{13}$, and $Đ_{23}$ in the liquid phase using the interpolation formula

$$Đ_{ij} = \left(Đ_{ij}^{x_i\to1}\right)^{x_i}\left(Đ_{ij}^{x_j\to1}\right)^{x_j}\left(Đ_{ij}^{x_k\to1}\right)^{x_k}$$

The six infinite dilution values of the pair diffusivities $Đ_{ij}^{x_j\to 1}$ are estimated the Wilke-Chang correlation.[12] For estimation of $Đ_{ij}^{x_k\to 1}$, the *i* - *j* pair diffusivity when both *i* and *j* are present in infinitely dilute concentrations, the following formula has been suggested[11]

$$Đ_{ij}^{x_k\to 1} = \left(Đ_{ik}^{x_k\to 1}\right)^{x_i/(x_i+x_j)}\left(Đ_{jk}^{x_k\to 1}\right)^{x_j/(x_i+x_j)}$$

At the liquid composition on the tray: $x_1 = 0.067$, $x_2 = 0.44$, and $x_3 = 0.493$, we calculate the following values of the M-S diffusivities of the binary pairs

$$Đ_{12} = 6.4; \quad Đ_{13} = 5.6; \quad Đ_{23} = 3.8\times 10^{-9}\ \mathrm{m^2 s^{-1}}$$

For estimation of the Fick diffusivity, we use the approximation[6]

$$[D] = |\Lambda|^{1/2}[\Gamma]$$

The value of the scalar diffusivity is

$$|\Lambda|^{1/2} = \sqrt{\frac{Đ_{12}Đ_{13}Đ_{23}}{x_1Đ_{23}+x_2Đ_{13}+x_3Đ_{12}}} = 4.8\times 10^{-9}\ \mathrm{m^2 s^{-1}}$$

The matrix of thermodynamic factors is

$$[\Gamma] = \begin{bmatrix} 0.86952 & -0.03937 \\ -0.20988 & 0.75351 \end{bmatrix}$$

The Fick diffusivity matrix in the liquid phase is calculated as

$$[D] = |\Lambda|^{1/2}[\Gamma] = \begin{bmatrix} 4.16901 & -0.18874 \\ -1.00627 & 3.61281 \end{bmatrix}\times 10^{-9}$$

The mass transfer coefficient external to the bubble can be estimated from the surface renewal theory[15, 16]

$$[k_c] = 2\sqrt{\frac{[D]}{\pi t_{renewal}}}$$

The characteristic time for surface renewal can be estimated is $t_{renewal} = d_{bubble}/V_{bubble}$ = 0.0225 s; this value is lower than the time the bubble takes to rise through the dispersion, 0.046 s.

For a surface renewal time of 0.0225 s, the mass transfer in the continuous liquid phase can be estimated from the surface renewal theory (cf. schematic in Figure 27)

$$[k_c] = 2\sqrt{\frac{[D]}{\pi t_{renewal}}} = \begin{bmatrix} 4.84999 & -0.11406 \\ -0.60812 & 4.51386 \end{bmatrix} \times 10^{-4}$$

The overall mass transfer coefficient can be calculated from the addition of resistances formula

$$[K_{Od}]^{-1} = [k_d]^{-1} + \frac{c_{tV,d}}{c_{tL,c}} \begin{bmatrix} \frac{y_{1,eq}}{x_1} & 0 \\ 0 & \frac{y_{2,eq}}{x_2} \end{bmatrix} [k_c]^{-1}$$

Inserting the values of the partial mass transfer coefficients, we have for the overall mass transfer coefficients

$$[K_{Od}]^{-1} = \begin{bmatrix} 343.52901 & -1.00639 \\ -55.27758 & 205.97396 \end{bmatrix}^{-1} \times 10^4 + \frac{36.32105}{1.48899 \times 10^4} \begin{bmatrix} \frac{0.04335}{0.067} & 0 \\ 0 & \frac{0.25907}{0.44} \end{bmatrix} \begin{bmatrix} 4.84999 & -0.11406 \\ -0.60812 & 4.51386 \end{bmatrix}^{-1} \times 10^4$$

The matrix of overall mass transfer coefficients is

$$[K_{Od}] = \begin{bmatrix} 309.00758 & -1.34179 \\ -49.04598 & 193.33745 \end{bmatrix} \times 10^{-4}.$$

We note that $[K_{Od}] \approx [k_d]$, indicating that the mass transfer is controlled by diffusion within the vapor bubbles; the liquid phase mass transfer resistance is of negligible importance.

The matrix for the overall number of transfer units can be calculated from

$$[NTU_{Od}] = [K_{Od}]at$$

The interfacial area per unit volume of bubble is

$$a = \frac{6}{d_{bubble}} = 1.333 \times 10^3$$

Therefore, for contact time t = 0.046 s is

$$[NTU_{Od}] = \begin{bmatrix} 1.89525 & -0.00823 \\ -0.30082 & 0.99427 \end{bmatrix}$$

The matrix describing departure from equilibrium can be determined from

$$[Q] = \exp[-[NTU_{Od}]]$$

$$[Q] = \begin{bmatrix} 0.15052 & 1.8013 \times 10^{-3} \\ 0.06584 & 0.3058 \end{bmatrix}$$

The composition of the vapor bubble exiting the tray at t = 0.046 s is determined from

$$(y - x_{eq}) = [Q](y_0 - x_{eq})$$

The calculated value is

y_1 = 0.04724, y_2 = 0.31596, and y_3 = 0.6368.

This vapor composition is very close to the value calculated above by ignoring the liquid phase resistance. Boundary crossing persists even if we ignore the liquid phase mass transfer resistance. The Geddes provides an accurate prediction of boundary crossing of water(1)/ethanol(2)/acetone(3) mixture.

For various vapor compositions entering any given stage, we have plotted in Figure 35c the actual composition vector $(y_{i,L} - y_{i,E})$, calculated from the NEQ model (taking bubble diameter of 4.5 mm) along with the equilibrium vector $(y_i^* - y_{i,E})$. The angle between the NEQ trajectory (red line) and the EQ trajectory (blue line) increases when the differences in the component efficiencies increase. If all the component efficiencies were equal to one another, the NEQ and EQ trajectories would coincide. We see from Figure 35c that the NEQ trajectory has a tendency to cut across to the right of the EQ trajectory, precisely as has been observed in Run T2-26; cf. Figure **30**. It is this tendency to cut towards the right of the composition space that causes boundary crossing. By performing several NEQ simulations with various starting compositions of the vapor entering the condenser we can determine the region within which the column trajectories will cross the distillation boundary and end up with reboiler compositions in the right region. This boundary crossing region is shown as the orange shaded area in Figure 35d.

17. NEQ vs EQ models for design of column to separate water/ethanol/acetone mixtures

The *design* of a distillation column to meet the required specification with regard to product purity is distinctively different to that of simulation as discussed above. In this section, our objective is to demonstrate the inclusion of diffusional coupling effects will lead to different requirements on the number of trays, in order to achieve a desired level of purity, when compared to a conventional approach of using equal component efficiencies. The material presented in this section are taken from an unpublished manuscript (P.A.M. Springer, R. Baur, R. Krishna, Influence of Diffusional Coupling on Distillation Column Design, 2004), that is based on the contents of Chapter 9 of the Ph.D. Dissertation of Springer.[33] The chosen mixture for investigation is water(1)/ethanol(2)/acetone(3) that has been investigated by Springer in the context of boundary crossing. The column hardware details are tabulated in Table 16. The distillation column was maintained at a total pressure of 101.3 kPa and the ideal gas law was applied. The vapor pressures were calculated using the Antoine equation. The reflux ratio = 3; this is an optimum value reached after an optimization study. The bottoms product flow rate was specified as 1.75 mol/s. The chosen parameters are summarized in Table 17.

Two different feed compositions are chosen, either side of the distillation boundary.

For feed on the left side of the distillation boundary, the feed was introduced in such a way that 20% of all column-stages were located above the feed stage. In this case, a purity level of 96% ethanol in the bottom product is specified.

For feed on the right side of the distillation boundary, the feed tray was located exactly halfway through the distillation column. In this case, a purity level of 100% water in the bottom product is specified.

The simulations were carried out using ChemSep developed by Kooijman and Taylor.[30] The ChemSep manual, that can be downloaded online, contains details of all thermodynamics, hydrodynamics and mass transfer models for tray columns that have been implemented into the software. The mass transfer coefficients for the NEQ stage model were estimated using the AIChE 1958

correlation for sieve tray columns with inclusion of the liquid phase mass transfer resistance. Both the vapor and liquid were assumed to be well-mixed. No pressure drop or entrainment was considered. The equilibrium data (NRTL parameters) for the water – ethanol – acetone system are specified in Table 18. For comparison purposes, simulations were also carried out with and EQ model assume that all the trays have the same efficiency, and that all component efficiencies are identical. The choice of the efficiency value is chosen as the average of that calculated by the NEQ model, averaged over all the trays.

Let us first consider the results for feed on the distillation region on the left side of the distillation boundary for the system water (1) – ethanol (2) – acetone (3); see Figure 36. For the purity requirement of 96% ethanol in the reboiler, the NEQ model requires 39 stages; see Figure 36b. The EQ model (with equal component efficiencies) requires only 25 stages to attain this product purity. The reason for the extra stages required by the NEQ is evident on examination of the column composition trajectory in Figure 36a. The NEQ trajectory appears to veer towards the water vertex because of the higher component efficiency of water (Figure 36c). Water is the least volatile of the three components, and its transfer is directed from vapor to the liquid phase; a higher efficiency of water ensures that the liquid phase is richer in water than anticipated on the basis of equal component efficiencies.

For the feed mixture right of the distillation boundary, the results are shown in Figure 37. In this case, the NEQ model requires 30 stages to reach 100% water purity in the bottoms product; the EQ model (with equal component efficiencies) requires 38 trays to reach the same purity target; see Figure 37b. The corresponding composition trajectories, plotted in Figure 37a, the higher number of stages required by the EQ model is because it takes the "scenic" route in proceeding to the bottom of the column. Due to the higher component efficiency of water (see Figure 37c), the composition trajectory followed by the NEQ model veers towards the water vertex and consequently demands fewer number of stages. In other words, the NEQ model takes a shorter route, and the EQ model follows the scenic route in the column.

The overall conclusion to be drawn from our design study is that use of the conventional EQ model may be either overly optimistic or pessimistic, depending on the which side of the distillation column the operation is taking place.

18. Boundary crossing in water/ethanol/methanol mixture

Consider distillation of water(1)/ethanol(2)/methanol(3) mixture in a tray column operating at total reflux at a total pressure of 101.3 kPa. For a specified tray, the composition of the vapor entering the tray is y_{10} = 0.082, y_{20} = 0.68, and y_{30} = 0.238. This composition is right of the distillation boundary. For total reflux operations, the compositions of the liquid leaving that stage will be equal to that of the vapor entering the stage, i.e. x_1 = 0.082, x_2 = 0.68, and x_3 = 0.238. The composition of vapor in equilibrium with the liquid leaving the tray can be determined using the NRTL parameters provided in Table 15. The bubble point temperature is 348 K and the equilibrium composition is $y_{1,eq}$ = 0.06767, $y_{2,eq}$ = 0.59691, and $y_{3,eq}$ = 0.33542. The final equilibrated composition is also right of the distillation boundary, as is to be expected.

The driving forces are $\Delta y_1 = y_{10} - y_{1,eq} = 0.01433$, and $\Delta y_2 = y_{20} - y_{2,eq} = 0.08309$. Both driving forces are positive, i.e. directed from vapor to the liquid phase.

The values of the vapor phase M-S diffusivities of the binary pairs, calculated using the Fuller-Schettler-Giddings (FSG)[32] method, are $Đ_{12} = 2.1$; $Đ_{13} = 2.72$; $Đ_{23} = 1.36\times10^{-5}$ m^{2}s^{-1}. These diffusivities are independent of composition. The differences in the binary pair diffusivities cannot be ignored, as we demonstrate below. At the average composition between the entering compositions and the equilibrated compositions, use of

$$[D] = \begin{bmatrix} \Lambda_{11} & \Lambda_{12} \\ \Lambda_{21} & \Lambda_{22} \end{bmatrix} = \frac{\begin{bmatrix} Đ_{13}\left(x_1 Đ_{23} + (1-x_1)Đ_{12}\right) & x_1 Đ_{23}\left(Đ_{13} - Đ_{12}\right) \\ x_2 Đ_{13}\left(Đ_{23} - Đ_{12}\right) & Đ_{23}\left(x_2 Đ_{13} + (1-x_2)Đ_{12}\right) \end{bmatrix}}{x_1 Đ_{23} + x_2 Đ_{13} + x_3 Đ_{12}}$$

results in

$$[D] = \begin{bmatrix} 2.28276 & 0.02578 \\ -0.52706 & 1.39446 \end{bmatrix} \times 10^{-5} \text{ m}^2 \text{ s}^{-1}$$ in which the D_{21} is seen to non-negligible in comparison with

D_{22}. We can also determine a "magnitude" of the Fick diffusivity for use in the calculation of the Fourier number: $|D|^{1/2} = 1.8 \times 10^{-5}$ in order to plot the results in terms of dimensionless times.

The diffusion equilibration trajectory, calculated using the Geddes model is shown in Figure 38a. Figure 38b presents a plot of the component Murphree efficiencies, E_i, as function of the Fourier number. The curvilinear equilibration trajectory crosses the distillation boundary during a portion of this traject. The Murphree point efficiency of ethanol, E_2, is the lowest; this is because of the negative contribution of $D_{21}\Delta y_1$; the Murphree point efficiency of water, E_1, is higher than that of ethanol: $E_1 > E_2$. Due to $E_1 > E_2$, a higher proportion of water is transferred to the liquid phase as compared to ethanol; this implies that the vapor phase is poorer in water than predicted by calculations based on equal component efficiencies.

The contact time of the bubble with the liquid phase is finite. For a 4.5 mm bubble, with a rise velocity of 0.2 m s^{-1} in a dispersion of height 9.2 mm, the contact time t = 0.046 s; these are the input parameters used by Springer et al.[21, 23, 25, 26] in the NEQ model implementation.[23]

For this contact time, the composition of the vapor bubble leaving the tray is

y_1 =0.06856, y_2 = 0.61221, and y_3 = 0.31943.

This vapor composition is on the other side of the distillation boundary. Such boundary crossing is observed in Run T4-13 of the experiments of Springer et al.[23] (cf. Figure 32).

The time-averaged mass transfer coefficient for the dispersed bubbles, for contact time t = 0.046 s is

$$[k_d] = -\ln[Q]\frac{d_{bubble}}{6t}$$

For t = 0.046 s, we have the matrix describing the departure from equilibrium is

$$[Q] = \begin{bmatrix} 0.07794 & -2.797 \times 10^{-3} \\ 0.05719 & 0.17432 \end{bmatrix}$$

and

$$[k_d] = \begin{bmatrix} 414.846671 & 3.79431 \\ -77.57228 & 284.10861 \end{bmatrix} \times 10^{-4}$$

If the diffusion coupling effects are completely ignored, and the simplest Fickian relation

$$J_i = -c_t D \frac{dx_i}{dz}; \quad i = 1,2,3$$

is employed, the equilibration trajectory will be linear, running parallel to the residue curves (pink lines) in Figure 38a.

Let us examine what influence inclusion of liquid phase mass transfer resistance has on the composition trajectories.

At the liquid composition on the tray: $x_1 = 0.082$, $x_2 = 0.68$, and $x_3 = 0.238$, we calculate the following values of the M-S diffusivities of the binary pairs

$$Đ_{12} = 6.2; \quad Đ_{13} = 5.6; \quad Đ_{23} = 4.1 \times 10^{-9} \text{ m}^2\text{s}^{-1}$$

For estimation of the Fick diffusivity, we use the approximation[6]

$$[D] = |\Lambda|^{1/2} [\Gamma]$$

The value of the scalar diffusivity is

$$|\Lambda|^{1/2} = \sqrt{\frac{Đ_{12} Đ_{13} Đ_{23}}{x_1 Đ_{23} + x_2 Đ_{13} + x_3 Đ_{12}}} = 5 \times 10^{-9} \text{ m}^2\text{s}^{-1}$$

The matrix of thermodynamic factors is

$$[\Gamma] = \begin{bmatrix} 0.95488 & 0.03852 \\ 0.13448 & 0.98609 \end{bmatrix}$$

The Fick diffusivity matrix in the liquid phase is calculated as

$$[D] = |\Lambda|^{1/2} [\Gamma] = \begin{bmatrix} 4.79312 & 0.193364 \\ 0.67501 & 4.94981 \end{bmatrix} \times 10^{-9}$$

The mass transfer coefficient external to the bubble can be estimated from the surface renewal theory[15, 16]

$$[k_c] = 2\sqrt{\frac{[D]}{\pi t_{renewal}}}$$

The characteristic time for surface renewal can be estimated is $t_{renewal} = d_{bubble}/V_{bubble}$ = 0.0225 s; this value is lower than the time the bubble takes to rise through the dispersion, 0.046 s.

For a surface renewal time of 0.0225 s, the mass transfer in the continuous liquid phase can be estimated from the surface renewal theory

$$[k_c] = 2\sqrt{\frac{[D]}{\pi t_{renewal}}} = \begin{bmatrix} 5.20438 & 0.10428 \\ 0.36402 & 5.28888 \end{bmatrix} \times 10^{-4}$$

The overall mass transfer coefficient can be calculated from the addition of resistances formula

$$[K_{Od}]^{-1} = [k_d]^{-1} + \frac{c_{tV,d}}{c_{tL,c}} \begin{bmatrix} \frac{y_{1,eq}}{x_1} & 0 \\ 0 & \frac{y_{2,eq}}{x_2} \end{bmatrix} [k_c]^{-1}$$

Inserting the values of the partial mass transfer coefficients, we have for the overall mass transfer coefficients

$$[K_{Od}]^{-1} = \begin{bmatrix} 414.846671 & 3.79431 \\ -77.57228 & 284.10861 \end{bmatrix}^{-1} \times 10^4 + \frac{34.73188}{1.83151 \times 10^4} \begin{bmatrix} \frac{0.06767}{0.082} & 0 \\ 0 & \frac{0.59691}{0.68} \end{bmatrix} \begin{bmatrix} 5.20438 & 0.10428 \\ 0.36402 & 5.28888 \end{bmatrix}^{-1} \times 10^4$$

The matrix of overall mass transfer coefficients is

$$[K_{Od}] = \begin{bmatrix} 368.73607 & 3.66694 \\ -61.14586 & 260.74857 \end{bmatrix} \times 10^{-4}.$$

We note that $[K_{Od}] \approx [k_d]$, indicating that the mass transfer is controlled by diffusion within the vapor bubbles; the liquid phase mass transfer resistance is of negligible importance.

The matrix for the overall number of transfer units can be calculated from

$$[NTU_{Od}] = [K_{Od}]at$$

The interfacial area per unit volume of bubble is

$$a = \frac{6}{d_{bubble}} = 1.333 \times 10^3$$

Therefore, for contact time t = 0.046 s is

$$[NTU_{Od}] = \begin{bmatrix} 2.26158 & 0.02249 \\ -0.37503 & 1.59926 \end{bmatrix}$$

The matrix describing departure from equilibrium can be determined from

$$[Q] = \exp[-[NTU_{Od}]]$$

$$[Q] = \begin{bmatrix} 0.10363 & -3.31843 \times 10^{-3} \\ 0.05533 & 0.20136 \end{bmatrix}$$

The composition of the vapor bubble exiting the tray at t = 0.046 s is determined from

$$(y - x_{eq}) = [Q](y_0 - x_{eq})$$

The calculated value is

y_1 = 0.06888, y_2 = 0.61443, and y_3 = 0.31668.

This vapor composition is very close to the value calculated above by ignoring the liquid phase resistance. Boundary crossing persists even if we ignore the liquid phase mass transfer resistance. The Geddes provides an accurate prediction of boundary crossing for water(1)/ethanol(2)/methanol(3) mixture.

For various vapor compositions entering any given stage, we have plotted in Figure 38c the actual composition vector $(y_{i,L} - y_{i,E})$, calculated from the NEQ model (taking bubble diameter of 4.5 mm) along with the equilibrium vector $(y_i^* - y_{i,E})$. The angle between the NEQ trajectory (red line) and the EQ trajectory (blue line) increases when the differences in the component efficiencies increase. If all the component efficiencies were equal to one another, the NEQ and EQ trajectories would coincide. We see from Figure 38c that the NEQ trajectory has a tendency to cut across to the right of the EQ trajectory, precisely as has been observed in Run T4-13; cf. Figure 32. It is this tendency to cut towards the right of the composition space that causes boundary crossing. By performing several NEQ simulations with various starting compositions of the vapor entering the condenser we can determine the region within which the column trajectories will cross the distillation boundary and end up with reboiler

compositions in the right region. This boundary crossing region is shown as the orange shaded area in Figure 38d.

19. Boundary crossing in water/ethanol/methylacetate mixture

Consider distillation of water(1)/ethanol(2)/methylacetatel(3) mixture in a tray column operating at total reflux at a total pressure of 101.3 kPa. For a specified tray, the composition of the vapor entering the tray is y_{10} = 0.095, y_{20} = 0.6345, and y_{30} = 0.2705. The chosen vapor composition is right of the distillation boundary. For total reflux operations, the compositions of the liquid leaving that stage will be equal to that of the vapor entering the stage, i.e. x_1 = 0.095, x_2 = 0.6345, and x_3 = 0.2705. The composition of vapor in equilibrium with the liquid leaving the tray can be determined using the NRTL parameters provided in Table **15**. The bubble point temperature is 337 K and the equilibrium composition is $y_{1,\text{eq}}$ = 0.06324, $y_{2,\text{eq}}$ = 0.36863, and $y_{3,\text{eq}}$ = 0.56813. The final equilibrated composition is also right of the distillation boundary, as is to be expected.

The driving forces are $\Delta y_1 = y_{10} - y_{1,eq} = 0.03176$, and $\Delta y_2 = y_{20} - y_{2,eq} = 0.26587$.

The values of the vapor phase M-S diffusivities of the binary pairs, calculated using the Fuller-Schettler-Giddings (FSG)[32] method, are $Đ_{12} = 2$; $Đ_{13} = 1.62$; $Đ_{23} = 7.91\times10^{-5}$ m^{2}s^{-1}. These diffusivities are independent of composition. The differences in the binary pair diffusivities cannot be ignored, as we demonstrate below. At the average composition between the entering compositions and the equilibrated compositions, use of

$$[D] = \begin{bmatrix} \Lambda_{11} & \Lambda_{12} \\ \Lambda_{21} & \Lambda_{22} \end{bmatrix} = \frac{\begin{bmatrix} Đ_{13}\left(x_1 Đ_{23} + (1-x_1)Đ_{12}\right) & x_1 Đ_{23}\left(Đ_{13} - Đ_{12}\right) \\ x_2 Đ_{13}\left(Đ_{23} - Đ_{12}\right) & Đ_{23}\left(x_2 Đ_{13} + (1-x_2)Đ_{12}\right) \end{bmatrix}}{x_1 Đ_{23} + x_2 Đ_{13} + x_3 Đ_{12}}$$

results in

$$[D] = \begin{bmatrix} 1.79479 & -0.01346 \\ -0.56871 & 0.83543 \end{bmatrix} \times 10^{-5} \text{ m}^2 \text{ s}^{-1}$$

in which the D_{21} is seen to non-negligible in comparison with D_{22}. We can also determine a "magnitude" of the Fick diffusivity for use in the calculation of the Fourier number: $|D|^{1/2} = 1.22\times10^{-5}$ in order to plot the results in terms of dimensionless times.

The diffusion equilibration trajectory, calculated using Geddes model is shown in Figure 39a. Figure 39b presents a plot of the component Murphree efficiencies, E_i, as function of the Fourier number. The curvilinear equilibration trajectory crosses the distillation boundary during a portion of this traject.

The Murphree point efficiency of ethanol is the lowest; this is because of the negative contribution of the $D_{21}\Delta y_1$. A lower amount of ethanol is transferred to the liquid phase than predicted by an uncoupled equation; i.e. the vapor phase is richer in ethanol. The component efficiency of water is higher than that of partner species; see Figure 39b. Water is the least volatile of the three components, and its transfer is directed from vapor to the liquid phase; a higher efficiency of water ensures that the liquid phase is richer in water than anticipated on the basis of equal component efficiencies.

The contact time of the bubble with the liquid phase is finite. For a 4.5 mm bubble, with a rise velocity of 0.2 m s^{-1} in a dispersion of height 9.2 mm, the contact time t = 0.046 s; these are the input parameters used by Springer et al. in the NEQ model implementation.[23]

For this contact time, the composition of the vapor bubble leaving the tray is

y_1 =0.06778, y_2 = 0.45057, and y_3 = 0.48165.

This vapor composition is on the other side of the distillation boundary. Such boundary crossing is observed in Run T3-23 of the experiments of Springer et al.[21, 23, 25, 26] (cf. Figure 33). The component efficiency of water is higher than that of partner species; see Figure 39b. Water is the least volatile of the three components, and its transfer is directed from vapor to the liquid phase; a higher efficiency of water ensures that the liquid phase is richer in water than anticipated on the basis of equal component efficiencies.

The time-averaged mass transfer coefficient for the dispersed bubbles, for contact time t = 0.046 s is

$$[k_d] = -\ln[Q]\frac{d_{bubble}}{6t}$$

For t = 0.046 s, we have the matrix describing the departure from equilibrium is

$$[Q] = \begin{bmatrix} 0.12238 & 2.43476\times10^{-3} \\ 0.10287 & 0.2959 \end{bmatrix}$$

and

$$[k_d] = \begin{bmatrix} 343.22267 & -2.0244 \\ -85.52786 & 198.94608 \end{bmatrix} \times 10^{-4}$$

If the diffusion coupling effects are completely ignored, and the simplest Fickian relation

$$J_i = -c_t D \frac{dx_i}{dz}; \quad i = 1,2,3$$

is employed, the equilibration trajectory will be linear, running parallel to the residue curves (pink lines) in Figure 39a.

Let us examine what influence inclusion of liquid phase mass transfer resistance has on the composition trajectories.

At the liquid composition on the tray: x_1 = 0.095, x_2 = 0.6345, and x_3 = 0.2705, we calculate the following values of the M-S diffusivities of the binary pairs

$$Đ_{12} = 6.06; \quad Đ_{13} = 4.95; \quad Đ_{23} = 3.1 \times 10^{-9} \text{ m}^2\text{s}^{-1}$$

For estimation of the Fick diffusivity, we use the approximation[6]

$$[D] = |\Lambda|^{1/2} [\Gamma]$$

The value of the scalar diffusivity is

$$|\Lambda|^{1/2} = \sqrt{\frac{Đ_{12} Đ_{13} Đ_{23}}{x_1 Đ_{23} + x_2 Đ_{13} + x_3 Đ_{12}}} = 4.28 \times 10^{-9} \text{ m}^2\text{s}^{-1}$$

The matrix of thermodynamic factors is

$$[\Gamma] = \begin{bmatrix} 0.81047 & -0.06719 \\ -0.27874 & 0.67141 \end{bmatrix}$$

The Fick diffusivity matrix in the liquid phase is calculated as

$$[D] = |\Lambda|^{1/2} [\Gamma] = \begin{bmatrix} 3.46945 & -0.28763 \\ -1.19322 & 2.874181 \end{bmatrix} \times 10^{-9}$$

The mass transfer coefficient external to the bubble can be estimated from the surface renewal theory[15, 16]

$$[k_c] = 2\sqrt{\frac{[D]}{\pi t_{renewal}}}$$

The characteristic time for surface renewal can be estimated is $t_{renewal} = d_{bubble}/V_{bubble}$ = 0.0225 s; this value is lower than the time the bubble takes to rise through the dispersion, 0.046 s.

For a surface renewal time of 0.0225 s, the mass transfer in the continuous liquid phase can be estimated from the surface renewal theory

$$[k_c] = 2\sqrt{\frac{[D]}{\pi t_{renewal}}} = \begin{bmatrix} 4.41342 & -0.19315 \\ -0.80125 & 4.0137 \end{bmatrix} \times 10^{-4}$$

The overall mass transfer coefficient can be calculated from the addition of resistances formula

$$[K_{Od}]^{-1} = [k_d]^{-1} + \frac{c_{tV,d}}{c_{tL,c}} \begin{bmatrix} \frac{y_{1,eq}}{x_1} & 0 \\ 0 & \frac{y_{2,eq}}{x_2} \end{bmatrix} [k_c]^{-1}$$

Inserting the values of the partial mass transfer coefficients, we have for the overall mass transfer coefficients

$$[K_{Od}]^{-1} = \begin{bmatrix} 343.22267 & -2.0244 \\ -85.52786 & 198.94608 \end{bmatrix}^{-1} \times 10^4 + \frac{36.16254}{1.45983 \times 10^4} \begin{bmatrix} \frac{0.06324}{0.095} & 0 \\ 0 & \frac{0.36863}{0.6345} \end{bmatrix} \begin{bmatrix} 4.41342 & -0.19315 \\ -0.80125 & 4.0137 \end{bmatrix}^{-1} \times 10^4$$

The matrix of overall mass transfer coefficients is

$$[K_{Od}] = \begin{bmatrix} 304.303387 & -2.69663 \\ -74.45095 & 185.81078 \end{bmatrix} \times 10^{-4}.$$

We note that $[K_{Od}] \approx [k_d]$, indicating that the mass transfer is controlled by diffusion within the vapor bubbles; the liquid phase mass transfer resistance is of negligible importance.

The matrix for the overall number of transfer units can be calculated from

$$[NTU_{Od}] = [K_{Od}]at$$

The interfacial area per unit volume of bubble is

$$a = \frac{6}{d_{bubble}} = 1.333 \times 10^3$$

Therefore, for contact time $t = 0.046$ s is

$$[NTU_{Od}] = \begin{bmatrix} 1.86639 & -0.01654 \\ -0.45663 & 1.13964 \end{bmatrix}$$

The matrix describing departure from equilibrium can be determined from

$$[Q] = \exp[-[NTU_{Od}]]$$

$$[Q] = \begin{bmatrix} 0.15544 & 3.76551 \times 10^{-3} \\ 0.10396 & 0.3209 \end{bmatrix}$$

The composition of the vapor bubble exiting the tray at $t = 0.046$ s is determined from

$$(y - x_{eq}) = [Q](y_0 - x_{eq})$$

The calculated value is

$y_1 = 0.06918$, $y_2 = 0.45725$, and $y_3 = 0.47357$.

This vapor composition is very close to the value calculated above by ignoring the liquid phase resistance. Boundary crossing persists even if we ignore the liquid phase mass transfer resistance. The Geddes provides an accurate prediction of boundary crossing for the system water(1)/ethanol(2)/methylacetate(3).

For various vapor compositions entering any given stage, we have plotted in Figure 39c the actual composition vector $(y_{i,L} - y_{i,E})$, calculated from the NEQ model (taking bubble diameter of 4.5 mm) along with the equilibrium vector $(y_i^* - y_{i,E})$. The angle between the NEQ trajectory (red line) and the EQ trajectory (blue line) increases when the differences in the component efficiencies increase. If all the component efficiencies were equal to one another, the NEQ and EQ trajectories would coincide. We see from Figure 39c that the NEQ trajectory has a tendency to cut across to the right of the EQ trajectory, precisely as has been observed in Run T3-23; cf. Figure 33. It is this tendency to cut towards the right of the composition space that causes boundary crossing. By performing several NEQ

simulations with various starting compositions of the vapor entering the condenser we can determine the region within which the column trajectories will cross the distillation boundary and end up with reboiler compositions in the right region. This boundary crossing region is shown as the orange shaded area in Figure 39d.

20. Boundary crossing in heterogeneous azeotropic distillation

For heterogeneous azeotropic distillation, experimental data on column composition trajectories for water/acetone/toluene, and water/ethanol/cyclohexane show boundary crossing characteristics that are attributable to diffusional coupling.[22]

The experimental data for Run WAT-1, and WAT-2 for water(1)/acetone(2)/toluene(3) mixtures are shown in Figure 40, and Figure 41. The NEQ model simulations, taking due account of coupling in both vapor and liquid phases are indicated by the continuous red lines. The EQ model simulations (i.e. ignoring diffusional coupling, and assuming that the efficiencies of all components are the same) are indicated by the dashed red lines.

For the heterogeneous azeotropic distillation with water(1)/ethanol(2)/cyclohexane(3) mixture, boundary crossing is observed in Run WEC-12; see Figure 42. For Run WEC-8, no boundary crossing is observed; see Figure 43.

For rationalization and quantitative description of the observed experimental boundary crossing phenomena, Springer et al.[22] used rigorous non-equilibrium (NEQ) stage-wise contacting model, as implemented in ChemSep.[18, 30] The NEQ model uses the Maxwell-Stefan formulation for diffusion in the vapor and the two liquid phases. There are four mass transfer resistances to contend with, as sketched in Figure 44; Springer et al. provide the modelling details. [22]

The important conclusion reached in their work is that boundary crossing effects are primarily attributable to diffusional coupling effects, that cause the component Murphree efficiencies to be unequal to one another. Unequal component efficiencies cause column composition trajectories to deviate from those of the residue curve maps. Put another way, the NEQ model does not follow the tramline guides of the RCM.

21. Separating azeotropic alcohol/water mixture by diffusional distillation

If we distill a 2-propanol(1)/water (2) mixture of azeotropic composition in say a sieve tray column, the compositions of the vapor and liquid phases will remain unchanged as the vapor bubbles traverse along the height of the dispersion. The situation is changed if the distillation is carried out in the presence of an inert gas, say nitrogen (3); cf. Figure 45. Separation of the azeotropic mixture is attained because of diffusional coupling effects. For quantitative demonstration of this separation, let us consider a sieve tray column operating at a total pressure of 101.3 kPa and temperature of 313.15 K. The liquid composition entering the tray is x_1 = 0.6226, x_2 = 0.3774; this composition corresponds to that of the azeotrope at 313.15 K, calculated using the NRTL parameters provided in Table 19.

We bubble pure nitrogen (3) through the tray, i.e. the vapor composition entering the tray is y_{1E} = 0.0, y_{2E} = 0.0, y_{3E} = 1.0. If the vapor bubble is allowed to equilibrate, the composition of the equilibrated vapor is $y_{1,eq}$ = 0.09836, $y_{2,eq}$ = 0.05963, y_{3E} = 0.84201. The ratio of the compositions of water (2) to that of 2-propanol (1) at equilibrium, $\frac{y_{2,eq}}{y_{1,eq}}$ is that same as that of the ratio of water to 2-propanol in the liquid phase, $\frac{y_{2,eq}}{y_{1,eq}} = \frac{x_2}{x_1} = 0.606$.

Let us consider the dispersion to consist of uniform and rigid vapor bubbles of diameter, d_{bubble}. The transient equilibration process within a rigid spherical bubble is described by Geddes model that was originally developed for describing binary diffusion inside vapor bubbles on distillation trays.[7] For ternary mixtures, the Geddes model can be written in two-dimensional matrix differential equation[4, 31]

$$\left(y - x_{eq}\right) = [Q]\left(y_0 - x_{eq}\right); \quad [Q] \equiv \frac{6}{\pi^2}\sum_{m=1}^{\infty}\frac{1}{m^2}\exp\left[-m^2\pi^2\frac{4[D]t}{d_{bubble}^2}\right]$$

In the above equation, $\left(y_0\right)$ denotes the vapor composition entering the tray. The Sylvester theorem, detailed in Appendix A of Taylor and Krishna,[4] is required for explicit calculation of the composition trajectories described by the Geddes model. For vapor bubbles rising on a sieve tray, the effective

contact time of the dispersed phase bubbles with the surrounding continuous phase is $t = h_f / V_{bubble}$, where h_f is the froth dispersion height, and V_{bubble} is the bubble rise velocity.

We choose a bubble diameter, d_{bubble} = 4.5 mm, rising at a velocity V_{bubble} = 0.2 m s^{-1} through a froth dispersion h_f of height 9.2 m. These parameters are representative of the sieve-tray experimental set of Springer et al.[21, 23, 25, 26]

In Figure 46a, the mole fractions of 2-propanol (1) and water (2) are plotted as a function of time, *t*. The ratio of the mole fraction of water (2) to that of 2-propanol (1) in the vapor phase as a function of time, *t* is plotted in Figure 46a; this ratio equilibrates to the value of $\frac{y_{2,eq}}{y_{1,eq}} = \frac{x_2}{x_1} = 0.606$, as is expected. During the initial transience, however, the vapor is richer in water vapor than 2-propanol. For the contact time of the vapor bubbles, $t = h_f / V_{bubble}$ = 0.46 s, the ratio of the mole fraction of water (2) to that of 2-propanol (1) is 0.738; this value is significantly higher than that of the azeotrope as seen in Figure 46b. This implies that the 2-propanol/water azeotrope can be separated by bubbling nitrogen through the tray.

In order to understand the mechanism of the separation, let us examine the diffusivities and fluxes in the ternary mixture. The values of the vapor phase M-S diffusivities of the three binary pairs at 313.15 K, calculated using the Fuller-Schettler-Giddings[32] method, are $Đ_{12} = 1.47;\quad Đ_{13} = 1.15;\quad Đ_{23} = 2.81\times10^{-5}$ m^{2}s^{-1}; these diffusivities are independent of composition. At the average composition between the entering vapor compositions and the equilibrated compositions, the Fick matrix of diffusivities $[D] = \begin{bmatrix} 1.186 & -0.15399 \\ 0.159 & 2.16759 \end{bmatrix} \times 10^{-5}$ m^2 s^{-1}. Water vapor is the smallest of the three molecules and the mobility of water molecules in the vapor phase is the highest. This is evident because of the significantly larger value of D_{22} as compared to D_{11}. The driving forces are $\Delta y_1 = y_{10} - y_{1,eq} = -0.09859$, and $\Delta y_2 = y_{1o} - y_{2,eq} = -0.05615$. Both driving forces are negative, i.e. directed from liquid to the vapor phase. The ratio of the flux of water to that of 2-propanol is

$\frac{D_{21}\Delta y_1 + D_{22}\Delta y_2}{D_{11}\Delta y_1 + D_{12}\Delta y_2} = 1.35$. This ratio is higher than that corresponding to the azeotropic composition. Taking account of coupling effects results in a higher proportion of water vapor in the bubble during equilibration. Coupling effects enhance the flux of water, relative to that of 2-propanol, due to two reasons. Firstly, the contribution of $D_{21}\Delta y_1$ has the same sign as that of $D_{22}\Delta y_2$; therefore flux of water is enhanced. Secondly, the contribution of $D_{12}\Delta y_2$ reduces the flux of 2-propanol because D_{12} is negative in sign.

The experiments of Fullarton and Schlunder[34] confirm that the concept of diffusion distillation is effective for separation of 2-propanol/water azeotrope.

If helium is used as inert gas in place of nitrogen, the separations are less effective; see the comparisons of the ratio of water to 2-propanol in the vapor phase presented in Figure 46c. With helium, the ratio of the flux of water to that of 2-propanol is $\frac{D_{21}\Delta y_1 + D_{22}\Delta y_2}{D_{11}\Delta y_1 + D_{12}\Delta y_2} = 0.85$; this ratio is lower than that with nitrogen as inert gas. Use of argon as inert gas improves the separations because in this case the ratio of the flux of water to that of 2-propanol is $\frac{D_{21}\Delta y_1 + D_{22}\Delta y_2}{D_{11}\Delta y_1 + D_{12}\Delta y_2} = 1.46$.

Figure 46d compares the diffusion equilibration trajectories in composition space. Coupling effects are strongest with argon and this explains why the equilibration trajectories deviates the most from the linear equilibration that results with uncoupled diffusion.

Diffusional distillation can be also used to separate ethanol/water mixture of azeotropic composition. For quantitative demonstration of this separation, let us consider a sieve tray column operating at a total pressure of 101.3 kPa and temperature of 313.15 K. The liquid composition entering the tray is x_1 = 0.87013, x_2 = 0.12987; this composition corresponds to that of the azeotrope at 313.15 K, calculated using the NRTL parameters provided in Table 20.

We bubble pure nitrogen (3) through the tray, i.e. the vapor composition entering the tray is y_{1E} = 0.0, y_{2E} = 0.0, y_{3E} = 1.0. If the vapor is allowed to equilibrate, the composition of the equilibrated vapor is $y_{1,eq}$ = 0.15266, $y_{2,eq}$ = 0.02279, y_{3E} = 0.82455. The ratio of the compositions of water (2) to that of

ethanol (1) at equilibrium, $\frac{y_{2,eq}}{y_{1,eq}}$ is that same as that of the ratio of water to ethanol in the liquid phase,

$\frac{y_{2,eq}}{y_{1,eq}} = \frac{x_2}{x_1} = 0.14925$.

In Figure 47a, the mole fractions of ethanol (1) and water (2) are plotted as a function of time, *t*. The ratio of the mole fraction of water (2) to that of ethanol (1) in the vapor phase as a function of time, *t* is plotted in Figure 47b; this ratio equilibrates to the value of $\frac{y_{2,eq}}{y_{1,eq}} = \frac{x_2}{x_1} = 0.14925$, as is expected. During the initial transience, however, the vapor is richer in water vapor than ethanol. For the contact time of the vapor bubbles, $t = h_f / V_{bubble}$ = 0.46 s, the ratio of the mole fraction of water (2) to that of ethanol (1) is 0.1726; this value is higher than that of the azeotrope as seen in Figure 47b. This implies that the ethanol/water azeotrope can be separated by bubbling nitrogen through the tray.

In order to understand the mechanism of the separation, let us examine the diffusivities and fluxes in the ternary mixture. The values of the vapor phase M-S diffusivities of the three binary pairs at 313.15 K, calculated using the Fuller-Schettler-Giddings[32] method, are $Đ_{12} = 1.75$; $Đ_{13} = 1.37$; $Đ_{23} = 2.81 \times 10^{-5}$ $m^2 s^{-1}$; these diffusivities are independent of composition. At the average composition between the entering vapor compositions and the equilibrated compositions, the Fick matrix of diffusivities $[D] = \begin{bmatrix} 1.38892 & -0.20907 \\ 0.04335 & 2.21543 \end{bmatrix} \times 10^{-5}$ m^2 s^{-1}. Water vapor is the smallest of the three molecules and the mobility of water molecules in the vapor phase is the highest. This is evident because of the significantly larger value of D_{22} as compared to D_{11}. The driving forces are $\Delta y_1 = y_{10} - y_{1,eq} = -0.15266$, and $\Delta y_2 = y_{1o} - y_{2,eq} = -0.02278$. Both driving forces are negative, i.e. directed from liquid to the vapor phase. The ratio of the flux of water to that of ethanol is $\frac{D_{21}\Delta y_1 + D_{22}\Delta y_2}{D_{11}\Delta y_1 + D_{12}\Delta y_2} = 0.27546$. This ratio is higher than that corresponding to the azeotropic composition. Taking account of coupling effects results in a higher proportion of water vapor in the bubble during

equilibration. Coupling effects enhance the flux of water, relative to that of ethanol, due to two reasons. Firstly, the contribution of $D_{21}\Delta y_1$ has the same sign as that of $D_{22}\Delta y_2$; therefore flux of water is enhanced. Secondly, the contribution of $D_{12}\Delta y_2$ reduces the flux of ethanol because D_{12} is negative in sign.

If helium is used as inert gas in place of nitrogen, the separations are less effective; see the comparisons of the ratio of water to ethanol in the vapor phase presented in Figure 47c. With helium, the ratio of the flux of water to that of ethanol is $\frac{D_{21}\Delta y_1 + D_{22}\Delta y_2}{D_{11}\Delta y_1 + D_{12}\Delta y_2} = 0.197$; this ratio is lower than that with nitrogen as inert gas. Use of argon as inert gas improves the separation of the azeotrope because the ratio of the flux of water to that of ethanol is $\frac{D_{21}\Delta y_1 + D_{22}\Delta y_2}{D_{11}\Delta y_1 + D_{12}\Delta y_2} = 0.291$.

Figure 47d compares the diffusion equilibration trajectories in composition space. Coupling effects are strongest with argon and this explains why the equilibration trajectories deviates the most from the linear equilibration that results with uncoupled diffusion.

Experimental confirmation of the validity of the diffusional distillation concept to separate ethanol/water azeotrope is provided by Singh and Prasad.[35] Of particular interest is their experimental observation that use of helium as inert gas yields lower separation selectivity as compared to nitrogen. Singh and Prasad[35] also report that use of argon as inert gas improves the separation selectivity.

The technique of bubbling inert gas to break azeotropes also applies to non-aqueous mixtures such as acetone/methanol. For quantitative demonstration of this separation, let us consider a sieve tray column operating at a total pressure of 101.3 kPa and temperature of 313.15 K. The liquid composition entering the tray is $x_1 = 0.85259$, $x_2 = 0.14741$; this composition corresponds to that of the azeotrope at 313.15 K, calculated using the NRTL parameters provided in Table 21

We bubble pure nitrogen (3) through the tray, i.e. the vapor composition entering the tray is $y_{1E} = 0.0$, $y_{2E} = 0.0$, $y_{3E} = 1.0$. If the vapor is allowed to equilibrate, the composition of the equilibrated vapor is $y_{1,eq} = 0.4798$, $y_{2,eq} = 0.08296$, $y_{3E} = 0.43724$. The ratio of the compositions of methanol (2) to that of

acetone (1) at equilibrium, $\frac{y_{2,eq}}{y_{1,eq}}$ is that same as that of the ratio of water to ethanol in the liquid phase, $\frac{y_{2,eq}}{y_{1,eq}} = \frac{x_2}{x_1} = 0.1729$.

In Figure 48a, the mole fractions of acetone (1) and methanol (2) are plotted as a function of time, *t*. The ratio of the mole fraction of methanol (2) to that of acetone (1) in the vapor phase as a function of time, *t* is plotted in Figure 48b; this ratio equilibrates to the value of $\frac{y_{2,eq}}{y_{1,eq}} = \frac{x_2}{x_1} = 0.129$, as is expected. During the initial transience, however, the vapor is richer in water vapor than ethanol. For the contact time of the vapor bubbles, $t = h_f / V_{bubble}$ = 0.46 s, the ratio of the mole fraction of methanol (2) to that of acetone (1) is 0.1908; this value is higher than that of the azeotrope as seen in Figure 48b. This implies that the acetone/methanol azeotrope can be separated by bubbling nitrogen through the tray.

In order to understand the mechanism of the separation, let us examine the diffusivities and fluxes in the ternary mixture. The values of the vapor phase M-S diffusivities of the three binary pairs at 313.15 K, calculated using the Fuller-Schettler-Giddings[32] method, are $Đ_{12} = 0.98$; $Đ_{13} = 1.186$; $Đ_{23} = 1.79 \times 10^{-5}$ $m^2 s^{-1}$; these diffusivities are independent of composition. At the average composition between the entering vapor compositions and the equilibrated compositions, the Fick matrix of diffusivities $[D] = \begin{bmatrix} 1.17224 & 0.11647 \\ 0.05285 & 1.3305 \end{bmatrix} \times 10^{-5}$ m^2 s^{-1}. The driving forces are $\Delta y_1 = y_{10} - y_{1,eq} = -0.4798$, and $\Delta y_2 = y_{1o} - y_{2,eq} = -0.08296$. Both driving forces are negative, i.e. directed from liquid to the vapor phase. The ratio of the flux of methanol to that of acetone is $\frac{D_{21}\Delta y_1 + D_{22}\Delta y_2}{D_{11}\Delta y_1 + D_{12}\Delta y_2} = 0.23725$. This ratio is higher than that corresponding to the azeotropic composition. Taking account of coupling effects results in a higher proportion of methanol vapor in the bubble during equilibration.

If helium is used as inert gas in place of nitrogen, the separations are less effective; see the comparisons of the ratio of methanol to acetone in the vapor phase presented in Figure 48c. With helium, the ratio of the flux of water to that of ethanol is $\frac{D_{21}\Delta y_1 + D_{22}\Delta y_2}{D_{11}\Delta y_1 + D_{12}\Delta y_2} = 0.19682$; this ratio is lower than that with nitrogen as inert gas. Use of argon as inert gas improves the separation of the azeotrope because the ratio of the flux of water to that of ethanol is $\frac{D_{21}\Delta y_1 + D_{22}\Delta y_2}{D_{11}\Delta y_1 + D_{12}\Delta y_2} = 0.24574$.

Figure 48d compares the diffusion equilibration trajectories in composition space. Coupling effects are strongest with argon and this explains why the equilibration trajectories deviates the most from the linear equilibration that results with uncoupled diffusion.

22. Notation

A_m	constant in Kronig-Brink model, dimensionless
c_t	total molar concentration of mixture, mol m^{-3}
d_{bubble}	bubble diameter, m
d_{drop}	droplet diameter, m
$Đ_{ij}$	M-S binary pair diffusivity, m^2 s^{-1}
$[D]$	Fick diffusivity matrix, m^2 s^{-1}
$\lvert D \rvert$	Determinant of the Fick diffusivity matrix, m^4 s^{-2}
$\lvert D \rvert^{1/2}$	Square-root of determinant of $[D]$, m^2 s^{-1}
E_i	Component Murphree efficiency, dimensionless
Fo	Fourier number, dimensionless
$[I]$	Identity matrix, dimensionless
J_i	molar diffusion flux of species *i* with respect to u, mol m^{-2} s^{-1}
$[k]$	Matrix of mass transfer coefficients, m s^{-1}
$[K]$	Matrix of overall mass transfer coefficients, m s^{-1}
$[NTU]$	Matrix of number of transfer units, dimensionless
p	system pressure, Pa
$[Q]$	matrix quantifying fractional departure from equilibrium, dimensionless
R	gas constant, 8.314 J mol^{-1} K^{-1}
t	time, s
T	absolute temperature, K
x_i	mole fraction of component *i* in liquid phase, dimensionless
y_i	mole fraction of component *i* in vapor phase, dimensionless
u	molar average mixture velocity, m s^{-1}
V_{bubble}	bubble rise velocity, m s^{-1}
V_{drop}	droplet rise velocity, m s^{-1}

z	direction coordinate, m

Greek letters

β	constant used for equilibration in Lewis stirred cell, m^{-2}
δ_{ij}	Kronecker delta, dimensionless
γ_i	activity coefficient of component *i*, dimensionless
$[\Gamma]$	matrix of thermodynamic factors, dimensionless
$\lvert\Gamma\rvert^{1/2}$	Square-root of determinant of $[\Gamma]$, dimensionless
λ_m	constant in Kronig-Brink model, dimensionless
$[\Lambda]$	matrix defined by Equation (4), $m^2\ s^{-1}$
$\lvert\Lambda\rvert^{1/2}$	Square-root of determinant of $[\Lambda]$, $m^2\ s^{-1}$
μ_i	molar chemical potential, J mol^{-1}

Subscript

0	Referring to starting compositions, $t = 0$
bubble	Referring to bubble
c	Referring to continuous phase
d	Referring to dispersed phase
drop	Referring to droplet
eq	Referring to final equilibrated compositions, $t \to \infty$
E	Referring to vapor compositions entering tray
i	Component number
j	Component number
L	referring to liquid phase
O	referring to overall parameter
L	referring to vapor phase

Table 1. NRTL parameters for heptane(1)/toluene(2)/sulpholane(3). The parameters are taken from Table 6.8 of the PhD dissertation of Meindersma.[36]

	τ_{ij}	τ_{ji}	$\alpha_{ij} = \alpha_{ji}$
	dimensionless	dimensionless	dimensionless
heptane(1)/ toluene(2)	$-0.756 + 48.1/T$	$0.269 + 31.74/T$	0.3
heptane(1)/ sulpholane(3)	$-0.039 + 1365/T$	$-0.215 + 1188/T$	0.3
toluene(2)/ sulpholane(3)	$-1.057 + 1017/T$	$0.428 - 165.7/T$	0.3

Table 2. The values of A_m and λ_m are tabulated by Sideman and Shabtai.[14]

Integer counter, *m*	A_m	λ_m
1	1.29	1.656
2	0.596	9.08
3	0.386	22.2
4	0.35	36.5
5	0.28	63
6	0.22	89.8
7	0.16	123.8

Table 3. NRTL parameters for NMP(1)/propylbenzene(2)/tetradecane(3) at 298.15 K. The parameters are from Al-Jimaz et al.[37]

	$\tau_{ij} = A_{ij}/T$	$\tau_{ji} = A_{ji}/T$	$\alpha_{ij} = \alpha_{ji}$
	dimensionless	dimensionless	dimensionless
NMP(1)/ propylbenzene(2)	-2.8661	1.5931	0.2
NMP(1)/tetradecane(3)	3.4745	0.4103	0.2
propylbenzene(2)/ tetradecane(3)	0.2851	-2.678	0.2

Table 4. NRTL parameters for glyercol(1)/acetone(2)/water(3) at 298 K. These parameters are from Krishna et al.[5]

	$\tau_{ij} = A_{ij}/T$	$\tau_{ji} = A_{ji}/T$	$\alpha_{ij} = \alpha_{ji}$
	dimensionless	dimensionless	dimensionless
glycerol(1)/acetone(2)	0.868	2.467	0.2
glycerol(1)/water(3)	-1.29	-1.52	0.2
acetone(2)/water(3)	-0.665	2.095	0.2

Table 5. NRTL parameters for water(1)/acetone(2)/phenol(3) at 323.15 K. These parameters are taken from Table 2 of Zuber et al.[38]

	$\tau_{ij} = A_{ij}/T$	$\tau_{ji} = A_{ji}/T$	$\alpha_{ij} = \alpha_{ji}$
	dimensionless	dimensionless	dimensionless
water(1)/acetone(2)	0.1024	1.826	0.2
water(1)/phenol(3)	5.332	-1.585	0.2
acetone(2)/phenol(3)	-1.504	-2.78	0.2

Table 6. UNIQUAC parameters for acetone(1)/ethyl-acetate(2)/water(3) at 293 K. These parameters are from Pertler.[39]

	r_i	q_i
	dimensionless	dimensionless
acetone(1)	2.5735	2.336
ethyl-acetate(2)	3.4786	3.116
water(3)	0.92	1.4

	$\tau_{ij} = \exp(-A_{ij}/T)$	$\tau_{ji} = \exp(-A_{ji}/T)$
	dimensionless	dimensionless
acetone(1)/ethyl-acetate(2)	1.3068	0.827
acetone(1)/water(3)	0.488	1.328
ethyl-acetate(2)/water(3)	0.2538	0.7705

Table 7. UNIQUAC parameters for water(1)/caprolactam(2)/toluene(3) at 298.15 K. These parameters are from Table 1, Chapter 7 of the PhD dissertation of Bollen.[40]

	r_i	q_i
	dimensionless	dimensionless
water(1)	0.92	1.4
caprolactam(2)	4.6106	3.724
toluene(3)	3.9928	2.968

	$\tau_{ij} = A_{ij}/T$	$\tau_{ji} = A_{ji}/T$
	dimensionless	dimensionless
water(1)/caprolactam(2)	0.1027043	3.647516849
water(1)/ toluene(3)	0.2563201	0.0964476
caprolactam(2)/toluene(3)	0.3324973	1.4351863

Table 8. NRTL parameters for water(1)/acetic acid(2)/isophorone(3) at 298.15 K. The parameters are from Colombo et al.[41]

	$\tau_{ij} = A_{ij}/T$	$\tau_{ji} = A_{ji}/T$	$\alpha_{ij} = \alpha_{ji}$
	dimensionless	dimensionless	dimensionless
water(1)/acetic acid (2)	0.7074	0.2455	0.2
water(1)/isophorone(3)	6.466	-0.2852	0.2
Acetic acid(2)/ Isophorone(3)	-1.489	1.381	0.2

Table 9. NRTL parameters for water(1)/acetic acid(2)/MTBE (3) at 298.15 K. The parameters are from Zhang and Wang.[42]

	$\tau_{ij} = A_{ij}/T$	$\tau_{ji} = A_{ji}/T$	$\alpha_{ij} = \alpha_{ji}$
	dimensionless	dimensionless	dimensionless
water(1)/acetic acid (2)	0.354	-1.2151	0.47
water(1)/MTBE(3)	3.9737	1.2998	0.2
Acetic acid(2)/ MTBE(3)	-0.2774	-2.8068	0.37

Table 10. NRTL parameters for [omim][Cl](1)/ethanol(2)/TAEE(3) at 298 K. The parameters are from Aznar.[43]

	$\tau_{ij} = A_{ij}/T$	$\tau_{ji} = A_{ji}/T$	$\alpha_{ij} = \alpha_{ji}$
	dimensionless	dimensionless	dimensionless
[omim][Cl](1)/ethanol(2)	-1.674	-3.035	0.2
[omim][Cl](1)/TAEE(3)	1.365	9.3245	0.204
ethanol(2)/TAEE(3)	0.3034	1.399	0.307

Table 11. UNIQUAC parameters for [bmim][TfO](1)/ethanol(2)/TAEE(3) at 298 K. The parameters are from Tables 2, 3, and 4 of Santiago et al.[44]

	r_i	q_i
	dimensionless	dimensionless
[bmim][TfO]	8.9463	7.135
ethanol(2)	2.5755	2.588
TAEE(3)	5.417	4.712

	$\tau_{ij} = \exp(-A_{ij}/T)$	$\tau_{ji} = \exp(-A_{ji}/T)$
	dimensionless	dimensionless
[bmim][TfO](1)/ethanol(2)	0.8331298	2.91830955
[bmim][TfO](1)/TAEE(3)	1.4677043	0.004246414
ethanol(2)/TAEE(3)	3.74432548	0.048064224

Table 12. NRTL parameters for water(1)/ethanol(2)/cyclohexane (3). These parameters are from the DECHEMA Dortmund data bank, as reported in Table 1 of Springer et al.[22] These parameters are used along with $G_{ij} = \exp\left(-\alpha_{ij}\tau_{ij}\right)$ and $\tau_{ij} = B_{ij}/T$.

Component i	Component j	B_{ij} / K	B_{ji} / K	α_{ij}
Water	Ethanol	557.48	29.09	0.348
Water	Cyclohexane	4422.3	1688.3	0.212
Ethanol	Cyclohexane	440.61	717.68	0.463

Table 13. NRTL parameters for toluene(1)/ethanol(2)/water(3) at 298 K. The toluene/water parameters are from Wang et al.[45] The remaining parameters are from the DECHEMA Dortmund data bank; the ethanol/toluene τ_{ji} has been modified to match experimental binodal data.[46, 47]

	τ_{ij}	τ_{ji}	$\alpha_{ij} = \alpha_{ji}$
	dimensionless	dimensionless	dimensionless
toluene(1)/ethanol(2)	1.938	0.6	0.529
toluene(1)/water(3)	15.219	7.529	0.2
ethanol(2)/water(3)	-0.0978	2.096	0.293

Table 14. NRTL parameters for water(1)/acetone(2)/toluene(3). These parameters are from the DECHEMA Dortmund data bank, as reported in Table 1 of Springer et al.[22] These parameters are used along with $G_{ij} = \exp\left(-\alpha_{ij}\tau_{ij}\right)$ and $\tau_{ij} = B_{ij}/T$.

Component i	Component j	B_{ij} / K	B_{ji} /K	α_{ij}
Water	Acetone	653.89	377.58	0.586
Water	Toluene	2160.8	2839.4	0.200
Acetone	Toluene	-124.77	366.1	0.295

Table 15. NRTL parameters used in homogeneous and heterogeneous distillation systems.

NRTL parameters from Dortmund data bank.
$G_{ij} = \exp(-\alpha_{ij}\tau_{ij})$ and $\tau_{ij} = B_{ij}/T$

Component *i*	Component *j*	B_{ij} / K	B_{ji} / K	α_{ij}
		water/ethanol/acetone		
Water	Ethanol	624.9174	-29.169	0.2937
Water	Acetone	602.6252	330.4768	0.5103
Ethanol	Acetone	188.8983	22.83319	0.3006
		water/methanol/isopropanol		
Water	Methanol	594.6299	-182.6052	0.297
Water	Isopropanol	729.2208	70.6619	0.288
Methanol	Isopropanol	65.71121	-89.74272	0.304
		water/ethanol/methanol		
Water	Ethanol	624.9174	-29.169	0.2937
Water	Methanol	594.6299	-182.605	0.297
Ethanol	Methanol	73.413	-79.1718	0.3029
		water/ethanol/cyclohexane		
Water	Ethanol	557.4826	29.08636	0.3475
Water	Cyclohexane	4422.3	1688.273	0.21159
Ethanol	Cyclohexane	440.6134	717.6762	0.46261
		water/acetone/toluene		
Water	Acetone	653.885	377.577	0.5859
Water	Toluene	2160.78	2839.37	0.2
Acetone	Toluene	-124.774	366.098	0.295
		water/ethanol/methylacetate		
Water	Ethanol	624.9174	-29.169	0.2937
Water	Methylacetate	796.8165	334.6706	0.35
Ethanol	Methylacetate	198.9705	134.162	0.3

Table 16. Sieve tray distillation hardware details

Parameter	value
Column diameter	0.8 m
Tray spacing	0.6 m
Number of flow passes	1
Liquid flow path length	0.52 m
Downcomer clearance	0.038 m
Deck thickness	0.0025 m
Hole diameter	0.005 m
Hole pitch	0.012 m
Active area	76.0 %
Total hole area	15.0 %
Downcomer area	12.0 %
Weir type	Segmental
Weir length	0.7408 m
Weir height	0.05 m

Table 17. Specifications of operating conditions for design for water(1)/ethanol(2)/acetone(3) mixtures.

Parameter	Value
Total pressure	101.3 kPa
Pressure drop per tray	0
Reflux ratio	3
Bottoms flow rate	1.75 mol s^{-1}
Mole fractions in feed (left of distillation boundary)	$x_1 = 0.015$ $x_2 = 0.25$ $x_3 = 0.735$
Mole fractions in feed (right of distillation boundary)	$x_1 = 0.2$ $x_2 = 0.05$ $x_3 = 0.75$

Table 18. NRTL parameters for water(1)/ethanol(2)/acetone (3). These parameters are from the DECHEMA Dortmund data bank, as reported in Table 1 of Springer et al.[23] These parameters are used along with $G_{ij} = \exp\left(-\alpha_{ij}\tau_{ij}\right)$ and $\tau_{ij} = B_{ij}/T$.

Component i	Component j	B_{ij} / K	B_{ji} / K	α_{ij}
Water	Ethanol	624.9174	-29.169	0.2937
Water	Acetone	602.6252	330.4768	0.5103
Ethanol	Acetone	188.8983	22.83319	0.3006

Table 19. NRTL parameters for 2-propanol(1)/water (2) mixture. These parameters are from the DECHEMA Dortmund data bank, and are used along with $G_{ij} = \exp\left(-\alpha_{ij}\tau_{ij}\right)$.

Component 1	Component 2	τ_{12}	τ_{21}	α_{12}
2-propanol(1)	water (2)	$\tau_{12} = \frac{70.6619}{T}$	$\tau_{21} = \frac{729.2208}{T}$	0.288

Table 20. NRTL parameters for ethanol(1)/water (2) mixture. These parameters are from the DECHEMA Dortmund data bank, and are used along with $G_{ij} = \exp\left(-\alpha_{ij}\tau_{ij}\right)$.

Component 1	Component 2	τ_{12}	τ_{21}	α_{12}
ethanol(1)	water (2)	$\tau_{12} = -\frac{29.169}{T}$	$\tau_{21} = \frac{624.9174}{T}$	0.2937

Table 21. NRTL parameters for acetone(1)/methanol (2) mixture. These parameters are from the Kurihara et al.[48], and are used along with $G_{ij} = \exp\left(-\alpha_{ij}\tau_{ij}\right)$.

Component 1	Component 2	τ_{12}	τ_{21}	α_{12}
ethanol(1)	water (2)	$\tau_{12} = \frac{770.15}{RT}$	$\tau_{21} = \frac{1023.18}{RT}$	0.1099

23. References

(1) PTC MathCad 15.0, http://www.ptc.com/, PTC Corporate Headquarters, Needham, 3 November 2015.

(2) Krishna, R.; Goswami, A. N.; Nanoti, S. M.; Rawat, B. S.; Khanna, M. K.; Dobhal, J. Extraction of aromatics from 63-69 ^{o}C Naphtha fraction for food grade hexane production using sulpholane and NMP as solvents, *Indian Journal of Technology* **1987**, *25*, 602-606.

(3) Seader, J. D.; Henley, E. J.; Roper, D. K. *Separation Process Principles*; 3rd Edition, John Wiley: New York, 2011.

(4) Taylor, R.; Krishna, R. *Multicomponent mass transfer*; John Wiley: New York, 1993.

(5) Krishna, R.; Low, C. Y.; Newsham, D. M. T.; Olivera Fuentes, C. G.; Paybarah, A. Liquid Liquid Equilibrium in the System Glycerol Water Acetone at 25 ^{o}C, *Fluid Phase Equilib.* **1989**, *45*, 115-120.

(6) Krishna, R. Serpentine Diffusion Trajectories and the Ouzo Effect in Partially Miscible Ternary Liquid Mixtures, *Phys. Chem. Chem. Phys.* **2015**, *17*, 27428-27436.

(7) Geddes, R. L. Local efficiencies of bubble-plate fractionators, *Trans. Am. Inst. Chem. Engrs.* **1946**, *42*, 79-105.

(8) Krishna, R.; Nanoti, S. M.; Goswam, A. N. Mass-Transfer Efficiency of Sieve Tray Extraction Columns, *Ind. Eng. Chem. Res.* **1989**, *28*, 642-644.

(9) Treybal, R. E. *Mass-Transfer Operations*; 3rd Edition, McGraw-Hill: New York, 1980.

(10) Robbins, L. A.; Cusack, R. W. *Chaper 15, Liquid-Liquid Extraction Operations and Equipment*. Perry's Chemical Engineers' Handbook; 7th Edition, Edited by R.H. Perry and D.W. Green, McGraw-Hill: New York, 1999.

(11) Krishna, R.; van Baten, J. M. The Darken relation for multicomponent diffusion in liquid mixtures of linear alkanes. An investigation using Molecular Dynamics (MD) simulations, *Ind. Eng. Chem. Res.* **2005**, *44*, 6939-6947.

(12) Reid, R.C.; Prausnitz, J. M.; Poling, B. E. *The Properties of Gases and Liquids*; 4th Edition, McGraw-Hill: New York, 1986.

(13) Kronig, R.; Brink, J. C. On the Theory of Extraction from Falling Droplets, *Appl. Sci. Res.* **1950**, *A2*, 142-154.

(14) Sideman, S.; Shabtai, H. Direct-Contact Heat Transfer Between a Single Drop and an Immiscible Liquid Medium, *Can. J. Chem. Eng.* **1964**, *42*, 107-116.

(15) Sherwood, T. K.; Pigford, R. L.; Wilke, C. R. *Mass Transfer*; Mc-Graw Hill: New York, U.S.A., 1975.

(16) Cussler, E. L. *Diffusion: Mass Transfer in Fluid Systems*; 3rd Edition, Cambridge University Press: Cambridge, 2007.

(17) Krishna, R.; Low, C. Y.; Newsham, D. M. T.; Olivera-Fuentes, C. G.; Standart, G. L. Ternary mass transfer in liquid-liquid extraction, *Chem. Eng. Sci.* **1985**, *40*, 893-903.

(18) Taylor, R.; Krishna, R.; Kooijman, H. Real-World Modeling of Distillation, *Chem. Eng. Prog.* **2003**, *99 (7)*, 28-39.

(19) Krishna, R.; Martinez, H. F.; Sreedhar, R.; Standart, G. L. Murphree point efficiencies in multicomponent systems, *Trans. Inst. Chem. Eng.* **1977**, *55*, 178-183.

(20) Krishna, R.; Standart, G. L. Mass and energy transfer in multicomponent systems, *Chem. Eng. Commun.* **1979**, *3*, 201-275.

(21) Springer, P. A. M.; Baur, R.; Krishna, R. Influence of interphase mass transfer on the composition trajectories and crossing of boundaries in ternary azeotropic distillation, *Sep. Purif. Technol.* **2002**, *29*, 1-13.

(22) Springer, P. A. M.; Baur, R.; Krishna, R. Composition trajectories for heterogeneous azeotropic distillation in a bubble-cap tray column: Influence of mass transfer, *Chem. Eng. Res. Des.* **2003**, *81*, 413-426.

(23) Springer, P. A. M.; Buttinger, B.; Baur, R.; Krishna, R. Crossing of the distillation boundary in homogeneous azeotropic distillation: Influence of interphase mass transfer, *Ind. Eng. Chem. Res.* **2002**, *41*, 1621-1631.

(24) Springer, P. A. M.; Krishna, R. Crossing of boundaries in ternary azeotropic distillation: Influence of interphase mass transfer, *Int. Commun. Heat Mass Transf.* **2001**, *28*, 347-356.

(25) Springer, P. A. M.; van der Molen, S.; Baur, R.; Krishna, R. Experimental verification of the necessity to use the Maxwell-Stefan formulation in describing trajectories during azeotropic distillation, *Chem. Eng. Res. Des.* **2002**, *80*, 654-666.

(26) Springer, P. A. M.; van der Molen, S.; Krishna, R. The need for using rigorous rate-based models for simulations of ternary azeotropic distillation, *Comput. Chem. Eng.* **2002**, *26*, 1265-1279.

(27) Baur, R.; Taylor, R.; Krishna, R.; Copati, J. A. Influence of mass transfer in distillation of mixtures with a distillation boundary, *Chem. Eng. Res. Des.* **1999**, *77*, 561-565.

(28) Levy, S. G.; Van Dongen, D. B.; Doherty, M. F. Design and synthesis of homogeneous azeotropic distillation. 2. Minimum reflux calculations for nonideal and azeotropic columns, *Ind. Eng. Chem. Fundamentals* **1985**, *24*, 463-474.

(29) Li, Y. H.; Chen, H. F.; Liu, J. Q. Composition profile of an azeotropic continuous distillation with feed composition on a ridge or in a valley, *Ind. Eng. Chem. Res.* **1999**, *38*, 2482-2484.

(30) Kooijman, H. A.; Taylor, R. *The ChemSep Book*; 2nd Edition, www.chemsep.com: 2006.

(31) Krishna, R. Model for prediction of point efficiencies for multicomponent distillation, **1985**, *63*, 312-322.

(32) Fuller, E. N.; Schettler, P. D.; Giddings, J. C. A new method for prediction of binary gas-phase diffusion coefficients, *Ind. Eng. Chem.* **1966**, *58*, 19-27.

(33) Springer, P. A. M. *Mass Transfer Effects in Distillation*, University of Amsterdam, Amsterdam, 2004.

(34) Fullarton, D.; Schlünder, E. U. Diffusion Distillation - A New Separation .Process for Azeotropic Mixtures - Part I: Selectivity and Transfer Efficiency, *Chem. Eng. Process.* **1986**, *20*, 255-263.

(35) Singh, N.; Prasad, R. Experimental studies on the effect of inert gases on diffusion distillation of ethanol–water mixtures, *J. Chem. Technol. Biotechnol.* **2011**, *86*, 1495-1500.

(36) Meindersma, G. W. *Extraction of Aromatics from Naphtha with Ionic Liquids*, Ph.D. Dissertation, University of Twente, The Nethelands, Enschede, 2005.

(37) Al-Jimaz, A. S.; Fandary, M. S.; Al-Kandary, J. A.; Fahim, M. A. Liquid–liquid equilibria for n-alkanes (C12, C14,C17) + propylbenzene +NMP mixtures at temperatures between 298 and 328K, *Fluid Phase Equilib.* **2005**, *231*, 163-170.

(38) Zuber, A.; Raimundo, R.; Mafra, M. R.; Filho, L. C.; Oliveira, J. V.; Corazza, M. L. Thermodynamic Modeling of Ternary Liquid-Liquid Systems with Forming Immiscibility Islands, *Braz. Arch. Biol. Technol.* **2013**, *56*, 1034-1042.

(39) Pertler, M. *Die Mehrkomponenten-Diffuson in nicht vollständig mischbaren Flüssigkeiten*, Technische Universität München, München, 1996.

(40) Bollen, A. M. *Collected tales on mass transfer in liquids*, Ph.D. Dissertation, Rijksuniversiteit Groningen, Groningen, 1999.
http://dissertations.ub.rug.nl/faculties/science/1999/a.m.bollen/

(41) Colombo, A.; Battilana, P.; Ragaini, V.; Bianchi, C. L. Liquid-Liquid Equilibria of the Ternary Systems Water + Acetic Acid + Ethyl Acetate and Water + Acetic Acid + Isophorone (3,5,5-Trimethyl-2-cyclohexen-1-one), *J. Chem. Eng. Data* **1999**, *44*, 35-39.

(42) Zhang, H.; Wang, T. Measurement and Correlation of Liquid-Liquid Equilibrium Data for Water + Acetic Acid + Methyl tert-Butyl Ether + NaCl, *J. Chem. Eng. Data* **2009**, *54*, 945-949.

(43) Aznar, M. Correlation of (Liquid + Liquid) Equilibrium of Systems Including Ionic Liquids, *Braz. J. Chem. Eng.* **2007**, *24*, 143-149.

(44) Santiago, R. S.; Santos, G. R.; Aznar, M. UNIQUAC correlation of liquid–liquid equilibrium in systems involving ionic liquids: The DFT–PCM approach, *Fluid Phase Equilib.* **2009**, *278*, 54-61.

(45) Wang, H.; Wang, Q.; Xiong, Z.; Chen, C. Liquid–liquid equilibria for ternary system water + toluene + benzaldehyde at (303.2–343.2) K, *Fluid Phase Equilib.* **2014**, *383*, 43-48.

(46) Ruiz, F.; Prats, D.; Gomis, V. Quaternary Liquid-Liquid Equilibrium: Water-Ethanol-ChtoroformToluene at 25 ^{o}C. Experimental Determination and Graphical and Analytical Correlation of Equillbrium Data, *J. Chem. Eng. Data* **1985**, *30*, 412-416.

(47) Washburn, E. R.; Beguin, A. E.; Beckford, O. C. The Ternary System: Ethyl Alcohol, Toluene and Water at 25^{o}, *J. Am. Chem. Soc.* **1939**, *61*, 1694-1695.

(48) Kurihara, K.; Hori, H.; Kojima, K. Vapor-Liquid Equilibrium Data for Acetone + Methanol + Benzene, Chloroform + Methanol + Benzene, and Constituent Binary Systems at 101.3 KPa, *J. Chem. Eng. Data* **1998**, *43*, 264-268.

24. Caption for Figures

Figure 1. Schematic showing a variety of applications of liquid extraction processes in petroleum refining.

Figure 2. Schematic of agitated, and un-agitated column contactors used for liquid-liquid extraction processes.

Figure 3. Schematic of single-stage contacting in sieve-tray column.

Figure 4. (a, b) Transient equilibration trajectories for the system heptane(1)/toluene(2)/sulpholane(3) at 348.2 K. For the extract phase, the initial mole fractions in the drop are x_{10} = 0.0, x_{20} = 0.0, and x_{30} = 1.0; the final equilibrium composition is $x_{1,eq}$ = 0.062684992, $x_{2,eq}$ = 0.406432625, and $x_{3,eq}$ = 0.53088. (c) Plot of the component Murphree efficiencies in the hydrocarbon-rich heptane(1)/toluene(2)/sulpholane(3) mixture, E_i, as function of the Fourier number. (d) The composition trajectory followed during S-E equilibration. (c) Calculations of the ratios $-k_{12}/k_{11}$, and $-k_{21}/k_{22}$ as a function of the Fourier number. The NRTL parameters are provided in Table 1.

Figure 5. Interphase mass transfer resistances in liquid-liquid extraction.

Figure 6. (a) Transient equilibration trajectories for the system NMP(1)/propylbenzene(2)/tetradecane(3) at 298 K. The initial mole fractions in the drop are x_{10} = 1.0, x_{20} = 0.0, and x_{30} = 0.0. The final equilibrium composition is $x_{1,eq}$ = 0.689463372, $x_{2,eq}$ = 0.208896097, and $x_{3,eq}$ = 0.101640532. (b) Plot of the component Murphree efficiencies in the extract phase, E_i, as function of the Fourier number. (c) Calculations of the ratios $-k_{12}/k_{11}$, and $-k_{21}/k_{22}$ as a function of the Fourier number. The NRTL parameters are provided in Table 3.

Figure 7. Transient equilibration trajectories for the system glycerol(1)/acetone(2)/water(3) mixtures at 298 K. For the acetone-rich phase (left hand side), the initial mole fractions in the drop are x_{10} = 0.0, x_{20} = 0.77, and x_{30} = 0.23; the final equilibrium composition is $x_{1,eq}$ = 0.042, $x_{2,eq}$ = 0.894, and $x_{3,eq}$ = 0.064. For the glycerol-rich phase (right hand side), the initial mole fractions in the drop are x_{10} = 0.85, x_{20} = 0.0, and x_{30} = 0.15; the final equilibrium composition is $x_{1,eq}$ = 0.552, $x_{2,eq}$ = 0.164, and $x_{3,eq}$ = 0.284. The experimental data for the equilibration paths for glycerol(1)/acetone(2)/water(3) mixture measured in a stirred Lewis cell by Krishna et al.[17] are also indicated. The two trajectories are calculated using $[D]=|\Lambda|^{1/2}[\Gamma]$ with $|\Lambda|^{1/2}=(D_{1,self})^{x_1}(D_{2,self})^{x_2}(D_{3,self})^{x_3}$, taking $D_{1,self}$= 0.01, $D_{2,self}$= 3.2, $D_{3,self}$= 0.5 with units 10^{-9} m^2 s^{-1}; this diffusivity information has been derived from our earlier work.[6] In these calculations, the equilibration trajectories are determined using the exponential decay model $(x-x_{eq})=[Q](x_0-x_{eq})$; $[Q]\equiv\exp[-A[D]t]$. The phase equilibrium is determined from the NRTL parameters in Table 4.

Figure 8. Transient equilibration trajectories for the system water(1)/acetone(2)/ethylacetate(3) at 293 K. The initial mole fractions in the drop are x_{10} = 0.1, x_{20} = 0.25, and x_{30} = 0.0. The final equilibrium

compositions is $x_{1,eq}$ = 0.354107973, $x_{2,eq}$ = 0.307050572, and $x_{3,eq}$ = 0.338841456. The UNIQUAC parameters for calculation of the phase equilibrium thermodynamics are provided in Table 6.

Figure 9. Transient equilibration trajectories for the system water(1)/acetone(2)/ethylacetate(3) at 293 K. The initial mole fractions in the drop are binary acetone(2)/ethylacetate(3) mixtures of varying compositions. The final equilibrium composition is $x_{1,eq}$ = 0.354107973, $x_{2,eq}$ = 0.307050572, and $x_{3,eq}$ = 0.338841456. The UNIQUAC parameters for calculation of the phase equilibrium thermodynamics are provided in Table 6.

Figure 10. Transient equilibration trajectories for the system water(1)/caprolactam(2)/toluene(3) at 298 K. The initial mole fractions in the drop are x_{10} = 0.0, x_{20} = 0.6, and x_{30} = 0.4. The final equilibrium composition is $x_{1,eq}$ = 0.087810088, $x_{2,eq}$ = 0.108474359, and $x_{3,eq}$ = 0.803715553. The UNIQUAC parameters for calculation of the phase equilibrium thermodynamics are provided in Table 7.

Figure 11. Transient equilibration trajectories for the system water(1)/caprolactam(2)/toluene(3) at 298 K. The initial mole fractions in the drop are binary caprolactam(2)/toluene(3) mixtures of varying compositions. The final equilibrium composition is $x_{1,eq}$ = 0.76316675, $x_{2,eq}$ = 0.200866022, and $x_{3,eq}$ = 0.035967228. The UNIQUAC parameters for calculation of the phase equilibrium thermodynamics are provided in Table 7.

Figure 12. Transient equilibration trajectories for the system water(1)/acetic acid(2)/isophorone(3) at 298 K. The initial mole fractions in the drop are x_{10} = 0.0, x_{20} = 0.0, and x_{30} = 1.0. The final equilibrium

composition is $x_{1,eq}$ = 0.544129988, $x_{2,eq}$ = 0.223048947, and $x_{3,eq}$ = 0.23282106. The NRTL parameters for calculation of the phase equilibrium thermodynamics are provided in Table 8.

Figure 13. Transient equilibration trajectories for the system water(1)/acetic acid(2)/isophorone(3) at 298 K. The initial mole fractions in the drop are binary acetic acid(2)/isophorone(3) mixtures of varying compositions. The final equilibrium composition is $x_{1,eq}$ = 0.544129988, $x_{2,eq}$ = 0.223048947, and $x_{3,eq}$ = 0.23282106. The NRTL parameters for calculation of the phase equilibrium thermodynamics are provided in Table 8.

Figure 14. Transient equilibration trajectories for the system water(1)/acetic acid(2)/MTBE(3) at 298.15 K. The initial mole fractions in the drop are x_{10} = 0.0, x_{20} = 0.0, and x_{30} = 1. The final equilibrium composition is $x_{1,eq}$ = 0.424393, $x_{2,eq}$ = 0.243211571, and $x_{3,eq}$ = 0.332395429. The NRTL parameters for calculation of the phase equilibrium thermodynamics are provided in Table 9.

Figure 15. Transient equilibration trajectories for the system water(1)/acetic acid(2)/MTBE(3) at 298.15 K. The initial mole fractions in the drop are binary acetic acid(2)/MTBE(3) mixtures of varying compositions. The final equilibrium composition is $x_{1,eq}$ = 0.424393, $x_{2,eq}$ = 0.243211571, and $x_{3,eq}$ = 0.332395429. The NRTL parameters for calculation of the phase equilibrium thermodynamics are provided in Table 9.

Figure 16. Transient equilibration trajectory for the system [omim][Cl](1)/ethanol(2)/TAEE(3) at 298.15. Here we denote the ionic liquid 1-octyl-3-methylimidazolium chloride in the abbreviated form

[omim][Cl]. TAEE is the abbreviated name for tert-amyl ethyl ether. The initial mole fractions in the drop are x_{10} = 1.0, x_{20} = 0.0, and x_{30} = 0.0. The final equilibrium composition is $x_{1,eq}$ = 0.150072736, $x_{2,eq}$ = 0.47026855, and $x_{3,eq}$ = 0.379658714. The NRTL parameters are provided in Table 10.

Figure 17. Transient equilibration trajectory for the system [omim][Cl](1)/ethanol(2)/TAEE(3) at 298.15. Here we denote the ionic liquid 1-octyl-3-methylimidazolium chloride in the abbreviated form [omim][Cl]. TAEE is the abbreviated name for tert-amyl ethyl ether. The initial mole fractions in the drop are x_{10} = 1.0, x_{20} = 0.0, and x_{30} = 0.0. The final equilibrium composition is $x_{1,eq}$ = 0.397919131, $x_{2,eq}$ = 0.381690314, and $x_{3,eq}$ = 0.22039056. The NRTL parameters are provided in Table 10.

Figure 18. Transient equilibration trajectories for the system [omim][Cl](1)/ethanol(2)/TAEE(3) at 298.15. Here we denote the ionic liquid 1-octyl-3-methylimidazolium chloride in the abbreviated form [omim][Cl]. TAEE is the abbreviated name for tert-amyl ethyl ether. The initial mole fractions in the drop are all devoid of TAEE, and contain different proportions of [omim][Cl] and ethanol(2). The final equilibrium composition for all starting compositions is $x_{1,eq}$ = 0.397919131, $x_{2,eq}$ = 0.381690314, and $x_{3,eq}$ = 0.22039056. The NRTL parameters are provided in Table 10.

Figure 19. Transient equilibration trajectory for the system [bmim][TfO](1)/ethanol(2)/TAEE(3) at 298.15 K. Here [bmim][TfO] = 1-butyl-3-methylimidazolium trifluoromethanesulfonate. TAEE is the abbreviated name for tert-amyl ethyl ether. The initial mole fractions in the drop are x_{10} = 0.6, x_{20} = 0.2, and x_{30} = 0.0. The final equilibrium composition is $x_{1,eq}$ = 0.316915772, $x_{2,eq}$ = 0.361266258, and $x_{3,eq}$ = 0.32181797. The UNIQUAC parameters are provided in Table 11.

Figure 20. Transient equilibration trajectories for the system [bmim][TfO](1)/ethanol(2)/TAEE(3) at 298.15 K. Here [bmim][TfO] = 1-butyl-3-methylimidazolium trifluoromethanesulfonate. TAEE is the abbreviated name for tert-amyl ethyl ether. The initial mole fractions in the drop contain varying compositions of the binary mixtures [bmim][TfO](1)/ethanol(2). The final equilibrium composition for all starting compositions is $x_{1,eq}$ = 0.397919131, $x_{2,eq}$ = 0.381690314, and $x_{3,eq}$ = 0.22039056. The UNIQUAC parameters are provided in Table 11.

Figure 21. Transient equilibration trajectory for the system water(1)/ethanol(2)/cyclohexane(3) at 298 K. The initial mole fractions in the drop are x_{10} = 0.3, x_{20} = 0.7, and x_{30} = 0.0. The final equilibrium composition is $x_{1,eq}$ = 0.325889064, $x_{2,eq}$ = 0.563182958, and $x_{3,eq}$ = 0.11093. The NRTL parameters for calculation of the phase equilibrium thermodynamics are provided in Table 12.

Figure 22. Transient equilibration trajectory for the system water(1)/ethanol(2)/cyclohexane(3) at 298 K. The initial mole fractions in the drop are binary water(1)/ethanol(2) mixtures of varying compositions. The final equilibrium composition is $x_{1,eq}$ = 0.325889064, $x_{2,eq}$ = 0.563182958, and $x_{3,eq}$ = 0.11093. The NRTL parameters for calculation of the phase equilibrium thermodynamics are provided in Table 12.

Figure 23. Transient equilibration trajectory for the system toluene(1)/ethanol(2)/water(3) at 298 K. The initial mole fractions in the drop are x_{10} = 0.25, x_{20} = 0.75, and x_{30} = 0.0. The final equilibrium

composition is $x_{1,eq}$ = 0.2952817, $x_{2,eq}$ = 0.454727223, and $x_{3,eq}$ = 0.24999108. The NRTL parameters for toluene(1)/ethanol(2)/water(3) are provided in Table 13.

Figure 24. Transient equilibration trajectory for the system toluene(1)/ethanol(2)/water(3) at 298 K. The initial mole fractions in the drop are binary toluene(1)/ethanol(2) mixtures of varying compositions. The final equilibrium composition is $x_{1,eq}$ = 0.2952817, $x_{2,eq}$ = 0.454727223, and $x_{3,eq}$ = 0.24999108. The NRTL parameters for toluene(1)/ethanol(2)/water(3) are provided in Table 13.

Figure 25. Transient equilibration trajectory for the system water(1)/acetone(2)/toluene(3) at 298 K. The initial mole fractions in the drop are x_{10} = 0.3, x_{20} = 0.7, and x_{30} = 0.0. The final equilibrium composition is $x_{1,eq}$ = 0.057357706, $x_{2,eq}$ = 0.600380623, and $x_{3,eq}$ = 0.342261671. The NRTL parameters for calculation of the phase equilibrium thermodynamics are provided in Table 14.

Figure 26. Transient equilibration trajectory for the system water(1)/acetone(2)/toluene(3) at 298 K. The initial mole fractions in the drop are binary water(1)/acetone(2) mixtures of varying compositions. The final equilibrium composition is $x_{1,eq}$ = 0.057357706, $x_{2,eq}$ = 0.600380623, and $x_{3,eq}$ = 0.342261671. The NRTL parameters for calculation of the phase equilibrium thermodynamics are provided in Table 14.

Figure 27. Transfer resistances in vapor/liquid contacting on a distillation tray.

Figure 28. (a) Residue curve map for the Methanol - Isopropanol - Water system, showing a straight-line distillation boundary and feed locations F1 and F2 on either side of the distillation boundary. (b) Residue curve map for the Acetone - Chloroform - Methanol system, showing feed locations F1 and F2 on the concave and convex sides of the highlighted distillation boundary respectively.

Figure 29. (a) Schematic of a laboratory-scale distillation column used in the experiments of Springer et al.[21, 23] which includes a total condenser (1), a partial reboiler (12), 10 bubble-cap trays (2-11), and 13 draw-off faucets, 9 for vapor samples and 4 for liquid samples.

Figure 30. Residue curve maps for distillation of water(1)/ethanol(2)/acetone(3) mixtures. The blue circles represent the experimental data for T2-26 of Springer et al.[21, 23, 25, 26] on composition trajectories in a bubble-cap tray column operating at total reflux implying $x_i = y_i$.

Figure 31. (a) Ethanol driving force $\Delta y_{2E} = \left(y_{2E} - y_{2,eq}\right)$ on each stage for the system water(1)/ethanol(2)/acetone(3). (b) Murphree component efficiencies for the system water(1)/ethanol(2)/acetone(3).

Figure 32. Residue curve maps for distillation of water(1)/ethanol(2)/methanol(3) mixtures. The blue circles represent the experimental data for T4-13 of Springer et al.[21, 23, 25, 26] on composition trajectories in a bubble-cap tray column operating at total reflux implying $x_i = y_i$.

Figure 33. Residue curve maps for distillation of water(1)/ethanol(2)/methylacetate(3) mixtures. The blue circles represent the experimental data for T3-23 of Springer et al.[21, 23, 25, 26] on composition trajectories in a bubble-cap tray column operating at total reflux implying $x_i = y_i$.

Figure 34. Experimental data (blue circles) of Springer et al.[25] for Run Q6 with quaternary water(1)/ethanol(2)/methanol(3)/acetone(4) mixtures. Also shown as insets are the Murphree component efficiencies and component driving forces.

Figure 35. (a) Transient equilibration trajectories for the system water(1)/ethanol(2)/acetone(3) at 335.5 K. The initial mole fractions in the rigid spherical vapor bubble are y_{10} = 0.067, y_{20} = 0.44, and y_{30} = 0.493; the final equilibrium compositions are $y_{1,eq}$ = 0.04335, $y_{2,eq}$ = 0.25907, and $y_{3,eq}$ = 0.69758. (b) Plot of the component Murphree efficiencies, E_i, as function of the Fourier number. (c) NEQ and EQ trajectory vectors for various entering tray compositions. (d) The orange shaded region indicate vapor compositions that will have trajectories that cross the distillation boundary.

Figure 36. Design result for feed left of distillation boundary. (a) Comparison of column composition trajectories calculated using the NEQ with EQ stage model. (b) Required number of stages for a bottom product of 96 mol% ethanol. (c) Murphree component efficiencies.

Figure 37. Design result for feed right of distillation boundary. (a) Comparison of column composition trajectories calculated using the NEQ with EQ stage model. (b) Required number of stages for a bottom product of 100 mol% water. (c) Murphree component efficiencies.

Figure 38. (a) Transient equilibration trajectories for the system water(1)/ethanol(2)/methanol(3) at 348 K. The initial mole fractions in the rigid spherical vapor bubble are $y_{10} = 0.082$, $y_{20} = 0.68$, and $y_{30} = 0.238$; the final equilibrium compositions are $y_{1,eq} = 0.06767$, $y_{2,eq} = 0.59691$, and $y_{3,eq} = 0.33542$. (b) Plot of the component Murphree efficiencies, E_i, as function of the Fourier number. (c) NEQ and EQ trajectory vectors for various entering tray compositions. (d) The orange shaded region indicate vapor compositions that will have trajectories that cross the distillation boundary.

Figure 39. (a) Transient equilibration trajectories for the system water(1)/ethanol(2)/methylacetate(3) at 337 K. The initial mole fractions in the rigid spherical vapor bubble are $y_{10} = 0.095$, $y_{20} = 0.6345$, and $y_{30} = 0.2705$; the final equilibrium compositions are $y_{1,eq} = 0.06324$, $y_{2,eq} = 0.36863$, and $y_{3,eq} = 0.56813$. (b) Plot of the component Murphree efficiencies, E_i, as function of the Fourier number. (c) NEQ and EQ trajectory vectors for various entering tray compositions. (d) The orange shaded region indicate vapor compositions that will have trajectories that cross the distillation boundary.

Figure 40. Residue curve maps for distillation of water(1)/acetone(2)/toluene(3) mixtures. The blue circles represent the experimental data for WAT-1 of Springer et al.[22] (blue circles) showing the column composition trajectories in the bubble-cap tray column operating at total reflux implying $x_i = y_i$.

Figure 41. Residue curve maps for distillation of water(1)/acetone(2)/toluene(3) mixtures. The blue circles represent the experimental data for WAT-2 of Springer et al.[22] (blue circles) showing the column composition trajectories in the bubble-cap tray column operating at total reflux implying $x_i = y_i$.

Figure 42. Residue curve maps for distillation of water(1)/ethanol(2)/cyclohexane(3) mixtures. The blue circles represent the experimental data for WEC-12 of Springer et al.[22] (blue circles) showing the column composition trajectories in the bubble-cap tray operating at total reflux implying $x_i = y_i$.

Figure 43. Residue curve maps for distillation of water(1)/ethanol(2)/cyclohexane(3) mixtures. The blue circles represent the experimental data for WEC-8 of Springer et al.[22] (blue circles) showing the column composition trajectories in the bubble-cap tray column operating at total reflux implying $x_i = y_i$.

Figure 44. Transfer resistances in heterogeneous azeotropic distillation. This scheme is adapted from Springer et al.[22]

Figure 45. Diffusional distillation of alcohol(1)-water(2) binary mixture by introduction of pure inert gas (3) at the inlet to the tray.

Figure 46. Transient equilibration in the vapor phase determined using the Geddes model. (a) The mole fractions of 2-propanol (1) and water (2) plotted as a function of time, *t*.The total pressure is 101.3 kPa, and the temperature is 313.15 K. The well-mixed liquid composition on the tray is x_1 = 0.637, x_2 = 0.363. The vapor composition entering the tray is y_{1E} = 0.0, y_{2E} = 0.0, y_{3E} = 1.0. The composition of the vapor in equilibrium with the liquid is $y_{1,eq}$ = 0.09836, $y_{2,eq}$ = 0.05963, y_{3E} = 0.84201. The phase equilibrium is calculated using the NRTL parameters provided in Table 19. (b) Ratio of the mole fraction of water (2) to that of 2-propanol (1) in the vapor phase as a function of time, *t*. (c) Comparisons of the ratios of the mole fraction of water (2) to that of 2-propanol (1) in the vapor phase as a function of time, *t* using nitrogen, argon, and helium as inert gas. (d) Comparison of diffusion equilibration trajectories in composition space.

Figure 47. Transient equilibration in the vapor phase determined using the Geddes model. (a) The mole fractions of ethanol (1) and water (2) plotted as a function of time, *t*.The total pressure is 101.3 kPa, and the temperature is 313.15 K. The well-mixed liquid composition on the tray is x_1 = 0.87, x_2 = 0.13. The vapor composition entering the tray is y_{1E} = 0.0, y_{2E} = 0.0, y_{3E} = 1.0. The composition of the vapor in equilibrium with the liquid is $y_{1,eq}$ = 0.09859, $y_{2,eq}$ = 0.02278, y_{3E} = 0.82455. The phase equilibrium is calculated using the NRTL parameters provided in Table 20. (b) Ratio of the mole fraction of water (2) to that of ethanol (1) in the vapor phase as a function of time, *t*. (c) Comparisons of the ratios of the mole fraction of water (2) to that of ethanol (1) in the vapor phase as a function of time, *t* using nitrogen, argon, and helium as inert gas. (d) Comparison of diffusion equilibration trajectories in composition space.

Figure 48. Transient equilibration in the vapor phase determined using the Geddes model. (a) The mole fractions of acetone (1) and methanol (2) plotted as a function of time, *t*.The total pressure is 101.3 kPa,

and the temperature is 313.15 K. The well-mixed liquid composition on the tray is $x_1 = 0.85259$, $x_2 = 0.14741$. The vapor composition entering the tray is $y_{1E} = 0.0$, $y_{2E} = 0.0$, $y_{3E} = 1.0$. The composition of the vapor in equilibrium with the liquid is $y_{1,eq} = 0.4798$, $y_{2,eq} = 0.08296$, $y_{3E} = 0.43724$. The phase equilibrium is calculated using the NRTL parameters provided in Table 21. (b) Ratio of the mole fraction of methanol (2) to that of acetone (1) in the vapor phase as a function of time, t. (c) Comparisons of the ratios of the mole fraction of methanol (2) to that of acetone (1) in the vapor phase as a function of time, t using nitrogen, argon, and helium as inert gas. (d) Comparison of diffusion equilibration trajectories in composition space.

LLE applications in Petroleum Refining

Fig. S1

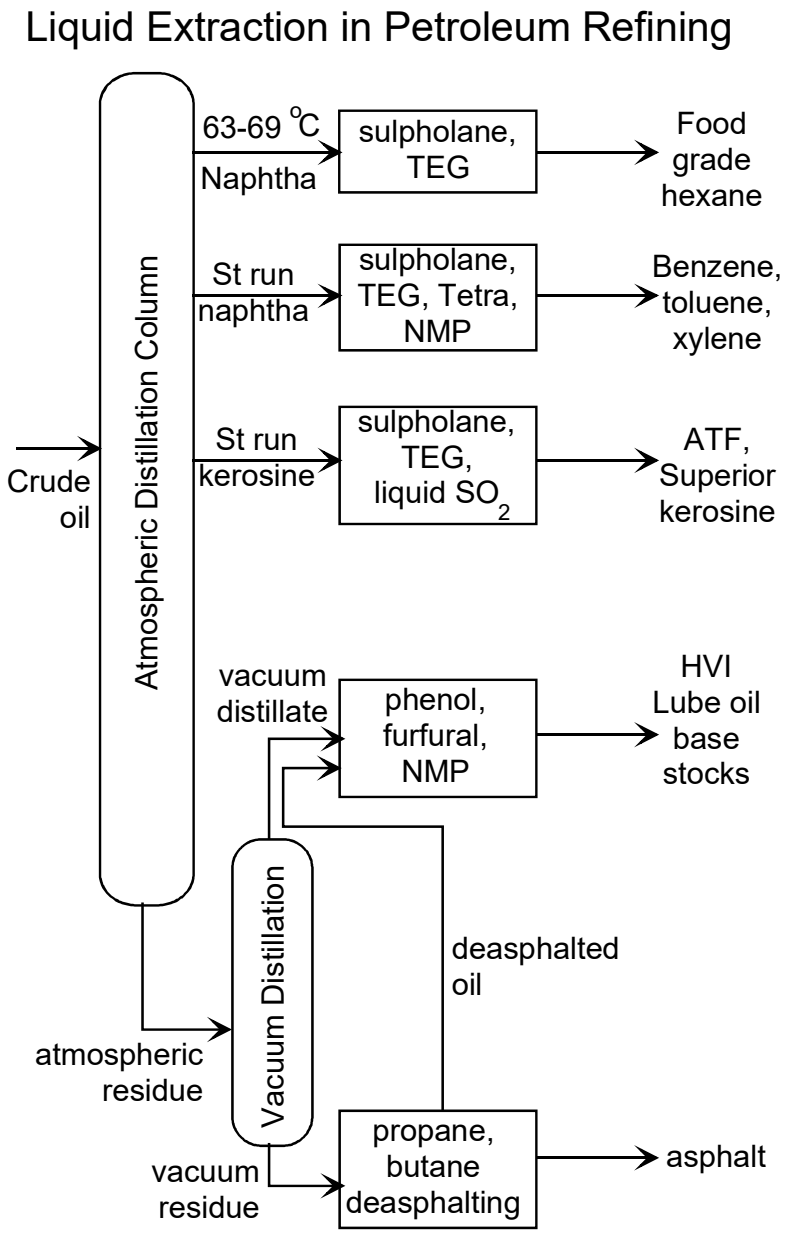

Agitated and Un-Agitated Contactors

Fig. S2

Multi-Stage Mechanically Agitated Columns

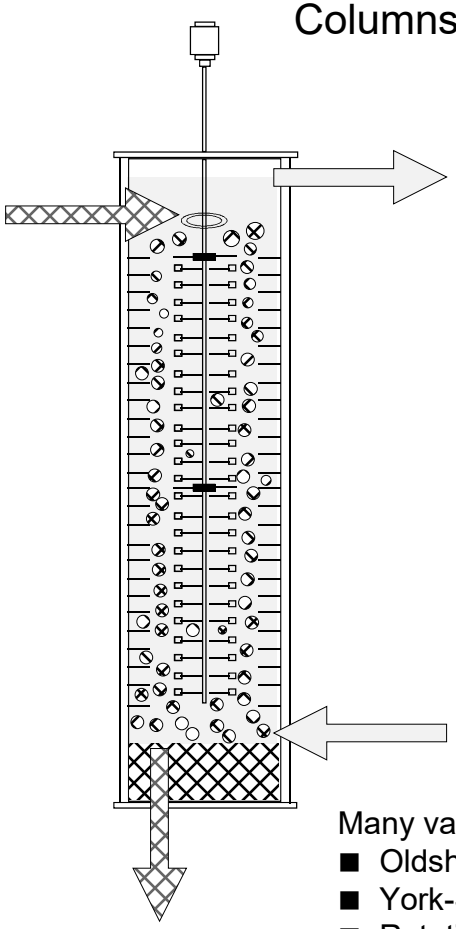

Many variants are possible

- Oldshue-Rushton
- York-Schiebel
- Rotating Disc Contactor
- Kühni
- Asymmetric Rotating Disc Contactor

Un- Agitated Columns

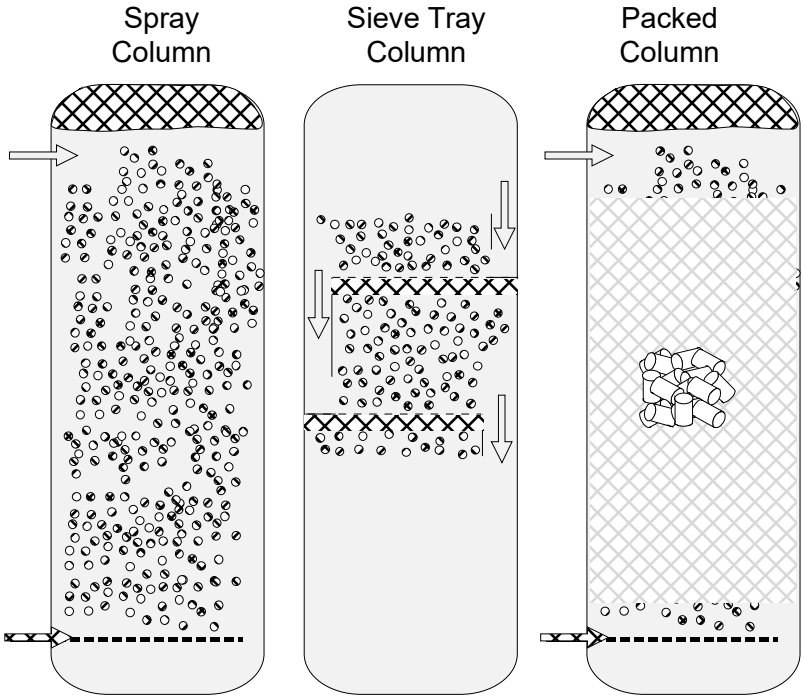

- large amount of backmixing of both phases
- some back-mixing of drops
- channelling and maldistr-bution in large diameter columns

Fig. S3

Single stage mass transfer

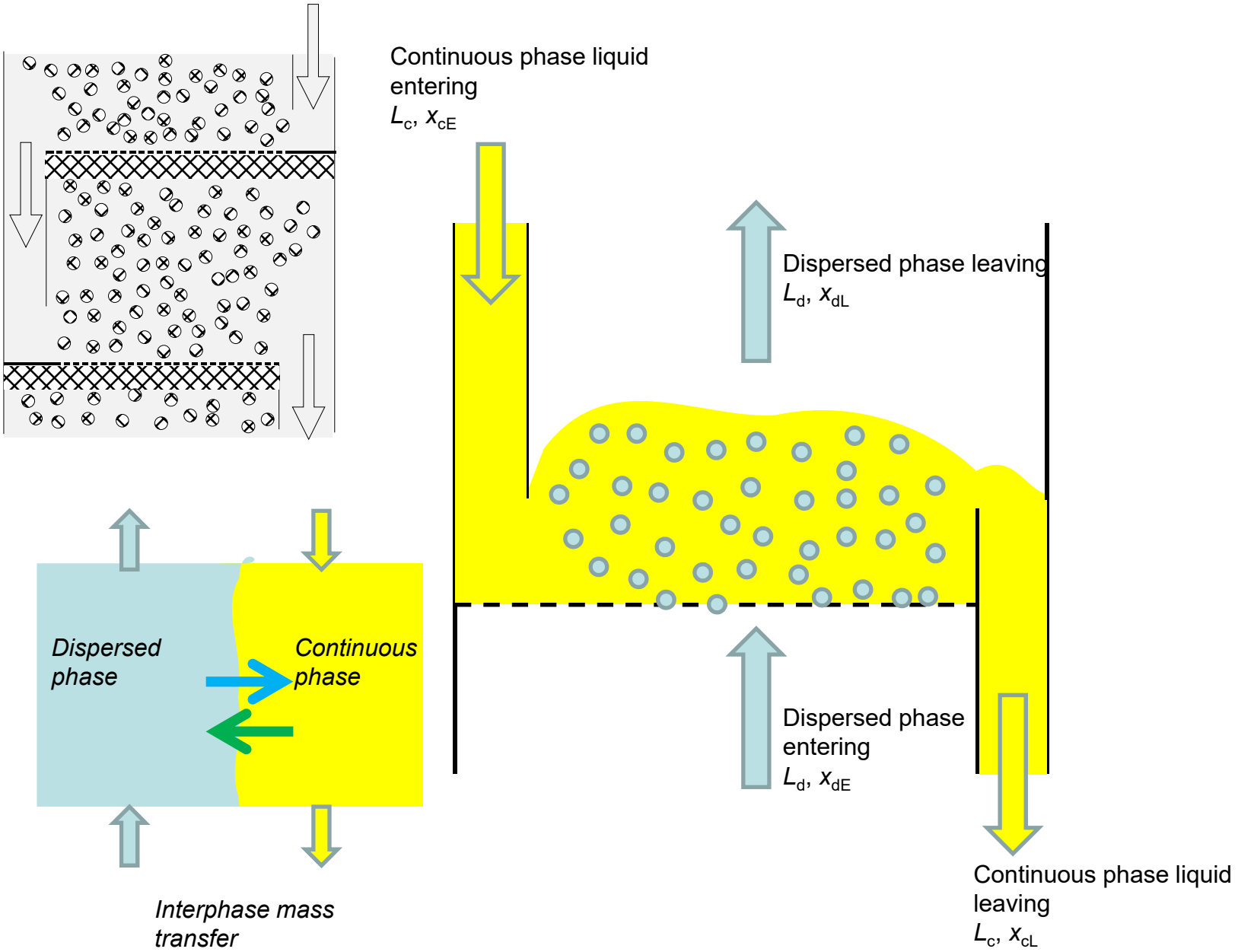

Heptane/toluene/sulpholane equilibration

Fig. S4

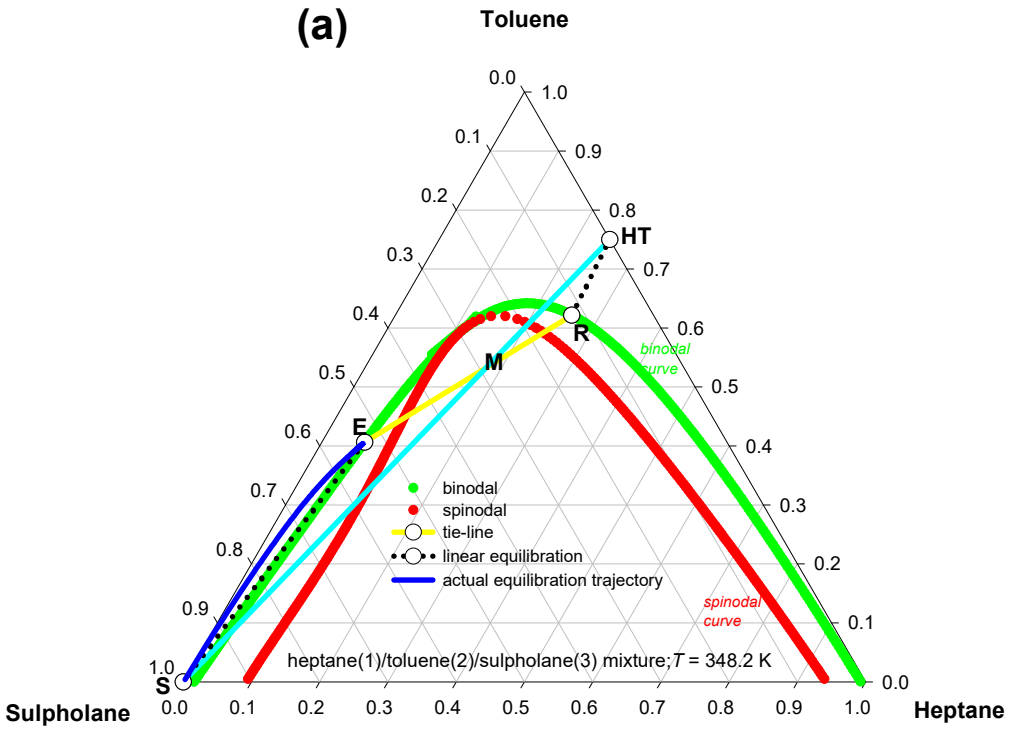

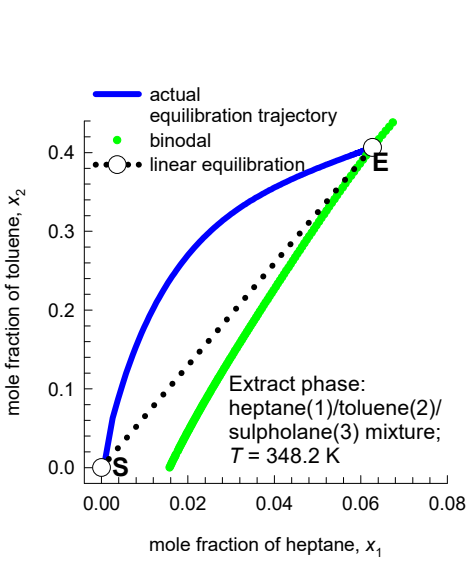

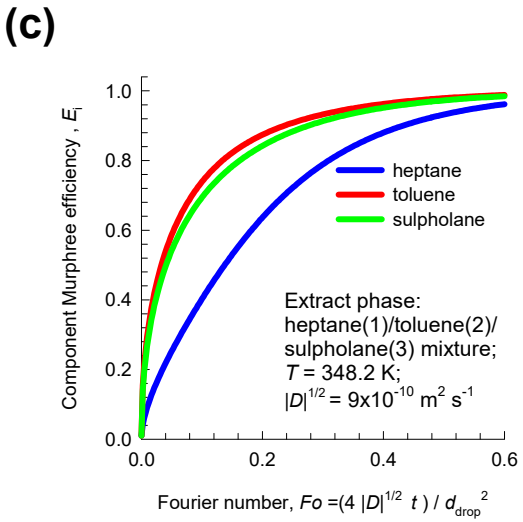

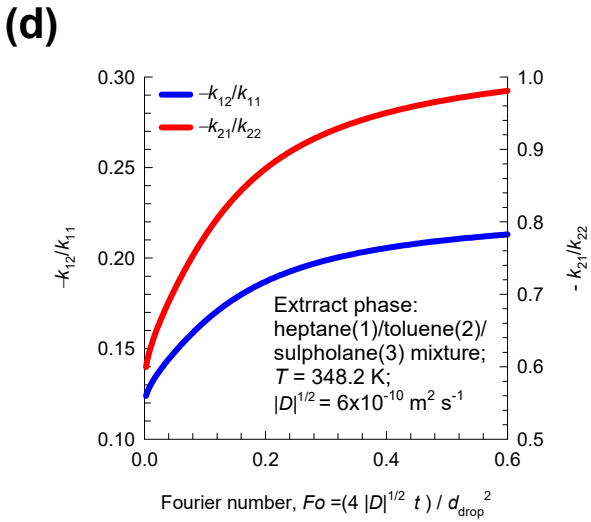

Fig. S5

Mass transfer resistances: Liquid-Liquid Extraction

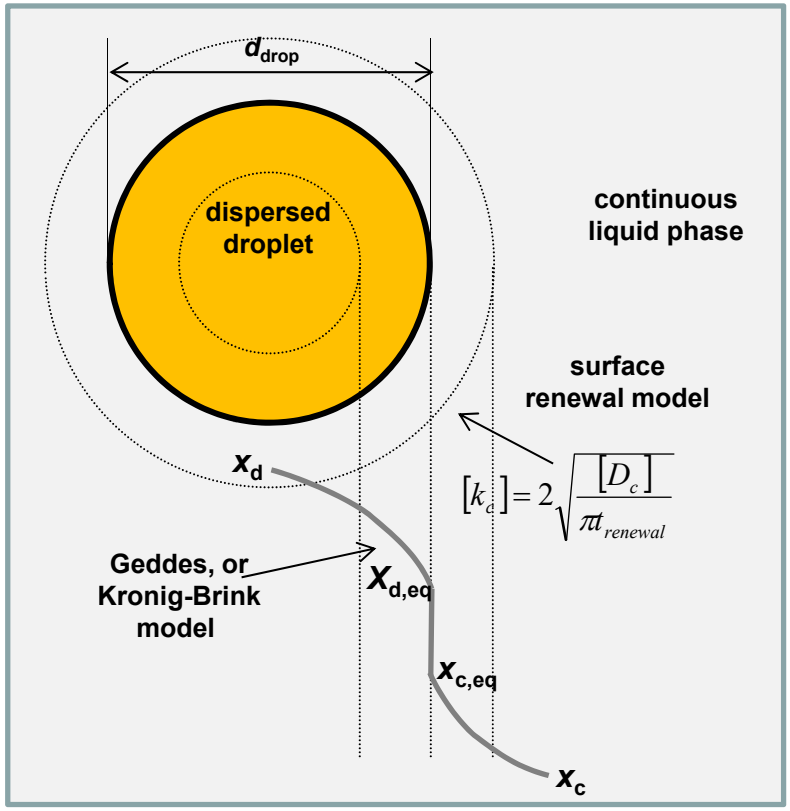

NMP/propylbenzene/tetradecane equilibration

Fig. S6

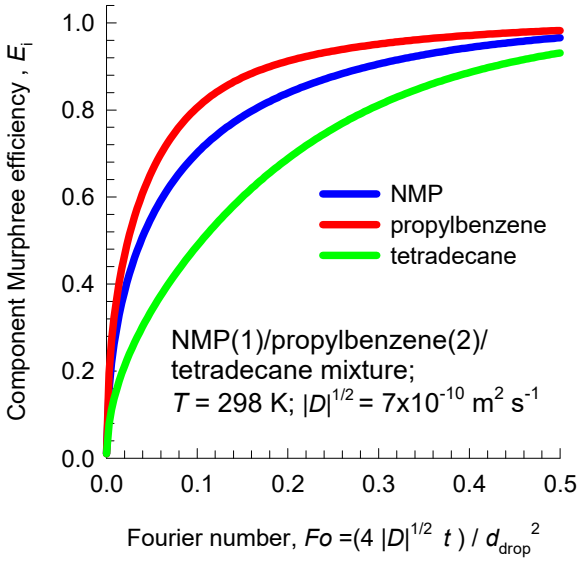

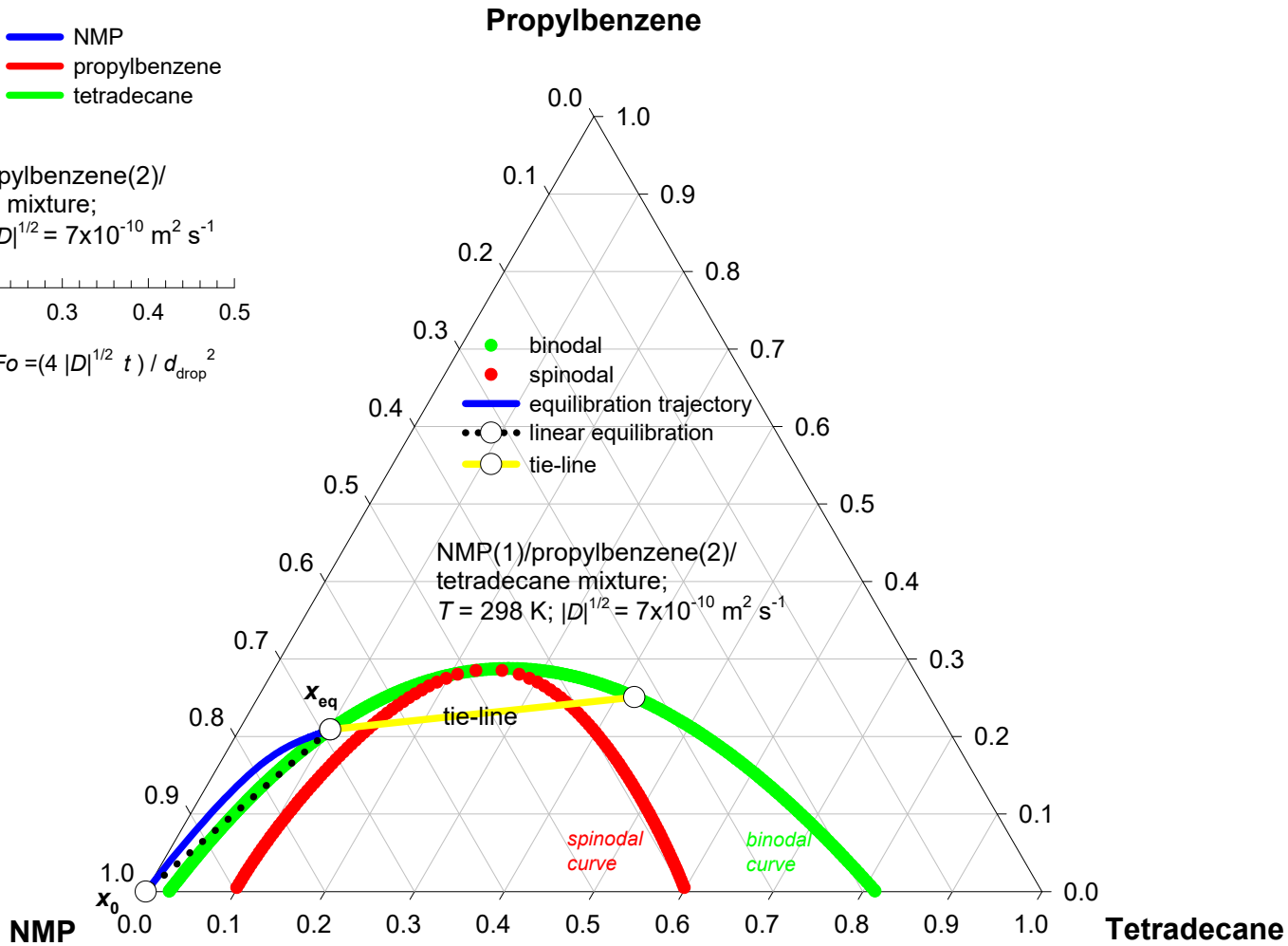

Glycerol/Acetone/Water Equilibration

Fig. S7

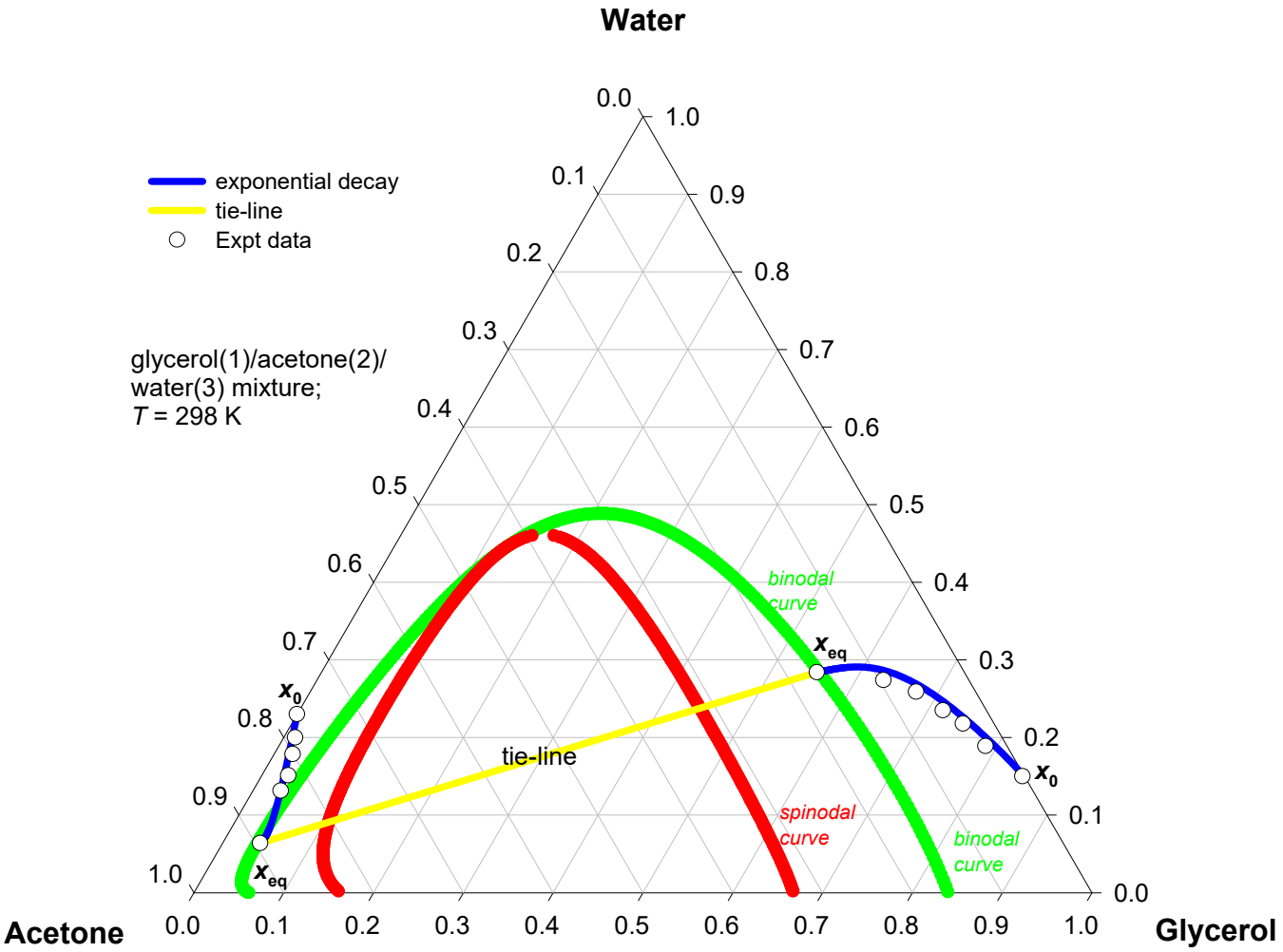

Krishna, R., Low, C.Y., Newsham, D.M.T., Olivera-Fuentes, C.G. and Standart, G.L., Ternary mass transfer in liquid-liquid extraction, *Chem. Engng Sci.*, 40, 893-903 (1985)

Fig. S8

Water/Acetone/Ethylacetate equilibration

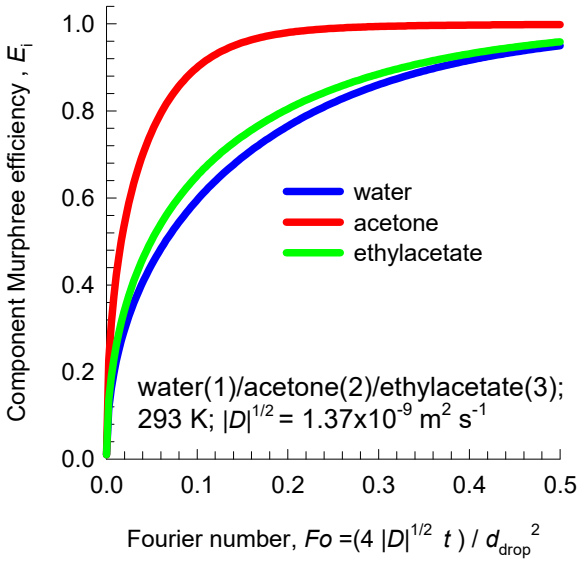

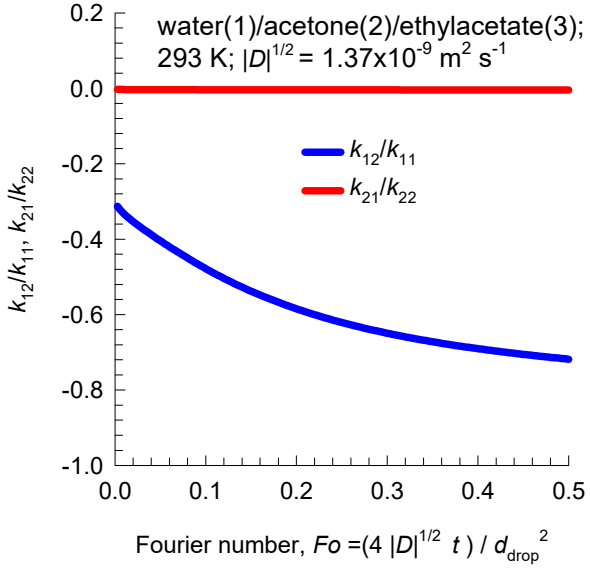

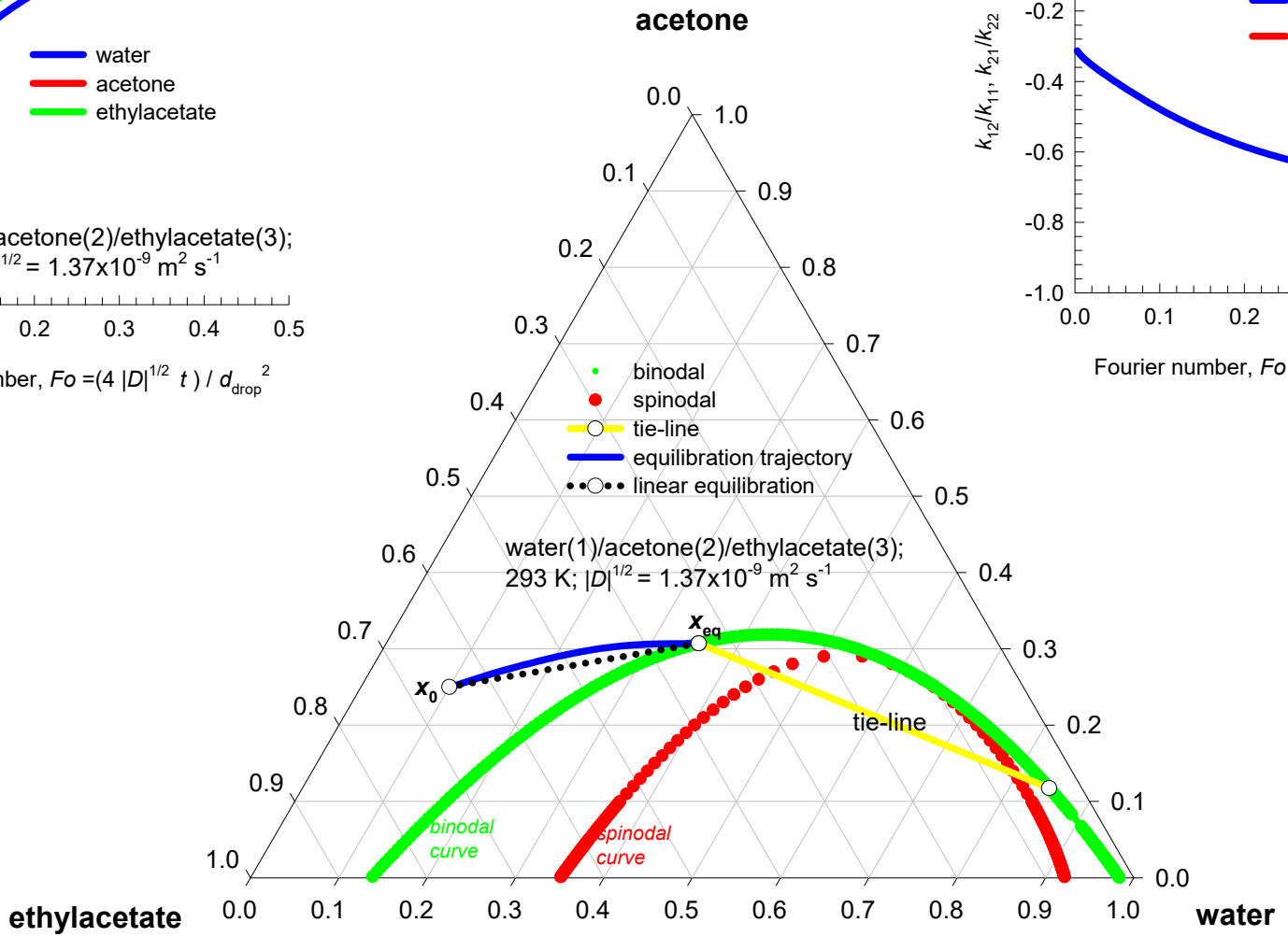

Fig. S9

Water/Acetone/Ethylacetate equilibration

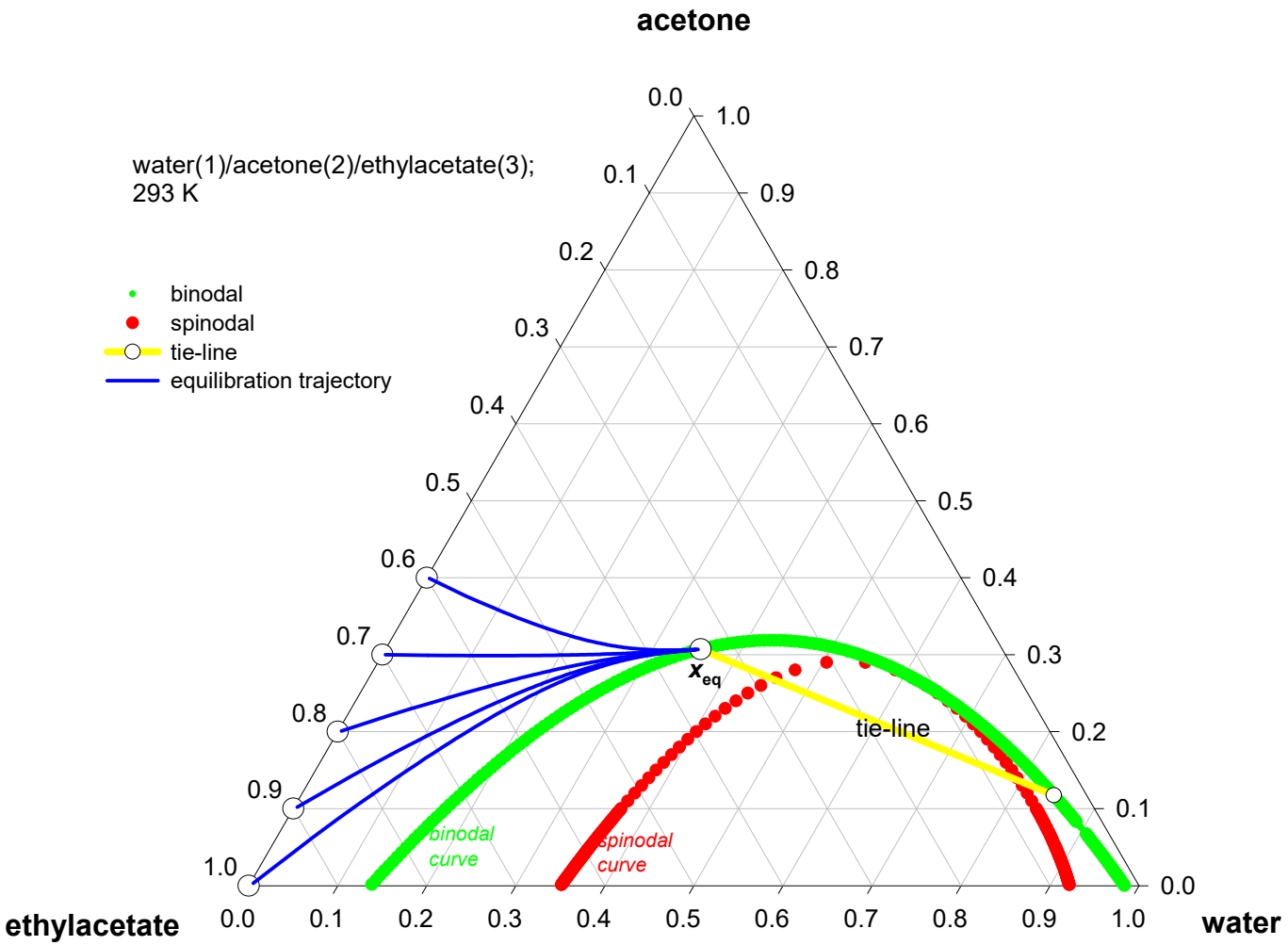

Water/Caprolactam/Toluene equilibration

Fig. S10

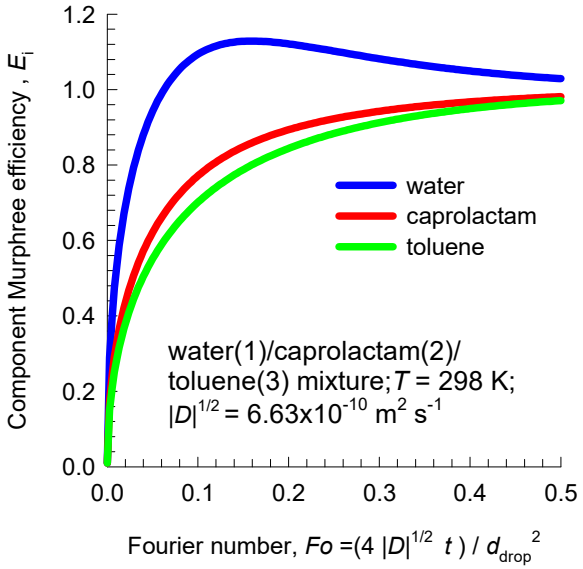

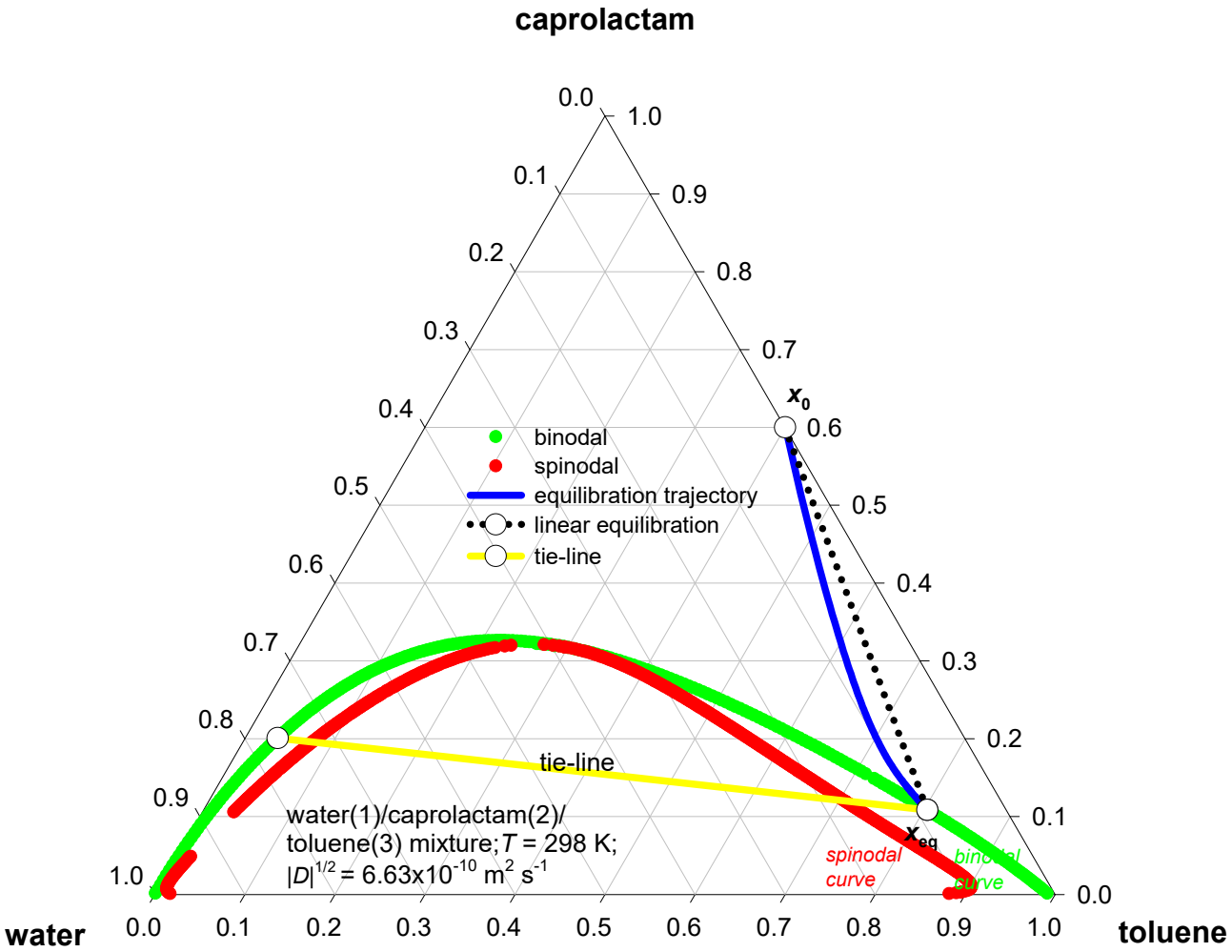

Water/Caprolactam/Toluene equilibration

Fig. S11

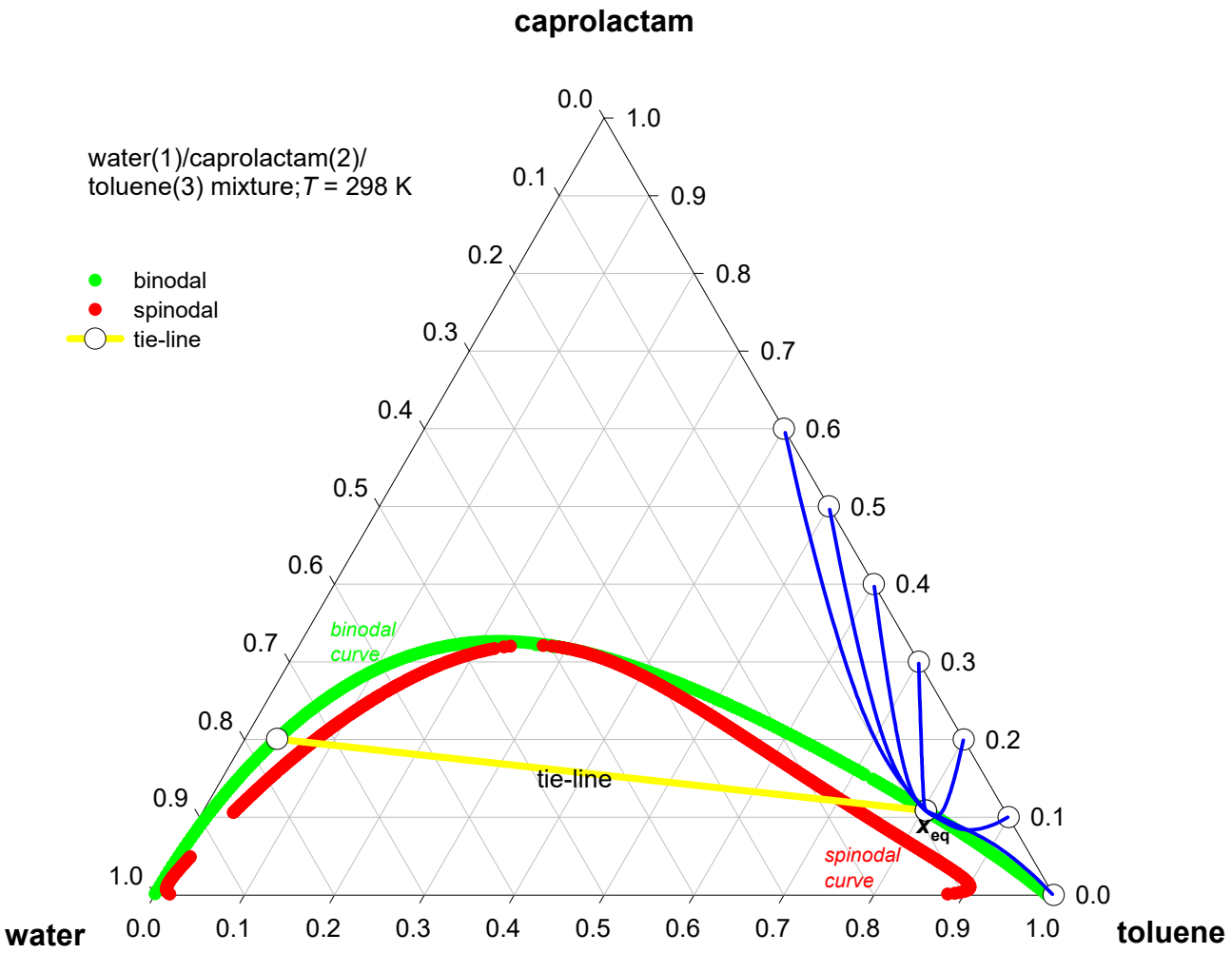

Fig. S12

Water/acetic acid/isophorone equilibration

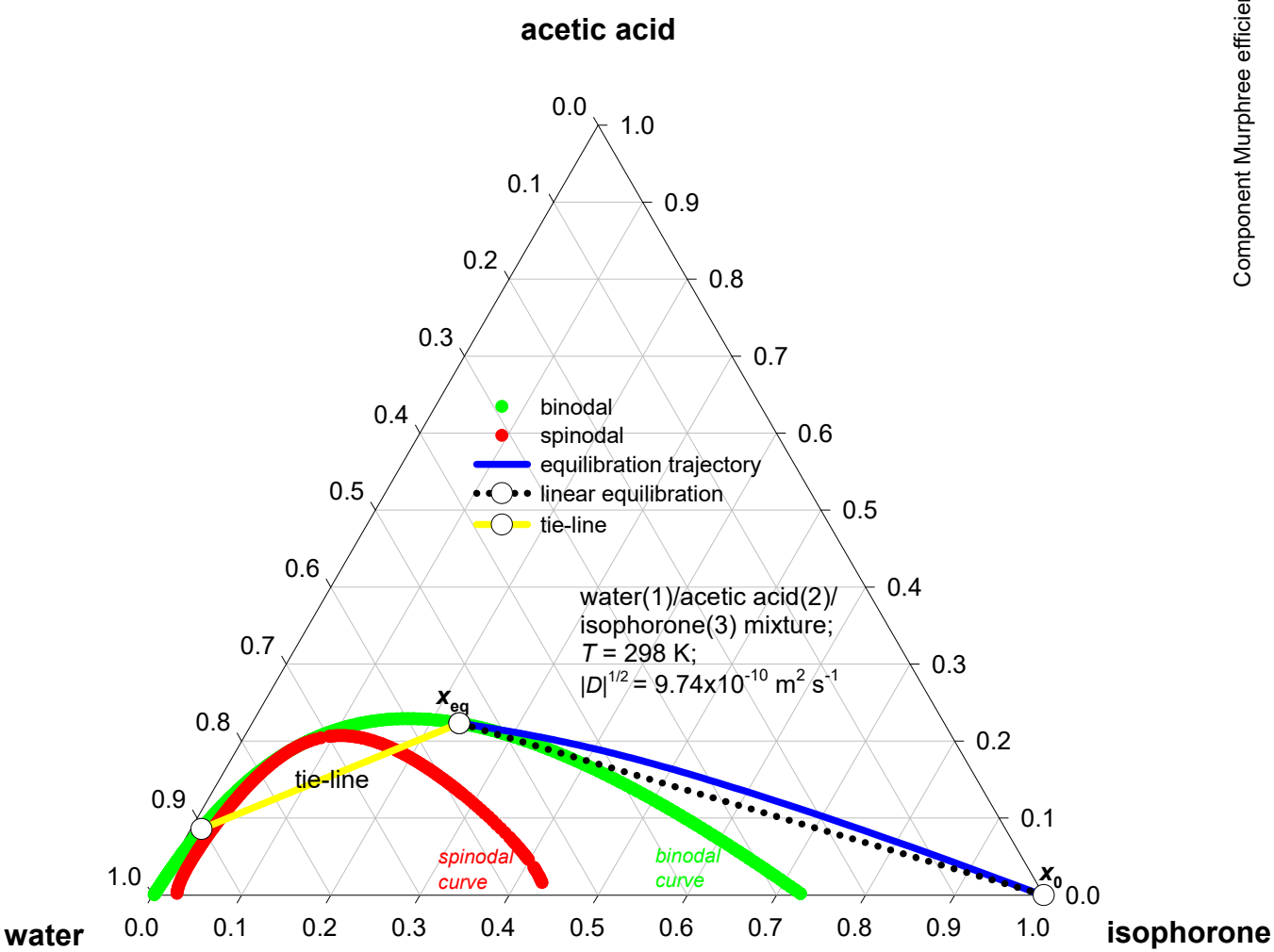

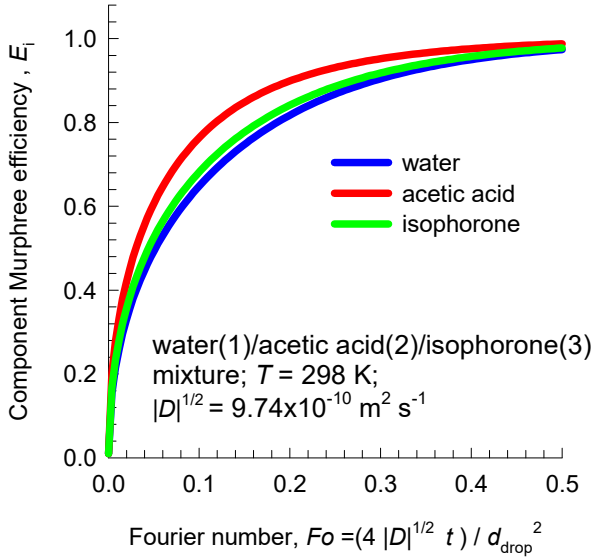

Fig. S13

Water/acetic acid/isophorone equilibration

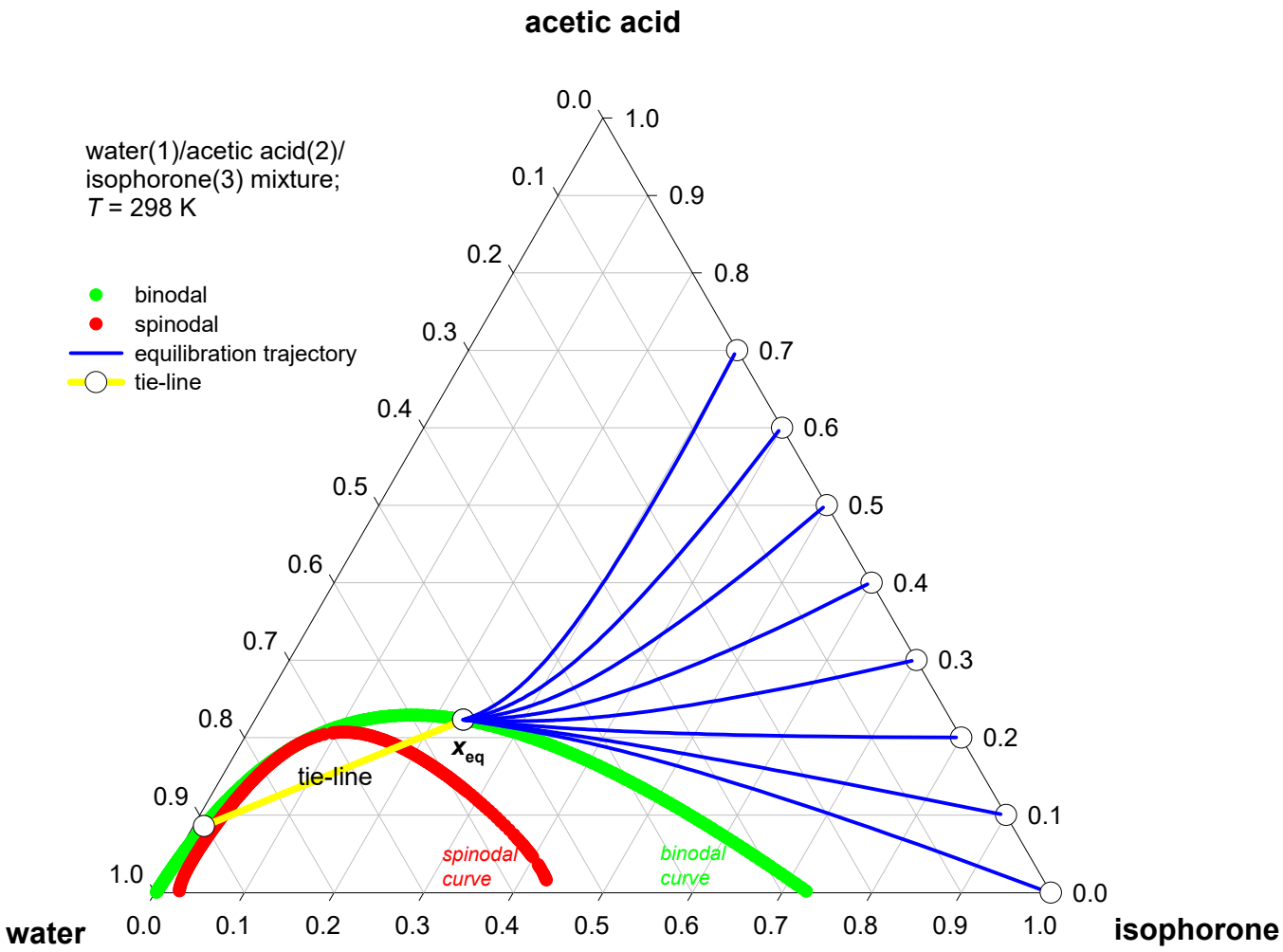

Fig. S14

Water/acetic acid/MTBE equilibration

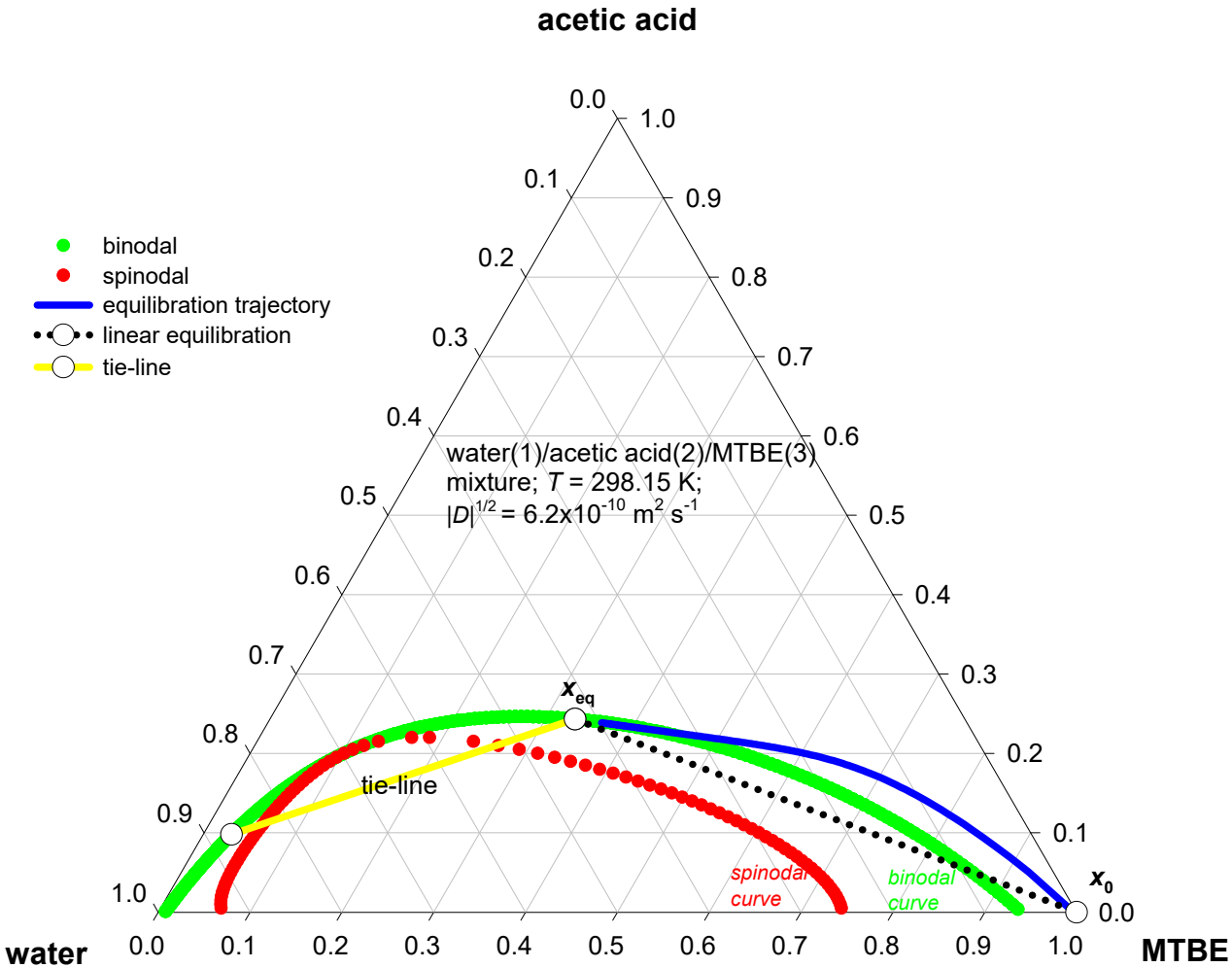

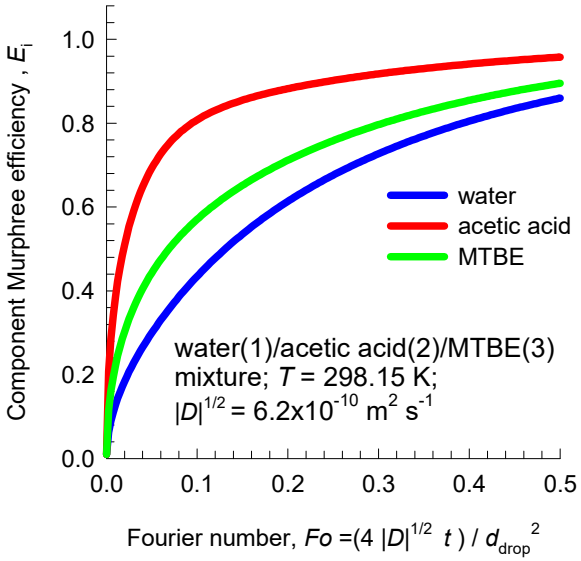

Fig. S15

Water/acetic acid/MTBE equilibration

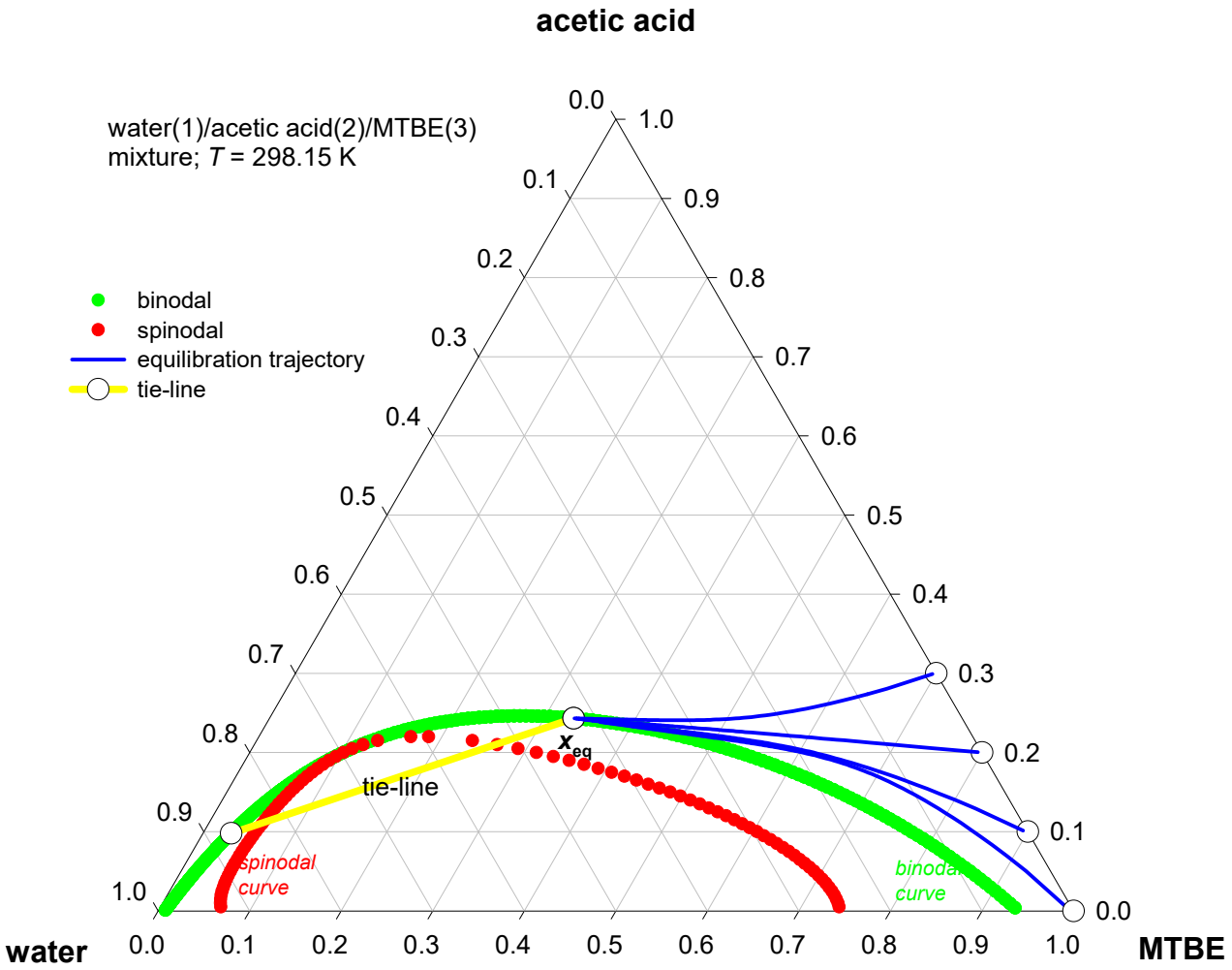

[omim][Cl]/ethanol/TAEE equilibration

Fig. S16

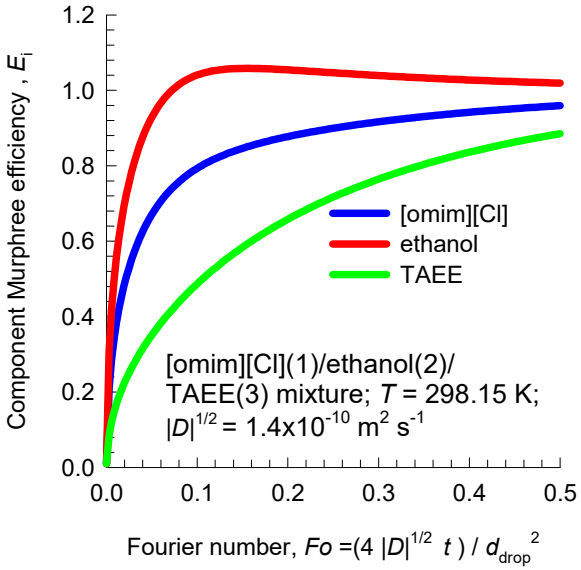

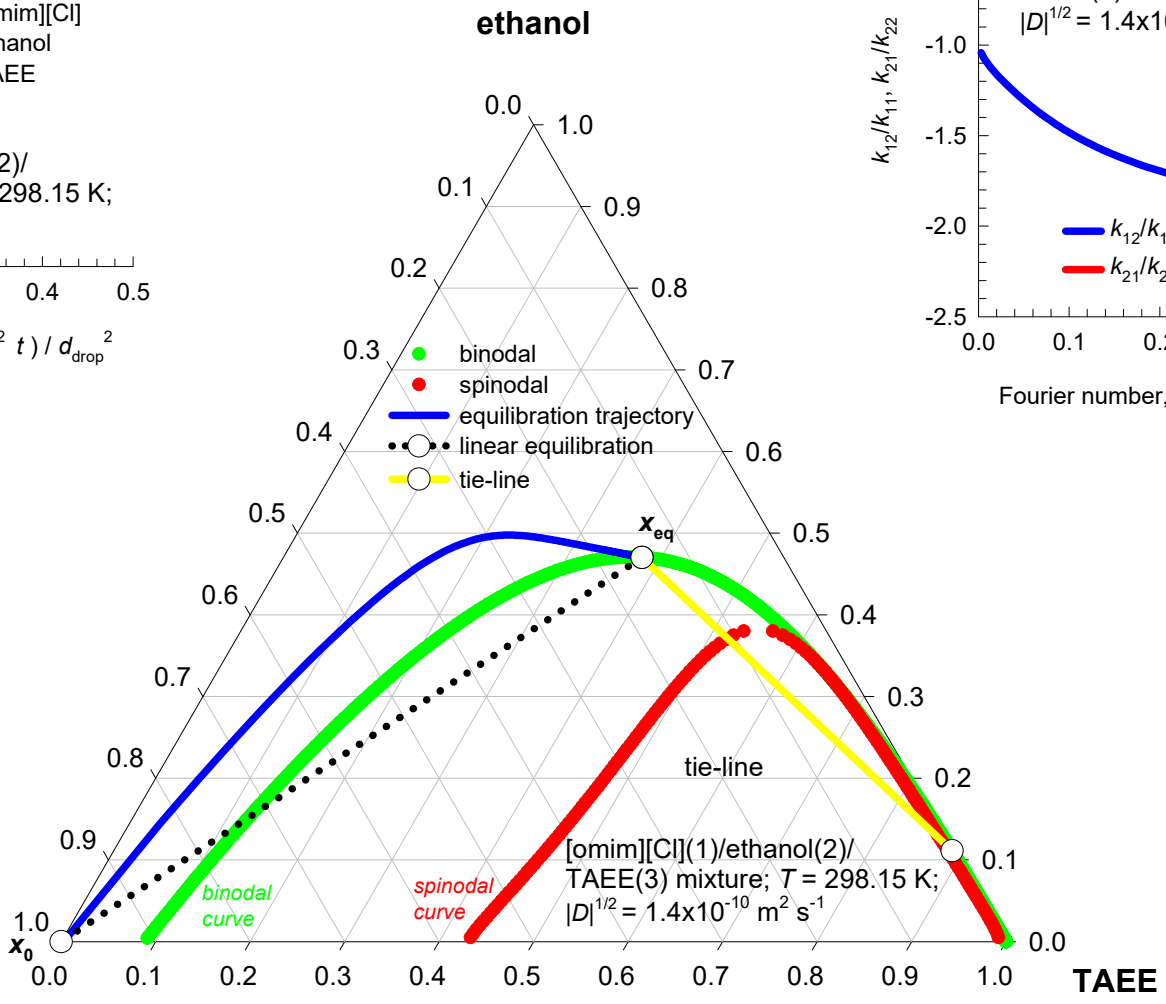

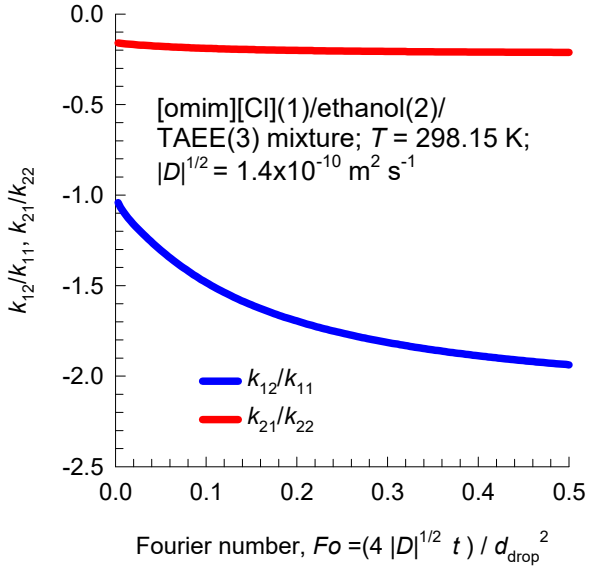

[omim][Cl]/ethanol/TAEE equilibration

Fig. S17

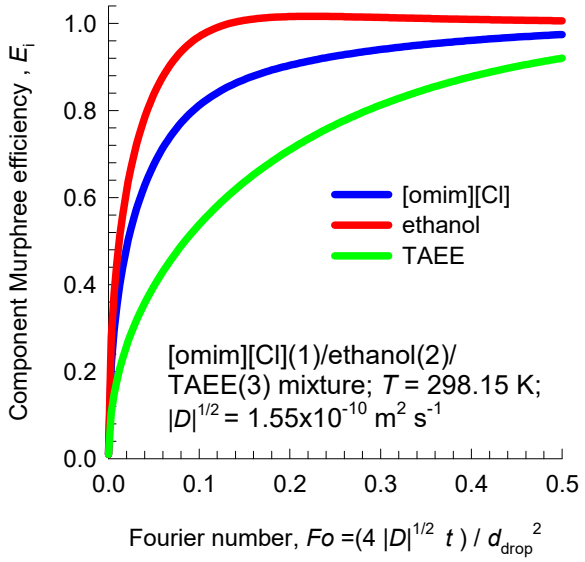

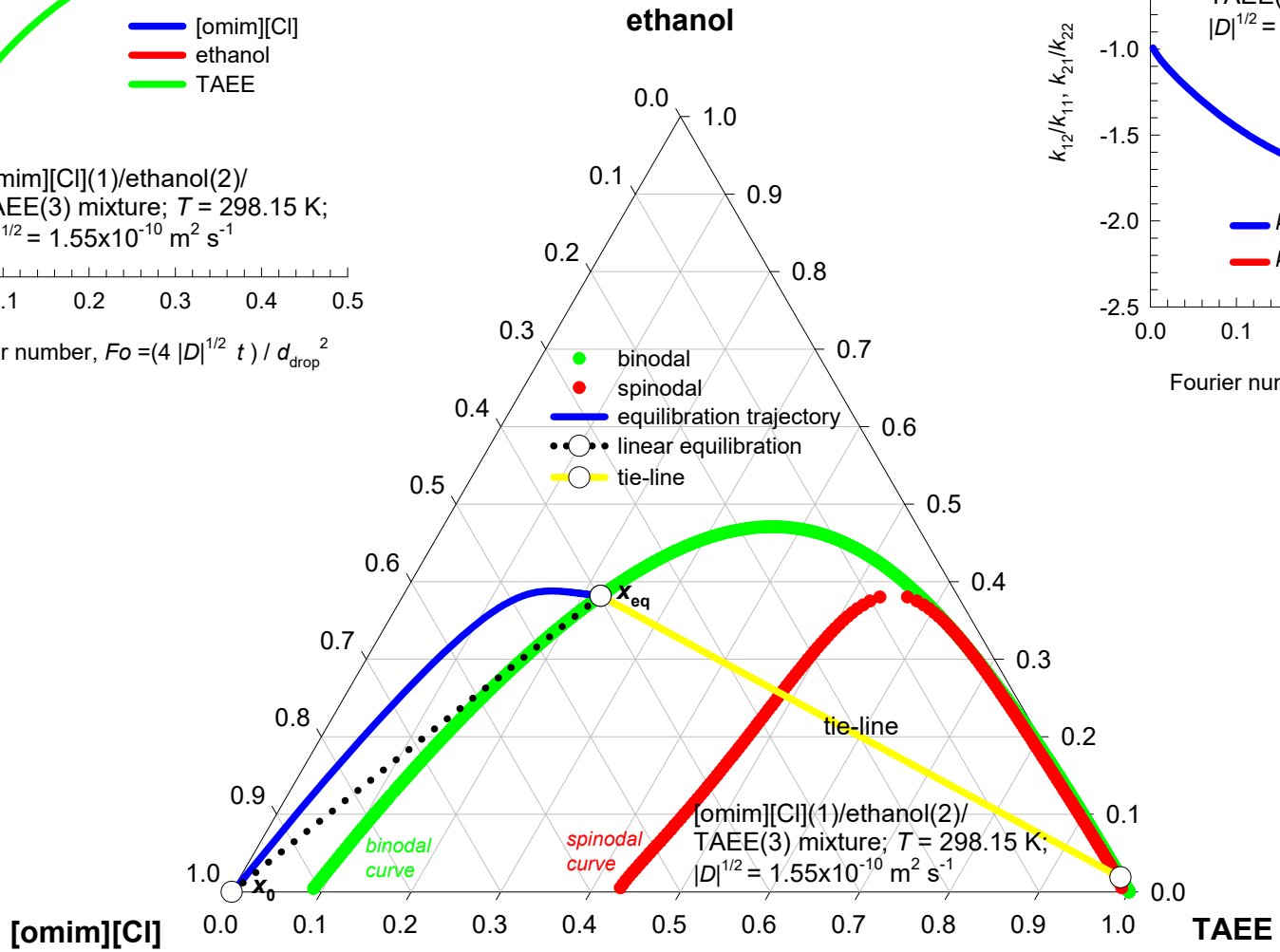

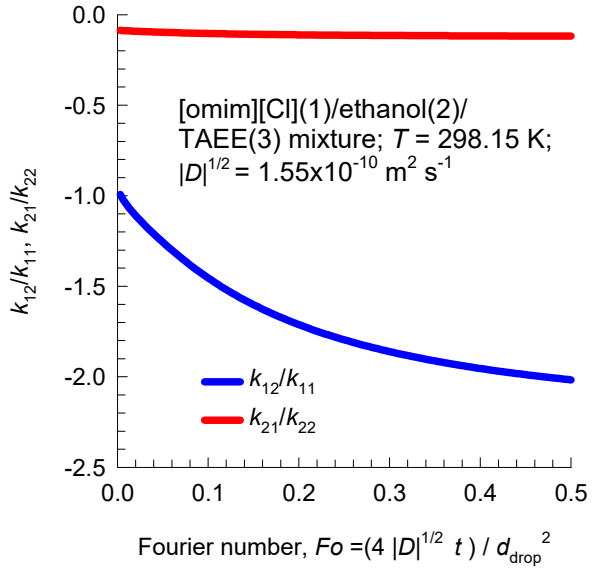

[omim][Cl]/ethanol/TAEE equilibration

Fig. S18

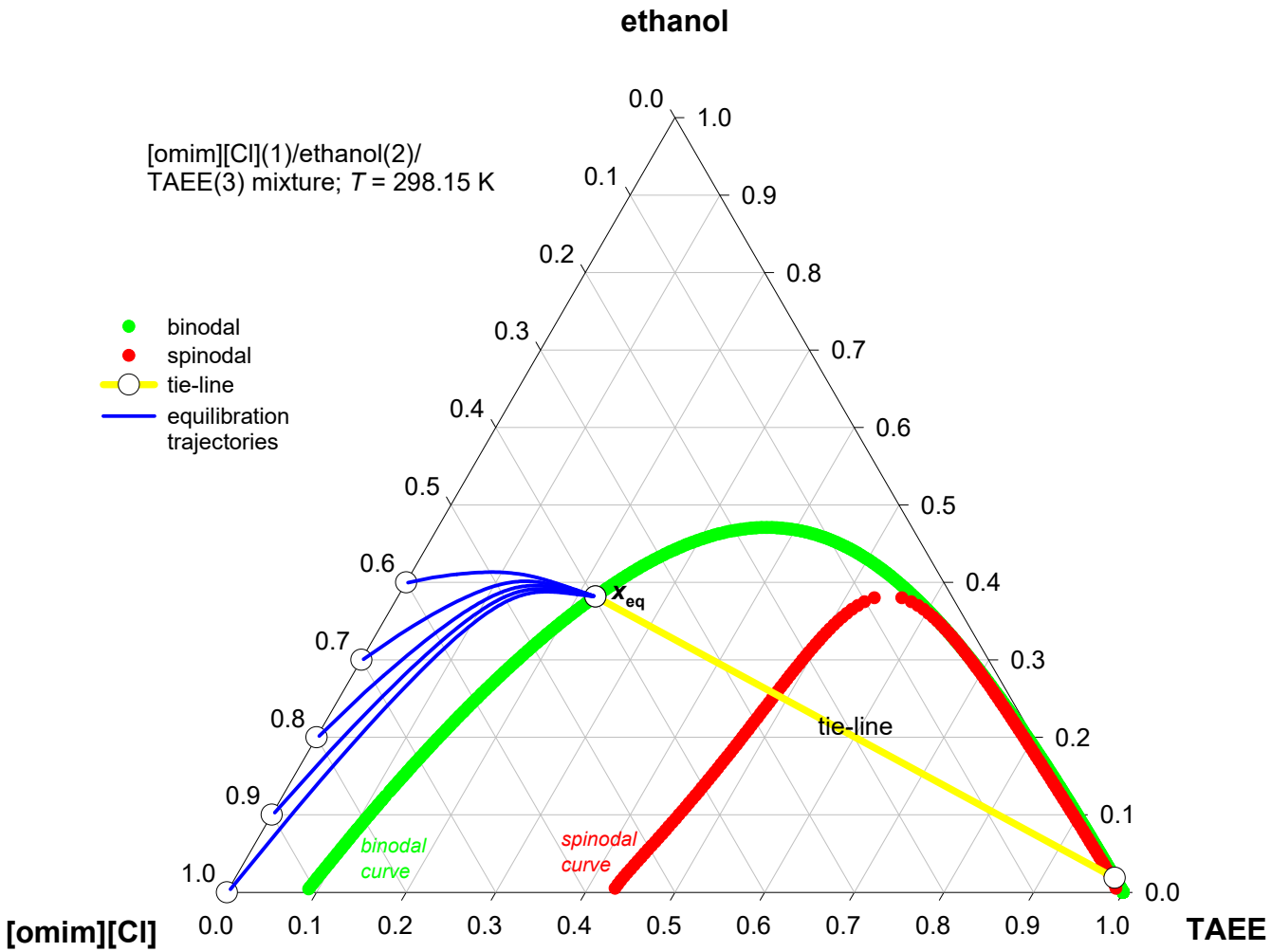

[bmim][TfO]/ethanol/TAEE equilibration

Fig. S19

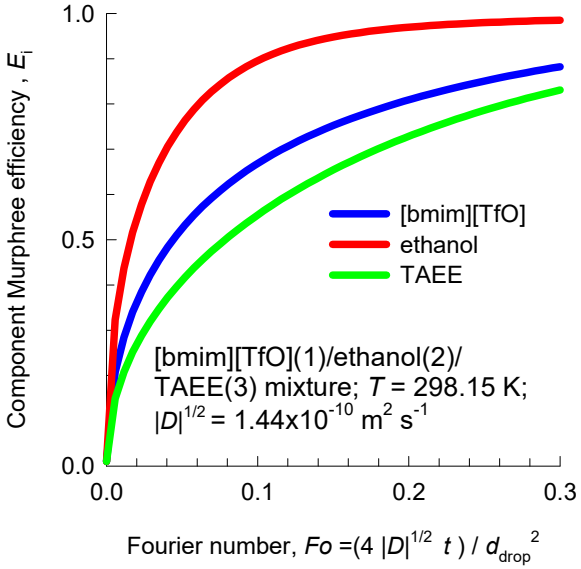

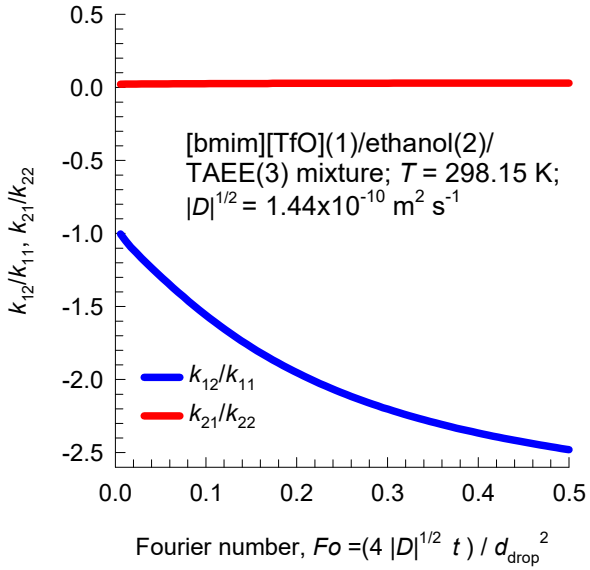

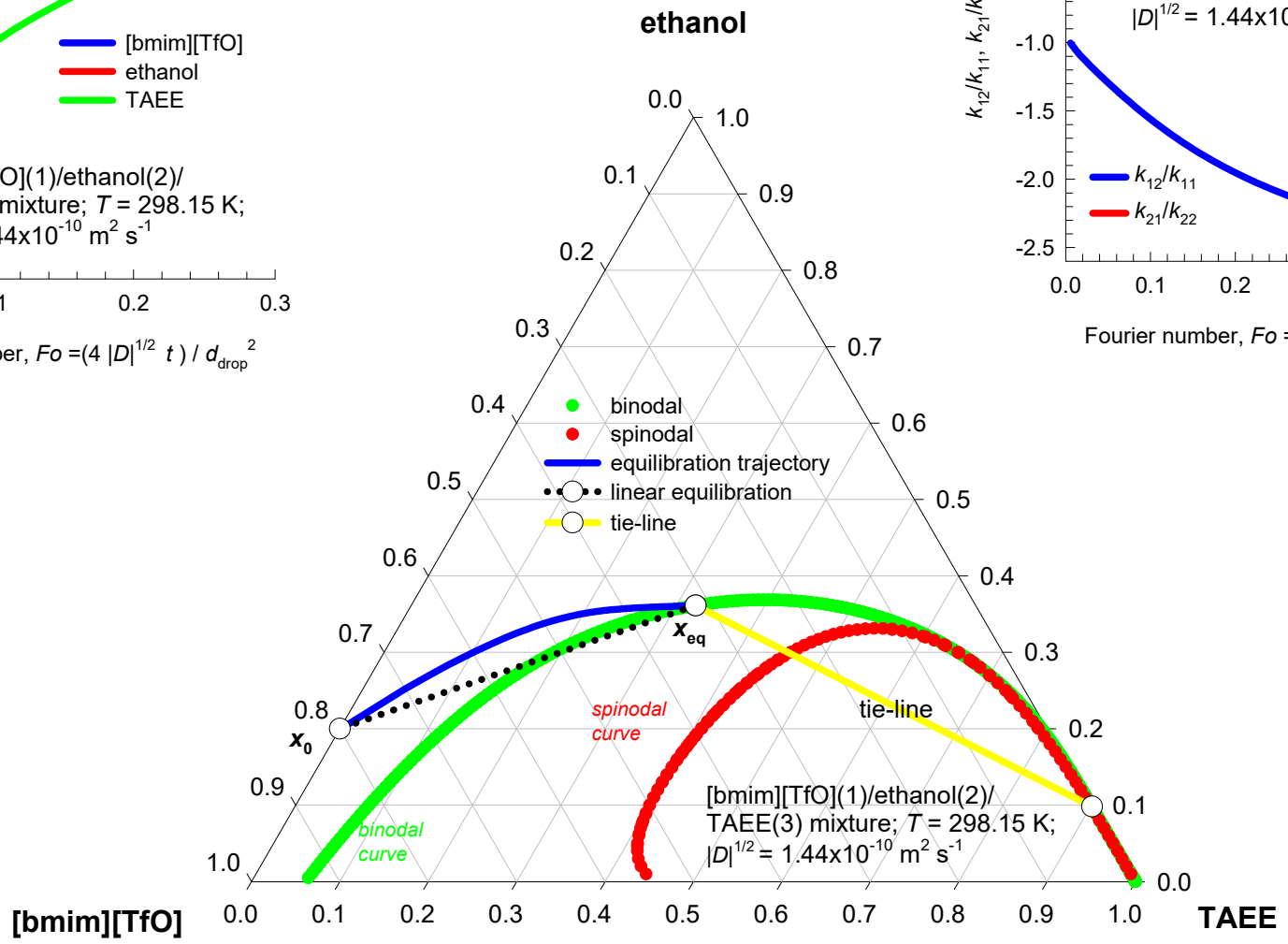

[bmim][TfO]/ethanol/TAEE equilibration

Fig. S20

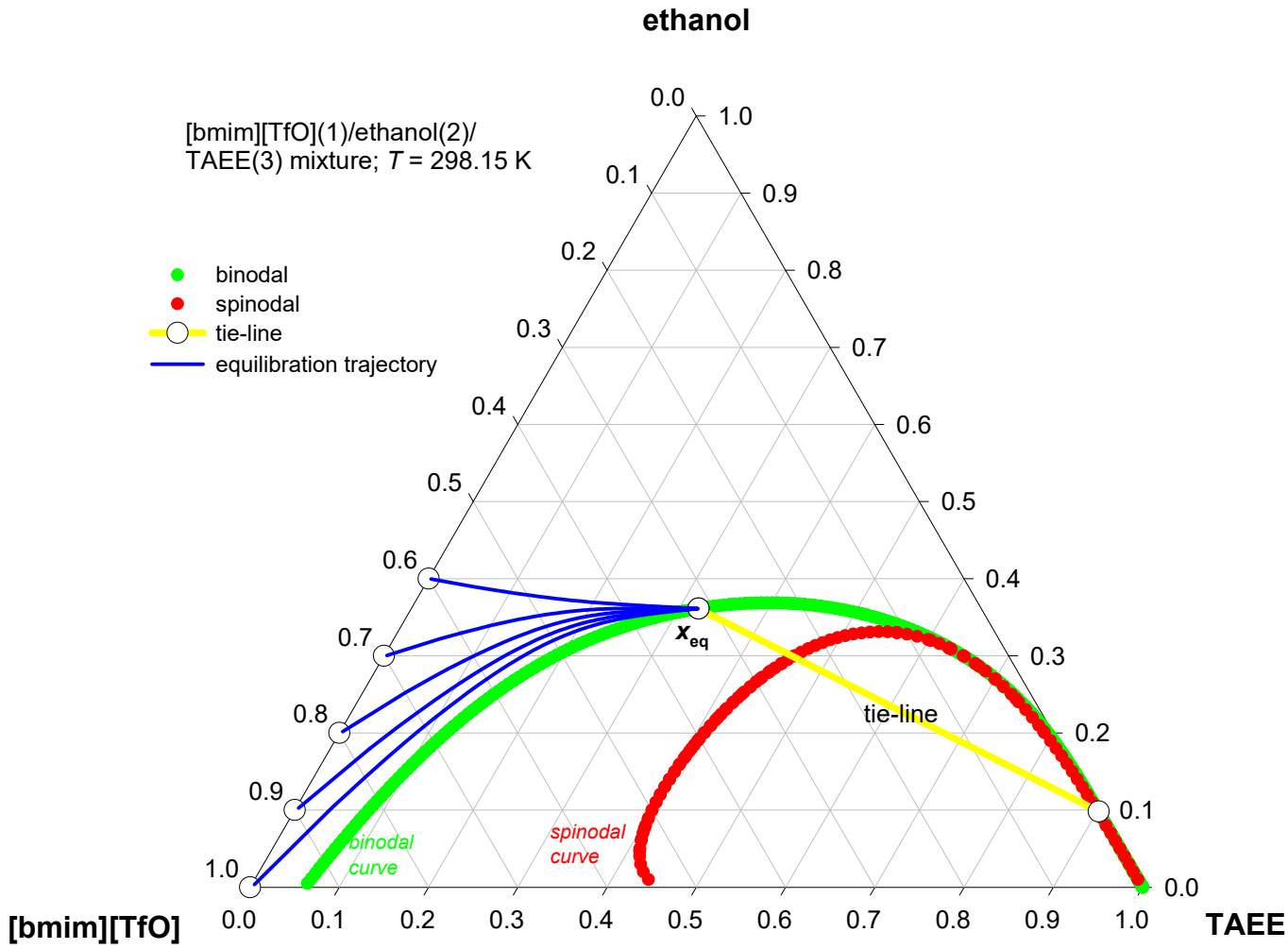

Water/Ethanol/Cyclohexane equilibration

Fig. S21

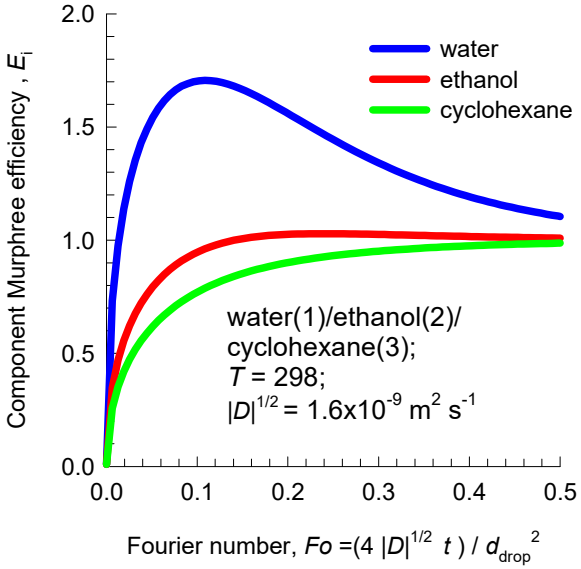

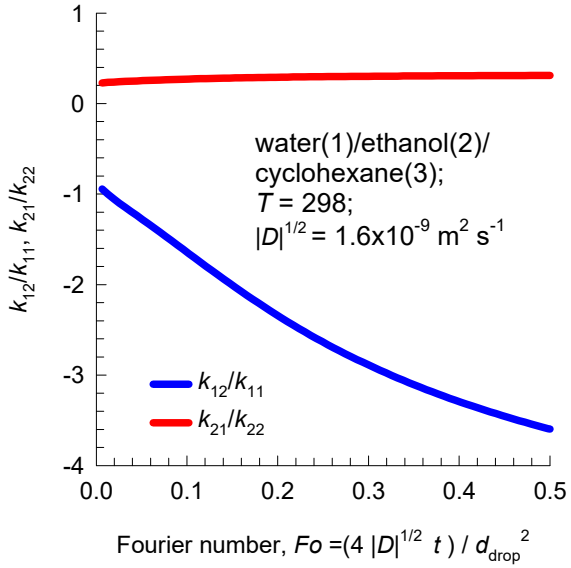

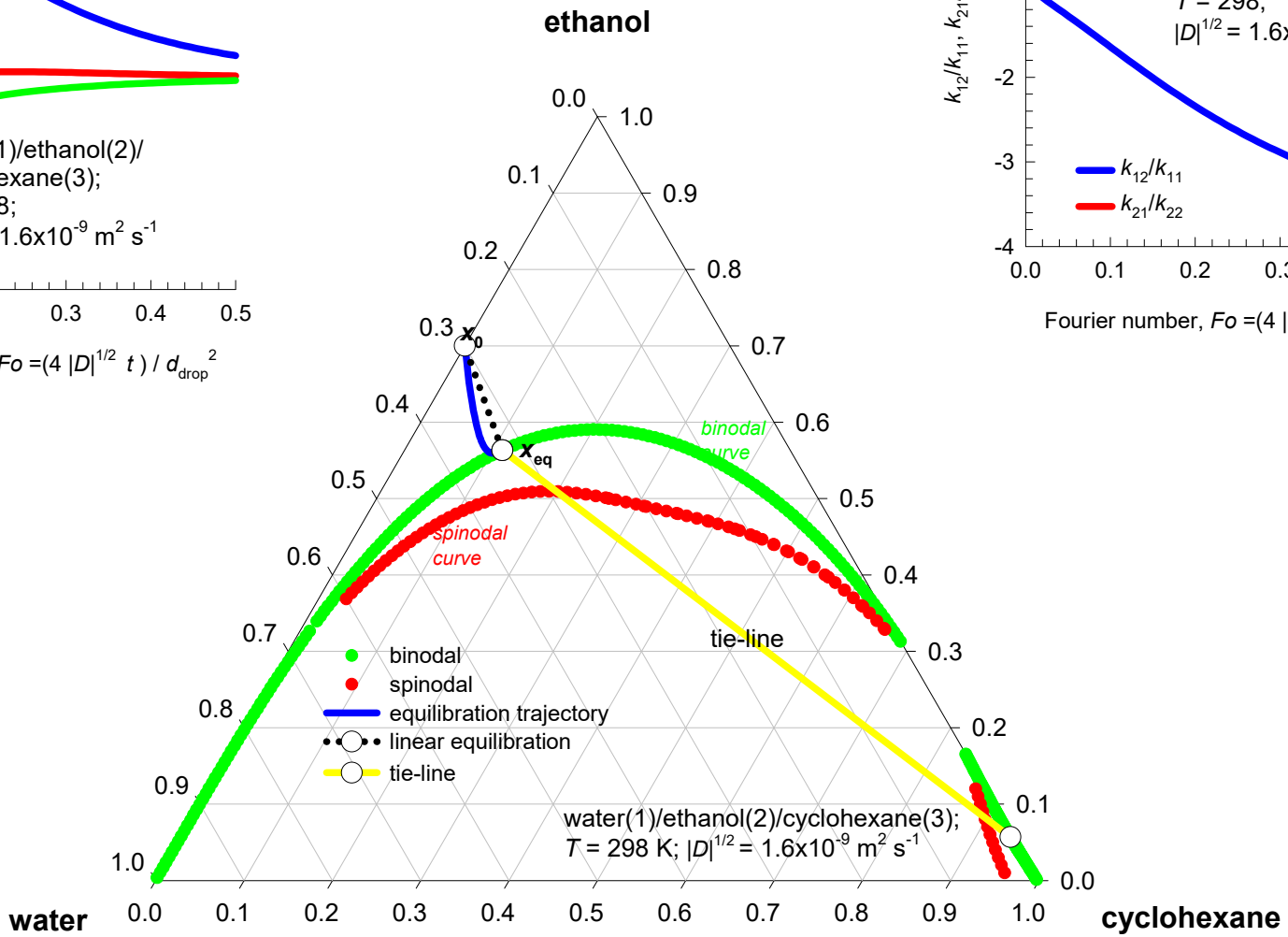

Water/Ethanol/Cyclohexane equilibration

Fig. S22

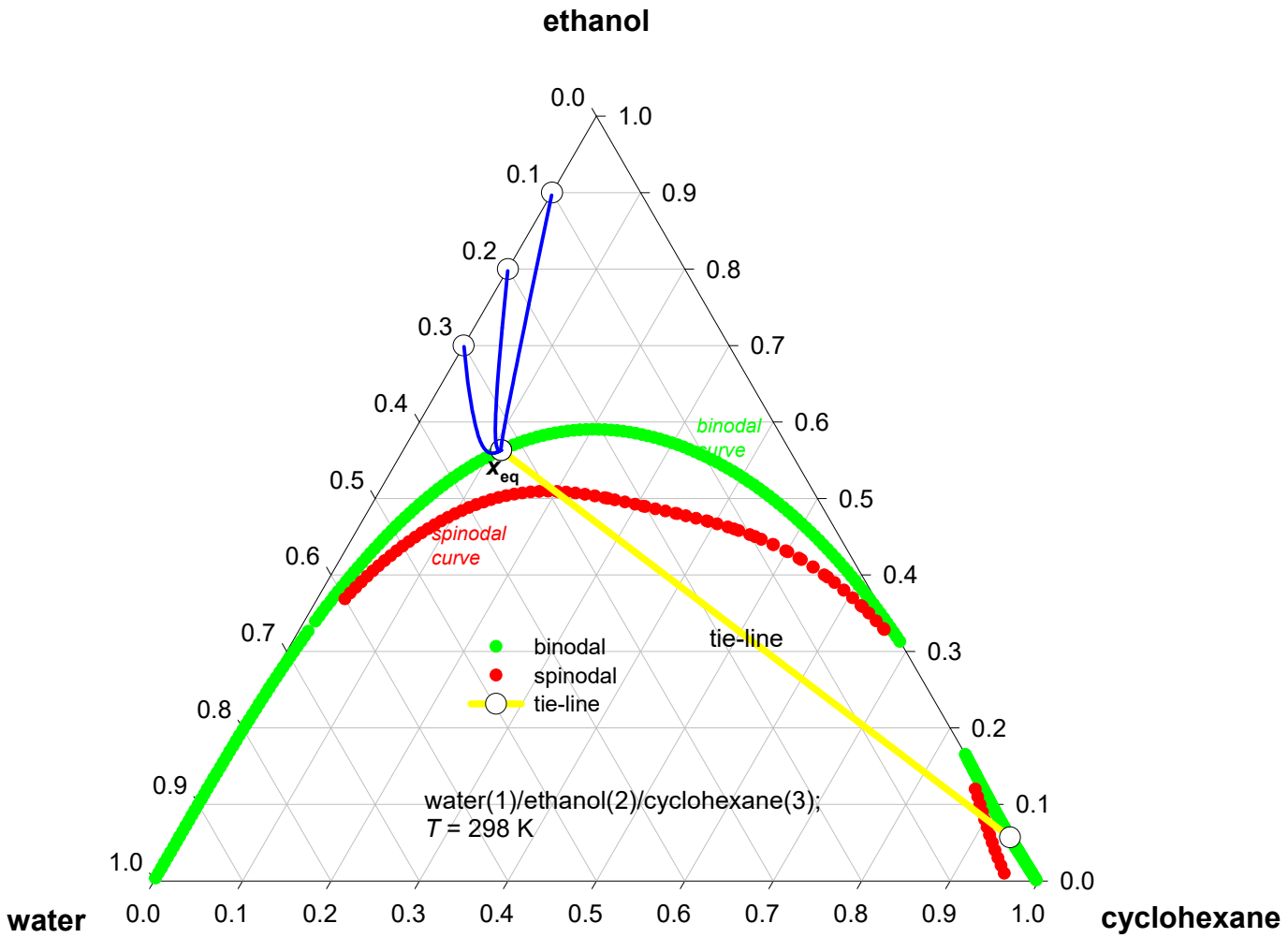

Toluene/ethanol/water equilibration

Fig. S23

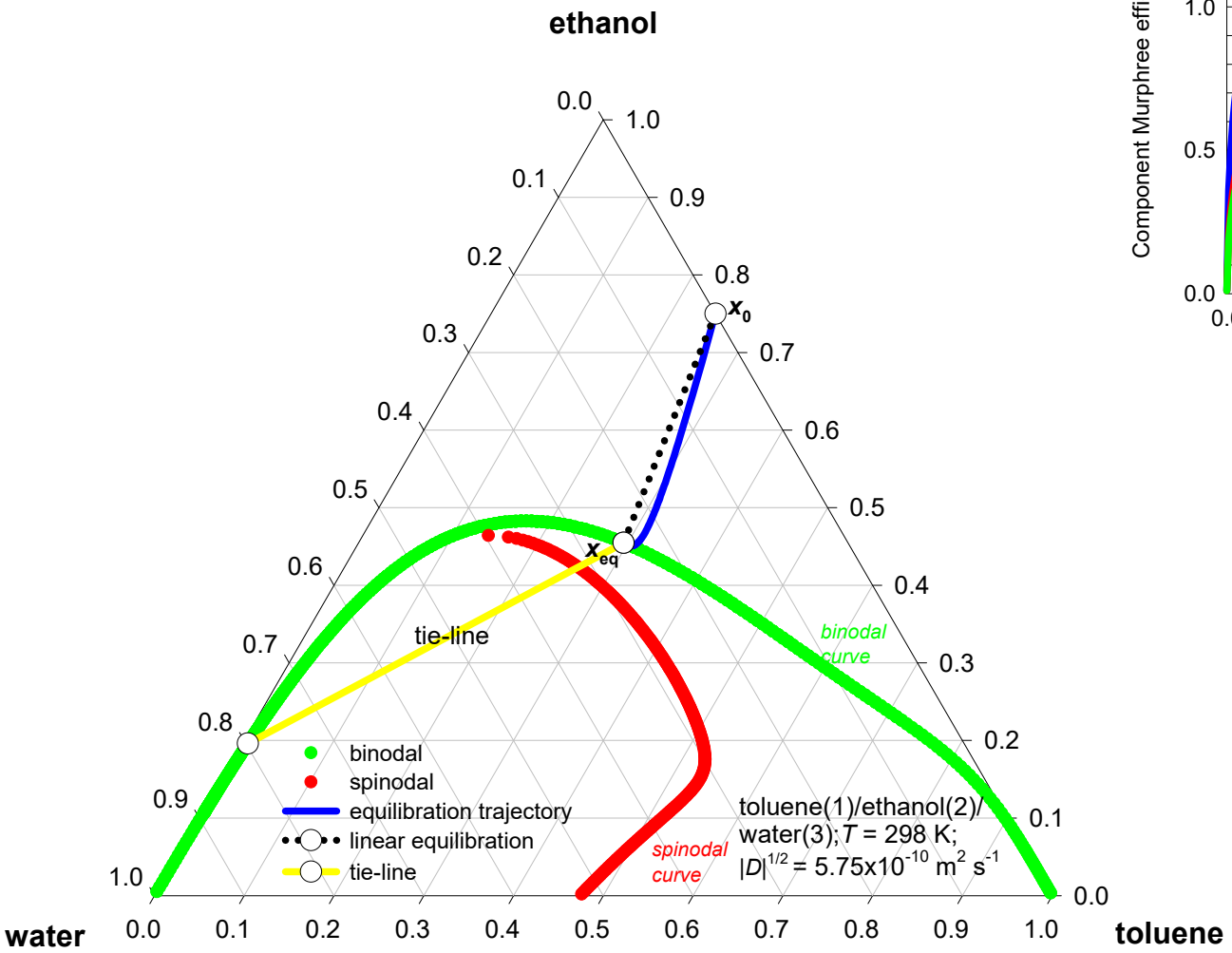

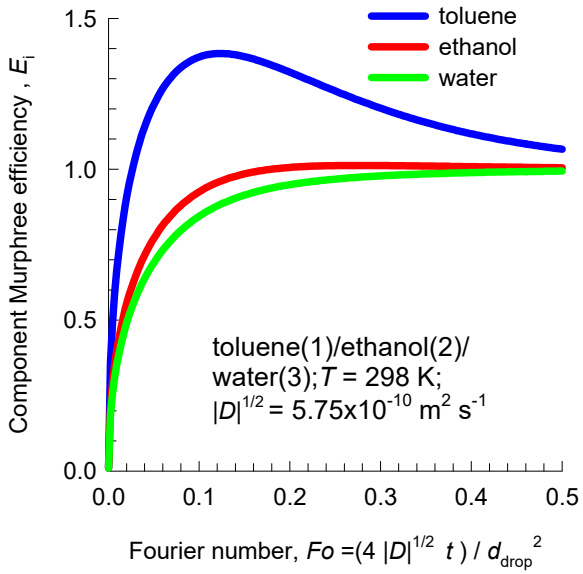

Toluene/ethanol/water equilibration

Fig. S24

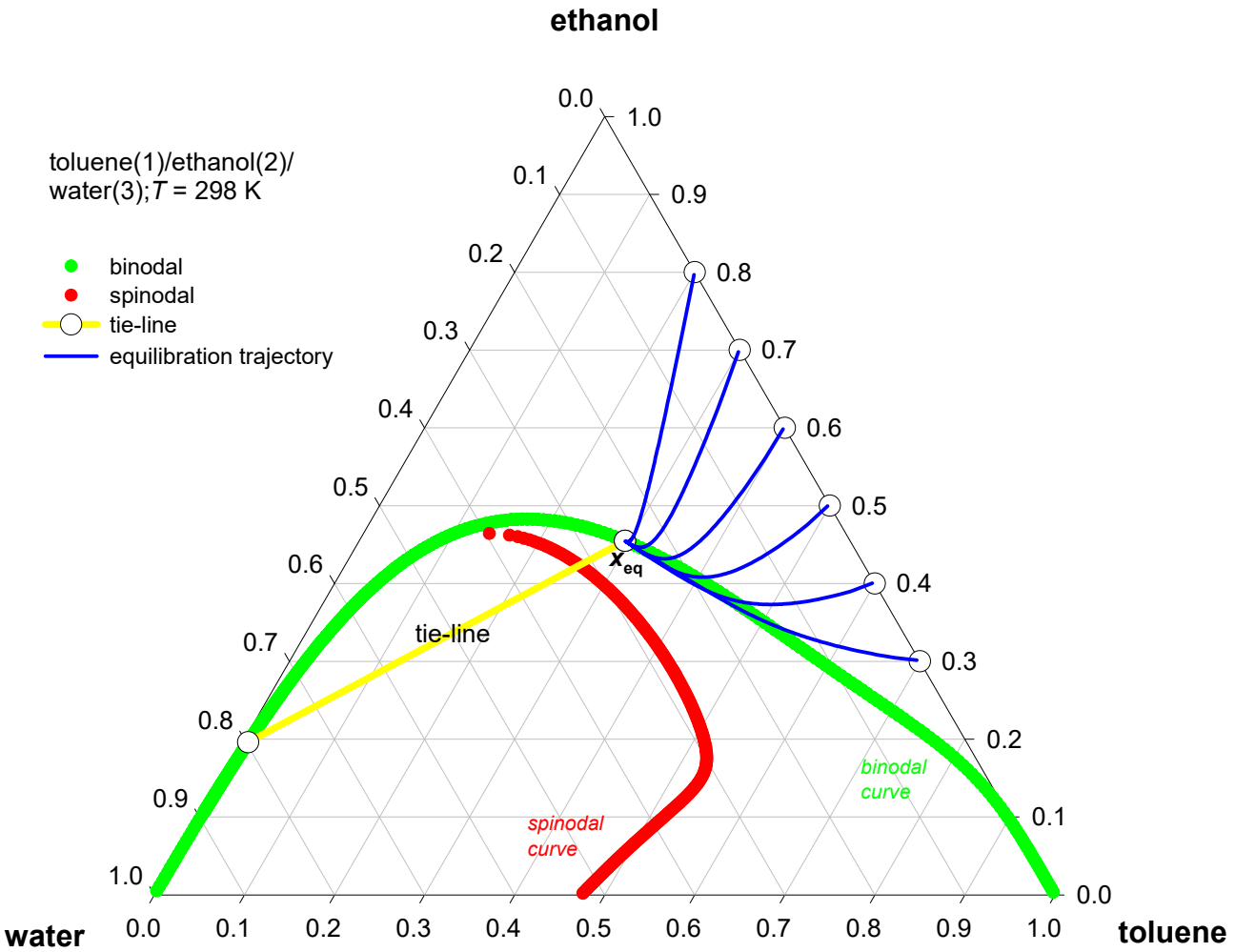

Water/Acetone/Toluene equilibration

Fig. S25

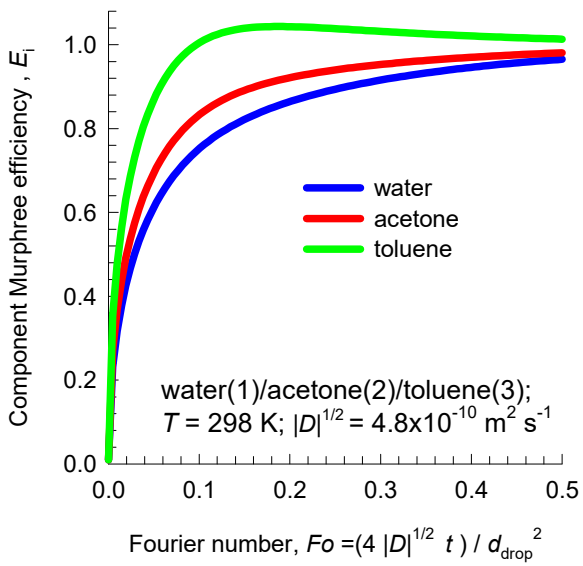

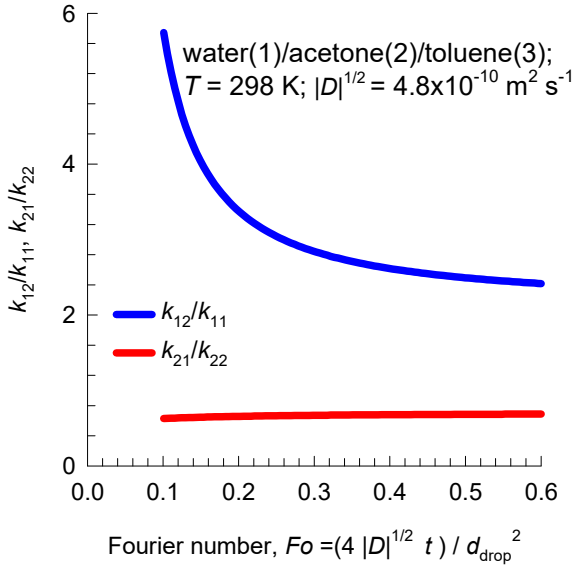

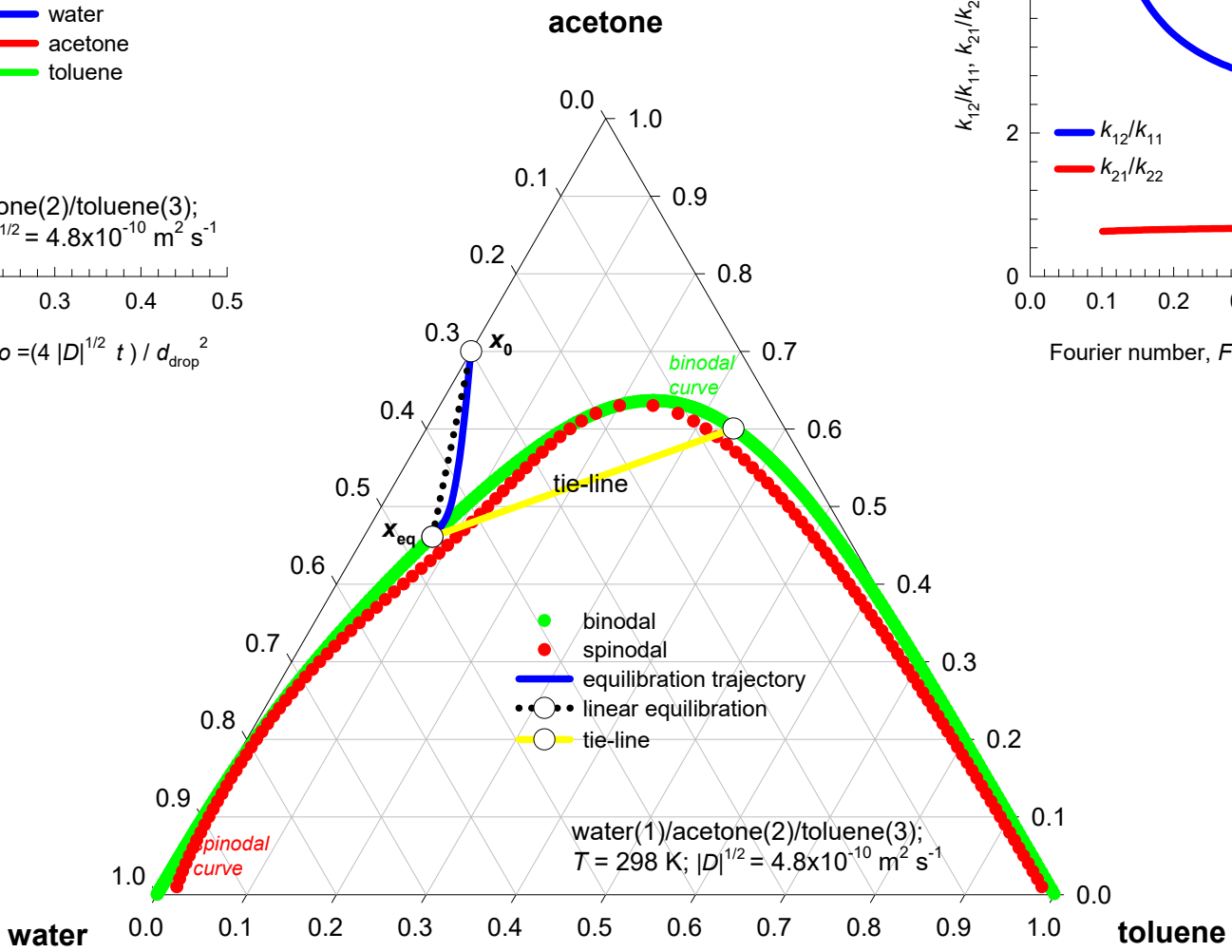

Water/Acetone/Toluene equilibration

Fig. S26

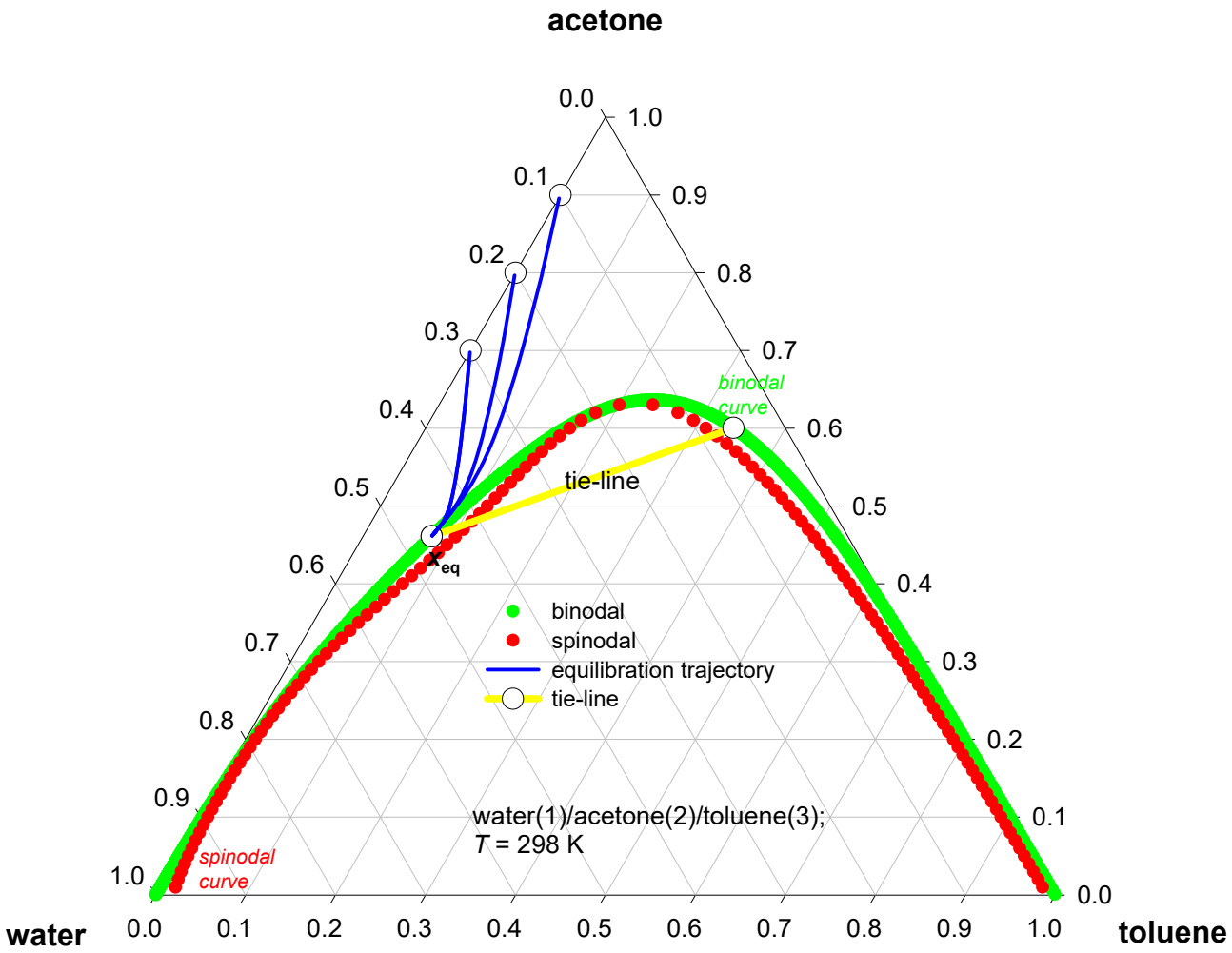

Vapor/liquid contacting on distillation tray

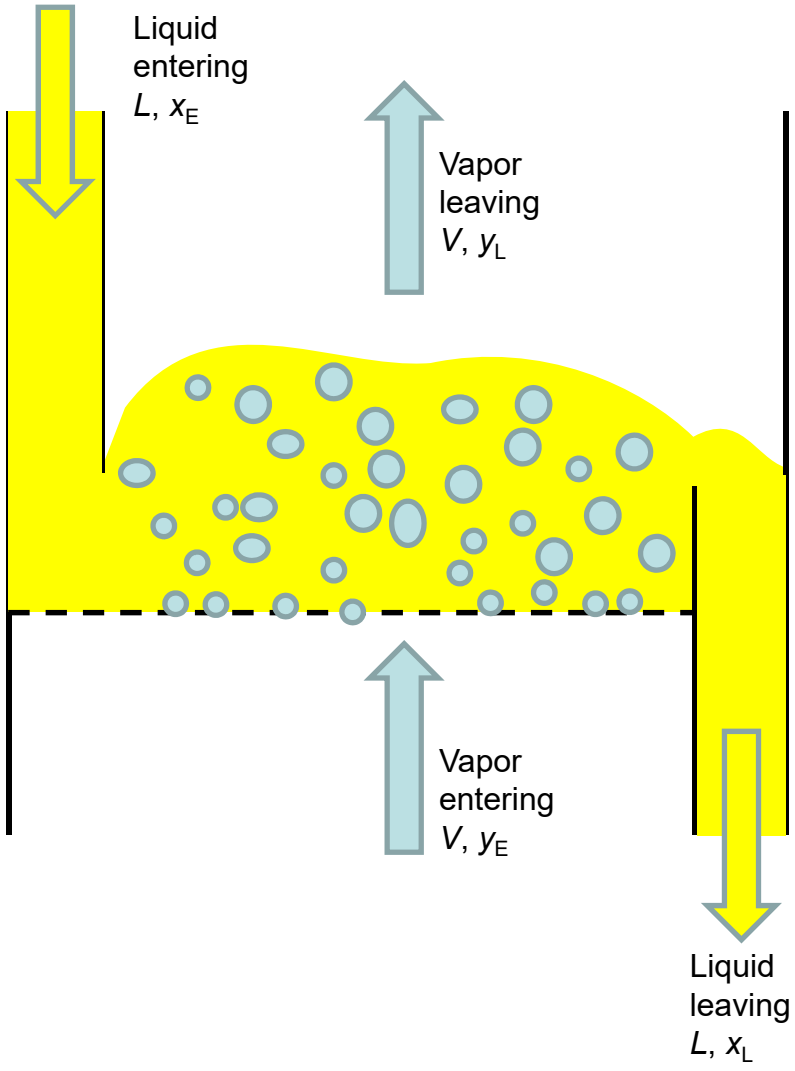

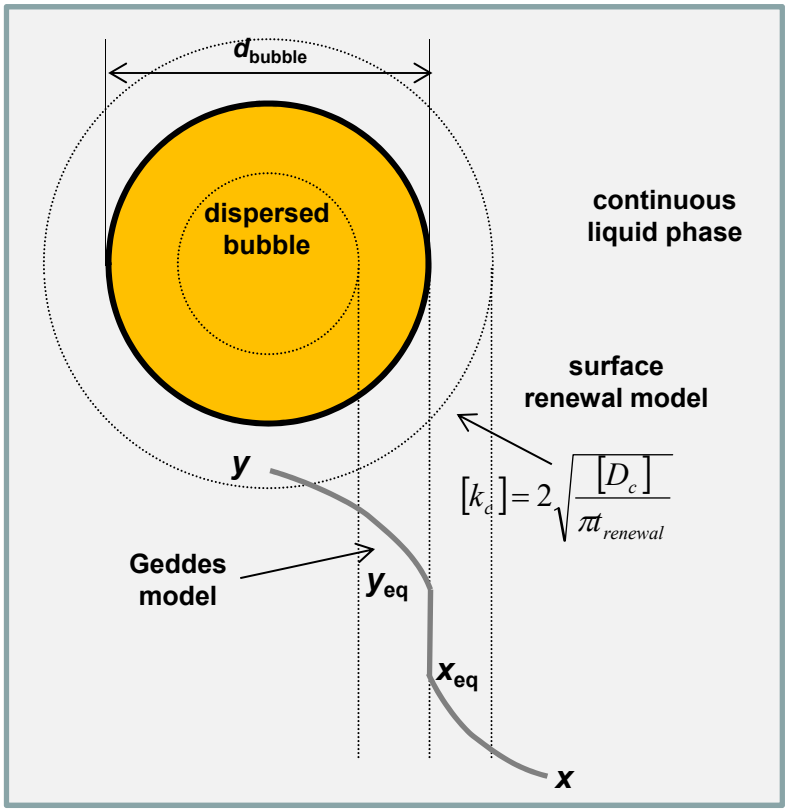

Levy rules for boundary crossing

Fig. S28

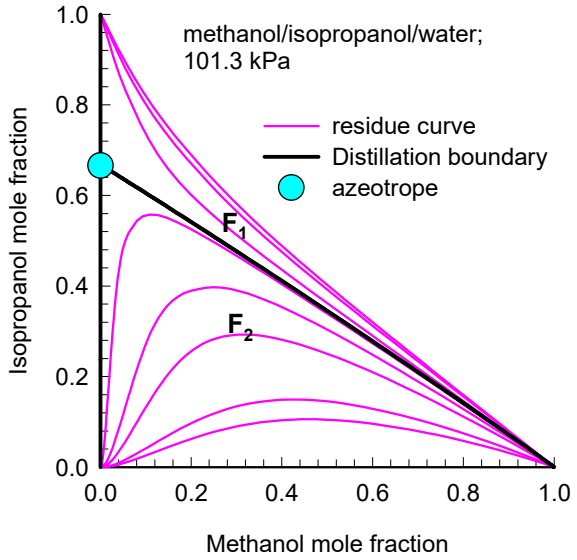

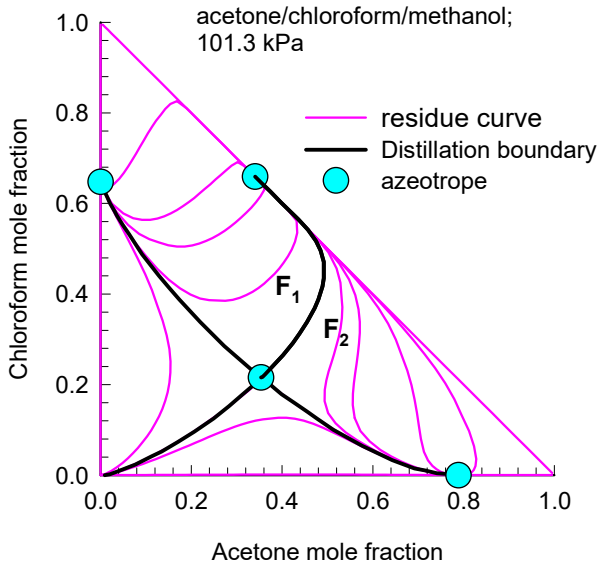

Springer experimental set-up

Fig. S29

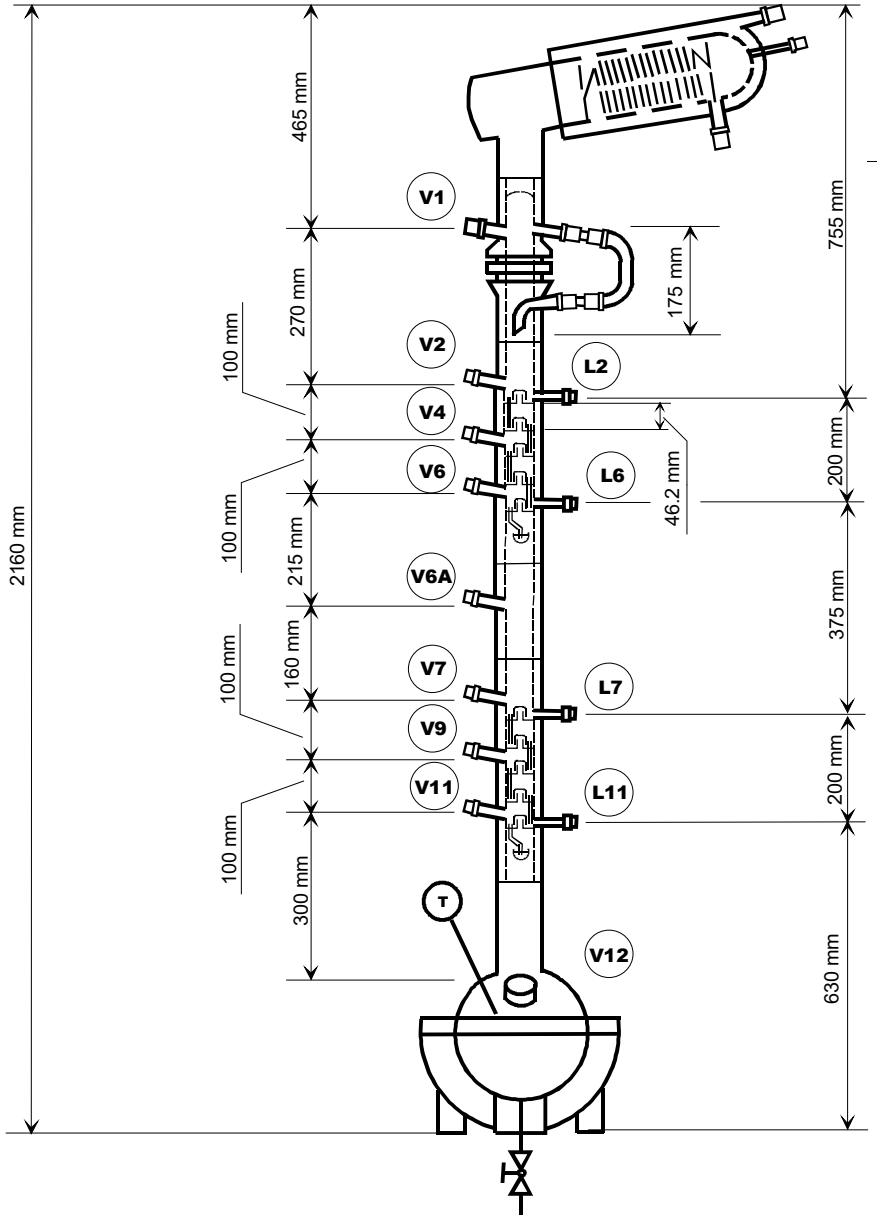

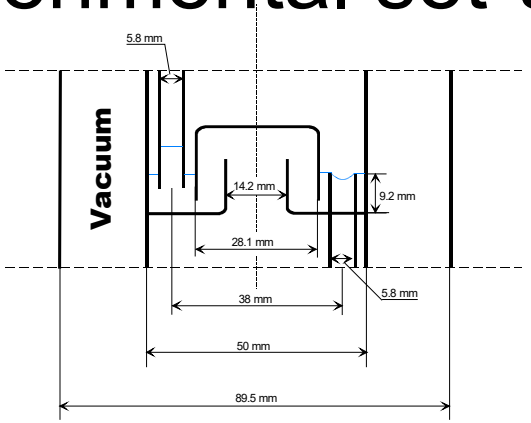

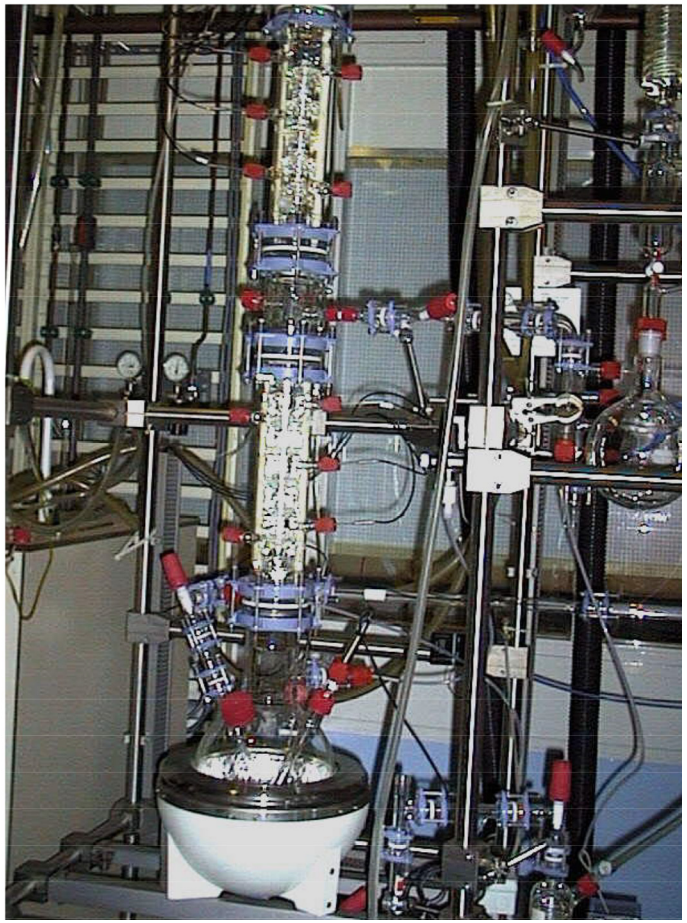

Water/Ethanol/Acetone Distillation

Fig. S30

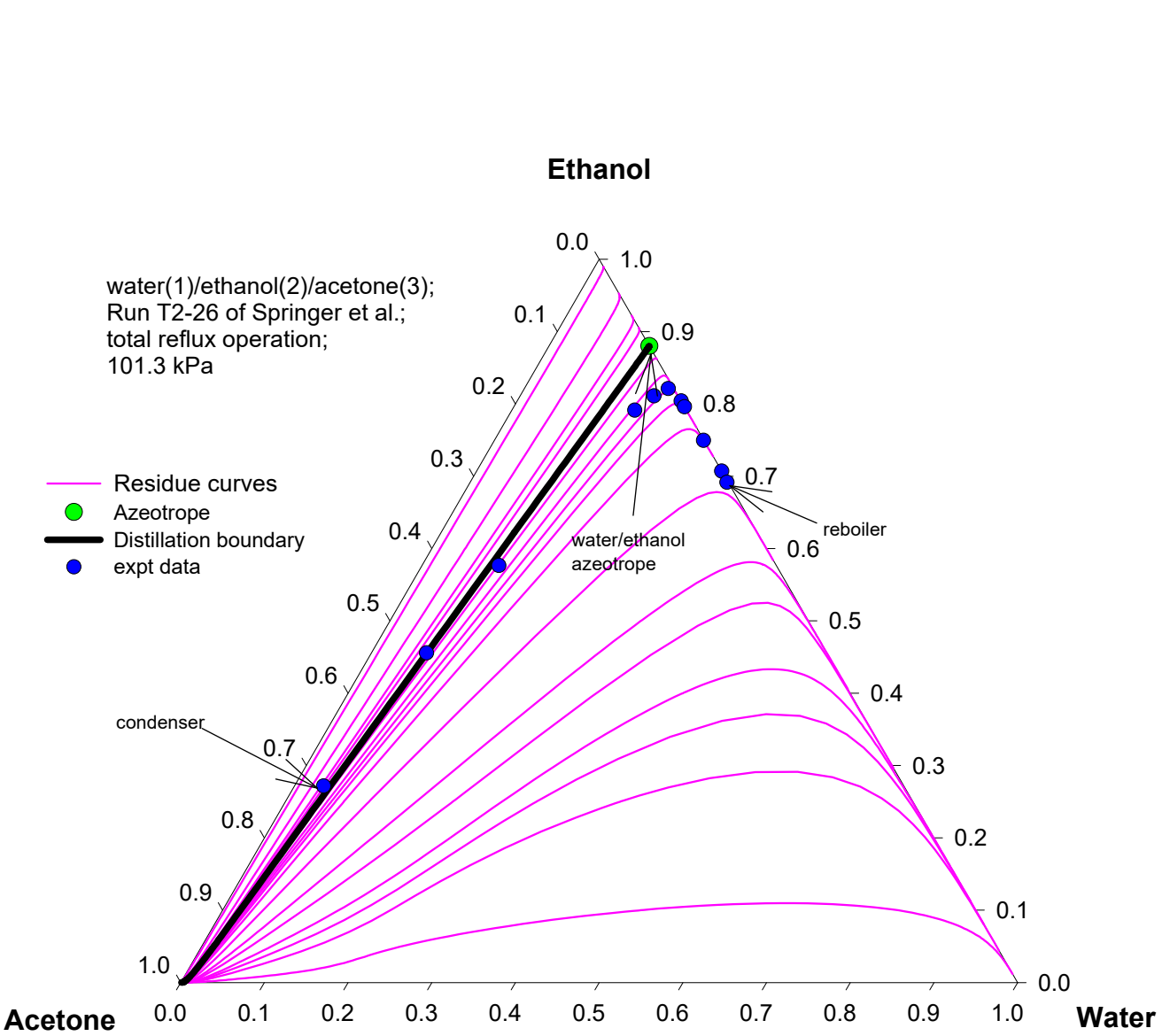

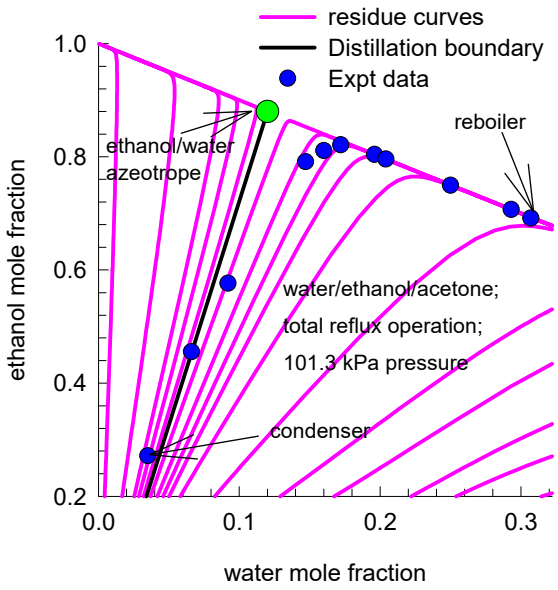

Murphree component efficiencies

Fig. S31

(a)

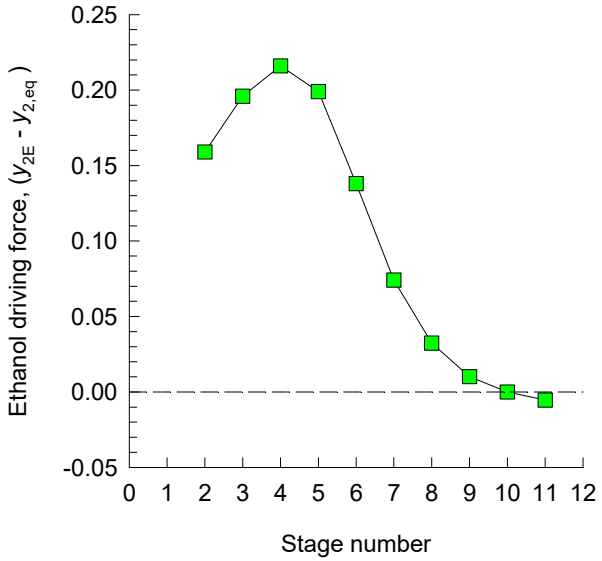

(b)

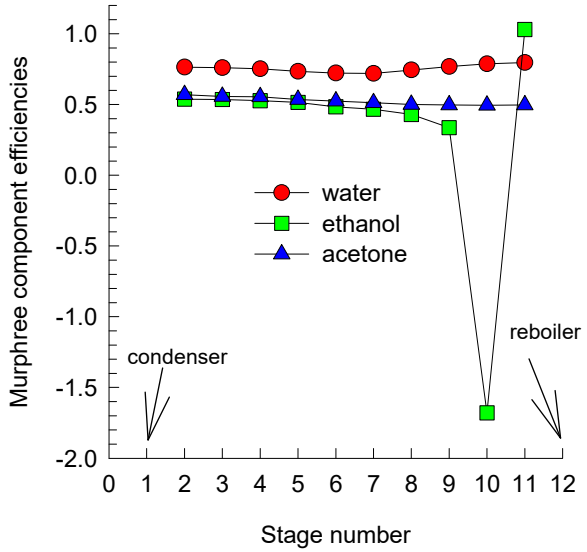

Water/Ethanol/Methanol Distillation

Fig. S32

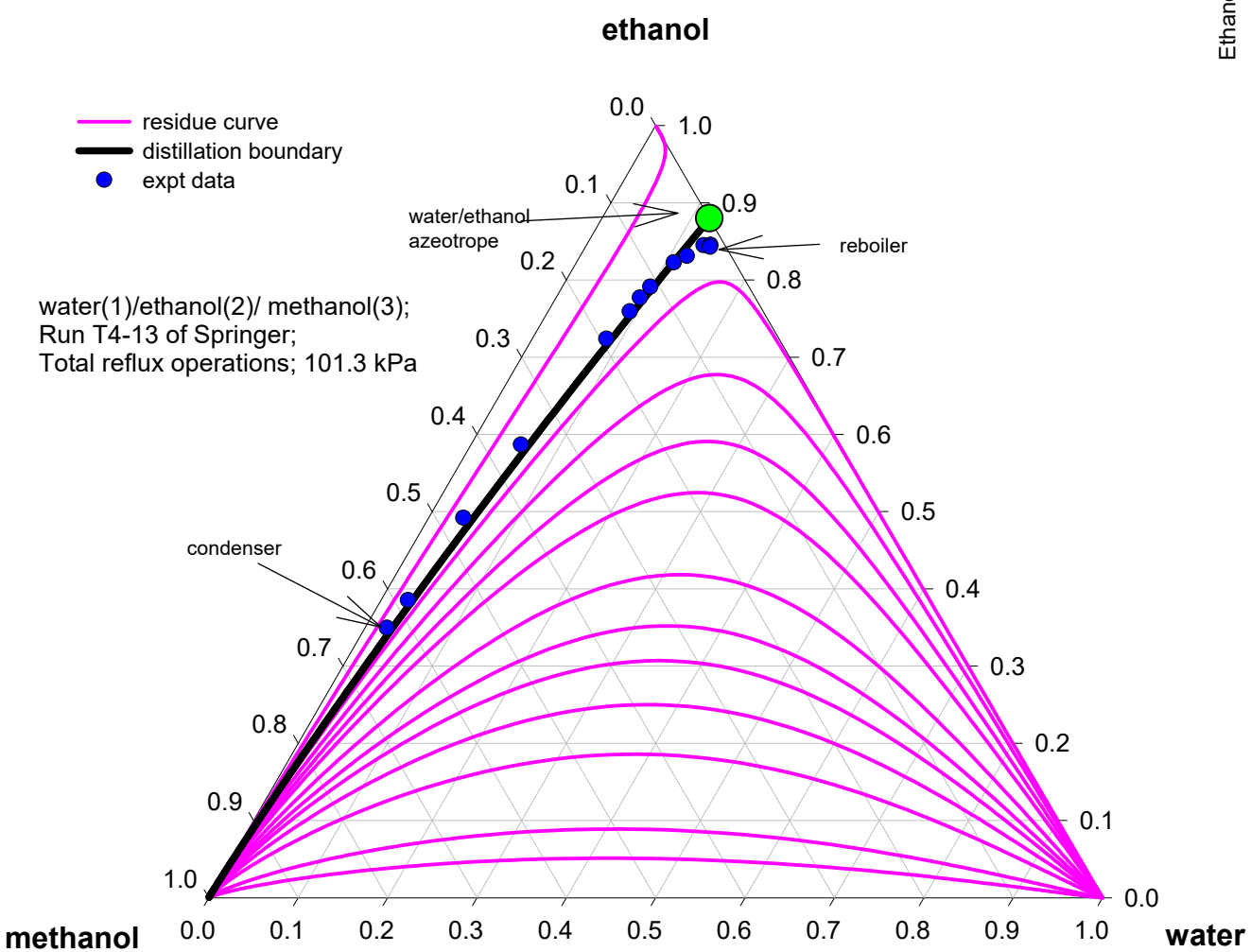

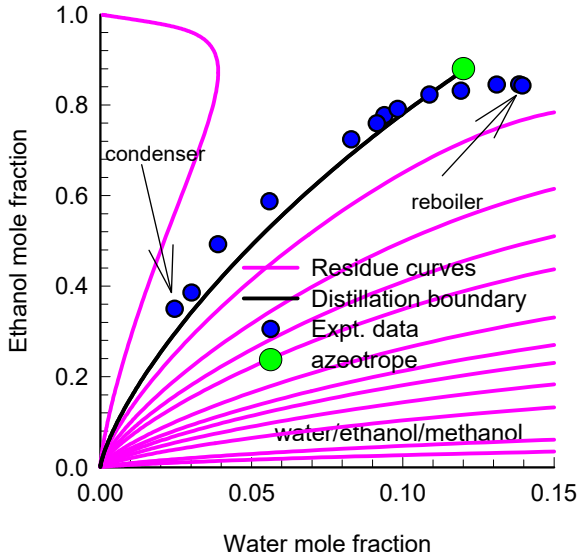

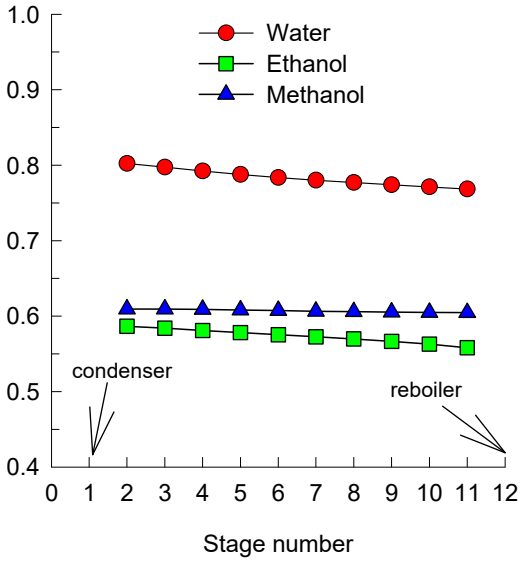

Water/Ethanol/Methylacetate Distillation

Fig. S33

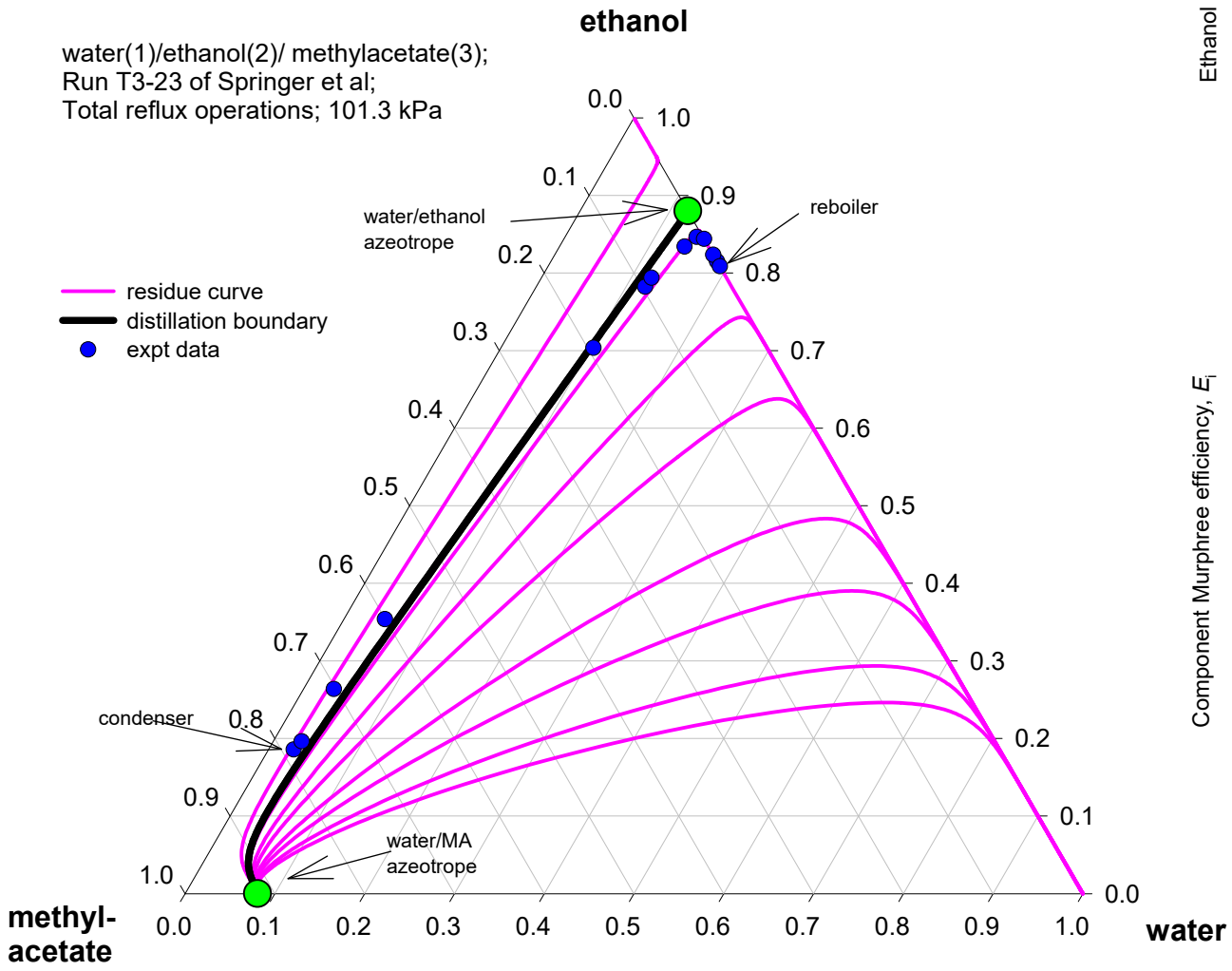

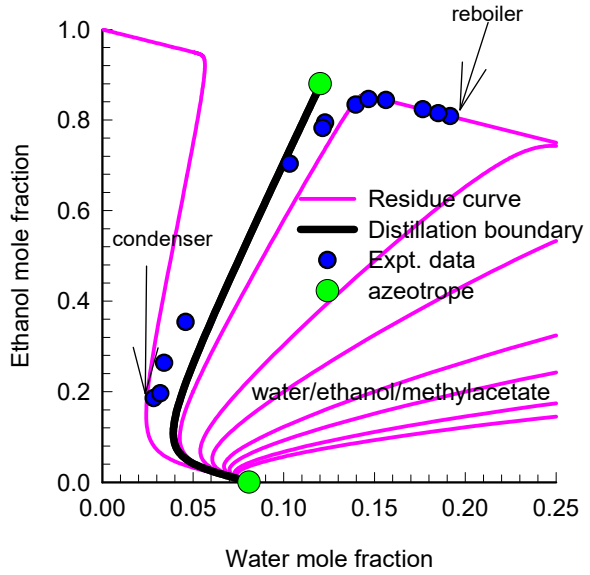

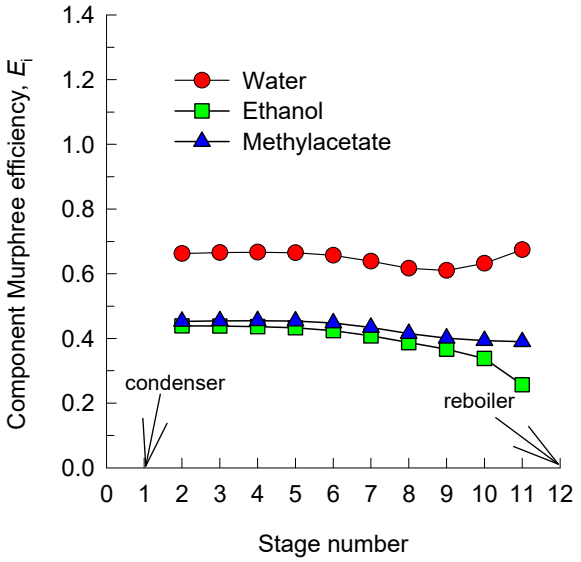

Water/Ethanol/Acetone/Methanol Distillation

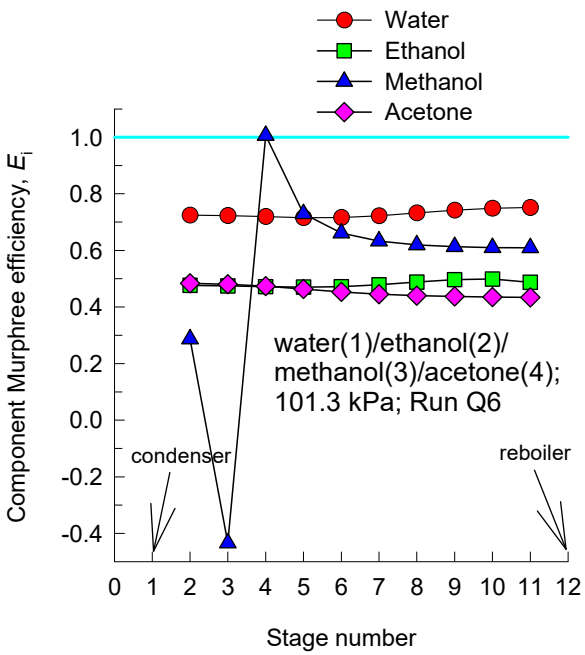

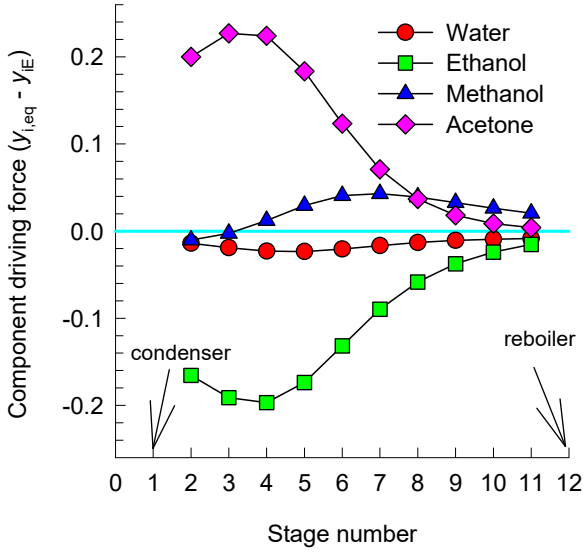

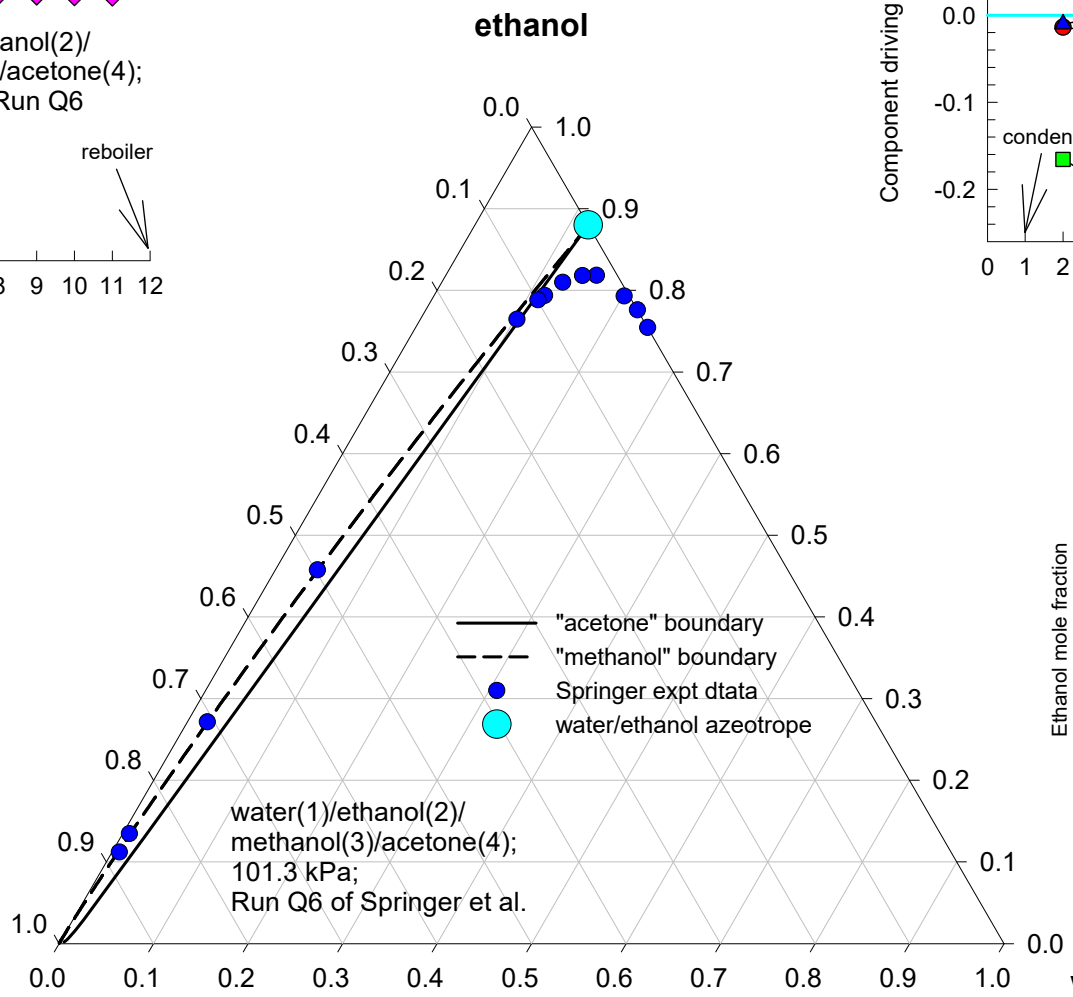

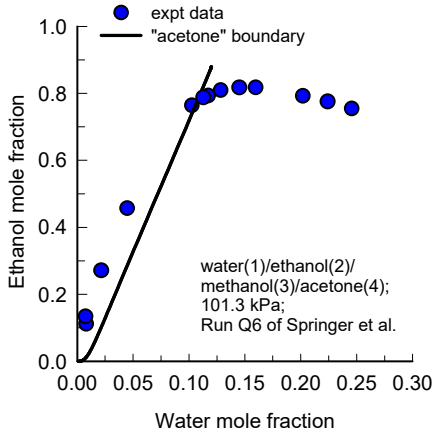

Water/Ethanol/Acetone Distillation

Fig. S35

(a)

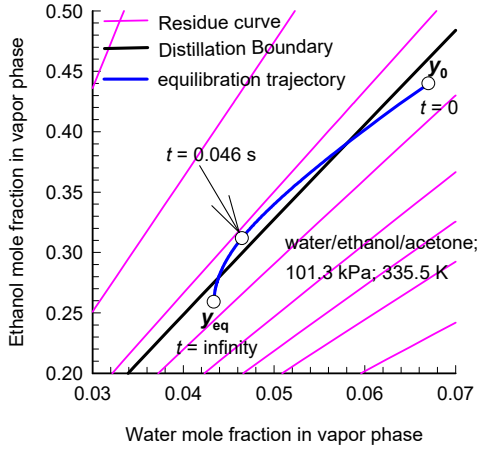

(b)

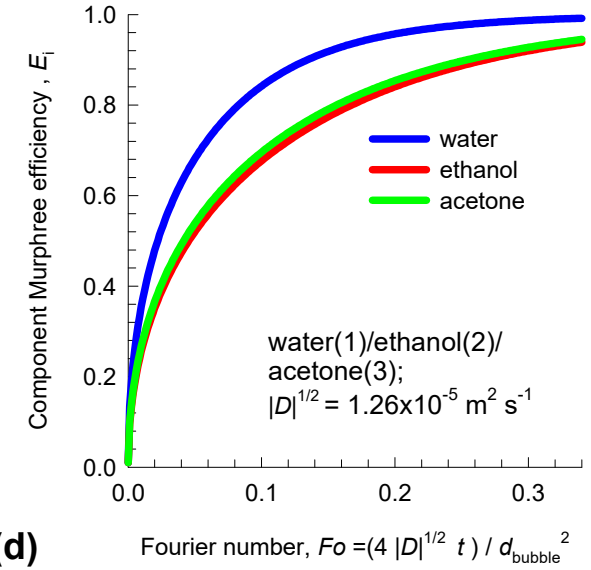

(c)

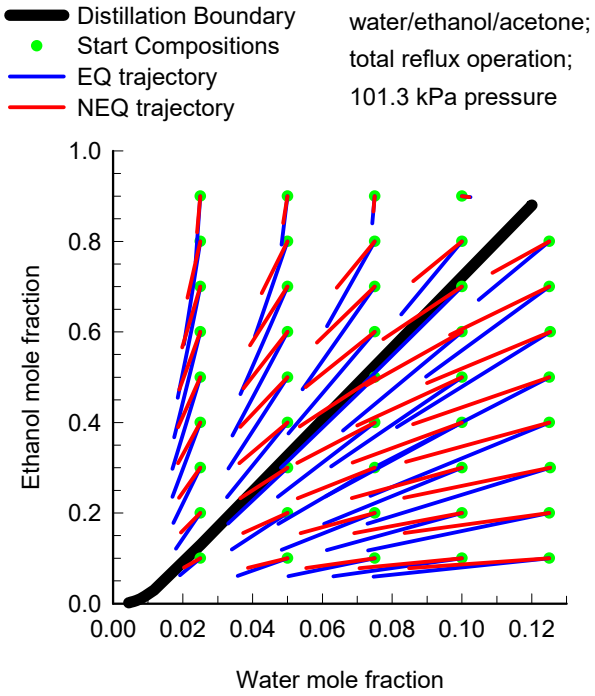

(d)

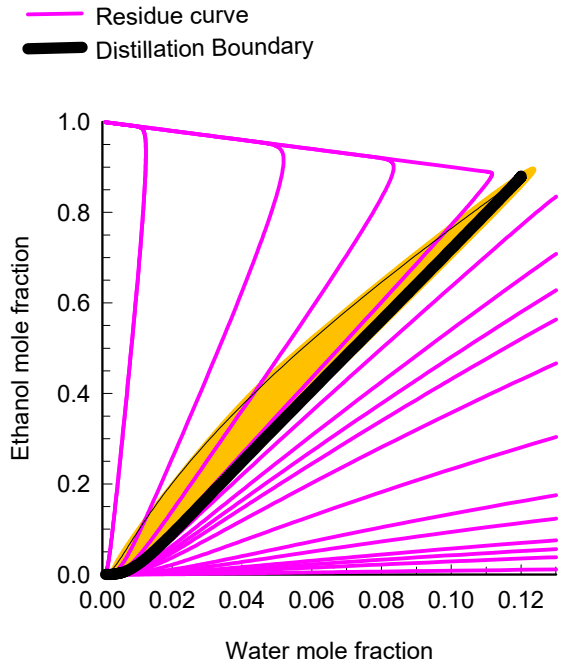

Design of column: Left of boundary

Fig. S36

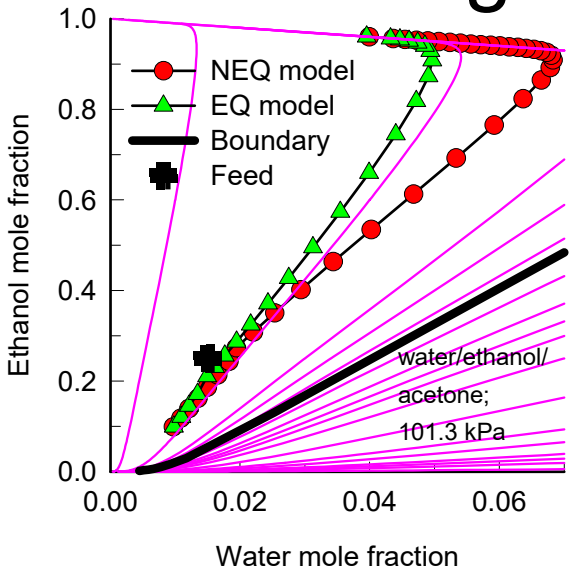

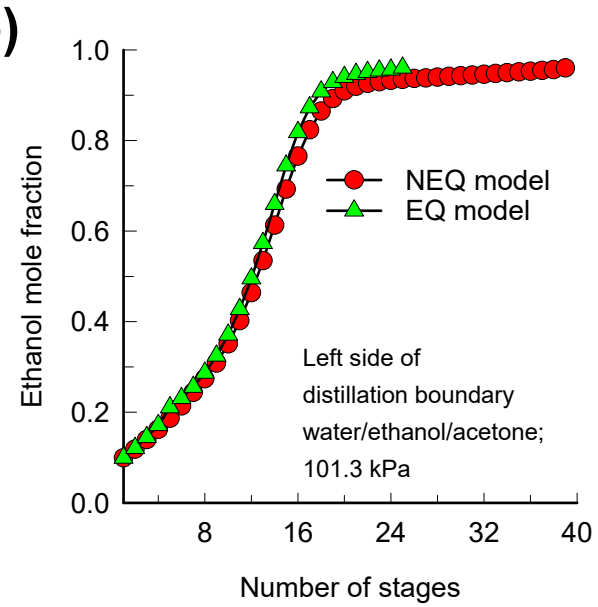

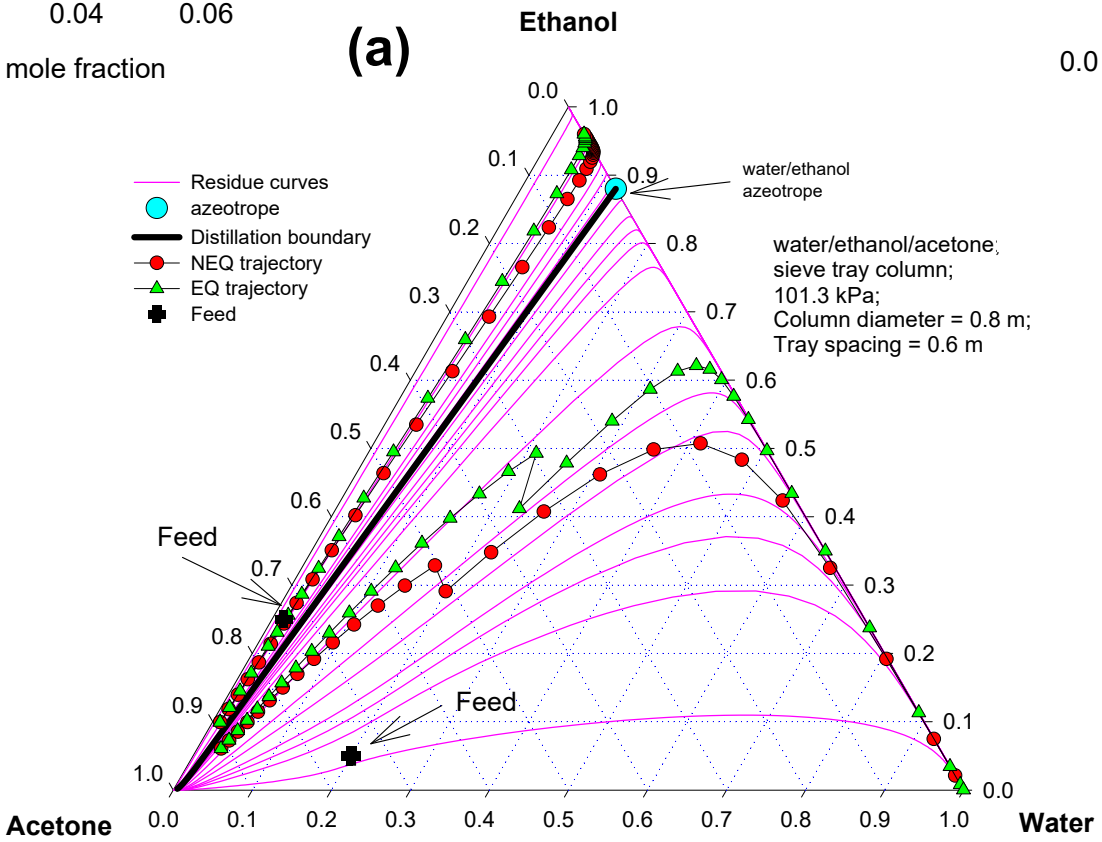

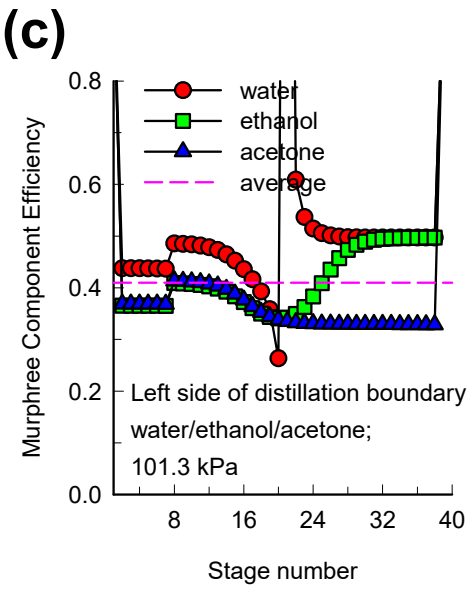

Design of column: Right of boundary

Fig. S37

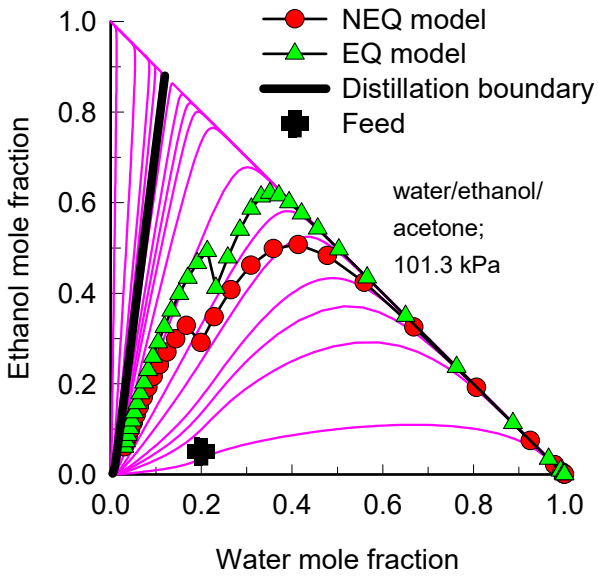

(a)

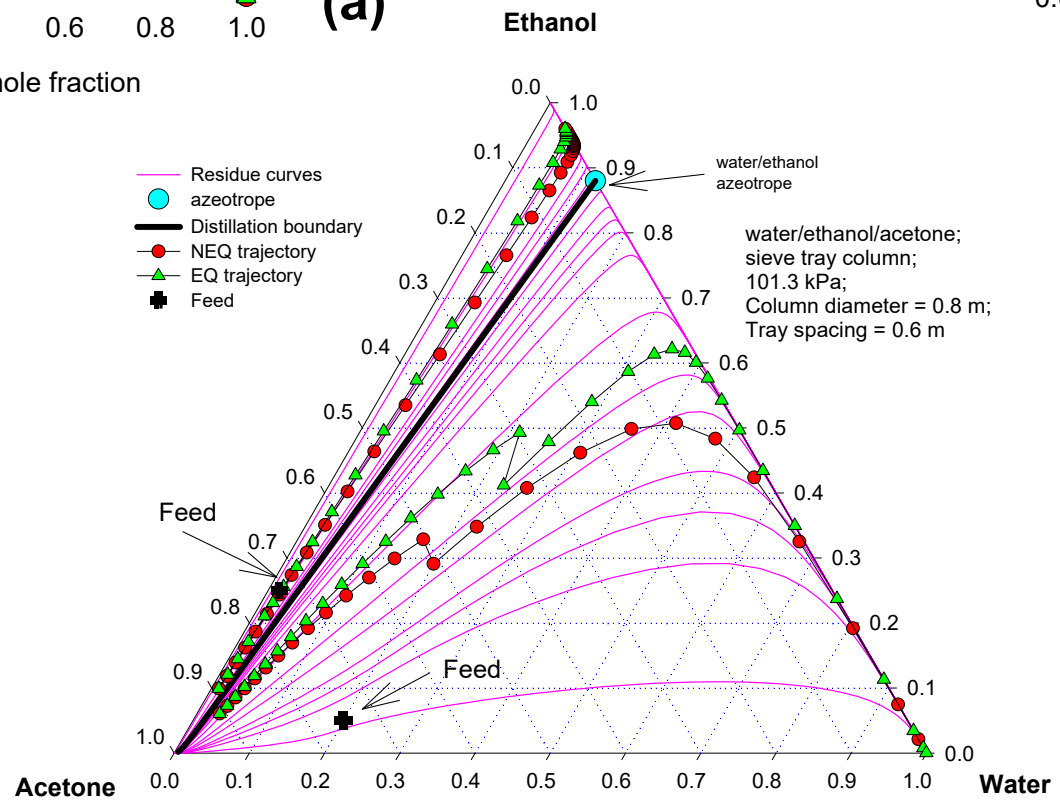

(b)

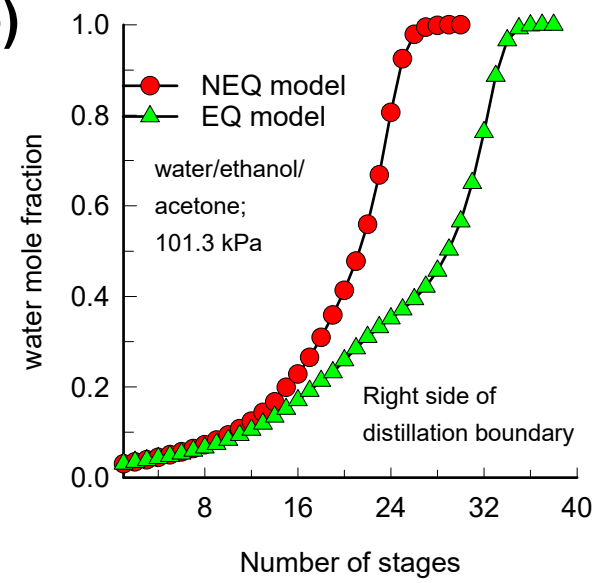

(c)

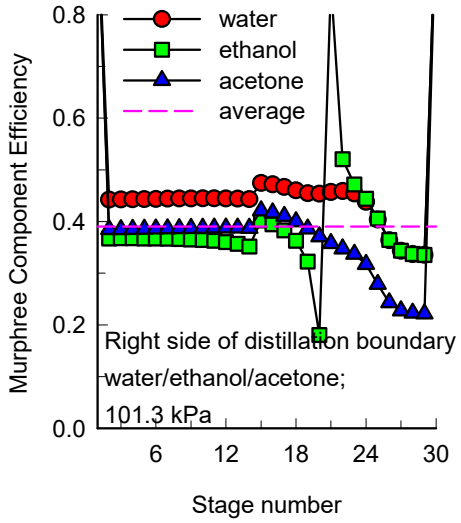

Water/Ethanol/Methanol Distillation

Fig. S38

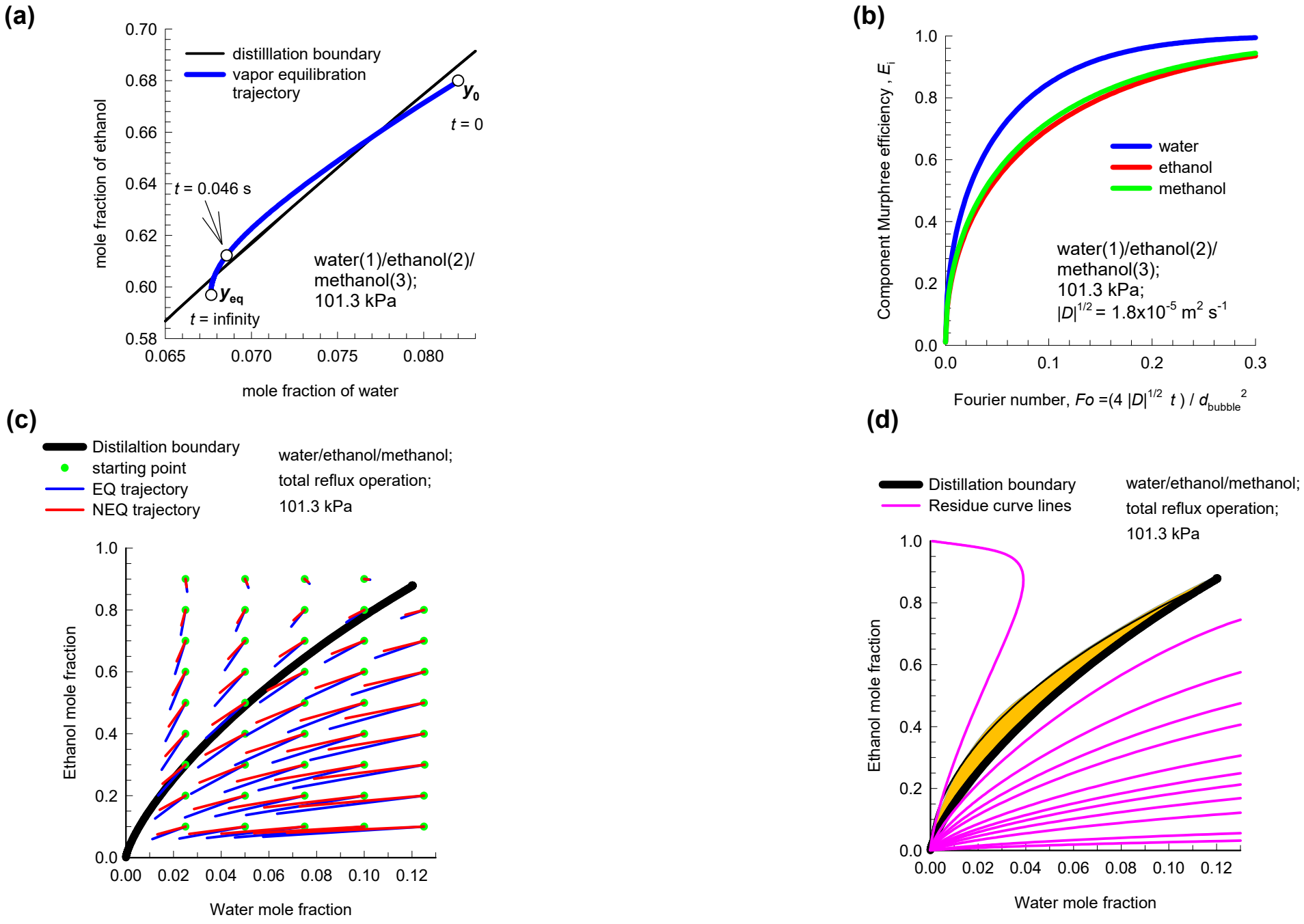

Water/Ethanol/Methylacetate Distillation

Fig. S39

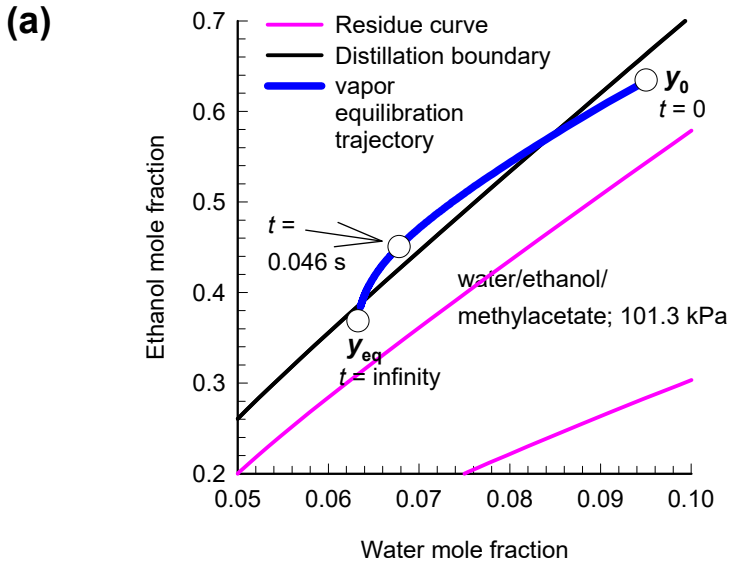

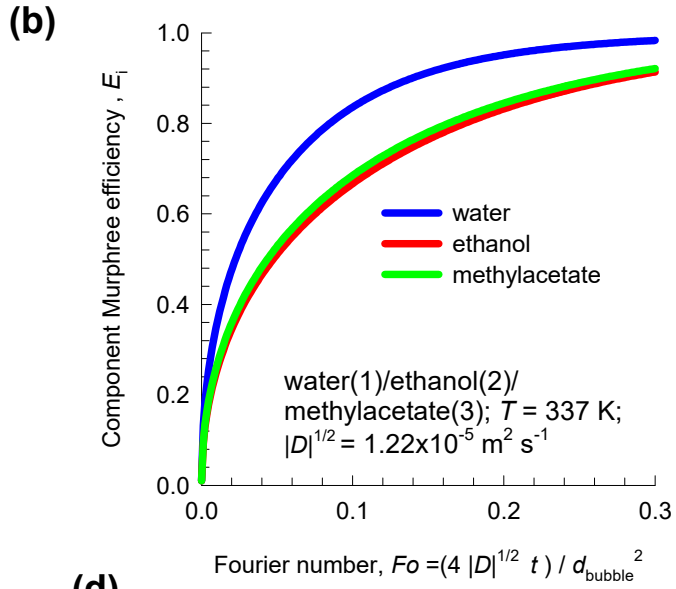

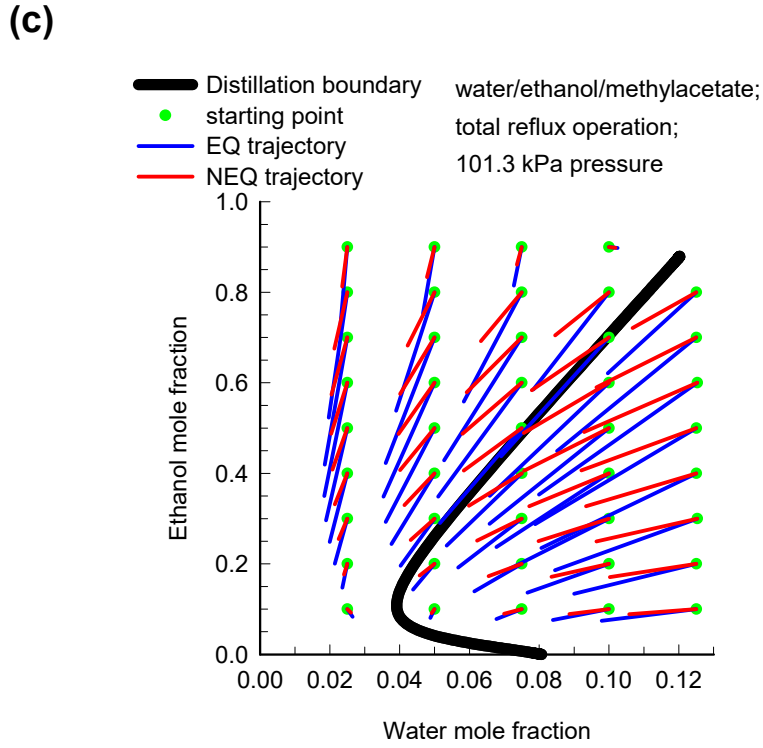

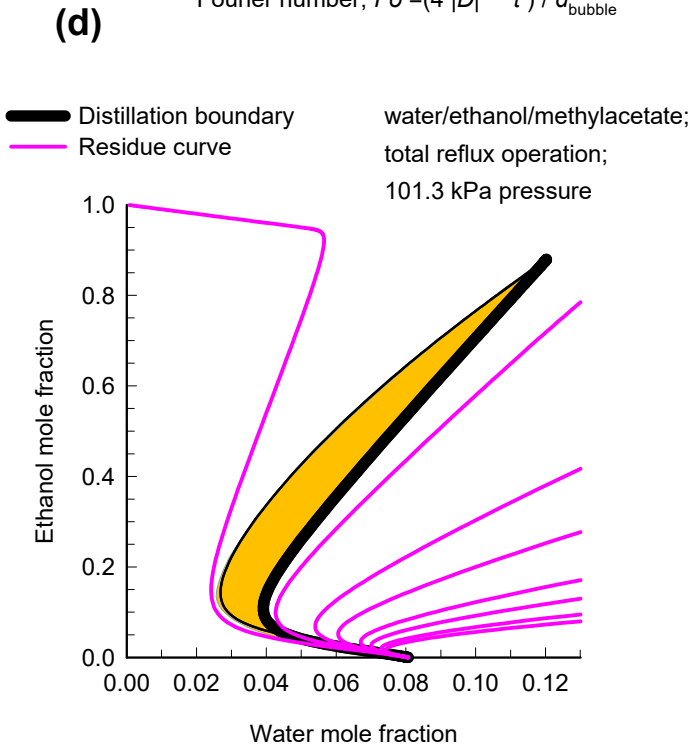

Water/Acetone/Toluene Distillation

Fig. S40

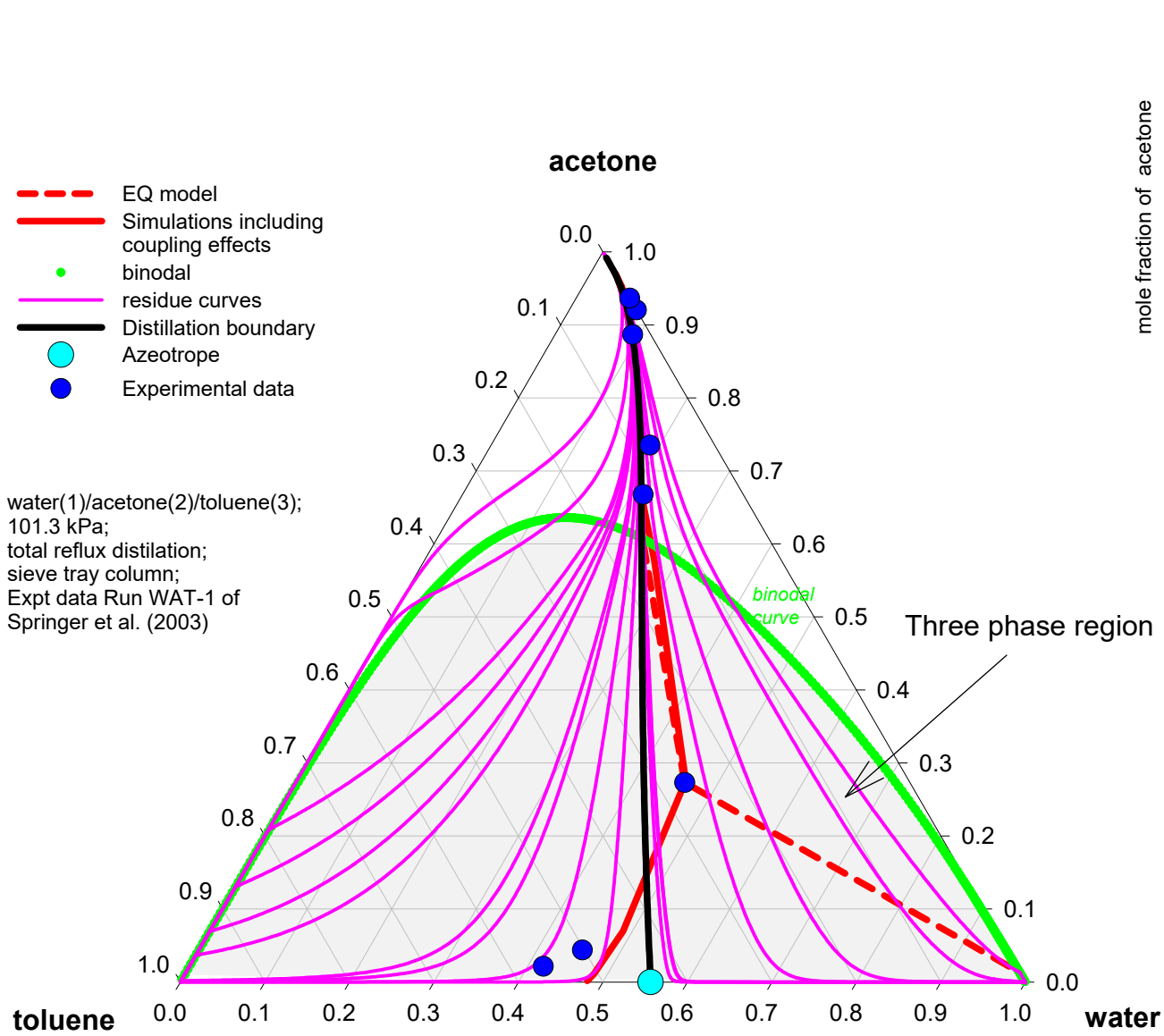

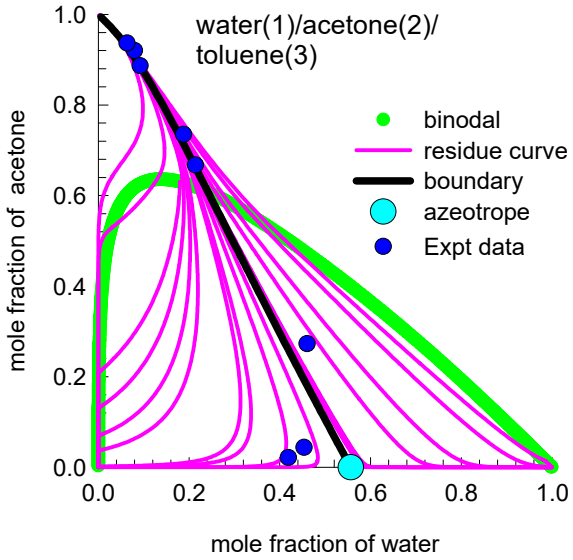

Water/Acetone/Toluene Distillation

Fig. S41

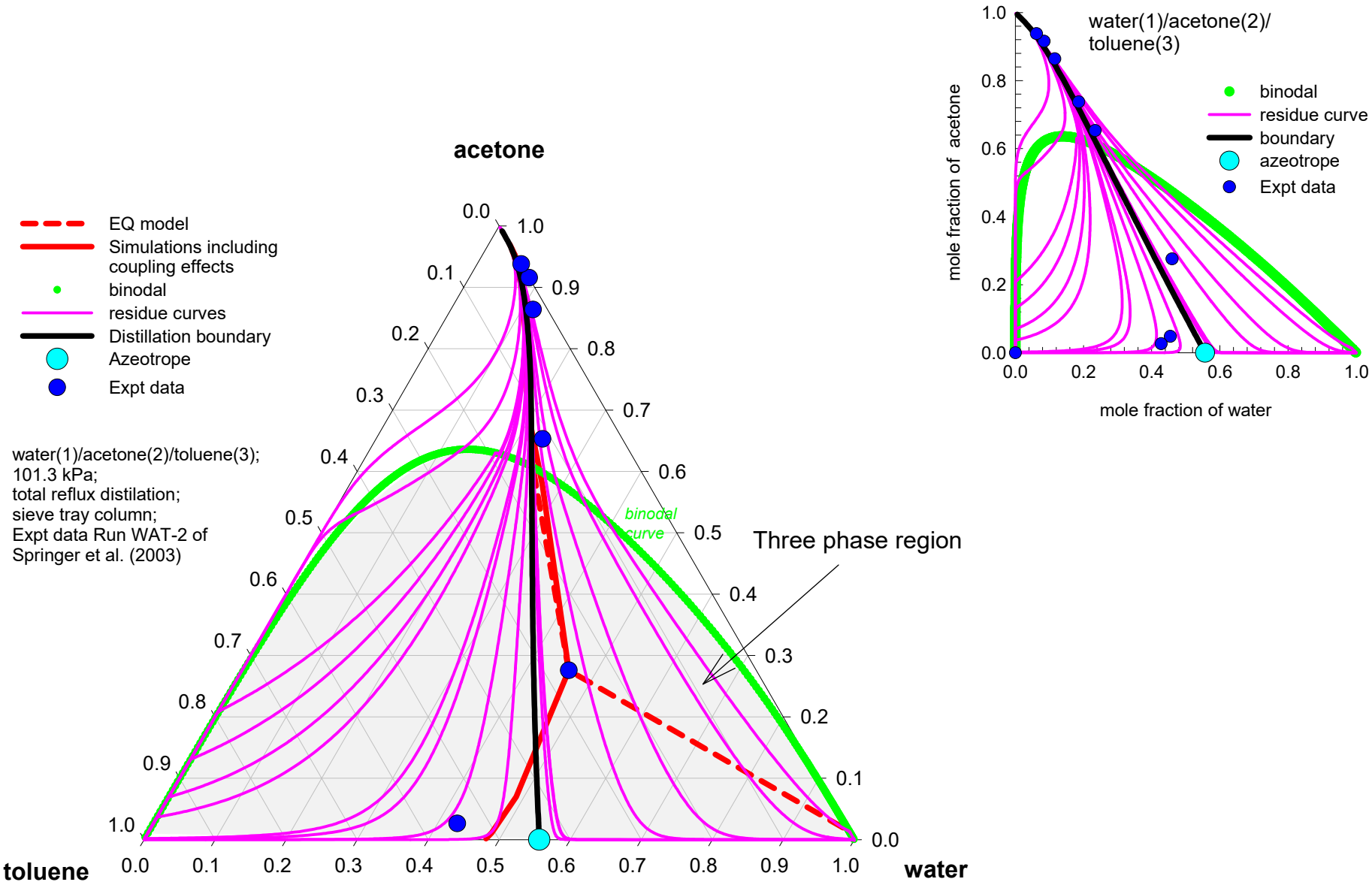

Water/Ethanol/Cyclohexane Distillation

Fig. S42

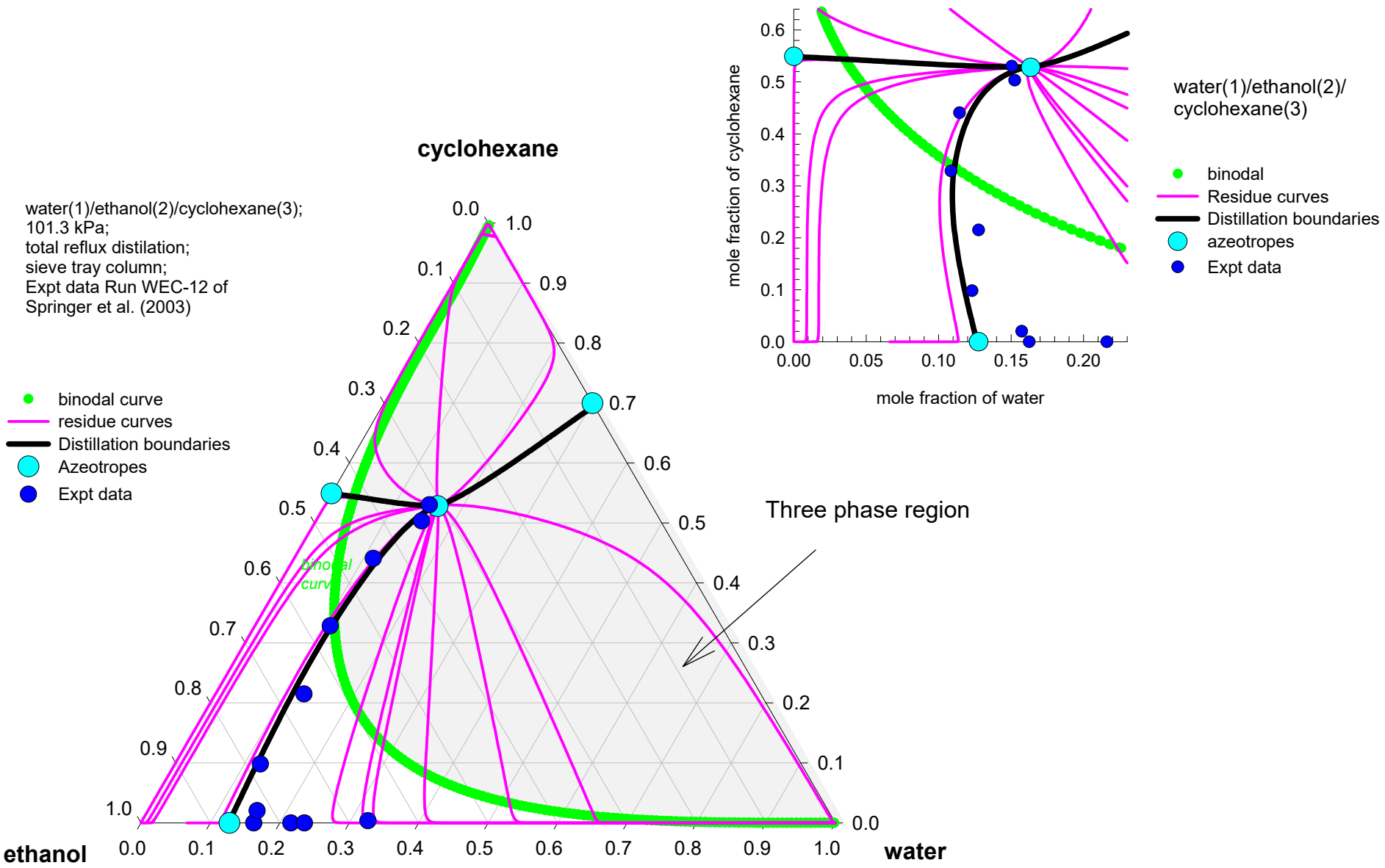

Water/Ethanol/Cyclohexane Distillation

Fig. S43

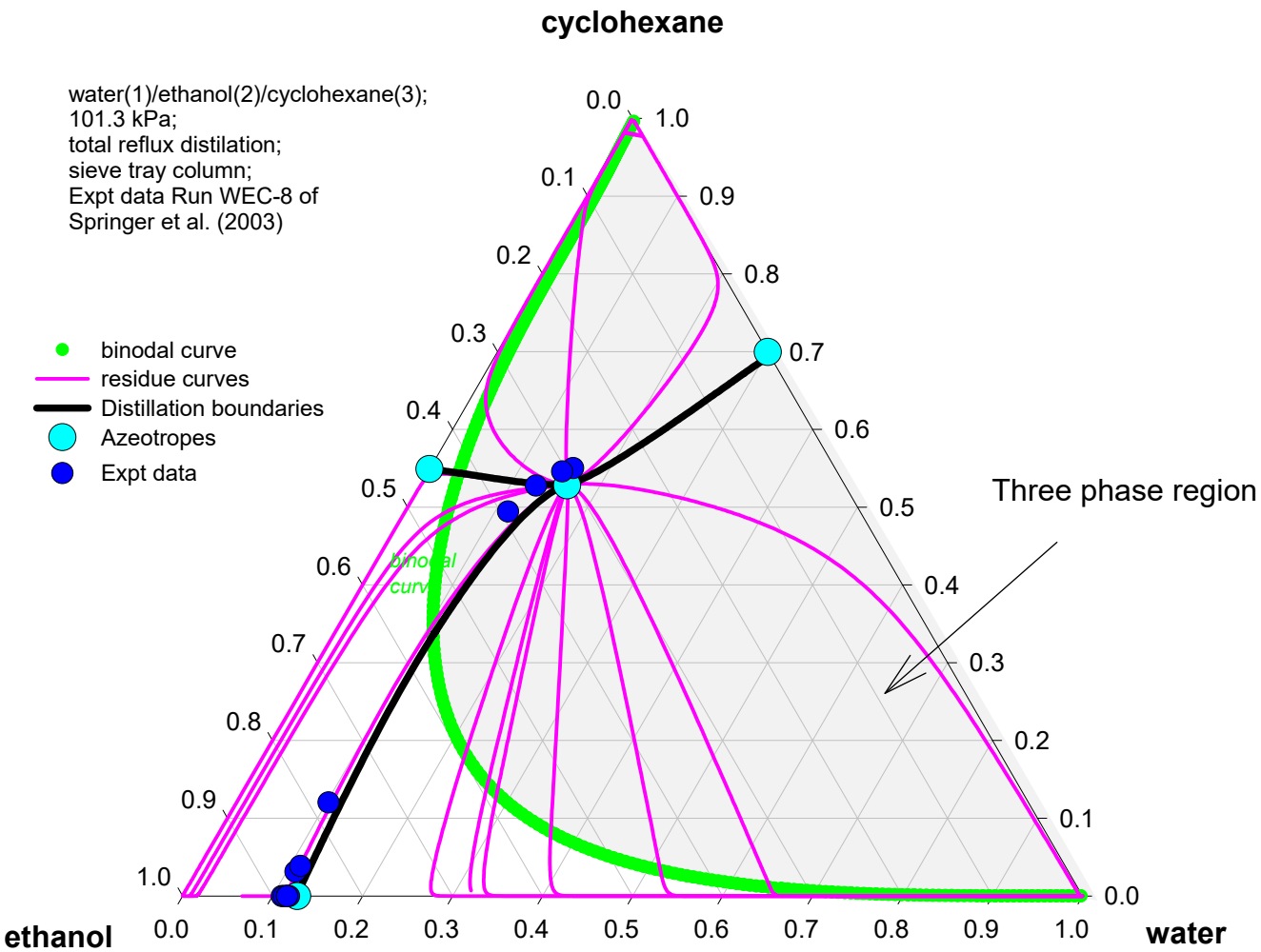

Mass transfer resistances:Heterogeneous Azeotropic Distillation

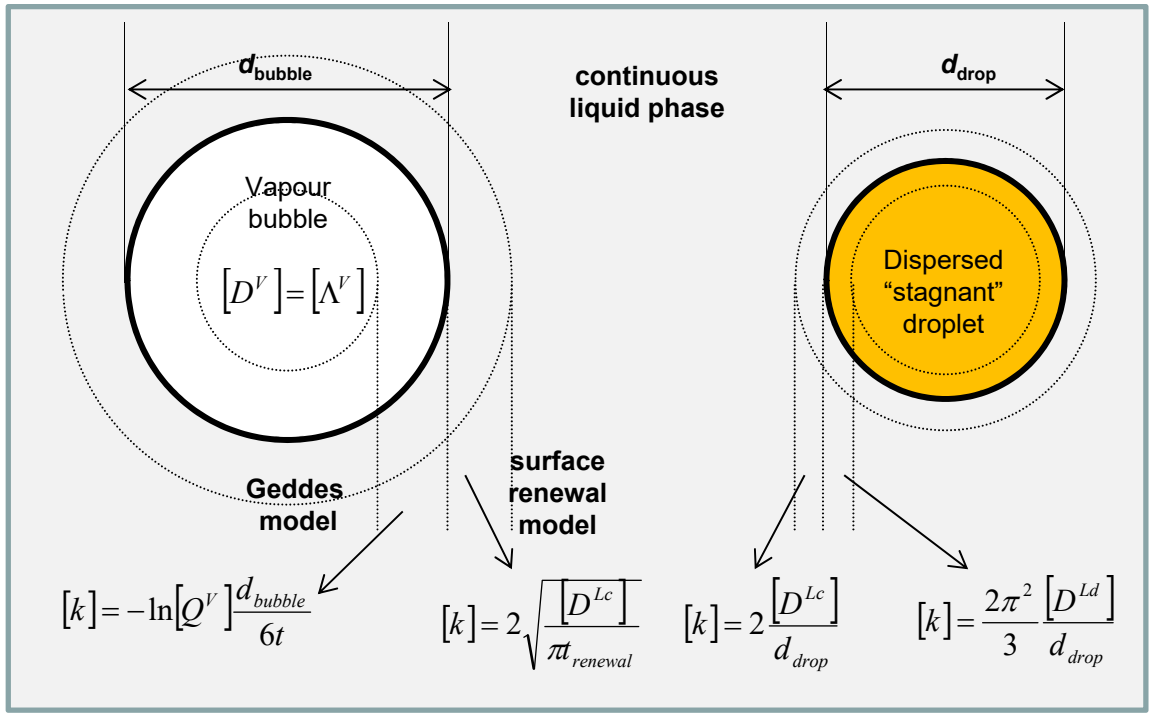

Fig. S45

Diffusional Distillation

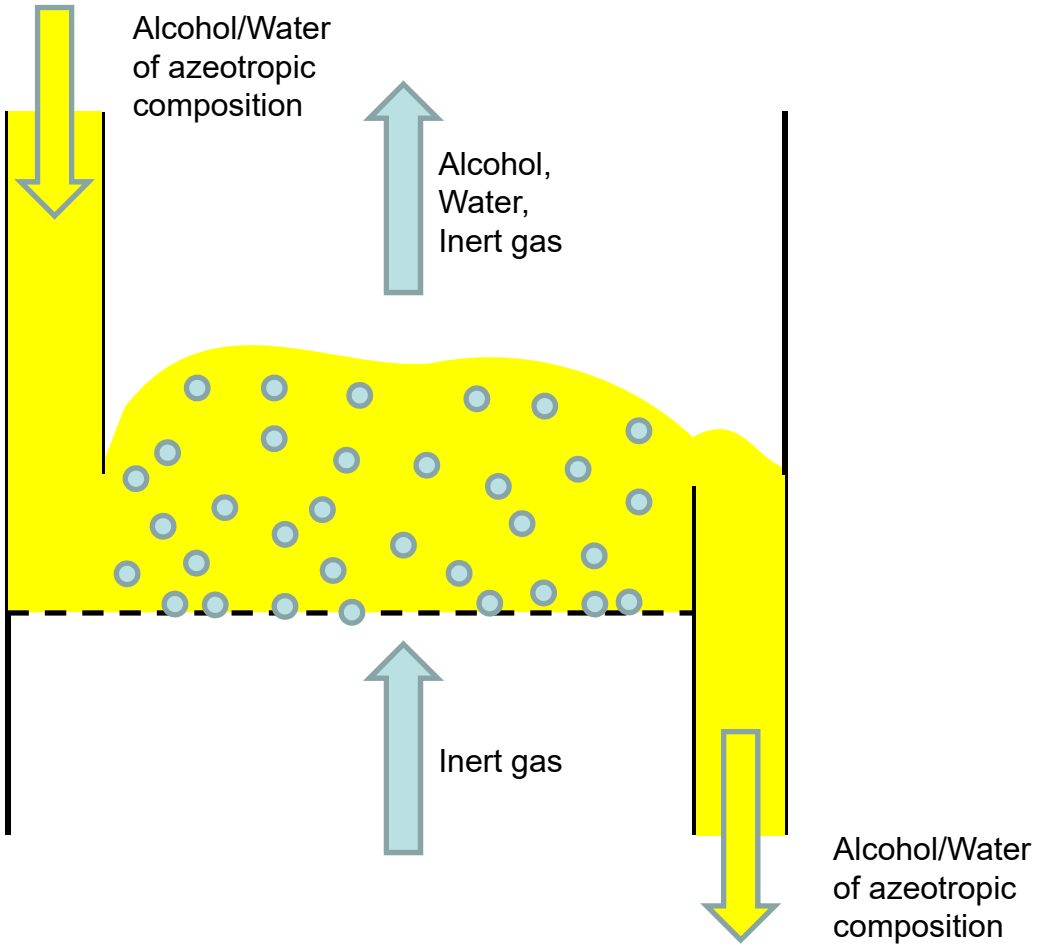

Bubbling inert gas to break azeotrope

Fig. S46

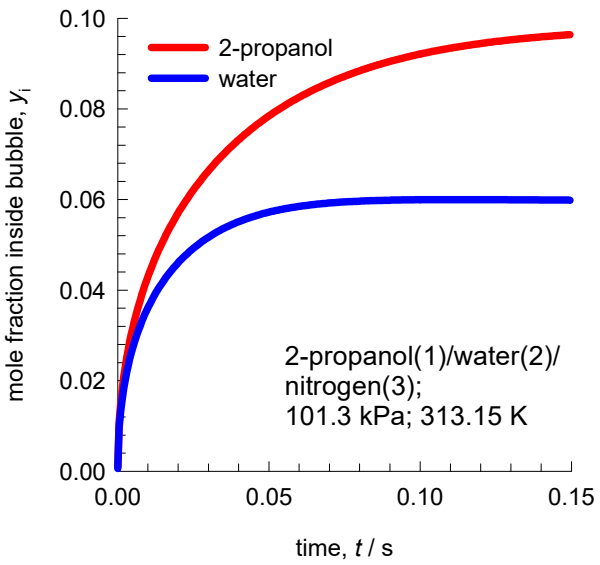

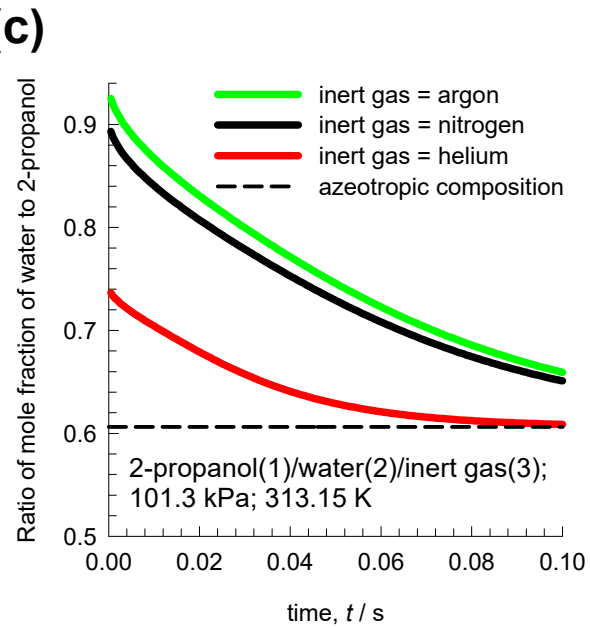

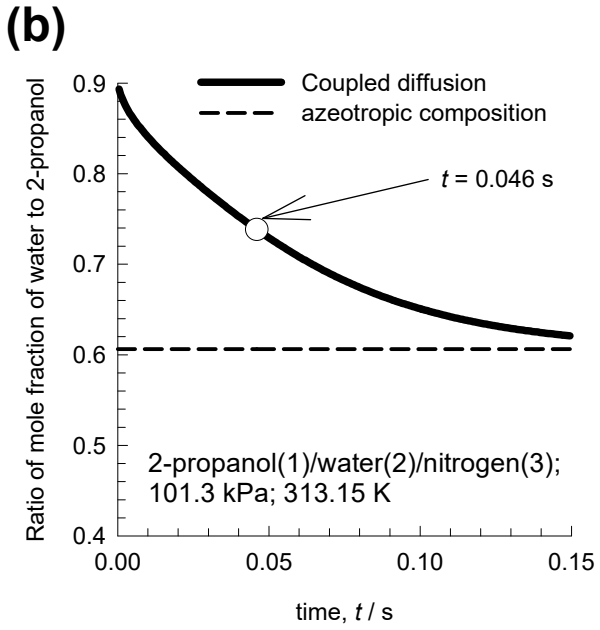

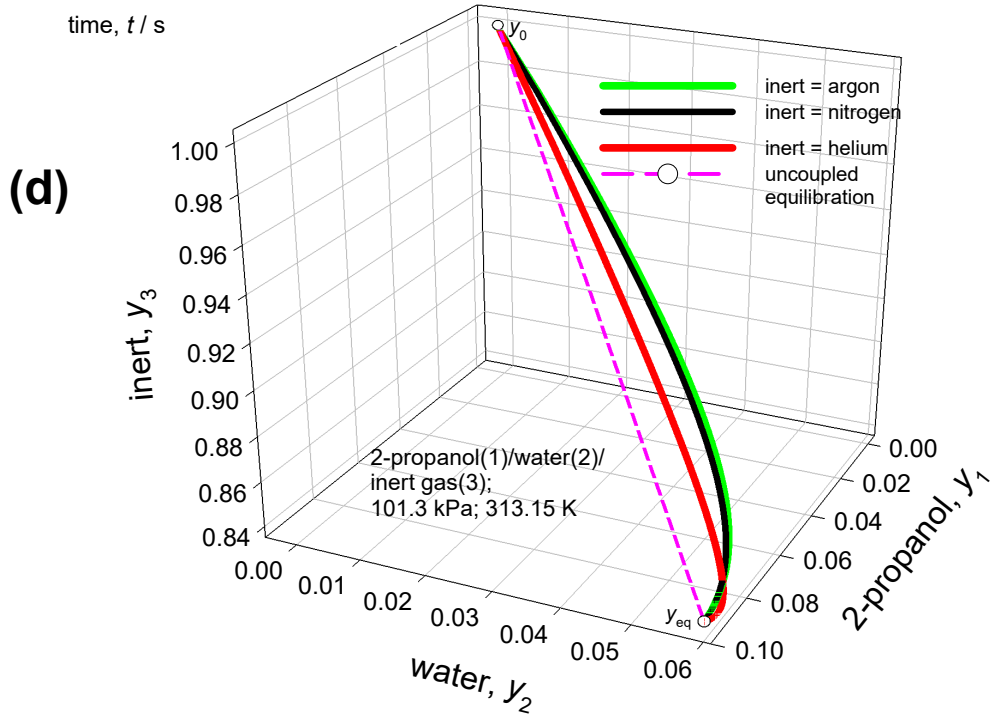

Bubbling inert gas to break azeotrope

Fig. S47

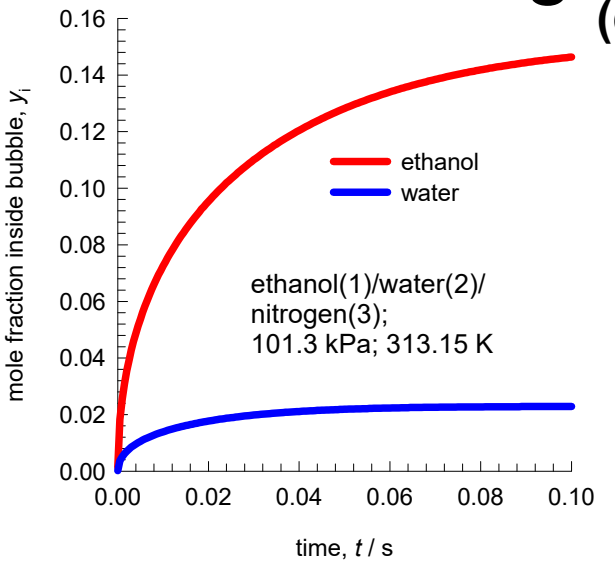

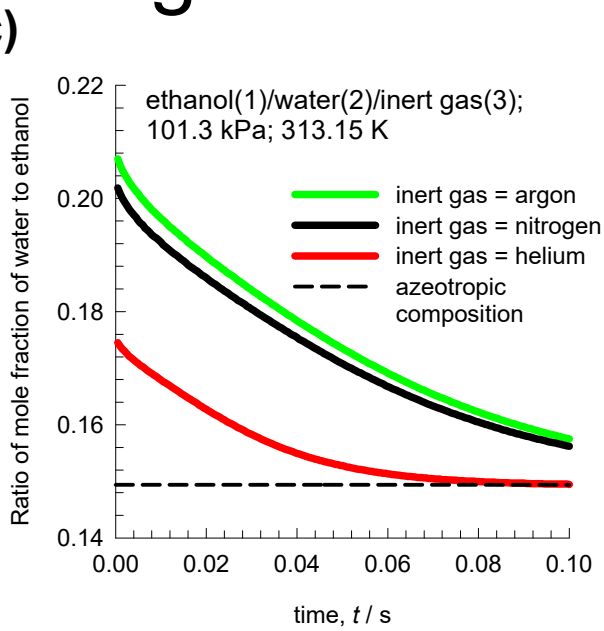

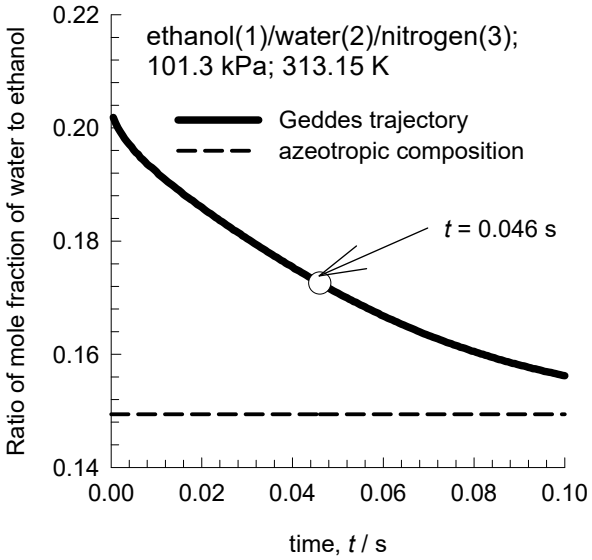

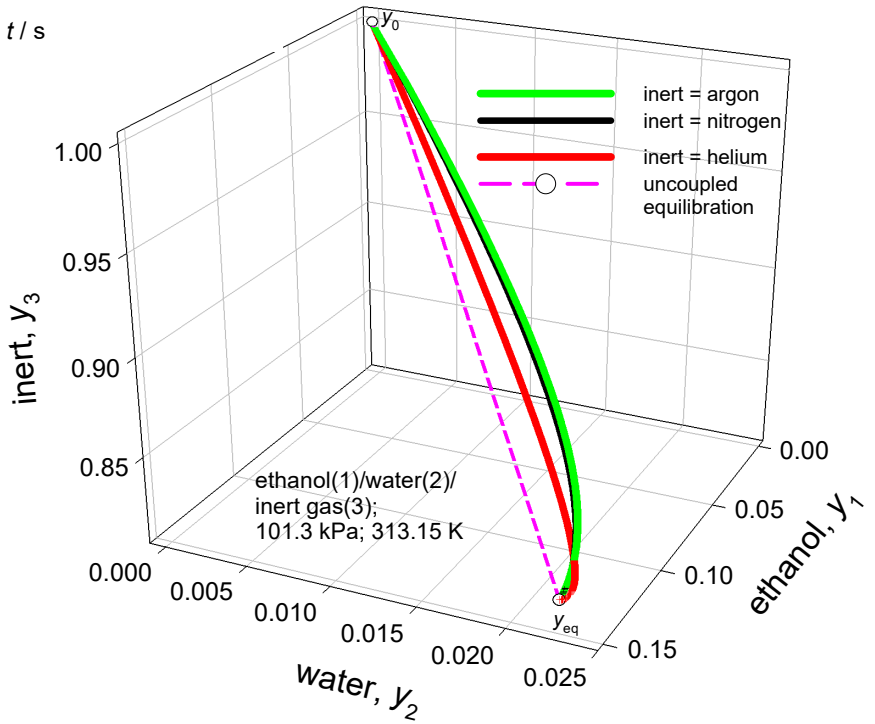

Bubbling inert gas to break azeotrope

Fig. S48